

UNIVERSITÉ DU QUÉBEC

RAPPORT PRÉSENTÉ À
L'UNIVERSITÉ DU QUÉBEC À TROIS-RIVIÈRES

COMME EXIGENCE PARTIELLE
DU DOCTORAT EN SCIENCES ET GÉNIE
DES MATÉRIAUX LIGNOCELLULOSIQUES

PAR
MICHEL SCHENKER

ÉTUDE DES SUSPENSIONS DE MICRO-NANOCELLULOSE
FIBRILLÉE (MNFC)

MAI 2019

Université du Québec à Trois-Rivières

Service de la bibliothèque

Avertissement

L'auteur de ce mémoire ou de cette thèse a autorisé l'Université du Québec à Trois-Rivières à diffuser, à des fins non lucratives, une copie de son mémoire ou de sa thèse.

Cette diffusion n'entraîne pas une renonciation de la part de l'auteur à ses droits de propriété intellectuelle, incluant le droit d'auteur, sur ce mémoire ou cette thèse. Notamment, la reproduction ou la publication de la totalité ou d'une partie importante de ce mémoire ou de cette thèse requiert son autorisation.

UNIVERSITÉ DU QUÉBEC À TROIS-RIVIÈRES
SCIENCES ET GÉNIE DES MATÉRIAUX LIGNOCELLULOSIQUE (PH.D.)

Direction de recherche :

Patrice MANGIN

Prénom et nom

directeur de recherche

Patrick GANE

Prénom et nom

Aalto University

codirecteur de recherche

Jury d'évaluation

Bruno CHABOT

Prénom et nom

Président de Jury

Nicole DEMARQUETTE

Prénom et nom

École de technologie supérieure (ETS)

Évaluateur externe

Joachim SCHOELKOPF

Prénom et nom

OMYA

Évaluateur externe

Foreword

The origins of this study go back to a joint work between UQTR (Prof. Patrice Mangin) and Omya International AG within the ArboraNano framework, which started in 2012. The goal of this initial project was to demonstrate the feasibility of applying micro nanofibrillated cellulose (MNFC)-based coatings directly on a paper machine, up to pilot scale. After successfully achieving this goal on the pilot paper machine of Innofibre, Trois Rivières Québec, the cooperation between Prof. Mangin and Omya continued to develop this technology further, and to advance a more fundamental aspect in related areas. A mid-term research proposal was set up, including several Master- and PhD theses. I had the honour to be asked by Prof. Patrick Gane, vice president of R&D at Omya International AG, to work on one of those PhD thesis projects, and to be accepted as a candidate by my supervisor Prof. Patrice Mangin. The goal of this work was set to obtain a better understanding of the stability and homogeneity of MNFC-containing suspensions. Soon it became apparent, that the initial scope was too broad, and it was decided to focus on a specific investigation of the rheology of such suspensions. As this project was funded by the industry, an eye was kept on product relevance and practicability. Due to the complex rheological behaviour of fibrillar cellulose suspensions, special attention was paid to adequate measurement set-ups and protocols, as well as meaningful parametrisation and quantification of the obtained rheological data. Finally, the influence of suspension solids content and the degree of fibrillation on their rheological behaviour was investigated specifically adopting an extensive experimental matrix.

Acknowledgments

This work would not have been possible without the encouragement and the constant support of my former managers from Omya International AG, Joachim Schoelkopf and Patrick Gane, as well as my supervisor Patrice Mangin. I would like to thank them for their guidance, but also for giving me a lot of freedom and independence to carry out this work. Also, I would like to thank them for all the interesting discussions, exchanges and chats we have had on, or off, the topic of this work. *Dear gentlemen, thank you very much!* To become a scientist, one has to be curious as well as persistent sometimes. These are only two of many useful traits that my parents taught me. I am deeply grateful for your encouragements, support and help I have experienced, also in difficult times. Without you, I wouldn't be where I am today. *Mami, Papi, danke vöumou!* Cathrin, thank you for supporting my enthusiasm, for your honest interest in my work and for giving me balance in my life. *You rock!* And, finally, Fay, thank you for teaching me life lessons without even knowing.

Big thanks also go to my colleagues at Omya and FiberLean for their valuable discussions, moral support and helpful inputs. It was, and still is a pleasure to work with you. I would also like to thank the members of the CRML at UQTR I had the pleasure to meet and work with, I felt always welcome and supported during my visits and stays.

Finally, but not less importantly, Omya International AG as well as FiberLean Technologies Ltd. are gratefully acknowledged for not only funding this research as well as providing me all the resources I needed to carry out this thesis.

Résumé

Bien que connu depuis environ 30 ans, la micro-nanocellulose fibrillée (MNFC) n'a suscité de véritable intérêt que depuis les dix dernières années. Depuis, non seulement les universités, mais aussi l'industrie, étudient ce matériau polyvalent pour diverses applications. Un facteur limitant était, et est encore dans une certaine mesure, les processus de fabrication généralement longs et coûteux. Cependant, des développements récents ont montré qu'il est possible de produire économiquement diverses qualités de MNFC en utilisant des procédés de fibrillation mécanique, éventuellement assistés par des aides au broyage tels que des particules minérales qui peuvent apporter des propriétés par synergie énergétique.

Alors que le MNFC possède des propriétés très intéressantes, comme la résistance mécanique, la rhéologie et les fonctionnalités barrière, les mêmes propriétés peuvent également poser des problèmes majeurs de manipulation et d'application. L'un de ces aspects est le comportement d'écoulement visqueux du flux de suspension de MNFC, c'est-à-dire son profil rhéologique. Non seulement le comportement rhéologique est complexe, mais aussi la morphologie des particules de suspension sous-jacente.

Ce travail a été initié pour étudier l'interaction entre différents paramètres de suspension et les propriétés de la suspension résultante alors que la rhéologie n'était que l'un des aspects d'intérêt. Après avoir réalisé le niveau de complexité de la rhéologie des suspensions de MNFC, la recherche a été recentrée sur les investigations rhéologiques qui, à notre analyse, pouvait également fournir de nombreuses informations utiles.

Des travaux expérimentaux initiaux, ainsi qu'une analyse bibliographique approfondie, ont révélé que même une mesure fiable de la rhéologie d'une suspension MNFC n'est pas simple, pour de nombreuses raisons pratiques liées à son comportement rhéologique complexe.

Ainsi, une première partie du travail est consacrée à analyser et préciser les réglages et conditions de mesures appropriés pour les rhéomètres à cisaillement. Constatant qu'une telle recherche n'avait pas encore été effectuée systématiquement auparavant pour les suspensions de MNFC, il convient de souligner que différents matériaux à base de nanocellulose peuvent répondre différemment à certaines conditions de mesure. Par

conséquent, toutes les recommandations figurant dans la littérature ne peuvent pas être appliquées de manière ponctuelle aux suspensions de MNFC. Nous avons montré, par exemple, qu'une palette dans un système à cupule dentelée semblait moins susceptible aux artefacts de mesure que d'autres systèmes plus classiques à base de cylindres coaxiaux. Cependant, les données ont également indiqué que les tendances en fonction de la teneur en solides peuvent également être reproduites avec des systèmes influencés par des artefacts, qui peuvent même être quantifiés.

Une autre partie de ce travail consistait à décrire les données rhéologiques obtenues de manière comparable, c'est-à-dire quantitatives plutôt que qualitatives. Plusieurs descripteurs rhéologiques quantitatifs sont bien connus, par exemple la viscosité et le module de stockage. Cependant, les suspensions de MNFC ont un profil de viscosité complexe et plutôt distinct (courbe d'écoulement). Même si cela est rapporté fréquemment, il est rarement paramétré et quantifié, ce qui rend difficile la comparaison avec d'autres ensembles de données. Nous avons donc introduit de nouveaux descripteurs qui quantifient spécifiquement le comportement observé des trois zones. Les nouveaux descripteurs traduisent d'une part les taux de cisaillement auxquels la suspension de MNFC entre et sort de la zone de transition, et d'autre part, ils décrivent le comportement de la courbe d'écoulement dans les différentes zones de réponse. Une autre approche que nous avons introduite est la description quantitative de l'hystérésis de la courbe d'écoulement qui est généralement observée lorsqu'une boucle de taux de cisaillement est réalisée, c'est-à-dire lorsque le taux de cisaillement est d'abord augmenté puis diminué dans une mesure de courbe d'écoulement (ou inversement).

Pour se garantir de la validité de notre approche expérimentale et des méthodes de traitement des données, des tests statistiques ont également été réalisés sur un ensemble de données sélectionné. En général, il a été constaté que les tendances apparentes visuelles étaient confirmées par les tests de variance respectifs.

Sur la base de toutes les parties susmentionnées de ce travail, une vaste étude expérimentale a été menée sur l'influence du degré de fibrillation (DoF) d'une suspension de MNFC sur son comportement rhéologique. Ceci a été réalisé par caractérisation rhéologique de mélanges de trois suspensions de DoF différentes. Alors qu'aucune quantification fiable et absolue de DoF n'a été obtenue, des mesures indirectes de DoF ont

montré que trois degrés de fibrillation étaient atteints dans la série de production d'échantillons, l'un peut être considéré comme non fibrillé, un autre moyennement fibrillé et le dernier hautement fibrillé. Pour pouvoir présenter l'ensemble complet de données de manière compacte et compréhensive, des diagrammes de mélange ternaires ont été utilisés comme format de visualisation, incluant des superpositions de cartes de couleurs pour tracer les données. À l'aide de ces diagrammes ternaires 2D ou 3D en courbes de niveau superposés, les tendances qualitatives sont facilement identifiables. Alors que certaines des tendances dominantes dans le domaine de la rhéologie des nano celluloses ont été confirmées par cette étude sur les suspensions de MNFC, d'autres effets précédemment jamais rapportés ont également été mis en évidence.

Les résultats obtenus tout au long de ce travail ont été discutés avec une vue sur les hypothèses de modèles morphologiques les plus récents. Plus précisément, notre argumentation était basée sur les résultats d'autres chercheurs qui utilisaient des méthodes rhéo-optiques pour étudier le changement macroscopique de la morphologie des particules de suspension dans des suspensions de MNFC en écoulement. En outre, nous avons également inclus d'autres travaux du domaine dans la discussion de nos données et de l'évolution des modèles respectifs. En conséquence, notre présent travail propose également un examen critique et une vue d'ensemble des avancées récentes dans le domaine de la rhéologie des suspensions de MNFC.

Le travail peut servir de base solide pour toutes recherches ultérieures, tout comme pour étudier l'influence des propriétés des autres types de suspensions de MNFC quant à leur comportement rhéologique et à leur morphologie.

Mai 2019

Summary

Despite being known for about thirty years, MNFC has only gained real attention about ten years ago. Since then, not only academia, but also industry, are investigating this versatile material for various purposes. A limiting factor was, and to some extent still is, the typically extensive and expensive manufacturing processes. Yet, recent developments have shown that it is possible to produce cost-effective grades using mechanical fibrillation processes, eventually assisted by grinding aids like mineral particles, which, themselves, can act to develop synergistic properties. Whereas MNFC has very interesting properties, for example, concerning mechanical strength, rheology and barrier functionality, the same properties can also lead to major challenges in handling and applying it. As mentioned, one of these aspects is the MNFC suspension flow behaviour, i.e. its rheology profile. Not only the rheological behaviour itself is complex, but also the respective underlying suspension particulate morphology reflected in that behaviour.

This work was set-up initially to investigate the interaction between different suspension/composition parameters and components and the resulting suspension properties, whereas rheology was one aspect of interest. After realising that the rheology of MNFC suspensions is very complex on its own, but might as well provide much useful information, the work was refocused on rheological investigations.

Initial experimental work, as well as a thorough literature review, have revealed that even a reliable measurement of an MNFC suspension's rheology in itself is not straightforward, for many practical reasons related to its complex rheological behaviour. So, an initial part of the work is dedicated to finding appropriate measurement set-ups and conditions for shear rheometer devices. It was found that such an investigation was not yet done systematically before for MNFC suspensions, and, in this context, it should be highlighted that different nanocellulose materials may respond differently to certain measurement conditions. So, not all recommendations that are found in the literature can be applied *ad hoc* to MNFC suspensions. We showed, for instance, that a vane-in-serrated-cup system appears to be less susceptible to measurement artefacts compared to the more common cylinder-in-cup-based systems. However, the data also indicated that trends as a function of solids content can also be reproduced with systems that are influenced by artefacts, sometimes even quantitatively.

Another part of this work was to describe the variously obtained rheological data in a way that they were comparable, i.e. to be quantitative rather than qualitative. Several quantitative rheological descriptors are well known, for instance viscosity and storage modulus. However, MNFC suspensions have a complex and rather distinct viscosity profile (flow curve). Even though this is reported frequently, it is seldom parametrised and quantified, making it difficult to compare to other datasets. We, therefore, introduced novel descriptors that quantify specifically the observed three-zone behaviour. On the one hand, they describe the shear rates at which the MNFC suspension enters and leaves the transition zone, and on the other hand, they describe the flow curve behaviour within the different response zones. Another approach we introduced was the quantitative description of the flow curve hysteresis that is typically observed when a shear rate loop is performed, i.e. when the shear rate is first increased and then decreased in a flow curve measurement (or vice versa). To get confidence in the experimental approach and the data treatment methods, statistical tests were performed on a selected dataset as well. In general, it was found that visually apparent trends were confirmed by respective variance tests.

Based on all the aforementioned parts of this work, an extensive experimental study was carried out, investigating the influence of the degree of fibrillation (DoF) of an MNFC suspension on its rheological behaviour. This was realised by rheologically characterising mixtures comprising up to three different suspensions of different DoFs. Unfortunately, no reliable, absolute quantification of the DoF was achieved, yet, indirect measurements of the DoF have shown that three grades of fibrillation were achieved in the sample production series, wherein one can be considered to be unfibrillated, another one medium fibrillated and the last one to be extensively fibrillated MNFC. To be able to present the extensive set of data in a compact and comprehensive way, ternary mixture diagrams were used as a visualisation format, including colourmap overlays to plot the data. Using these 2D contour, or 3D stacked, ternary diagrams, qualitative trends were easily identified. Whereas some prevailing trends in the field of nanocellulose rheology were confirmed by this study on MNFC suspensions, other, previously unreported effects were found as well. The findings obtained throughout this work were discussed with a view on recent morphological model hypotheses. Argumentation was based on results from other

researchers who used rheo-optical methods to investigate the macroscopical change of the suspension particulate morphology of flowing MNFC suspensions. In addition, other work in the field was included in the discussion of the data and respective model developments. As a result, the present work also provides a critical review and overview on recent advances in the field of the rheology of MNFC suspensions.

The work can be understood as a solid basis for continuing further, similar investigations researching the influence of other MNFC suspension properties and their influence on rheological behaviour and particulate flow morphology.

May 2019

Keywords

Microfibrillated cellulose (MFC); Micro nanofibrillated cellulose (MNFC); Rheology; Flow curve; Viscoelasticity; Vane rheometry; Degree of fibrillation; Aqueous suspension; Morphology; Data quantification

Contents

Foreword	i
Acknowledgments	ii
Résumé	iii
Summary	vi
Keywords	ix
Contents	x
List of figures	xvi
List of tables	xxii
List of equations	xxiii
List of abbreviations	xxv
Chapter 1 - Introduction	1
1.1 Nomenclature	1
1.2 Context	1
Chapter 2 - Literature review	4
2.1 Cellulose	4
2.1.1 Structure	4
2.1.2 Types	5
2.2 MNFC	7
2.2.1 Manufacturing	7
2.2.2 General properties	13
2.2.3 Applications and uses for MNFC	16
2.3 Matrix material for composites	20
2.4 Characterisation of MNFC suspensions	22
2.4.1 Challenging characterisation: multi-scale sized features	22

2.4.2	Characterisation methods	22
2.4.3	Conclusion	39
2.5	Rheology of MNFC suspensions	39
2.5.1	Pure MNFC systems	40
2.5.2	Influence of additives on MNFC suspensions	42
2.5.3	MNFC in complex systems	43
Chapter 3 - Hypothesis and objectives		47
3.1	Original goal	47
3.1.1	Material space	47
3.1.2	Properties and products characterisation	48
3.1.3	Stability and homogeneity assessment	49
3.2	Refined goal	50
3.3	Objectives	52
Chapter 4 - Materials and Methods		53
4.1	Materials	53
4.1.1	MNFC	53
4.2	Methods	58
4.2.1	Rheology	58
4.2.2	Data treatment and presentation	68
4.2.3	Particle size distribution analysis	72
Chapter 5 - Article 1: Rheological investigation of complex micro and nanofibrillated cellulose (MNFC) suspensions: discussion of flow curves and gel stability		74
5.1	Foreword	74
5.2	Abstract	74
5.2.1	Keywords	75

5.3	Introduction	75
5.4	Experimental.....	76
5.4.1	Materials.....	76
5.5	Results and Discussion	81
5.5.1	MNFC morphology	81
5.5.2	Influence of solids content on MNFC rheology.....	81
5.5.3	Influence of the degree of fibrillation on MNFC suspension rheology	84
5.5.4	Influence of additives on MNFC suspension rheology.....	88
5.6	Conclusions	100
5.7	Acknowledgements	100
5.8	References	100
Chapter 6 - Presentation 1: Rheological investigation of pigmented micro-nano-fibrillated cellulose (MNFC) suspensions: Discussion of flow curves		
6.1	Foreword.....	104
6.2	Summary.....	104
6.3	Presentation	105
Chapter 7 - Article 2: Influence of shear rheometer measurement systems on the rheological properties of microfibrillated cellulose (MFC) suspensions		
7.1	Foreword.....	115
7.2	Abstract.....	116
7.2.1	Keywords	116
7.3	Introduction	116
7.4	Methods	119
7.4.1	Materials.....	119
7.4.2	Imaging.....	121
7.4.3	Rheological measurements.....	122

7.5	Results	127
7.5.1	Viscoelastic properties	127
7.5.2	Flow curves	131
7.6	Conclusions	141
7.6.1	Acknowledgements	142
7.7	References	143
7.8	Supplementary information	147
7.8.1	Viscoelastic data	147
7.8.2	Flow curve data	150
7.8.3	References	152
7.9	Additional, unpublished data	152
7.9.1	Influence of individual measurement setup geometries	152
7.9.2	Conclusions	158
Chapter 8 - Article 3: Quantification of flow curve hysteresis data – a novel tool for characterising microfibrillated cellulose (MFC) suspensions		159
8.1	Foreword	159
8.2	Abstract	159
8.2.1	Keywords	160
8.3	Introduction	160
8.4	Experimental	162
8.4.1	Materials	162
8.4.2	Imaging	164
8.4.3	Rheological measurements	164
8.5	Results and discussion	171
8.5.1	Morphological model	171

8.5.2	Flow curves	172
8.5.3	Influence of solids content on hysteresis properties.....	172
8.5.4	Learnings.....	181
8.5.5	Hysteresis properties dependence on solids content	183
8.5.6	Comparison with other MFC suspension hysteresis data.....	183
8.6	Conclusions	185
8.6.1	Acknowledgements	186
8.7	References	186
8.8	Unpublished data	190
8.8.1	Introduction	190
8.8.2	Results	190
8.8.3	Conclusions	194
Chapter 9 - Article 4: Rheology of microfibrillated cellulose (MFC) suspensions – influence of the degree of fibrillation and residual fibre content on flow and viscoelastic properties.....		
9.1	Foreword.....	195
9.2	Graphical abstract	196
9.3	Highlights	196
9.4	Abstract.....	196
9.4.1	Keywords	197
9.5	Introduction	197
9.6	Methods	200
9.6.1	Materials.....	200
9.6.2	Data presentation.....	202
9.6.3	Degree of fibrillation analysis	202
9.6.4	Rheological measurements.....	203

9.7	Results	206
9.7.1	Degree of fibrillation.....	206
9.7.2	Suspension particulate morphology hypothesis	207
9.7.3	Influence of DoF on static structure morphology	208
9.7.4	Influence of DoF on yielding behaviour	209
9.7.5	Influence of DoF on aggregation behaviour	212
9.7.6	Influence of component mix on high shear behaviour.....	216
9.8	Conclusions	217
9.8.1	Acknowledgements	220
9.9	References	220
9.10	Supplementary information	225
9.10.1	Width distribution analysis	225
9.10.2	Ternary diagrams	226
9.11	References	237
9.12	Unpublished data.....	237
Chapter 10	- Conclusions	247
10.1	Rheometer system and measurement protocol	247
10.2	Quantification of rheological data of MNFC suspensions	249
10.3	Influence of DoF on the rheological properties of MNFC suspensions.....	250
10.4	Perspectives	252
References	254

List of figures

Figure 2.1: Overview on commonly used characterisation methods for MNFC materials	23
Figure 2.2: Common drag and pressure flow geometries.....	31
Figure 2.3: Shear rate dependent viscosity curves	33
Figure 2.4: Time-dependent viscosity curves.....	34
Figure 3.1: Original DoE matrix proposal with targeted parameters and predefined conditions and an estimate of experiments needed.	51
Figure 4.1: Photograph of the feed material (eucalyptus pulp), medium fibrillated- and highly fibrillated MFC suspension.....	54
Figure 4.2: Photograph of the MKCA 6-2 Supermasscolloider used for the MFC manufacturing	56
Figure 4.3: Photograph of the homogeniser used to manufacture the H-MFC	58
Figure 4.4: Photograph of the used MCR 300 rheometer	59
Figure 4.5: Confocal laser scanning microscopy images of a smooth (left) and roughened (right) CC27 bob.	60
Figure 4.6: Storage (full circles) and loss modulus (hollow circles) data, as well as phase angle (full triangles) data of a frequency sweep experiment of a 1 wt% MFC suspension, measured with a CC27 geometry.....	62
Figure 4.7: Storage-(full circles) and loss modulus (hollow circles) data (top and bottom left graphs) and phase angle data (top right graph) of a 1 wt% H-MFC suspension, measured with a VS geometry.	64
Figure 4.8: Comparison of flow curves obtained by different measurement protocols	65
Figure 4.9: Stacked diagram of acquisition time and viscosity data in dependence of shear rate for a 1 wt% MFC suspension measured with the CC27 (left) and VS system (right).	67
Figure 4.10: Ternary diagram of the planned mixtures for each of the total suspension solids contents	70
Figure 4.11: Example ternary diagrams	71

Figure 4.12: Example ternary contour plots with simulated property data.	72
Figure 5.1: SEM images of freeze dried MNFC suspension.....	81
Figure 5.2: Flow curves of MNFC samples at different solids contents	83
Figure 5.3: Schematic of the proposed conformations at high and low shear rate for higher and lower solids contents.....	83
Figure 5.4: Amplitude sweep curves of MNFC samples	84
Figure 5.5: Flow curves of MNFC suspensions at different degrees of fibrillation.....	86
Figure 5.6: Schematic of the proposed conformations at high and low shear rate for greater and lesser degrees of fibrillation.....	87
Figure 5.7: Amplitude sweep curves of MNFC suspensions at different degrees of fibrillation.	88
Figure 5.8: Flow curves of MNFC suspensions at different pigment filler loadings....	89
Figure 5.9: Amplitude sweep curves of MNFC suspensions at different pigment filler loadings.....	90
Figure 5.10: Flow curves of MNFC suspensions at different CMC loadings.....	93
Figure 5.11: Amplitude sweep curves of MNFC suspensions at different CMC loadings.	94
Figure 5.12: Flow curves of MNFC suspensions containing zero, one or two additives (CMC and/or fGCC).	95
Figure 5.13: Amplitude sweep curves of MNFC suspensions containing zero, one or two additives (CMC and/or fGCC).....	96
Figure 5.14: Schematic of the proposed conformations for MNFC suspensions with and without CMC and/or pigment.	96
Figure 5.15: Flow curves of MNFC suspensions containing no and the two different PHCH filler pigments, PHCHa and PHCHb.	97
Figure 5.16: Amplitude sweep curves of MNFC suspensions containing no pigment additive versus the two different PHCH pigments.	98
Figure 7.1: Optical microscopy image of MFC suspension at 0.5 wt% (top left), and SEM images of freeze-dried aerogels from 0.5 wt% suspensions at increasing magnifications	121
Figure 7.2: Typical flow curve of an MFC suspension characterised in this work.....	125

Figure 7.3: Storage and loss modulus (G' , G'') data of a 1 wt% MFC suspension measured with the CC27 geometry.....	126
Figure 7.4: Viscoelastic properties in dependence of the suspension solids content for the different measurement systems	130
Figure 7.5: Phase angle (δ) as a function of the shear stress (τ)	131
Figure 7.6: Flow curves of a viscosity standard oil measured with the different measurement setups	132
Figure 7.7: Description of zone 1 of the flow curve.....	136
Figure 7.8: Description of zone 2 of the flow curve.....	139
Figure 7.9: Description of transition zone properties	141
Figure 7.10: Amplitude sweep data of the 0.5 wt% for the different investigated measurement setups.	148
Figure 7.11: Amplitude sweep data of the 1 wt% for the different investigated measurement setups.	149
Figure 7.12: Amplitude sweep data of the 2 wt% for the different investigated measurement setups.	150
Figure 7.13: Flow curves of the 0.5 wt% MFC suspension for the different investigated measurement setups.	151
Figure 7.14: Flow curves of the 1 wt% MFC suspension for the different investigated measurement setups.	151
Figure 7.15: Flow curves of the 2 wt% MFC suspension for the different investigated measurement setups.	152
Figure 7.16: Viscoelastic properties of the 1 wt% MFC suspension, measured with the CC27 and the VS system, as well as with mixed setups, i.e. CC27 bob with serrated cup and vane with CC27 cup.....	154
Figure 7.17: Viscoelastic properties of the 1 wt% MFC suspension, measured with the smooth and roughened CC27 system, as well as with mixed setups, i.e. smooth bob with roughened cup and roughened bob with smooth cup....	155
Figure 7.18: Flow curve properties of the 1 wt% MFC suspension, measured with the CC27 and the VS system, as well as with mixed setups, i.e. CC27 bob with serrated cup and vane with CC27 cup.....	156

Figure 7.19: Flow curve properties of the 1 wt% MFC suspension, measured with the smooth and roughened CC27 system, as well as with mixed setups, i.e. smooth bob with roughened cup and roughened bob with smooth cup....	157
Figure 7.20: Power law fitting parameters of zone 1 and 2 flow curve sections of the 1 wt% MFC suspension, including the standard error of the respective parameters as calculated by the fitting software.	157
Figure 8.1: Optical microscopy image of MFC suspension at 0.5 wt% (top left), and SEM images of freeze-dried aerogels from 0.5 wt% suspensions at increasing magnifications (top right), (bottom left) and (bottom right). ...	163
Figure 8.2: Typical flow curve of an MFC suspension characterised in this work, showing the positive (+) and negative (-) defined hystereses.	166
Figure 8.3: Flow curves of averaged data for 1 (circles), 1.5 (triangles) and 2 wt% (squares) MFC suspensions including standard deviations (error bars). ...	172
Figure 8.4: Box charts of absolute hysteresis data	174
Figure 8.5: Box charts of normalised hysteresis data.....	175
Figure 8.6: Box charts of relative hysteresis data	176
Figure 8.7: Comparison of positive (full symbols) and negative (hollow symbols) relative hysteresis data obtained by the regular method (H_{R+} and H_{R-}) and the simplified method (H_{RS+} and H_{RS-}).	177
Figure 8.8: Hysteresis positioning data	180
Figure 8.9: Comparison of positive normalised hysteresis and positive relative hysteresis data	182
Figure 8.10: Box plots of the flow curve properties of the 9 individually evaluated flow curves per dilution.	192
Figure 8.11: Box plots of the flow curve properties with non-continuous values.	193
Figure 9.1: Flow curve (a) and amplitude sweep (b) measurement data of a 1 wt% MFC suspension.	205
Figure 9.2: Optical (top) and SEM images (bottom) of the pulp (a), MFC (b) and H-MFC materials (c).	207
Figure 9.3: Storage modulus (G'_{\max}) data presented in ternary mixture contour plots	209

Figure 9.4: Yield stress determined from the amplitude sweep measurements using the phase angle approach	210
Figure 9.5: Limit of linearity (<i>LoL</i>) data.	211
Figure 9.6: Apparent low shear viscosity ($\eta_{0.02}$) data.....	212
Figure 9.7: Position of the local minimum data.	214
Figure 9.8: Positive hysteresis data	215
Figure 9.9: High shear viscosity (η_{100}) data	216
Figure 9.10: Flow index of zone 2 (n_2) data	217
Figure 9.11: Fibre/fibril width histograms of pulp (a), MFC (b) and H-MFC (c).....	226
Figure 9.12: Ternary mixture diagram including investigated mixture ratios at all solids contents (blue circles) and additional ratios at 1.5 wt% (red triangles)....	227
Figure 9.13: Visual guide for reading out the composition from a ternary mixture diagram (left) and a visual guide for a simplified, general read out of the composition trends (right).....	228
Figure 9.14: Example of colourmap contour ternary diagrams.....	229
Figure 9.15: G'_{\max} data with individual scale bars for the single dilutions	230
Figure 9.16: $\tau_{Y,\delta}$ data with individual scale bars for the single dilutions.....	231
Figure 9.17: <i>LoL</i> data with individual scale bars for the single dilutions.....	232
Figure 9.18: $\eta_{0.02}$ data with individual scale bars for the single dilutions.....	233
Figure 9.19: Position of the local minimum data with individual scale bars for the single dilutions.....	234
Figure 9.20: H_{RS+} data with individual scale bars for the single dilutions	235
Figure 9.21: η_{100} data with individual scale bars for the single dilutions.....	236
Figure 9.22: n_2 data with individual scale bars for the single dilutions	237
Figure 9.23: Loss modulus data with individual scale bars for the single dilutions	238
Figure 9.24: Phase angle data with individual scale bars for the single dilutions	239
Figure 9.25: K_1 data with individual scale bars for the single dilutions.....	240
Figure 9.26: n_1 data with individual scale bars for the single dilutions	241
Figure 9.27: End of zone 1 data with individual scale bars for the single dilutions.....	242
Figure 9.28: Start of zone 2 data with individual scale bars for the single dilutions	243

Figure 9.29: Relative transition zone depth data with individual scale bars for the single dilutions	244
Figure 9.30: Negative hysteresis data with individual scale bars for the single dilutions ..	245
Figure 9.31: K_2 data with individual scale bars for the single dilutions.....	246
Figure 10.1: Initial mind map on potential topics for this work.....	253

List of tables

Table 2.1:	List of commercialised MNFC products or MNFC production processes. ...8
Table 4.1:	Details of measurement system components used in this work.....61
Table 7.1:	Fitting function parameters of selected viscoelastic properties.131
Table 7.2:	Fitting function parameters of selected flow curve properties.....140
Table 8.1:	Statistical test decisions including the ANOVA test power and strength of effect for hysteresis data.178
Table 8.2:	Statistical test decisions for the hysteresis positioning data.181
Table 8.3:	Average values and standard deviations of flow curve properties of the 9 individually evaluated flow curves per dilution.....191
Table 8.4	Summary of the ANOVA test for the three triplicates within a dilution for the tested flow curve properties.194
Table 9.1:	Specific surface area data of the pulp, MFC and H-MFC materials, including the standard deviations for the MFC and H-MFC materials.....207

List of equations

$D = \frac{k_B T}{6\pi\eta r_H}$	Equation 2.1	28
$\kappa = \frac{R_i}{R_0}$	Equation 2.2	32
$\dot{\gamma} = \frac{\Omega \frac{R_0 + R_i}{2}}{R_0 - R_i}$	Equation 2.3	32
$\tau = \frac{M}{2\pi R_i^2 L}$	Equation 2.4	32
$\dot{\gamma} = \frac{\Omega}{\beta}$	Equation 2.5	32
$\tau = \frac{3M}{2\pi R^3}$	Equation 2.6	32
$\eta = \frac{\tau}{\dot{\gamma}}$	Equation 2.7	32
$\tan \delta = \frac{G''}{G'}$	Equation 2.8	35
$\delta = \tan^{-1} \frac{G''}{G'}$	Equation 2.9	35
$\eta = K\dot{\gamma}^{n-1}$	Equation 4.1	69
$\delta = \tan^{-1} \frac{G''}{G'}$	Equation 5.1	80
$\eta_i = K_i \dot{\gamma}^{n_i-1}$	Equation 7.1	123
$\tau = K\dot{\gamma}^n \quad \text{for} \quad \tau \gg \tau_0$	Equation 7.2	123
$\Delta_{\min} = \frac{\eta_{\min,th} - \eta_{\min}}{\eta_{\min,th}}$	Equation 7.3	124
$\eta_{\min,th} = K_{\text{int}} \dot{\gamma}_{\min}^{n_{\text{int}}-1}$	Equation 7.4	124
$n_{\text{int}} - 1 = \frac{\log(\eta_{100}/\eta_{0.02})}{\log(100/0.02)}$	Equation 7.5	124
$K_{\text{int}} = \frac{\eta_{0.02}}{0.02^{n_{\text{int}}-1}}$	Equation 7.6	124
$\delta = \tan^{-1} \left(\frac{G''}{G'} \right)$	Equation 7.7	127
$\dot{\gamma}_i = 0.01 \cdot 10^{(5/29)^{i-1}} \text{ s}^{-1}$	Equation 8.1	165
$H_{A+}^* = \frac{1}{2} \sum_i \left((\dot{\gamma}_{i+1} - \dot{\gamma}_i) (\eta_1(\dot{\gamma}_i) - \eta_2(\dot{\gamma}_i) + \eta_1(\dot{\gamma}_{i+1}) - \eta_2(\dot{\gamma}_{i+1})) \right) : \text{for } \dot{\gamma}_i < \dot{\gamma}_a$	Equation 8.2	166

$H_{A-}^* = \frac{1}{2} \left \sum_i \left((\dot{\gamma}_{i+1} - \dot{\gamma}_i) (\eta_1(\dot{\gamma}_i) - \eta_2(\dot{\gamma}_i) + \eta_1(\dot{\gamma}_{i+1}) - \eta_2(\dot{\gamma}_{i+1})) \right) \right : \text{for } \dot{\gamma}_{a+1} < \dot{\gamma}_i < \dot{\gamma}_b$	Equation 8.3	166
$H_{A+}^{**} = \frac{\eta_1(\dot{\gamma}_a) - \eta_2(\dot{\gamma}_a)}{2} \cdot h$	Equation 8.4	167
$H_{A-}^{**} = \left \frac{\eta_1(\dot{\gamma}_{a+1}) - \eta_2(\dot{\gamma}_{a+1})}{2} \cdot ((\dot{\gamma}_{a+1} - \dot{\gamma}_a) - h) \right $	Equation 8.5	167
$h = \frac{(\dot{\gamma}_{a+1} - \dot{\gamma}_a) (\eta_1(\dot{\gamma}_a) - \eta_2(\dot{\gamma}_a))}{(\eta_1(\dot{\gamma}_a) - \eta_2(\dot{\gamma}_a)) + (\eta_2(\dot{\gamma}_{a+1}) - \eta_1(\dot{\gamma}_{a+1}))}$	Equation 8.6	167
$H_{A+} = H_{A+}^* + H_{A+}^{**}$	Equation 8.7	167
$H_{A-} = H_{A-}^* + H_{A-}^{**}$	Equation 8.8	167
$H_{N+}^* = 2 \sum_i \left(\frac{(\dot{\gamma}_{i+1} - \dot{\gamma}_i) (\eta_1(\dot{\gamma}_i) - \eta_2(\dot{\gamma}_i) + \eta_1(\dot{\gamma}_{i+1}) - \eta_2(\dot{\gamma}_{i+1}))}{\eta_1(\dot{\gamma}_i) + \eta_2(\dot{\gamma}_i) + \eta_1(\dot{\gamma}_{i+1}) + \eta_2(\dot{\gamma}_{i+1})} \right) : \text{for } \dot{\gamma}_i < \dot{\gamma}_a$	Equation 8.9	167
$H_{N-}^* = 2 \left \sum_i \left(\frac{(\dot{\gamma}_{i+1} - \dot{\gamma}_i) (\eta_1(\dot{\gamma}_i) - \eta_2(\dot{\gamma}_i) + \eta_1(\dot{\gamma}_{i+1}) - \eta_2(\dot{\gamma}_{i+1}))}{\eta_1(\dot{\gamma}_i) + \eta_2(\dot{\gamma}_i) + \eta_1(\dot{\gamma}_{i+1}) + \eta_2(\dot{\gamma}_{i+1})} \right) \right : \text{for } \dot{\gamma}_{a+1} < \dot{\gamma}_i < \dot{\gamma}_b$	Equation 8.10	167
$H_{N+}^{**} = \frac{2H_{A+}^{**}}{\frac{\eta_1(\dot{\gamma}_a) + \eta_2(\dot{\gamma}_a)}{2} + \left(\eta_1(\dot{\gamma}_a) + h \frac{\eta_1(\dot{\gamma}_{a+1}) + \eta_1(\dot{\gamma}_a)}{\dot{\gamma}_{a+1} - \dot{\gamma}_a} \right)}$	Equation 8.11	168
$H_{N-}^{**} = \left \frac{2H_{A-}^{**}}{\frac{\eta_1(\dot{\gamma}_{a+1}) + \eta_2(\dot{\gamma}_{a+1})}{2} + \left(\eta_1(\dot{\gamma}_a) + h \frac{\eta_1(\dot{\gamma}_{a+1}) + \eta_1(\dot{\gamma}_a)}{\dot{\gamma}_{a+1} - \dot{\gamma}_a} \right) \right $	Equation 8.12	168
$H_{N+} = H_{N+}^* + H_{N+}^{**}$	Equation 8.13	168
$H_{N-} = H_{N-}^* + H_{N-}^{**}$	Equation 8.14	168
$H_{R+}^* = \frac{1}{2} \sum_i \left(\log \frac{\eta_1(\dot{\gamma}_i)}{\eta_2(\dot{\gamma}_i)} + \log \frac{\eta_1(\dot{\gamma}_{i+1})}{\eta_2(\dot{\gamma}_{i+1})} \right) : \text{for } \dot{\gamma}_i < \dot{\gamma}_a$	Equation 8.15	168
$H_{R-}^* = \frac{1}{2} \left \sum_i \left(\log \frac{\eta_1(\dot{\gamma}_i)}{\eta_2(\dot{\gamma}_i)} + \log \frac{\eta_1(\dot{\gamma}_{i+1})}{\eta_2(\dot{\gamma}_{i+1})} \right) \right : \text{for } \dot{\gamma}_{a+1} < \dot{\gamma}_i < \dot{\gamma}_b$	Equation 8.16	169
$H_{R+}^{**} = \frac{\log \frac{\eta_1(\dot{\gamma}_a)}{\eta_2(\dot{\gamma}_a)}}{2} \cdot \frac{\log \frac{\eta_1(\dot{\gamma}_a)}{\eta_2(\dot{\gamma}_a)}}{\log \frac{\eta_1(\dot{\gamma}_a)}{\eta_2(\dot{\gamma}_a)} - \log \frac{\eta_1(\dot{\gamma}_{a+1})}{\eta_2(\dot{\gamma}_{a+1})}}$	Equation 8.17	169
$H_{R-}^{**} = \frac{\log \frac{\eta_1(\dot{\gamma}_{a+1})}{\eta_2(\dot{\gamma}_{a+1})}}{2} \cdot \left(1 - \frac{\log \frac{\eta_1(\dot{\gamma}_a)}{\eta_2(\dot{\gamma}_a)}}{\log \frac{\eta_1(\dot{\gamma}_a)}{\eta_2(\dot{\gamma}_a)} - \log \frac{\eta_1(\dot{\gamma}_{a+1})}{\eta_2(\dot{\gamma}_{a+1})}} \right)$	Equation 8.18	169
$H_{R+} = H_{R+}^* + H_{R+}^{**}$	Equation 8.19	169
$H_{R-} = H_{R-}^* + H_{R-}^{**}$	Equation 8.20	169
$H_{RS+} = \sum_i \left(\log \frac{\eta_1(\dot{\gamma}_i)}{\eta_2(\dot{\gamma}_i)} \right) : \text{for } \dot{\gamma}_i \leq \dot{\gamma}_a$	Equation 8.21	169
$H_{RS-} = \left \sum_i \left(\log \frac{\eta_1(\dot{\gamma}_i)}{\eta_2(\dot{\gamma}_i)} \right) \right : \text{for } \dot{\gamma}_{a+1} < \dot{\gamma}_i < \dot{\gamma}_b$	Equation 8.22	169

List of abbreviations

AFM	Atomic force microscopy
ANOVA	Analysis of variance
BC	Bacterial cellulose
BET	Brunauer–Emmett–Teller
CMC	Carboxymethyl cellulose
CPAM	Cationic poly acrylamide
CS	Cationic starch
CTE	Coefficient of thermal expansion
δ	Phase angle
Δ_{\min}	Relative transition zone depths
DLS	Dynamic light scattering
DoE	Design of experiments
DoF	Degree of fibrillation
EDL	Electrical double layer
ESD	Equivalent sphere diameter
G'	Storage modulus
G''	Loss modulus
$\dot{\gamma}$	Shear rate
η	Viscosity
GCC	Ground calcium carbonate
H-MNFC	High degree of fibrillation MNFC
IMC	Immobilisation cell
K	Consistency coefficient
L-MNFC	Low degree of fibrillation MNFC
LoL	Limit of linearity
LVE	Linear viscoelastic
MFC	Microfibrillated cellulose
MNFC	Micro-nano-fibrillated cellulose
n	Flow index

NCC.....	Nanocrystalline cellulose
NFC	Nanofibrillated cellulose
PCC	Precipitated calcium carbonate
PE	Poly ethylene
PEO	Poly ethylene oxide
PHCH	Pigment hydrocolloid hybrid
PLA	Poly lactic acid
PSD.....	Particle size distribution
r^2	Coefficient of determination
s.c.....	Solids content
SEM.....	Scanning electron microscopy
τ	Shear stress
τ_y	Yield stress
$\tan\delta$	Loss factor
TEM	Transmission electron microscopy
TEMPO	2,2,6,6-tetramethylpiperidine-1-oxyl
TMP.....	Thermo mechanical pulp
UQTR.....	University of Quebec in Trois-Rivières
UV/VIS.....	Ultraviolet-visible spectroscopy
wt%.....	Weight percent
ζ potential	Zeta potential

Chapter 1 - Introduction

1.1 Nomenclature

Please note that the term micro nanofibrillated cellulose (MNFC) is used to describe the material that was investigated in this study. In the early work when the terminology was still evolving (Chapter 5 - and Chapter 6 -), other notations were used as well for the same material (micro and nanofibrillated cellulose, micro-nano-fibrillated cellulose). For being more consistent with the currently used terms in this field, the term microfibrillated cellulose (MFC) is sometimes also used in this work (especially in later publications), again describing the same material. *Nanocellulose* is used as a collective term for different types of micrometre and nanometre sized cellulose materials. An overview on the different classes of cellulose materials, as well as an extensive discussion of the terms MNFC and MFC is given in section 2.1.2.4.

1.2 Context

Following recent announcements in the field of nanocelluloses made by research institutes and industrial companies, one can see that up-scaling of certain production processes is occurring and full scale operation is imminent or already up and running (Archambault and Hamel 2014; Gerrer 2014; Svending 2014). In addition, one can also see a trend going more in the direction of “cost-efficient” grades of MNFCs, especially for large volume applications like, for example, paper based packaging materials. The term “cost-efficient” in the case of MNFC grade typically means that extensive chemical or biological treatments are excluded from the mainly mechanical production process. As a result, these grades may most probably have a significantly broader distribution of their intrinsic size scales. This is mainly caused by the presence of residual and not or only partially fibrillated fibres or fibril aggregates.

One example of such a cost-efficient MNFC material is produced in the presence of mineral filler, therefore finally leading to a filler containing, namely “pigmented”, MNFC product (Schenker and Gane 2012; Svending 2014; Svending et al. 2016). On the one hand, the coprocessing of filler can positively influence the mechanical breakdown of pulp, but on the other hand, it also leads to an improved performance in some applications

when compared to a similar MNFC material that was initially processed without filler but with separately post-added filler (Schenker and Gane 2012; Schenker and Gane 2013; Schenker et al. 2015).

Whereas the up-scaling of the production process of MNFC products is on-going, it seems that only little progress is made when it comes to the up-scaling and/or commercialisation of potential MNFC applications. The one major application that was shown to be up-scalable is the use of MNFC as a wet and dry strength additive for certain paper grades which has been demonstrated in both pilot and full production scale (Svending 2014). However, as for most of the strength additive concepts, a major issue is the loss of bulk and, related to it, the typical loss of bending stiffness as macroscopic long fibres are replaced by the micro structures of MNFC. In addition, there are already several, well working concepts on the market being able to solve the same issue for which the MNFC-concept is competing, e.g. achieving higher filler load.

On the other hand, an alternative, very promising way of using MNFC in paper production was recently presented, in laboratory scale, but also with the announcement of successful trials in pilot scale (Charfeddine et al. 2014; Svending et al. 2016). In laboratory scale, a dynamic sheet former was used whereas in pilot scale the MNFC suspension was applied on-line in a wet-on-wet and wet-on-partially dewatered configuration on a paper machine forming a TMP base sheet by a Hydra-Sizer™ (Charfeddine et al. 2014) or on a unbleached Kraft base (Svending et al. 2016). It was shown that even a single side coating with low application weight is enough to maintain, or even increase, the bending stiffness compared to an uncoated reference paper having the same total weight, contrary to the experience, mentioned above, of adding the MNFC simply in bulk to the paper mass.

In the previous example, as the MNFC is applied during curtain coating as a dilute suspension through a narrow slit at relatively high rate, and furthermore onto a fast-moving substrate, the suspension is subjected to regions of high shear rate, extensional flow, and rapid changes of flow direction during the application process. Consequently, the rheological behaviour of such MNFC suspensions becomes a crucial issue, especially upon scale-up where even higher shear rates are to be expected. Additionally, the MNFC undergoes compound dewatering during the formation and drying of the sheet (Dimic-Misic et al. 2013c).

In addition to the well-known tendency for MNFC suspensions to exhibit a shear thinning behaviour, lately more work is published where an “irregular” rheological behaviour of such suspensions is observed at elevated shear rates (Roussière et al. 2014). Several hypotheses were proposed to explain these effects, however not yet fully supported by appropriate experimental confirmatory data. Furthermore, it was also shown that the rheological behaviour can be changed by the introduction of poly-electrolytes, or generally by changing the electrolytic conditions (Dimic-Misic et al. 2013a; Roussière et al. 2014; Sim 2014). In systems where additional materials, such as pigments and/or coating colour components, e.g. lattices, are present, the interactions, and consequently, the rheological behaviour is even more complex. For instance, there is evidence that in high consistency furnishes containing MNFC, the pigment particles, and eventual pulp fibres, are not bound to the MNFC-gel network but act more like inert particles enabling them to move relatively freely within the liquid water trapped in the strong gel network (Dimic-Misic et al. 2013b).

In order to be able to select an appropriate additive (polymer and/or pigment) to adjust an MNFC suspension rheology for a given application, or being able to predict the effect of the addition of MNFC to a given system, such as a coating colour (Dimic-Misic et al. 2013a), the specific interaction between the additive, the species present in the MNFC and eventually other species is needed. However, only few publications investigate complex (multi-component), MNFC based systems systematically in order to form hypotheses on interaction mechanisms within such systems.

Chapter 2 - Literature review

2.1 Cellulose

Cellulose is the most abundant organic polymer on earth (Klemm et al. 2005), and furthermore it is a bio-polymer that is produced by nature. Most of the cellulose is found in plants where it is a structural component of the primary cell wall providing dimensional stability of the cell wall and ultimately to the overall plant structure (Wagenführ and Scholz 2008). The following sections give an overview on the structure of cellulose in more detail, but also on different macroscopic types of cellulose that are manufactured from the raw material wood into technical grades.

2.1.1 Structure

Cellulose is a linear, high molecular weight polymer built up from β -D-glucose units that are linked via $\beta(1,4)$ bonds and belongs to the chemical group of poly saccharides. Cellulose of natural origin is organised in strongly bound bundles of cellulose polymers. The binding among the polymer chains happens via hydrogen bridges and is strong because one single β -D-glucose unit contains three hydroxyl groups. The hydrogen bridges on the one hand provide the stiffness of the cellulose molecules via intra-molecular interactions as well as the strong binding to other cellulose polymers via inter-molecular interactions. These bundles are called elementary fibrils, several of such elementary fibrils again bind together to form a micro fibril. The polymer chains within an elementary fibril can either be aligned (*i.e.* crystalline) respective to each other or randomly oriented. (*i.e.* amorphous) (Wagenführ and Scholz 2008). By the relative arrangement of the cellulose molecules in the crystal domains, cellulose can be further classified into different types. However, the topic will not be discussed further as the mechanical processes used in this work to process native wood cellulose into MNFC products do not change the crystalline morphology of the starting product; that is I_{β} for native cellulose in higher plants. It should be noted that in the following section the same terminology *Types* is used to describe the nano- and micro-scaled morphology, *i.e.* of higher hierarchical order than the morphology of the sole crystalline domains, and not to describe the difference in the crystalline morphology. The cellulose fibrils are found in

plants, providing mechanical stability as a rigid structure, together with other macromolecular compounds such as lignin, hemicellulose, and even proteins.

Depending of the source and the diminution procedure, different types of celluloses, not to be confused with the different allomorphs of cellulose, exist. The specific properties of those different types are further described in the next paragraph.

2.1.2 Types

Depending on how the cellulose polymer molecules are interacting and organised into larger entities, different types of celluloses with eventually significantly different properties occur. These different types are here briefly described.

2.1.2.1 Regenerated cellulose

Regenerated celluloses are produced by first dissolving pulp or another cellulose-containing source and then regenerating it by mixing with another liquid that is not a solvent for cellulose. The dissolution of cellulose can either be done directly using e.g. tetra-aminecopper-dihydroxide or carbon disulfide and a high alkalinity as in the viscose process, or indirectly, by first modifying the cellulose e.g. by nitration or acetylation to form a cellulose derivate that is soluble in other solvents. Those processed and products like viscose were already used around 1900. Recently, two new types of solvents for cellulose are investigated, namely ionic solvents and deep eutectic solvents (Francisco et al. 2012; Kosan et al. 2008).

Depending on the regeneration process, films, foils, compacts or fine fibres are produced. Fibre morphology, e.g. length, thickness, shape, etc. is being influenced by the process parameters. A drawback of the regeneration process is that the solvent for cellulose typically cannot be completely removed from the regenerated cellulose material, especially in the case of traditional solvents (Zhang et al. 2005).

2.1.2.2 Bacterial cellulose (BC)

In contrast to the other types of celluloses, bacterial cellulose is not produced via breaking down pulp fibres, or other cellulose sources, but is synthesised by bacteria (*Acetobacter* species). The cellulose fibrils have diameters typically below 100 nm at a very narrow

diameter distribution and are typically long compared to mechanically fibrillated fibrils (Iwamoto et al. 2005; Moon et al. 2011).

2.1.2.3 Nano crystalline cellulose (NCC)

By subjecting cellulose to strong acid treatment, such as sulfuric acid, the cellulose polymer is hydrolysed. As the amorphous parts of the fibrils are more accessible than the crystalline parts, the hydrolysis is faster in these regions. By adjusting the process conditions (acidity, time, etc.), it is possible to retain the crystalline residues. In contrast bacterial-, fibrillated and regenerated- in the case of spun fibres - cellulose that have a “string”-like morphology; i.e. a one very large dimension compared to the two other ones, the NCC entities are platelet- or whisker shaped. As indicated by the denomination, these particles are crystalline and in the low nanometre range (Moon et al. 2011).

2.1.2.4 Micro nanofibrillated cellulose (MNFC)

In literature, the terms for fibrillated cellulose types are not as well defined as e.g. bacterial cellulose that refers to the origin or nano crystalline cellulose that refers to the particle morphology. Especially the term *micro* in micro fibrillated cellulose (MFC) might be eventually misleading as these fibrils too may be in the <100 nm range. It is suggested by some authors, for example by Moon et al. (Moon et al. 2011), that the differentiation characteristic between nanofibrillated cellulose (NFC) and MFC is mainly the manufacturing process. Whereas MFC is typically obtained by purely mechanically disintegrating pulp, NFC manufacturing involves a pre-treatment like an oxidation, a grafting or an enzymatic treatment. The pre-treatment is on one hand used to reduce the amount of energy used in the mechanical fibrillation process step, and on the other hand leads to a decreased fibril size compared to MFC fibrils.

In contrast to the described terminology by Moon et al. (Moon et al. 2011), the term MNFC is used in this work to represent micro nanofibrillated cellulose, i.e. a product with a significant level of microscopic fibres, including a micro fraction, which have nanofibrils formed on their surface by a high energy fibrillation process, as well as individualised nanofibrils. Effectively, it can be considered as a collective term for MFC and NFC materials, as most, mainly mechanically fibrillated MFCs and NFCs having both, micro- and nano-sized fibre/fibril fractions (Herrick et al. 1983; Roussi re et al.

2014). According to Moon et al. (Moon et al. 2011), an MNFC product would fall under the term MFC. However, due to the fact that very fine fibrils in the very low nm-range are also present in such products (individualised and on the surface of microfibrils), the term might be misleading. Therefore, it is here proposed that the term MNFC is more appropriate for fibrillated cellulose materials that do contain micro- as well as nano-sized features. Furthermore, it is suggested here to use the term NFC exclusively for products that contain fibrils solely in the low nm range, e.g. < 100 nm. This is well in line with the proposal of Kangas et al. (Kangas et al. 2014), yet they promote to use the term MFC rather than MNFC for materials that contain also coarser fibrils and/or fibres.

In short, MNFC is likely a more accurate term to describe a mechanically fibrillated cellulose material, because of its naturally broad fibril width distribution ranging from the nanometre to the micrometre scale. Furthermore, it is also very likely to have nanofibrillation on micrometre sized fibrils present in addition to individualised nanometre fibrils. So, materials named MFC and NFC in the literature can very likely named MNFC as well, unless they are fractionated and/or strongly chemically modified. The next section will have a focused look on the manufacturing, the properties and potential fields of applications only for MNFC products as this work is will be limited to this type of cellulose.

2.2 MNFC

This section describes the manufacturing, the intrinsic properties as well as the properties of MNFC in suspension, and potential applications of this material. The following sections focus on fibrillated cellulose qualities and do not discuss NCC or BC.

2.2.1 Manufacturing

In recent years, many companies and institutes invested in the upscaling of MNFC manufacturing processes and the process optimisation to be able to deliver a cost-effective product. Up to date (2015), there are several commercial technologies and accordingly products available as seen in Table 2.1. However, there are many more pilot- and/or pre-commercial systems in planning or already running (Bio-fibre 2015; Laurinsilta 2013; PaperMoney 2011; RISI 2014) that are just not yet commercial.

Table 2.1: List of commercialised MNFC products or MNFC production processes.

Company / Institute	Name	Type	Scale	Source
Imerys	FiberLean	MNFC	Onsite (several 1 000 dmt/a) Offsite	(Svending 2014)
American process	Bioplus	NFC / NCC	Demonstration plant	(Naderi 2014)
FP Innovations / Kruger	Cellulose Filaments	MNFC	5 t/d	(Kruger 2013)
GL&V UMaine	CNF	MNFC	Onsite	(Gerrer 2014)
Daicel	Celish	MNFC	Unknown	(Barnes 2000)

2.2.1.1 Mechanical process

As already known for a long time from papermaking, wood can be processed into pulp by mechanical action. If sufficient amounts of energy are introduced, pulp fibres can be released from wood, cut or fibrillated as represented by fibrils or fibril bundles that are partially or completely liberated from the fibre. Specialised equipment like stone grinders and refiners exists to break down wood into pulp fibres used for papermaking. These pieces of equipment are optimised to end up with suitable fibres for papermaking that typically have a diameter in the range of some tens of micrometres. To obtain MNFC, the processes have to be carried on further, until more fibres are broken down into fibrils. Typically, the technologies used to produce pulp fibres are not able to apply enough force to the fibres in order to carry on the fibrillation action, or lead to fibre cutting or other detrimental effects. Therefore, other processes or modification of existing technologies are necessary.

Homogenising

The firsts to describe such a new process were Turbak, Snyder and Sandberg in 1983 (Turbak et al. 1983). They used a homogeniser to convert different pulp grades into MFC within 12 passes at a pressure drop of 55 MPa. As described by Ankerfors (Ankerfors 2012), such purely mechanical processes typically are energy intensive, typically in the area of some tens of MWh per ton of cellulose. As a consequence, many researchers investigated and work in the field is still on-going, to find suitable pre-treatments of the pulp fibres or more energy efficient processes (see sections 2.2.1.2, 2.2.1.3, 2.2.1.4 and 2.2.1.5).

As mentioned above, homogenisers and micro-fluidisers are typical devices used for the production of MNFC products. Such machines typically consist of a pump that is able to produce high pressures (some 10 up to 200 MPa) and an according high pressure zone. The design of the zones then varies between the different models, but generally introduces high shear forces due to fast flow velocities (shear rates), high and fast pressure changes (drops) and eventually related secondary effects as for instance cavitation. These forces are then partially isolating the cellulose fibrils. The maximal processable consistency for such devices in laboratory scale is typically low, around 1 wt%. Intense pre-treatments are needed (Zimmermann et al. 2010), as the device's size demands small orifices and/or channels which would otherwise tend to clog.

Grinding

Another process that is often used to manufacture MNFC products is grinding, especially using an ultrafine friction grinder such as the Supermasscolloider of Masuko Sangyo Co., LTD. The suspension is forced between a fixed and a turning grinding stone in order to introduce high shear forces into the suspension, leading to a fibrillation of the pulp fibres. The three main parameters that influence the fibrillation process are the revolution speed of the turning stone, the clearance between the grinding stones, respectively the pressure on the stones when they are operated in contact mode, and the number of passes. Depending on the desired product and the feed material composition, different parameter sets are used by different groups. Whereas the revolution speed is typically around 1500 rpm (Josset et al. 2014; Kangas et al. 2014; Nogi et al. 2009; Suopajärvi et al. 2010), the stone clearance (Subramanian et al. 2008), respectively the pressure on the stones can be

very different (Josset et al. 2014; Suopajarvi et al. 2010) or is sometimes not described at all (Kangas et al. 2014; Nogi et al. 2009). All necessary parameters to fully understand the operating conditions are rarely given in a publication, making a reproduction difficult. The maximal pulp consistency that can be processed is typically higher, around 1.5 to 3 wt%, compared to the ones common in the homogenising processes.

Refining

A related process is proposed by GL&V, but also others, where a refiner with specially designed refiner discs is used to manufacture MNFC, described as NFC although the product appears to be rather coarse (Gerrer 2014). As an especially designed anti-clash system is mentioned in the presentation, it is very likely that the refiner operates at a very small gap compared to classical refining in order to be able to generate high enough forces to fibrillate pulp to the desired level of fineness.

Ultra-sonication

Another method that is able to break down fibres, however, only rarely described, is ultra-sonication. For instance Chen et al. (Chen et al. 2011) describe the use of a small laboratory ultrasonic generator to produce a NFC at high enough ultrasonic power outputs ($> 1000 \text{ W}$). However, if the specific energy input on final dry cellulose matter is calculated from the provided experimental data, values as high as 1 GWh t^{-1} are obtained. Of course, up-scaled systems may have a better efficiency and therefore the specific energy input may be smaller for larger systems, but still, the described energy levels are exorbitant. As a comparison, the net power output of modern nuclear reactors is in the area of 1 GW . Equipment that combines ultra-sonication with mechanical disintegration (shear forces) - e.g. the mechanical ultrasonic dispergator (ZRI) described by Suopajarvi et al. (Suopajarvi et al. 2010) is also used. The specific energy input levels are then drastically reduced, between 10 and 16 MWh t^{-1} . However, the obtained material is an MNFC type, rather than a true NFC. The two previous examples clearly illustrate two points. First, it seems that purely mechanical disintegration is too inefficient when it comes to the production of NFC material, but may be suitable for MNFC materials. Second, eventually the combination of different mechanical disintegration methods, either applied in series or in parallel, is the most efficient solution as the different processes have their highest efficiencies at different stages of fibrillation and/or degrees of fibrillation.

Cryo-crushing

Another, very rarely used method, is cryo-crushing, where moist cellulose is frozen in liquid nitrogen and then crushed mechanically. However, it appears that this method has its limitations as it is typically coupled with other, suspension based mechanical disintegration processes (Ayse and Sain 2008; Jonoobi et al. 2009).

2.2.1.2 Co-processing of pigment particles

As described by Schenker and Gane (Schenker and Gane 2012), pigment particles, namely calcium carbonate, was added to the feed pulp suspension in order to ease the grinding and homogenising processes. Furthermore, Gane et al. described that the fibrillation efficiency was increased by the presence of the pigment particles (Gane et al. 2012a; Gane et al. 2012b). Recently, the commercial launch of such a product, explicitly MFC produced in the presence of filler, was announced (Svending 2014). In both cases, additional beneficial effects of co-processing pigment particles are seen in later applications. The products obtained by such pigment particle co-processing belong to the MNFC type of products, meaning that the products do contain features with diameters in the μm -range as well as in the nm-range (Roussière et al. 2014; Schenker and Gane 2012). The specific effect(s) of the pigment particles on the fibrillation process are not yet fully understood nor described, but they might be attributed eventually to localised increase of pH and a better transduction of mechanical energy. Increase in locally available energy may either be due to because the pigment particles themselves acting as grinding medium and/or indirectly via changing the rheological properties of the processed suspension.

2.2.1.3 Chemical processes

Chemical processes used for the manufacturing of nano crystalline cellulose like extensive acid hydrolysis (Elazzouzi-Hafraoui et al. 2008) will not be described here as such treatments typically are too aggressive to retain the fibrillar structure of NFC. However, the TEMPO (2,2,6,6-tetramethylpiperidine-1-oxyl) radical-mediated oxidation is able to partly retain some fibril length under the right conditions. The resulting fibrils have diameters in the 3 to 5 nm range but length still in the micrometre range and are typically and selectively grafted with carboxylate groups (Isogai et al. 2011). Typically, the TEMPO treated cellulose suspension is subjected to an additional mechanical

disintegration step in order to completely individualise the nanofibrils (Isogai et al. 2011; Saito et al. 2006). However, as the TEMPO treatment separates the fibrils or weakens the inter-fibril bonding quite intensely, only very little mechanical input is needed (Saito et al. 2006).

Typically, pre-treatments, especially the TEMPO-treatment, are employed when NFC-type of products are targeted. On the one hand, such fine products cannot simply be obtained by pure mechanical processes, but on the other hand, such processes are rather extensive and therefore typically induce an increase a final product price. The latter case only can be justified by a “higher value” that would come from an NFC-type of product compared to an MNFC-type product.

2.2.1.4 Enzymatic process

An alternative to the TEMPO pre-treatment are enzymatic treatments. In contrast to chemical reactions, enzymes are typically more specific and selective in their reactions. Under the right conditions, it is possible to produce fibrils without too much a shortening as described e.g. by Henriksson et al. (Henriksson et al. 2007) and Pääkkö et al. (Pääkkö et al. 2007). However, as the enzymes typically used are endoglucanases (types of cellulases), a too extensive treatment will lead to a complete depolymerisation of the cellulose into glucose sugars. Both authors report that by using an enzymatic pre-treatment and further mechanical disintegration steps enable the pulp feed material to be manufactured into MNFC fibrils, with width around 15 to 50 nm, and true NFC fibrils, around 5 nm. Yet no indication is given about any potential residual fibre content.

Ankerfors (Ankerfors 2012) provides some calculations on the potential savings of mechanical energy input of an enzymatic pre-treatment compared to a pure mechanical fibrillation in a homogeniser. Yet, what is missing, and is also missing in other literature where the energy savings due to enzymatic pre-treatments are discussed, is the calculation of the additional costs due to the additional process steps, and eventual capacity limitations, and related extra capital investments, due to a comparatively long residence time in the bio-reactor.

As for the chemical pre-treatments, the targeted final product is more in the area of an NFC rather an MFC. However, recently an alternative, high consistency process involving

an enzymatic treatment was presented to produce rather coarse MNFC with a very efficient process called HefCel (Qvintus 2015).

2.2.1.5 Modifications

Chemical modifications of cellulose are often used in order to change the cellulose's functionality, like adding hydrophobic groups making the cellulose overall hydrophobic or improving the water re-dispersibility after drying by carboxymethylation (Eyholzer 2010). But besides the added functionality, the carboxymethylation helps do decrease the mechanical energy demand in the mechanical diminution step (Ankerfors 2012). An indication that the presence of carboxymethyl cellulose compared to the chemical grafting of carboxymethyl groups on cellulose is enough to reduce the mechanical energy demand as given by Cheng et al. (Cheng et al. 2013).

2.2.1.6 Conclusions

If fine products like NFC have to be produced, a pre-treatment is a necessary step in order not to end up with unrealistic energy consumption values. However, if a more MFC – or as previously proposed, the wording MNFC - type of product is targeted, then purely mechanical processes are suitable. Finally, these mechanical processes can be further optimised by eventually combining different technologies (Iwamoto et al. 2005) and/or by the addition of grinding and/or process aids like pigment particles (Schenker and Gane 2013; Svending 2014) and/or by using carboxymethyl cellulose (Cheng et al. 2013).

2.2.2 General properties

The following section presents the properties of MNFC in suspension and in a condensed, dry form. Some of the properties will be further detailed when discussing rheological properties of MNFC suspensions (Section 2.5).

2.2.2.1 MNFC suspensions

Cellulose molecules contain a large amount of hydroxyl groups which strongly interact with water molecules via the formation of hydrogen bonds. Even though some of the hydroxyl groups form inter-molecular hydrogen bonds with other cellulose molecules within a fibril and among other fibrils, the interaction of cellulose parts in MNFC with

water remains strong. Such strong interaction is reflected in a high water retention value, whereas for highly fibrillated grades, the water retention measurement procedure needs to be modified in order to provide meaningful results (Dimic-Misic et al. 2013c).

The strong interaction is also reflected in the rheological behaviour of MNFC suspensions. Indeed, even at high dilution levels, the MNFC suspensions exhibit non-Newtonian characteristics (Iotti et al. 2011). As rheology is used as one of the main characterisation tool in present work, a more in-depth discussion is later provided.

MNFC suspensions typically appear turbid as some features are still in the μm -range and therefore scatter light. As for other grades as NFC and NCC when such coarse μm -sized residues are missing and when only nm-sized features remain, the suspensions become clear, translucent. Within a fixed, pigment particle free system, the dependence of the light scattering on the cellulose feature size can be used to indirectly assess a MNFC suspensions degree of fibrillation as proposed by Chinga-Carrasco (Chinga-Carrasco 2013).

Another property that is typically measured when an MNFC suspension or MNFC material is assessed is charge, either as surface charge (Fall et al. 2011; Fardim et al. 2002; Liimatainen et al. 2009) or as ζ -potential (Dimic-Misic et al. 2014; Eronen et al. 2011; Fall et al. 2011; Liimatainen et al. 2009) which also indirectly indicates the degree of fibrillation. Yet, both methods are prone to produce misleading, even wrong, absolute numbers. Indeed, pulps also contain residuals like hemicellulose or lignin which most probably also contribute to the total charge that is determined, e.g. by titration methods. So, the comparison of MNFCs originating from different pulp sources remains very critical. Furthermore, the measurement of the ζ -potential on MNFC, or fibrous materials in general, is critical, as already indicated not only by providing different absolute values, but as they depend on the applied measurement technique (El-Gholabzouri et al. 1999). Yet, charge measurements may still be a good relative comparison parameter within a fixed recipe in order to monitor the evolution of the degree of fibrillation within a given manufacturing process; i.e. all other parameters remaining constant. This issue is further developed in sections 2.4.2.1 and 2.4.2.2.

2.2.2.2 Dry MNFC

MNFC can be manufactured in dry form in different materials or workpieces using different techniques, probably having different properties. Here, the focus is placed on

intrinsic material properties, independently of the final form or the manufacturing process. Therefore, the properties presented below were measured on MNFC films or bars, where one assumes the material exhibits the physics of continuously condensed matter. Specific application properties are presented in the respective following sections 2.2.3.1 to 2.3. Nevertheless, a direct comparison of published values for mechanical- and other properties is difficult as the manufacturing method, and the respective parameters, to obtain a condensed MNFC material influence the final properties as for instance shown by Yang et al. (Yang et al. 2012).

Depending on the pulp source and the degree of fibrillation, elastic moduli of MNFC in the range of 8 to 11 GPa (Josset et al. 2014; Österberg et al. 2013; Schenker and Gane 2013; Schenker et al. 2015; Spence et al. 2010) are typically reported, but values as high as 17 GPa have been found (Syverud and Stenius 2009b). Within a publication, tensile strength typically follows the same trend as the elastic modulus, with higher modulus materials presenting higher tensile strength (Österberg et al. 2013). However, the tensile strength, as also elastic modulus values, vary significantly among different publications. This indicates that the tensile strength might be more sensitive to the drying and consolidation process than the elastic modulus, or that the material is not fully consolidated in all examples. Typical values of the tensile strength are found ranging from 60 to 250 MPa (Josset et al. 2014; Österberg et al. 2013; Schenker and Gane 2013; Schenker et al. 2015; Spence et al. 2010; Syverud and Stenius 2009b; Yang et al. 2012). As a comparison, values for crystalline cellulose can be as high as 138 GPa (Nishino et al. 1995) but one can surmise that with better consolidation MNFC-based materials would increase beyond 17 GPa while still remaining below the maximum for crystalline cellulose (Nishino et al. 1995).

For certain applications, another very interesting property is the low coefficient of thermal expansion (CTE) of cellulose that is reported to be as low as 10^{-7} K^{-1} (Nishino et al. 2004). Depending on the used MNFC base-material, the MNFC-film manufacturing method and the used characterisation method for barrier, e.g. air, oxygen and oil, properties, the absolute values may differ (Aulin et al. 2010; Lavoine et al. 2012; Österberg et al. 2013; Syverud and Stenius 2009b; Yang et al. 2012). However, the common findings are that MNFC films, or MNFC layers (see chapter 2.2.3.3), have a very good oxygen barrier

property, i.e. low oxygen transmission rate, and therefore a good air barrier, i.e. low air permeability, at low relative humidity values. In fact, the oxygen permeability of MNFC films at low moisture contents is as low or even lower than technical polymers that are currently in use as oxygen barrier layers (Lavoine et al. 2012). Unfortunately, the MNFC films have a relatively high water vapour permeability (Lavoine et al. 2012) inducing a significantly increased oxygen permeability at increased relative humidity conditions (Aulin et al. 2010), as explained by the uptake of water vapour into the MNFC material. The intrinsic oil/grease barrier properties of MNFC is not described in literature. Only few publications exist where the property was measured on MNFC coated substrates (see chapter 2.2.3.3).

2.2.3 Applications and uses for MNFC

The following sections present the potential applications of MNFC that are currently investigated by research groups, institutes and companies. In addition, there are already few niche applications of MNFC (or NCC/BC) that are commercialised, for instance as food additive (E 460 (Wikipedia 2015)), but they will not be discussed here.

2.2.3.1 Additive in paper making

An extensively investigated application of MNFC is the use as a wet and/or dry strength additive to paper products (Eriksen et al. 2008; Gonzalez et al. 2012; Hii et al. 2012; Sehaqui et al. 2011; Svending 2014; Taipale et al. 2010). Typically, the loss of mainly mechanical properties because of increased filler content is compensated by the addition of MNFC to the paper composition. As bulky pulp fibres are replaced by small, mobile and “condensable” fibrils of the MNFC, the density inherently is increased. The effect is even more pronounced when additional pigment filler is introduced into the sheet as the MNFC is added to enable a higher filler content in the paper. Typically, this leads to a decrease in bending stiffness (Schenker and Gane 2012), even though elastic modulus, internal bond and tensile index are typically increased. A further consequence of the fine, film forming, fibrils is that inter-fibre pores become smaller or blocked and so the air permeability is reduced (Eriksen et al. 2008; Rantanen and Maloney 2013). Due to the more closed and densified structure, but also the stronger water binding of MNFC

compared to conventional pulp, dewatering time is typically also increased by the addition of MNFC to a paper composition (Hii et al. 2012; Rantanen and Maloney 2013).

Even though there is a substantial amount of academic research on MNFC as a wet and/or dry strength bulk-additive in paper-related applications, so far only one commercially available full scale technology has been reported (Svending 2014). However, by investigating the intrinsic mechanical properties of MNFC, the price structure of paper, and other available market solutions for increasing filler addition levels in paper, it is questionable whether the wet-end addition of MNFC is a meaningful economical application for such products.

2.2.3.2 MNFC films

Free standing films composed mainly of MNFC are usually produced in order to measure intrinsic properties, i.e. mechanical- and barrier, eventually printing-properties of the MNFC material and combinations (Henriksson et al. 2008; Österberg et al. 2013; Spence et al. 2010; Syverud and Stenius 2009a). Sometimes, the MNFC, or typically NFC, films are further used as a component in a composite material (Iwamoto et al. 2005) (see also Section 2.2.3.4). A commonly used method to manufacture MNFC films is solvent casting whereas the “solvent” is the MNFC suspension water. The typically diluted MNFC suspension at solids content < 0.5 wt% is poured in a Petri dish and the water is evaporated under mild conditions ($T < 50$ °C, eventually increased relative humidity) (Spence et al. 2010; Wu et al. 2012). Another commonly used method is vacuum or pressure filtration of diluted MNFC suspensions, followed by hot-pressing (Henriksson et al. 2008; Österberg et al. 2013; Sehaqui et al. 2011) or drying at ambient (Syverud and Stenius 2009a) or in controlled conditions (Iwamoto et al. 2005; Syverud et al. 2011). Typically, dilution of MNFC suspensions is necessary to have a good levelling to manufacture homogeneous thin films. At higher consistencies, the viscosity is too high, and the suspensions behave elastically. Such a procedure normally leads to significant shrinkage that induces stresses in the drying structure that ultimately leads to wrinkling or wrapping of the film. In order to control that, the drying in controlled conditions, and application of hot-pressing are preferred.

Potential applications of pure MNFC films mainly pertain to the field of printed electronics (Penttilä et al. 2013), flexible displays (Shimaoka 2015), as separator and/or

electrode base material (Kaukonen et al. 2015; Lee 2015) or even as potential oxygen barrier layers (Ho et al. 2012; Österberg et al. 2013; Syverud and Stenius 2009b; Wu et al. 2012).

The above presented MNFC film manufacturing processes work well at the small scale, but are yet unsuitable for continuous, larger scale applications. However, a continuous pilot scale process has been developed to produce MNFC films (Peresin 2013; Tammelin et al. 2013).

2.2.3.3 MNFC coatings

As pointed out by Lavoine et al. (Lavoine et al. 2012), few publications can be found on MNFC as a coating material before 2010. Recently more activity in this area can be observed. MNFC is investigated as additive in coating colour formulations as binder and or rheology modifier (Dimic-Misic et al. 2013a; Dimic-Misic et al. 2014), as pure coating (Lavoine et al. 2014; Ridgway and Gane 2011) or as pigmented, i.e. filler containing, composition (Charfeddine et al. 2014; Schenker and Gane 2012). These coatings are typically applied onto a paper substrate. Some publications indicate the possibility of using other substrates as MNFC tends to bind to certain polyolefinic plastics: MNFC films formed in polycarbonate Petri dishes could not be removed (Spence et al. 2010). This unwanted binding effect was used by Peresin (Peresin 2013) to produce coated plastic substrates. By changing the substrate surface chemistry, for instance by using PTFE (Spence et al. 2010), the adhesion can be avoided.

In contrast to wet end bulk addition of MNFC, surface coating exhibits several advantages. The fibrillary, and larger size compared to single polymer molecules, nature of MNFC typically leads to a good hold-out on even porous substrates (Charfeddine et al. 2014; Ridgway and Gane 2011) and therefore a distinct layer of consolidated MNFC on top of the substrate. As a consequence, the coating layer exhibits the MNFC having very interesting intrinsic properties such as a high elastic modulus or barrier properties. Considering the base material and the MNFC layer as two different materials, the formed composite will then present improved overall properties. For example, bending stiffness would be greatly increased by a surface layer of MNFC on a base substrate as the higher modulus MNFC is farthest away from the neutral deflection axis. It is therefore subjected to most of the deformation and, as a consequence, bears most of the applied load following

the I-beam principle (Lavoine et al. 2014). As far as barrier properties are concerned, while a bulk addition of MNFC to a porous base material does not lead to completely closed pores, a distinct surface dense layer application of MNFC is more likely to form a throughout consolidated layer impervious to a bulk flow of gas thus creating even barrier properties. As stated by Aulin et al. (Aulin et al. 2010) and Charfeddine et al. (Charfeddine et al. 2015), low application weights of MNFC as a distinct layer on a base substrate are already enough to reduce the air permeability significantly.

As seen in Lavoine et al. (Lavoine et al. 2014), a uniform application of MNFC on a substrate remains challenging. On the one hand, great quantities of water have to be removed as the solids content of MNFC suspensions should necessarily be very low as to maintain a low viscosity; MNFC suspensions forming gels at even 2-3 wt% concentration. Also, MNFC residual coarse materials exclude some application techniques. The selection of an appropriate application method for a given MNFC material is therefore crucial for any commercial scale application. First work on this topic is presented by Charfeddine et al. (Charfeddine et al. 2014) where pigmented MNFC is applied on a TMP base sheet using a dynamic sheet former. Furthermore, it is indicated that successful pilot-scale trials were carried out where the MNFC suspension was applied on a TMP base web using a curtain coater type device (HydraSizer™) (Roussière et al. 2015).

2.2.3.4 Reinforcement in polymer-based composites

Due to its high mechanical properties, namely elastic modulus and strength, MNFC and more specifically NCC and NFC have been evaluated as dispersed reinforcement phase in polymer-based composites (Alemdar and Sain 2008; Eichhorn et al. 2010; Hubbe et al. 2008; Iwamoto et al. 2005; Nogi et al. 2009; Siqueira et al. 2010). A further advantage, especially for NFC and NCC, is their optical transparency. Therefore, these forms of nanocellulose may be used as a reinforcement phase in applications where the polymer-based composite has to remain transparent (Iwamoto et al. 2005). Additionally, cellulose generally exhibits a low coefficient of thermal expansion (CTE) compared to thermosetting, e.g. of thermoplastic polymers. When included in composites, the nanocellulose materials are then able to reduce the overall CTE (Nakagaito and Yano 2008). Typically, low addition levels - below 10, more frequently below 5 and sometimes

even below 1 wt% - are already enough to measure an improvement in mechanical properties compared to the pure polymer matrix system.

However, in order to get the best reinforcement effect, two requirements have to be fulfilled. On the one hand, the MNFC has to be well dispersed in the matrix phase and on the other hand, the interaction between the MNFC and the reinforcement phase has to be strong enough. Depending on the composite matrix material, the second point is usually not an issue if the general chemistry is similar - as for example poly lactic acid (PLA) (Cheng et al. 2007), chitosan (Azeredo et al. 2010), and some thermoset resin systems (Nakagaito and Yano 2008). When the chemistry of the matrix material is different than the reinforcing phase, nanocellulose inclusion is not necessarily an advantage. As shown by deMenezes et al. (deMenezes et al. 2009), when NCC whiskers were used as reinforcement phase in poly ethylene (PE), tensile strength decreased, which is a sign for a poor NCC whiskers dispersion. By chemical modification, e.g. addition of aliphatic chains to the NCC, dispersion was improved. However, the tensile strength was still not improved as could be expected for a reinforced composite. Yet, there are examples where surface modification actually led to an increase in mechanical properties (Siqueira et al. 2009).

Another challenge of using MNFC or nanocellulose in composites is the up-scaling of manufacturing processes. Except few authors who use directly up-scalable processes like melt extrusion (deMenezes et al. 2009), extensive processes like water-based casting, and successive evaporation steps, and pre-forming of an MNFC pad followed by resin impregnation and hot-pressing are typically presented.

2.3 Matrix material for composites

Instead of being used as a reinforcing phase, MNFC can also be used as the matrix phase of a composite material. However, only little is published on the topic. Of course, an MNFC-based free-standing film could somehow be considered as a MNFC based composite. However, the increased bulk when compared to thin film forming brings further challenges. First, free water removal is impeded as the MNFC fibrils and fibres build up dense layers during the filtration processes. Second, the removal of bound water is hindered as diffusion of water molecules is slowed down in already dried and dense

outer layers of any work-piece. Finally, deformation takes place due to the occurrence of large internal stresses when large solids content gradients develop due to inhomogeneous drying.

Typically, such composites are manufactured in a two-step process. In the first step the free water is removed mechanically and in the second step, the bound water is removed thermally by controlling the spatial shape of the composite. As described by Schenker and Gane (Schenker and Gane 2012) and Yano and Nakahara (Yano and Nakahara 2004), the mechanical dewatering is achieved by a pressure filtration step either on a porous metal plate or a membrane filter. As mentioned earlier, the filtration time using pressure and/or vacuum filtration may be quite long for highly fibrillated MNFC qualities. Maloney (Maloney 2013) presents a potential approach to facilitate dewatering by the introduction of high shear at dewatering site, or slightly before, before the disturbed network is again relaxed. A process and device based on preliminary combined rheology and dewatering measurements has been described by Dimic-Misic et al. (Dimic-Misic et al. 2013c). Although the process is limited to a maximal composite or work-piece thickness, it has the advantage to be a continuous when compared to previously presented processes. In all cases, the final drying step remains hot-pressing. However, other possibilities such as *in-situ* precipitation of calcium carbonate have been investigated by Rantanen et al. (Rantanen et al. 2015) to facilitate the dewatering of MNFC containing composites.

As seen in chapter 2.2.2.2, mechanical properties strongly depend on the type of MNFC (pulp source, degree of fibrillation, etc.), and within a composite also on other added components. For example, the addition of calcium carbonate pigment filler to MNFC generally leads to a decrease of mechanical properties (Schenker and Gane 2012; Schenker and Gane 2013). However, the decrease can be reduced or compensated by, for example by co-processing the pigment (Schenker and Gane 2012; Schenker and Gane 2013; Schenker et al. 2015) during MNFC manufacturing, by the addition of carboxymethyl cellulose (CMC) (Schenker and Gane 2013; Schenker et al. 2015) and/or by using special hybrid pigments (Schenker et al. 2015). Hence, MNFC composites consisting of 20 wt% calcium carbonate and 5 wt% cellulose may be obtained with an elastic modulus of around 11 GPa and an ultimate strength of around 200 MPa. Alternatively, an MNFC composite consisting of 50 wt% hybrid pigment, and around only

1 wt% polymer content, may be obtained with still an elastic modulus of 7 GPa and an ultimate strength of 100 MPa (Schenker et al. 2015). Additionally, the authors show that such composite materials can be manufactured in complex shapes, providing eventually as much flexibility as for thermoplastic polymer work-pieces (Schenker et al. 2015).

2.4 Characterisation of MNFC suspensions

2.4.1 Challenging characterisation: multi-scale sized features

As already mentioned, a typical MNFC material may contain residual or partially broken down fibres, fibril bundles, fibrils as well as nano-fibrils, and eventually nano-crystals. So, the characteristic diameter scales range from several 10 μm to some nm whereas the characteristic length scales range from several mm to some nm (Miao and Hamad 2013; Roussière et al. 2014; Xu 2014). As most quantitative measurements typically are only reliable in some limited dimensional ranges, a thorough assessment using only one measurement technique is not adequate. Measurements characterising macroscopic properties present the shortcoming of measuring only an overall effect that may just be the result of a combination of several effects, without any possibility to separate among them.

As stated by Kangas et al. (Kangas et al. 2014), there is not yet a single measurement able to characterise an MNFC material in sufficient detail to describe it completely and properly. Therefore, it is recommended to characterise different MNFC properties with different complementary techniques in order to describe different, eventually crucial aspects of these materials.

The following section provides an overview on methods that are typically applied to characterise MNFC suspensions. It is followed by a section that provides a critical review of selected methods.

2.4.2 Characterisation methods

The objective of this section is to propose a critical review of the key methods used for characterising MNFC suspensions. The methods have mostly been developed for clean, simple systems. However,

MNFC suspensions are complex systems consisting basically of a solvent, typically water, and a solid, so-called “cellulose-based materials”, eventually more materials may be present like (bio-)polymers and pigment particles. However, the cellulose-based materials present different forms, or the same form, as aggregated cellulose molecules, but with dimensional scales that may be very different. Therefore, different characterisation techniques from different fields are needed to assess a system completely. In an MNFC material with a broad degree of fibrillation distribution, eventually different techniques have to be applied to assess only one property, but on all relevant dimensional scales, like for instance the diameter distribution.

Figure 2.1 gives an overview on typically methods used to characterise typical properties of MNFC suspensions. The following sub-topics give a short introduction to selected methods, whereas some of them are discussed critically.

Property	Characterization method
Amount of nanomaterial	Mechanical fractionation by combination of sieves and membranes (Tanaka et al. 2012) Fractionation by centrifugation (Ahola et al. 2008) Field / tube flow fractionation (Haapala et al. 2013)
Average particle size and size distribution	Light scattering measurements (for low aspect ratio materials) Transmittance by UV-vis spectroscopy (Saito et al. 2006) Fibre analysers Fractionators Turbidity Microscopy (for fibrillated materials) by scanning electron (SEM), transmission electron (TEM) or atomic force microscopes (AFM) (Vartiainen et al. 2011; Wang et al. 2012)
Rheology i.e. viscosity, yield stress, gel point, aspect ratio	Low shear viscosity by viscometers (Iotti et al. 2011) Gel strength, viscoelastic properties by rheometers (Pääkkö et al. 2007)
Appearance, dimensions, branching degree, fibril aspect ratio (length/width, L/w)	Microscopy by optical microscope (OM) and SEM/TEM/AFM (Pääkkö et al. 2007; Ahola et al. 2008)
Dissolved (colloidal) substance (amount and quality)	Gel permeation chromatography (GPC) Size-exclusion chromatography (SEC) High-performance liquid chromatography (HPLC) Microscopy by SEM/TEM/AFM
Crystallinity	X-ray diffraction (XRD) (Iwamoto et al. 2007)
Specific surface area	X-ray scattering by small-angle XRS (SAXS) (Leppänen et al. 2010) N ₂ adsorption, Brunauer-Emmett-Teller (BET) isotherms (Pääkkö et al. 2007)
Surface charge and chemistry (chemically modified cellulose)	Conductometric titration (Saito, Isogai 2004) Polyelectrolyte (PE) titration (Junka et al. 2013) Zeta -potential (Eronen et al. 2012) X-ray photoelectron spectroscopy (XPS) (Johansson et al. 2011) Fourier Transform Infrared Spectroscopy (FT-IR) (Saito et al. 2006)
Mechanical properties	Strength properties of cellulose films

Figure 2.1: Overview on commonly used characterisation methods for MNFC materials, taken from Kangas et al., 2014 (Kangas et al. 2014).

2.4.2.1 Surface and total charge

By the de-protonation of the hydroxyl groups, cellulose gets a net-charge that can be measured. However other residual molecules from the original wood source would also, sometimes strongly, add charge to the overall system. Whereas titration methods are able to determine the total amount of anionic groups in a system, polyelectrolyte adsorption methods can, depending on the selected conditions, eventually differentiate between total and surface anionic groups.

In an overview Fardim et al. (Fardim et al. 2002) describe several different methods to determine the amount of anionic groups of pulp fibres. Besides the generally reliable titration methods to determine the total charge, a very simple and easy to perform colorimetric method, namely methylene blue sorption, is pointed out to be almost as accurate as the conductometric titration, but without any extensive sample preparation. As already shown by Fardim et al. (Fardim et al. 2002), different pulp types will have different amounts of anionic groups because, among other reasons, of eventual residual species other than cellulose, for instance like hemicellulose and lignin. They also mentioned that pure mechanical pulping will not have an influence of the amount of total anionic groups, indicating that the methylene blue is able to diffuse completely through the pulp fibres, and therefore sorb onto anionic groups within a fibre. In essence, these methods are unable to measure a degree of fibrillation directly: i.e. with no modification of the method. They may probably serve as base line measurements of the total charge, to which a surface charge can be related and eventually, an overall, apparent degree of fibrillation can be estimated.

As seen previously (Fardim et al. 2002), polyelectrolyte titration can measure surface charge, without the bulk charge. However, to obtain reliable results, the experimental conditions have to be selected carefully (Fardim et al. 2002; Horvath et al. 2006). As the amount of surface charge is directly related to the amount of accessible surface that is moreover dependent on the degree of fibrillation of the MNFC material, the polyelectrolyte titration may be a suitable method to determine the degree of fibrillation.

As just seen, because not only cellulose is contributing to a charge measurement, but also the residual species (lignin, hemicelluloses) (Fardim et al. 2002), it is usually necessary to know the exact composition of the feed pulp. However, as the pulp source will not be

changed within this work, the relative contributions of non-cellulose compounds will not change among different experiments. In any way, the actual share of non-cellulose compounds should be small as a bleached pulp quality will be used. Because it is useful, not to say necessary, to know both the surface and the total charge to be able to calculate a relative degree of fibrillation if one assumes that the total charge equals the completely fibrillated state (see paragraph 2.4.2.1 for more details), one has still to ensure that the measured surface and total charge are adequately measured. It appears that polyelectrolyte titration is suitable to measure surface charge, if the measurement parameters are properly selected (Horvath 2003; Horvath et al. 2006; Hubbe et al. 2005). To assess the total charge, poly-electrolytes typically are not suitable as they are too large to penetrate completely into the cellulose structure. In this case, other titration methods like conductometric titration or colorimetric methods like methylene blue sorption can be used (Fardim et al. 2002).

2.4.2.2 Zeta potential

The charge on a surface of a particle creates a potential that is called surface potential ψ_0 right at the particle surface. This potential decreases with increasing distance to the particle surface and approaches zero for long enough distances. How the potential decreases depends mainly on the ion-speciation of the surrounding electrolyte. Some models, i.e. the Stern model, assume a layer of counter-ions that are bound to the surface (so-called “Stern-layer”). As a consequence of the counter-ion adsorption, the potential at the surface of the counter-ion layer is reduced. This potential typically is called the Stern-potential ψ_d .

Another potential exists when there is a relative movement between a particle and an electrolyte, which is the elektrokinetic- or ζ -potential. This potential is present at the so-called “slipping plane” which defines the region of transition between the electrolyte moving with the particle and the electrolyte moving relatively to the particle. Depending on the model, the slipping plane sometimes is defined to be at the Stern layer.

The presence of the ζ -potential leads to some electrokinetic effects that can be used to indirectly characterise colloidal suspensions (Jacobasch et al. 1985).

Electrokinetic effects:

- **Electro-osmosis:** The solid phase material is immobilised (by e.g. a diaphragm) and surrounded by the solvent. Then an electric field is applied that causes a movement of the ions of the electrolyte and therefore a net flow of the electrolyte that is measured.
- **Streaming current or –potential:** As in the electro-osmosis, the solid phase material is fixed and surrounded by the electrolyte. However, in this case an electrolyte flow is induced by applying a mechanical force (e.g. pressure) and the resulting potential (or current) between two electrodes is measured.
- **Electrophoresis:** A potential is applied between two electrodes that are in contact (immersed) with the suspension. The electric field leads to a net flow (rate) of the solid particles that are then measured with different techniques.
- **Sedimentation potential:** The sedimentation of the solid phase particles leads to a built up of a potential between two horizontally arranged, immersed electrodes compared to the initial, fully dispersed suspension state.

So even though the ζ -potential does not directly measure the surface charge, it does give information about the charge situation close to the surface but not independently of the bulk ion speciation. However, whether the ζ -potential can be used to describe the degree of fibrillation of an MNFC suspension is questionable, even though it is sometimes used as such in the literature.

As the zeta potential is assumed to be an inherent material or system property, the value that is obtained for a given system should be the same, independently of the used measure principle. However, especially in the case of zeta potential measurements performed on fibrous suspensions, it is seldom the case (El-Gholabzouri et al. 1999; Hubbe and Wang 2004; Jacobasch et al. 1985; Jaycock 1995). We surmise that the main reason is probably that assumptions made in the respective theory for a given measurement principle are not fulfilled in the actual measure. For instance in pad-forming streaming current detectors, the equation used applies to single, straight capillaries (Jaycock 1995), and not for fibre pads; other assumptions are also not accurate or verified (Hubbe and Wang 2004; Jaycock 1995).

As per Jaycock (Jaycock 1995) and Hubbe and Wang (Hubbe and Wang 2004), it is recommended to use electrophoretic mobility type of measurements to assess the zeta potential of MNFC suspensions. On the one hand, it is because the underlying theory is closer to the actual measuring conditions, and on the second hand, as no instrumentation changes are necessary. Nevertheless, although of minor importance, the filter-mesh would most likely have to be changed in a pad-formation device as the fine fraction of an MNFC would not be held back completely at the screen. However, as pointed out above, as the Debye-length and fibril/fibre diameter are not known (but with a probable broad distribution), it is not possible to adequately choose the right approximation. It is therefore not possible to reliably calculate a correct, absolute zeta potential value. Another condition that may lead to wrong absolute zeta potential values is the concentration, as particle interactions are not considered in widely used electrophoretic mobility and zeta potential relations (Dukhin and Goetz 2002). It is then further recommended to use the electrophoretic mobility values instead.

Finally, the system needs to be sufficiently diluted to be reliably measured by electrophoretic experiments (Dukhin and Goetz 2002); unless some specialised formula is used that accounts for additional effects in concentrated systems. In effect, the dilution is not reflecting the suspension state in the undiluted system anymore. As the zeta potential is not a property of the suspended phase alone, but one of the complete system, the actual measured value is likely to be different from the “true” undiluted system value.

Notwithstanding our thorough critical analysis, it is concluded that the zeta potential, respectively the electrophoretic mobility could be used as a relative measure within a system as long as the sample preparation is kept the same and accurately checked throughout the measurements.

2.4.2.3 “Particle size”

Depending on the particle size relative to the wavelength of light, particle size distribution can be determined using dynamic light scattering (DLS) or laser diffraction methods, whereas DLS is suitable for the condition of $r < \lambda$ and laser diffraction for $r \geq \lambda$, r being the radius of the “spherical” particle. For non-spherical particles, a volume-equivalent sphere radius is given as a result, that of course is relatively inaccurate for particles having high aspect ratios (length to width ratios). For colloids, the read-out radius is the

hydrodynamic radius of the colloidal particles. As MNFC suspensions can have entities smaller and larger than the wavelength of light, it is worth to have a quick look on the theory supporting both techniques:

Dynamic light scattering (DLS)

For small particles ($r < \lambda$), the Stokes-Einstein equation is used to describe particle diffusion:

$$D = \frac{k_B T}{6\pi\eta r_H} \quad \text{Equation 2.1}$$

where D is the diffusion coefficient, k_B is the Boltzmann-constant, η is the solvent viscosity and r_H is the hydrodynamic radius.

Due to relative movement of the colloidal particles originating from Brownian motion, the intensity of the measuring laser light beam is fluctuating. The frequency of the intensity fluctuation can then be related to the particle size distribution.

Laser diffraction

In this method, the Mie-theory is the basis for the particle size measurement method. It describes the elastic diffraction of waves on particles. As the diffraction angle, or the respective interference pattern of moving particles, is particle size dependent, one can calculate the particle size distribution by measuring the diffraction angles or the intensity fluctuation, respectively at given angles. In order to be able to calculate the particle size exactly, the refractive index and the extinction coefficient of the suspended material are needed. For larger particles ($r > \lambda$, $r > 50 \mu\text{m}$), the Fraunhofer-approximation can be used, in which case no refractive index and no extinction coefficient are needed anymore.

As stated above, the described techniques only give an equivalent sphere diameter (ESD) (Tschamuter 2000), respectively a hydrodynamic radius for colloids as a result but no information about the fibre length and diameter unless some additional data treatment is applied (Rodríguez-Fernández et al. 2007).

The ESD for a coiled chain-like particle is therefore giving information on the hydrodynamic radius, rather than on the actual length and width of the chain itself. Furthermore, it is very likely that the absolute size value of a given non-spherical particle will be different when measured with techniques with different measurement principles

(Jennings and Parslow 1988). ESD data can be combined with other physical properties of the non-spherical data; like with BET (Brunauer–Emmett–Teller) surface area for rod-like particles as stated by Gantenbein et al. (Gantenbein et al. 2011). However, this is seldom done when particle size data of MNFC are presented in literature (Dimic-Misic et al. 2013a; Dimic-Misic et al. 2014). Therefore we agree with Kangas et al. (Kangas et al. 2014) and recommend not to use any particle size measurement technique that is designed for spherical particles to measure the MNFC particle size distribution.

Alternatively, imaging methods are able to produce pictures of the actual material where dimensions can then be measured. Depending on the feature to be measured, the level of magnification has to be selected. For low magnifications optical microscopy is suitable. However, common resolution limits optical microscopy to measure, at most, partially fibrillated fibres to a size down to some μm . Scanning electron microscopy (SEM) can be used for higher magnifications, with a resolution down to some nm with a field emission electron source. However low magnifications can also be used. If even higher resolutions are required, either transmission electron microscopy (TEM) or atomic force microscopy (AFM) are required. Using image analysis software, it is then possible to evaluate pictures automatically.

Although the use of imaging techniques combined with image analysis to assess an MNFC's particle size distribution appears more reliable (Kangas et al. 2014) than previous techniques, some limitations have to be accepted and special experimental precautions have to be taken. The sample has to be homogeneous and the imaged surfaces have to be representative for the whole system. Furthermore, a good dispersion of the materials is mandatory, i.e. one has to ensure that individual entities are separated and not aggregated in a larger entity. In relationship with the aggregation factor, an appropriate drying technique has to be applied - as is, or should be, the case for most techniques that are able to image dry samples in the true nanometre scale - to prevent the condensation of the cellulose-based materials during drying. Finally, the amount of evaluated materials has to be large enough in order to have good representativity and reliable statistics. In order to assess the full size-scale spectrum of MNFC suspension materials, different techniques have to be considered. However, as all of these techniques can be scaled, it is not a problem to combine size data from one to the other. However, the determination of

cellulose fibril length is practically not possible using imaging techniques as the diameter (width) is too small compared to the length. It is one or the other: either the full length can be measured but at this low magnification the resolution is too weak to image the fibril diameter, or the diameter, can be measured at increased magnification, but the full length cannot be determined anymore, it being outside the field of measurement. Additionally, it is also quite difficult in practise to identify single fibrils as entanglements are quite frequent.

2.4.2.4 Rheology

Fundamentally, rheology is investigating how a material is responding to an applied force. Typically, rheology is measured on systems that consist of at least one material in a liquid phase. The response of the material to the applied force may be viscous, elastic or a mixture of both. Using different measurement procedures, rheology is able to characterise the individual contributions to the overall response and by applying adequate models and theories, it is then possible to make conclusions on the materials (micro-) structure and interactions.

There are two basic types of rheometers based on the way the force is applied to the material under investigation: shear- and extension. Within the shear rheometry, another classification is based on the way shear is introduced. On the one hand, it can be done by drag applied to relatively moving surfaces, or by pressure generated in order to force the material through a certain geometry (Figure 2.2).

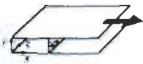
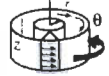
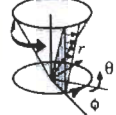

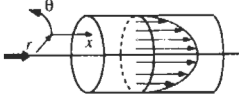
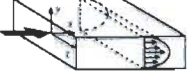
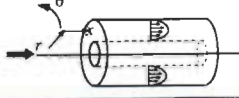
Drag Flows: Chapter 5 (section number)		Coordinates		
		x_1	x_2	x_3
Sliding plates (5.2)		x	y	z
Concentric cylinders (5.3) (Couette flow)		θ	r	z
Cone and plate (5.4)		ϕ	θ	r
Parallel disks (5.5) (torsional flow)		θ	z	r
Pressure Flows: Chapter 6 (section number)				
Capillary (6.2) (Poiseuille flow)		x	r	θ
Slit flow (6.3)		x	y	z
Axial annulus flow (6.4)		x	r	θ

Figure 2.2: Common drag and pressure flow geometries, image taken from Macosko, C.W., *Rheology - Principles, Measurements and Applications*, 1994 (Macosko 1994).

Different measuring geometries exist in shear rheometry. Commonly used designs include concentric cylinders (Couette flow), cone-plate and parallel discs for drag methods, and capillary flow (Poiseuille flow) for pressure methods (Figure 2.2).

A typical dynamic shear rheometer consists of a motor that creates a constant rotation at a required rotational speed and an oscillation at given amplitude and frequency. The response of the material is measured as the torque, either on the driven or the fixed geometry. The torque is then translated into shear rate and stress using, for example, following equations:

For concentric cylinders configuration

For $\kappa > 0.99$ (ratio of the two cylinders)

$$\kappa = \frac{R_i}{R_o} \quad \text{Equation 2.2}$$

Whereas R_o is the inner radius of the outer cylinder and R_i is the outer radius of the inner (moving) cylinder.

The shear rate is then calculated as:

$$\dot{\gamma} = \frac{\Omega \frac{R_o + R_i}{2}}{R_o - R_i} \quad \text{Equation 2.3}$$

with $\dot{\gamma}$ is the shear rate and Ω is the rotational speed.

The shear stress is:

$$\tau = \frac{M}{2\pi R_i^2 L} \quad \text{Equation 2.4}$$

with τ is the shear stress, M the torque and L the height of the inner (moving) cylinder.

For cone-plate configuration

For $\beta < 0.1$ rad, whereas β is the angle of the cone in relation to the bottom plate, the shear rate is:

$$\dot{\gamma} = \frac{\Omega}{\beta} \quad \text{Equation 2.5}$$

and the shear stress:

$$\tau = \frac{3M}{2\pi R^3} \quad \text{Equation 2.6}$$

whereas R is the radius of the bottom plate.

In order to assess the viscous properties of a material, a constant shear with respect to the direction of the shear is applied. Properties like the dynamic viscosity η can then be obtained:

$$\eta = \frac{\tau}{\dot{\gamma}} \quad \text{Equation 2.7}$$

Measuring the viscosity as a function of the applied shear rate and thus producing a so-called flow curve, will provide indication of the material fluid structure and structural changes, depending on the nature of the resulting flow curve. Whereas in the case of Newtonian behaviour, the viscosity is not depending on the applied shear rate, for many materials like polymer melts and material mixtures (suspensions, emulsions, colloids), viscosity is a function of the applied shear. The viscosity may decrease with increasing shear rate, for a pseudoplastic behaviour, or increase with increasing shear rate for a dilatant behaviour (Figure 2.3).

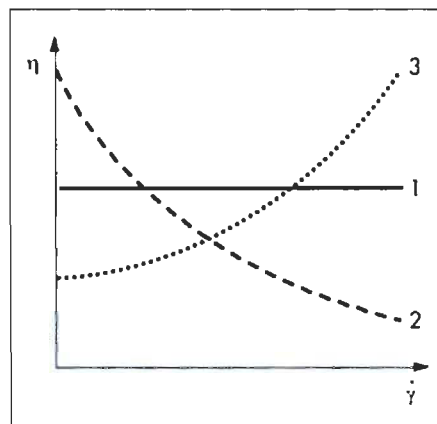


Figure 3.4: Viscosity functions, overview:
(1) ideally viscous/(2) shear-thinning/
(3) shear-thickening behavior

Figure 2.3: Shear rate dependent viscosity curves , taken from Mezger, T. G, The Rheology Handbook, 2014 (Mezger 2014).

Additionally, the viscosity can also be measured as a function of time at a given shear rate in order to characterise the time constant of eventual structuring processes induced by an applied shear or shear change. If the viscosity becomes smaller with time at a given shear rate, it is a thixotropic behaviour, in the opposite case when the viscosity increases with time at a given shear rate, it is a rheopectic behaviour (Figure 2.4).

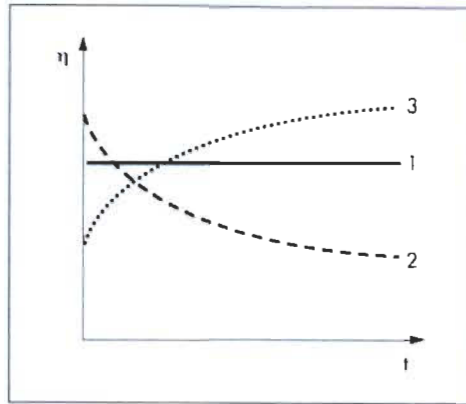


Figure 3.39: Time-dependent viscosity curves: for (1) to (3) see text of Figure 3.37

Figure 2.4: Time-dependent viscosity curves, taken from Mezger, T. G, *The Rheology Handbook*, 2014 (Mezger 2014).

To evaluate the elastic properties of a non-Newtonian (viscoelastic) material or the transformation from a solid-like to a fluid-like material, dynamic shear /oscillation experiments are to be considered. In such experiments, the moving geometry is not constantly rotating, but oscillating back and forth with a controlled frequency and amplitude. Depending on the property of interest, one can perform an amplitude sweep at a fixed frequency, or a frequency sweep at a fixed amplitude. The amplitude sweep gives more information about the structure of a material and the structural change induced by deformation compared to the frequency sweep which provides more insight in time-constants - and phase stability for heterogeneous system - of a system (Leung et al. 2014). Typical properties determined in dynamic shear experiments are, for instance, the storage modulus (G') describing the extent of elastic response of the material, and the loss modulus (G''), describing the extent of the viscous response of the material. In an amplitude sweep experiment of a viscoelastic material, those moduli are typically amplitude-independent up to a certain amplitude (or shear) value; the corresponding region is called the linear viscoelastic (LVE) region. Depending on which modulus is higher in absolute value, the material behaves like a viscoelastic liquid ($G'' > G'$) or a viscoelastic solid ($G' > G''$). After the LVE region, the moduli typically start to change with the amplitude further increasing. Eventually, the material starts to behave differently when the two moduli

curves cross over ($G' = G''$). The ratio between the two moduli rather than the absolute values may be of interest because it defines the materials overall appearance. Therefore, the loss factor is defined as

$$\tan \delta = \frac{G''}{G'} \quad \text{Equation 2.8}$$

or alternatively, the phase angle is defined as

$$\delta = \tan^{-1} \frac{G''}{G'} \quad \text{Equation 2.9}$$

For practical reasons, it might be more convenient to use the phase angle as it ranges from 0 to 90 ° whereas the loss factor ranges from 0 to ∞ . A phase angle of 0° then is describing a perfectly elastic solid material, whereas a phase angle of 90° is describing a Newtonian fluid. The crossing point of the two moduli, is then also easily to find at a phase angle of 45°. The yield point is defined at a certain deviation (reduction) of the storage modulus from the LVE plateau value. However, several other approaches and definitions to obtain the yield point exist as well and a more in-depth discussion can be found in paragraph 7.4.3.

Typically, an amplitude sweep measurement is performed prior to a frequency sweep measurement in order to determine the LVE region, and from this, selecting an appropriate amplitude (within the LVE region) for the frequency sweep measurement (unless specific investigations of the viscous-behaving suspension want to be made).

Finally, also more applied measurement protocols can be used where different measurement parameter sets are combined, like for instance in the three interval test (3ITT). This test consists of three intervals, in which the first and the last one each measure an actual material's condition like a low-shear dynamic viscosity or a specific modulus, and the second one is simulating a process condition like a high shear rate. Like this, one can investigate the time that the material needs to get back to the initial condition (a certain viscosity or modulus value), after the condition of the second interval. Performed like this, this test is able to characterise the time dependency of a structural change of the material, and by setting specific conditions for the intervals, it can be used to simulate specific application conditions.

As mentioned earlier (section 2.4.2.4), it is eventually possible to hypothesise structural- and interaction models from a combination of rheological measurements of a system. Yet, the rheological properties on their own are averaged, macroscopic properties of the complete system, including all contributing effects (that may be of very different nature). Rheology is a mature discipline based on a solid background and base for well accepted models and theories, as well as reliable equipment. However, the appropriate selection of measures is a crucial step in order to avoid as much as possible unwanted side effects as e.g. end-effects, secondary- and/or turbulent flows, shear banding, and wall slip. Only a few researchers have addressed these issues with a focus on the characterisation of MNFC applications.

In order to avoid wall slip and confinement typically observed in gel like systems (Karppinen 2014), Mohtaschemi et al. (Mohtaschemi et al. 2014b) have used a vane in cup geometry and wide gap set-up in place of the typically narrow gap Couette set up in the rheometer. However, the wide gap set-up led to a non-uniform shear profile. Consequently, the data had to be corrected in order to obtain the true, intrinsic flow curve. This was achieved via an iterative correction algorithm. The hysteresis of the shear stress, and/or viscosity (Iotti et al. 2011), originating from up- and downward shear rate sweep experiments was not uniquely attributed to the measurement set up and the used spatial dimensions, but also to a system-intrinsic characteristic. As hysteresis also occurs in narrow gap set-ups, it is assumed that the general behaviour of such MNFC suspensions can be characterised by the wide gap set-up; but probably with some error in the absolute values (Mohtaschemi et al. 2014a). Another effect related to the cup geometry is that secondary flows may occur at increased shear rates. Without any model to correct for the phenomena, we conclude that only shear rates with no secondary flows can be measured. It represents a major drawback of the method. Furthermore, the algorithm parameters have to be determined prior to the correction. As only one example is presented (one solids content of one NFC type), it is not clear whether the reported parameter values are universal but eventually related to system characteristics like solids content or have to be determined for every single system. Finally, additional extensive measurements would be necessary to validate the corrected curves, as so far no “truly correct” measurement exists.

In another work by Mohtaschemi et al. (Mohtaschemi et al. 2014a), a vane rotor mounted on a Brookfield viscometer was used to measure the torque on the rotor in dependence of different angular velocities for MFC and NFC suspensions at different dilution levels. The shear stress vs. shear rate flow curves were derived by two different methods, one taking into account the spatial heterogeneity of the shear rate in a complex fluid (denoted “corrected”), and the other without correction, assuming a linear shear rate profile across the gap. They found that the “corrected” shear stresses are lower than the uncorrected ones, and that the shear stress trends remained about the same. The critical shear stress calculated according to the Herschel-Bulkley model was also lower for the corrected data and the trends were also the same as presented in the flow curves. It may be concluded that relative trends are observed correctly, even when applied models do not take into account heterogeneous shear profiles. An interesting observation, mentioned by the authors, is that for NFC, the difference between corrected and uncorrected shear rate values seem to become bigger for increased shear rates for all solids contents. At the opposite, for MFC, the differences become smaller with increasing shear rates. The highest shear rate being only about 40 s^{-1} , an extrapolation of the trend would bring values of both models to converge in the case of MFC. We propose that a less fibrillated material would eventually show less shear banding as it is more likely to have less “mobile” entities that extend over a larger length. Therefore, it would transduce the shear force further away from the moving surface to the static surface. Consequently, after a certain time and/or shear rate, the shear rate profile becomes again linear). However, in the case of the fine NFC material, the shear banding increases with shear rates and therefore the misprediction of the uncorrected data becomes bigger, i.e. the non-linearity of the shear rate profile increases, and the error becomes larger when assuming a linear shear profile in the case of the “uncorrected” data.

With viscosity measured on a Brookfield viscometer, Sneek et al. (Sneek et al. 2011) found that the vane rotors set-up had a better reproducibility than the classical disc set-up which led to varying data. Furthermore, as the viscosity was measured at different rotational speeds, i.e. shear rates, at low shear rates, the absolute viscosity number did not differ too much between the two different measurement set-ups. However, when increasing shear rate, the disc set-up typically led to lower viscosity numbers. However,

as they used the same MFC suspension in both methods, the lower viscosity numbers were likely not originating from a different intrinsic effect. It could eventually be explained by a wall slip phenomenon leading to an overall reduced torque which translates into smaller viscosity numbers. The behaviour seems to agree with the observations by Mohtaschemi et al. (Mohtaschemi et al. 2014a) made in the case of the NFC material for corrected and uncorrected data. However, as repeatability in the parallel disc measurement was low, data interpretation should be subject to caution. Interestingly, Iotti et al. (Iotti et al. 2011) did not report repeatability issues with a disc-disc set-up, probably related to the use of roughened plates (no wall slip).

Although the vane cup geometry is less likely to create wall-slip, it may induce non-laminar flow at increased shear rates. Another option is worth considering as, if the contribution of the wall slip to the overall measured effect like the viscosity is known, one could correct the measured data accordingly. Yoshimura and Prud'homme (Yoshimura and Prud'homme 1988) provided a simple procedure to determine the wall slip for cylinder-cup (Couette) and plate-plate geometries.

2.4.2.5 Surface area measurement

The measurement of surface area of MNFC is sometimes used as an indicator for the degree of fibrillation assuming that one can measure the total surface of the material as more fine features will give a higher surface to volume ratio. One standard method is the Brunauer–Emmett–Teller (BET) nitrogen (N_2) adsorption (Kangas et al. 2014). The method requires a sample preparation that maintains the original, suspension-state structure of the fibre-fibril network, avoiding especially condensation and collapsing of the structure. Freeze drying is typically used for the purpose. Zheng et al. (Zheng et al. 2014) showed that BET surface area measurement is limited to a certain size range of the features. It means that the very fine NFC fraction cannot be measured by this method.

Alternatively, a Congo-Red absorption method can be applied to determine the specific surface area of MNFC materials in suspension (Spence et al. 2011). But, as mentioned by the authors, the method is prone to be influenced by the surface chemistry of the used pulp. Yet, as a relative measure within a given pulp system, the method is still suitable.

2.4.3 Conclusion

As presented by Kangas et al. (Kangas et al. 2014), as one single parameter is not able to describe adequately and in sufficient detail an MNFC suspension, and as often a single parameter is not even able to distinguish between different types of MNFC, an extensive set of parameters is required. However, for relative comparisons in fixed systems, a reduced set of parameters might be sufficient in order to form hypotheses for working or basic principles.

The size information of the cellulose entities is expected to be important in order to develop a model on the stability and the rheological behaviour of MNFC suspensions. As traditional particle size measurement methods are not able to give individual dimensions of non-spherical particles, those techniques remain highly questionable if a, often “coiled”, fibre-like particle is under investigation. Therefore, imaging techniques including image analysis look more appropriate, even though real quantification remains painstaking and difficult as different imaging techniques have to be used because of the large spread of diameters of the MNFC materials.

Furthermore, the characterisation of the charge situation in an MNFC suspension is important as the major part of the repulsive interaction in the system will derive from electronic interaction. As the determination of surface charge via poly electrolyte titration is relatively reliable, provided that the measurement parameters are properly selected (Horvath 2003), the method should normally be applied. The zeta potential measurement can be used, too, within a given experimental series for relative comparison. However, absolute values should be used with caution as they are most likely not comparable to other MNFC systems.

Finally, rheological measurements will provide a solid basis for getting information, although indirectly, on structural interactions in suspensions. The measurements typically are reliable, if side- and end-effects are controlled and/or considered.

2.5 Rheology of MNFC suspensions

Please note that the literature review provided in this section is a snap-shot of the time before the first article of this PhD work was published. It gives an overview on the basis on which the rheological aspect of this work was initially considered. More recent and

specific literature reviews are provided in the respective introductions of the publications (Chapter 5 - , Chapter 7 - , Chapter 8 - and Chapter 9 -).

2.5.1 Pure MNFC systems

Iotti et al. (Iotti et al. 2011) showed the viscosity of MFC suspensions in dependence of the shear rate (low shear: 0.1 to 1 000 s⁻¹ and high shear: 180 000 to 330 000 s⁻¹). Up- and downward sweeps were recorded for different solids contents (1, 2, 3 and 4 wt%) and at different temperatures (25, 40 and 60 °C). They reported both the typical shear thinning behaviour and the hysteresis between the downward- and the respective upward viscosity curve. The hysteresis seems to decrease for high solids contents but it is still well observable (Mohtaschemi et al. 2014a). The hysteresis also decreases at high temperatures. Furthermore, it appears that the hysteresis onset shear rate increases with temperature, whereas the hysteresis end-point remains unchanged; an observation not mentioned by the authors. Additionally, steady shear experiments (5 min), at representative shear rates within the hysteresis region showed that the viscosity is time-dependent. Whereas a thixotropic (viscosity decreases with time) behaviour is observed in the first part of the downward curve in the hysteresis area, rheopectic (viscosity increases with time) behaviour is observed both in the second part of the downward curve and on the upward curve of the hysteresis area. Finally, a shear-thickening (dilatant) behaviour is observed at high shear rates. As correctly pointed out by the authors, the upward shear sweep curve is rarely, if not at all, reported. Therefore, the hysteresis is generally not reported either. The hysteresis area (the relevant shear rate area) might however be a remarkable starting point to investigate the loss- and storage modulus as well as other properties, e.g. like time dependency, in order to get a deeper understanding of the interactions in MNFC suspensions. It becomes therefore of research interest to study how the hysteresis is modified or not by, for instance, changed electrolyte conditions, added polymers -dissolved and/or adsorbed (Liimatainen et al. 2009), and pigment particles.

Sneck et al. (Sneck et al. 2011) presented viscosity data of a mechanically (Supermasscolloider) produced MNFC suspension in dependence of the amount of passes through the grinder. They found that the shape of the viscosity versus shear rate curves looked similar, with increasing absolute values at increasing number of passes. Different

MNFC suspensions from different suppliers were thus characterised. The shear thinning behaviour, i.e. the slope of the viscosity versus shear rate curves, varied for different types of MNFC suspensions. When combined with observations by Kangas et al. (Kangas et al. 2014), we can conclude that a MNFC suspension rheology is a measure of various interactions occurring in such a system. It cannot directly be related solely to one parameter as, for instance, the degree or state of fibrillation. Previous statement is not only true for different types of MNFC suspensions, but also within a fixed system. This was further verified by the steady increase of viscosity with an increasing amount of passes (Sneck et al. 2011) while the viscosity was reduced for a different but more ground product (Kangas et al. 2014). These two sets of data indicate the counter-play of two effects in mechanically ground MNFC suspension.

At the start of the fibrillation treatment, the fibre suspension being inhomogeneous, only a small amount of charge carrying surface is available. It means that the main viscosity influence effect is most probably due to hindered relative motion of fibres or fibrils due to entanglement. As fibrillation proceeds, the fibres are broken down in smaller fibrils which then provide automatically a larger surface to volume ratio. It follows that they might easily separate from each other. On the one hand, it would mean that the interaction between fibrils is decreased due to a higher apparent charge per fibril volume which basically should lead to a decrease in viscosity. On the other hand, a better state of dispersion may lead to more entanglements resulting in the relative motion of fibrils being hindered. This second effect seems to be dominating during the initial phase of fibrillation (Kangas et al. 2014). After a certain fibrillation level, the fibrils exhibit a relatively high surface charge to volume ratio. Consequently, the repulsive interactions become more pronounced. However, the situation may be more complex when considering the likelihood that entanglements increase as the fibrils become finer. Indeed, if the fibrils become smaller and smaller, they might become more flexible as larger fibres tend to be stiffer than small fibrils alone. Therefore, entanglements could slip relatively to one another more easily. Furthermore, if some cutting of the fibres occurs during fibrillation, the aspect ratio of the fibrils decreases resulting in less hindering interactions between fibrils (as could be deduced from work by Kangas et al. (Kangas et al. 2014)). Overall one would expect a decrease in viscosity with increased fibrillation (Kangas et al. 2014).

From two different sets of experiments (Kangas et al. 2014; Sneek et al. 2011), above mentioned hypotheses could not by default be fully supported (even with similar processes). Therefore, simple viscosity measures based on the vane set-up of a MNFC material in dependence of the amount of passes up to maximum viscosity would be supporting our proposal and then become a valuable asset for present work in view of the development of an interaction-flow-structure comprehensive model.

2.5.2 Influence of additives on MNFC suspensions

Liimatainen et al. (Liimatainen et al. 2009) investigated the effect of free and adsorbed CMC on pulp fibres on the apparent yield stress of MNFC suspensions, filtration behaviour, and fines retention during filtration. In order to control CMC adsorption on the fibres, or upon need to avoid it, CMC was either added to the pure pulp suspension (almost no CMC adsorption) or to a 50 mM Ca^{2+} (CaCl_2) and 10 mM Na^+ (NaHCO_3) containing pulp suspension. At only about 0.04 to 0.1 wt% based on pulp fibres, CMC adsorbed on the pulp fibres. It was possible to adsorb up to 1.4 wt% CMC onto the fibres with increased electrolyte concentration and even higher loadings were possible by increasing CMC addition levels. It was shown, that independent of the CMC state (adsorbed and free), CMC did influence the investigated properties, e.g. the yield stress.

However, adsorbed CMC had a stronger impact on the characterised rheological properties than free CMC, e.g. a stronger reduction of the yield stress. The authors proposed that both free and adsorbed CMC would basically reduce the attractive interaction between pulp entities; namely a “reduction of fibre-to-fibre friction”. They also pointed out that CMC might promote the “disintegration” (probably meant as “liberation”) of fines from the pulp fibre surface and thus reduce the overall fibre-to-fibre contact points. Based on their work and on the findings of Xu et al. (Xu 2014), whether the presence of CaCO_3 pigments in an MNFC suspension provides enough Ca^{2+} ions to promote CMC adsorption (as adsorption data in (Xu 2014) indicate a very low CMC adsorption) or not would be worth investigating. Furthermore, CMC adsorption in an adequate electrolyte could be investigated for MNFC suspension having different degrees of fibrillation, assuming a higher adsorption for stronger fibrillated MNFC as more cellulose surface is accessible for adsorption.

Vesterinen et al. (Vesterinen et al. 2010) investigated the influence of salt concentration on the rheology of pure polymer solutions such as CMC, cationic starch (CS), cationic polyacrylamide (CPAM), and polyethylene oxide (PEO). The overall viscosity is reduced while the shear thinning behaviour is reduced or even disappears (CPAM, CS) at the higher salt concentrations, from 0.5 mM to 10 mM Na⁺. The charge density of the polymers is usually not taken into account to estimate the general colloidal stability of the individual polymers and thereof their sensitivity to salt concentrations. Nevertheless, previous results indicate that the ion speciation might not only change the adsorption behaviour of the polymers onto cellulose entities (Liimatainen et al. 2009), but also the intrinsic contribution of the polymers and the cellulose entities. From studies of high cationic starch, CMC, CPAM and PEO loadings on MFC suspensions (1:1 w/w dry), it was shown that the addition of polymers generally increases the loss factor ($\tan\delta$) of an MFC suspension, meaning that the system behaves more like a viscous material. Unfortunately, no loss factor curves were provided for the pure polymer suspensions. However, at such high polymer to MFC ratios, it can be assumed that the polymer would dominate the viscoelastic behaviour of the system. As the polymer levels (based on MFC) are rather high, one may surmise that substantial amounts of the added polymers remained free in solution; i.e. they were not adsorbed on the cellulose fibrils. As adsorption was not characterised, it is impossible to know if the polymer concentration in solution was the same for all polymers. The measured properties are then likely a combination of effects of polymer adsorbed on the fibrils changing their general interaction and of the structural change of the polyelectrolyte.

Based on our analysis of previous works, we propose that the rheological behaviour of MNFC suspensions could be investigated in dependence of the CMC addition levels in combination with adsorption data. Furthermore, oscillatory rheometry could be performed at different frequencies in order to find an eventual structure recovery time constant.

2.5.3 MNFC in complex systems

Dimic-Misic et al. (Dimic-Misic et al. 2013a) performed an extensive study of different rheological characteristics of coating colour formulations containing either only CMC as co-binder or CMC-MFC or CMC-NFC mixtures at a fixed ratio as co-binder to a latex binder. Rheological measurements were performed on pure mechanically ground MFC

and TEMPO oxidised NFC suspensions at different consistencies. As expected, the apparent yield stress of a given suspension increased with an increasing consistency of the suspension. Interestingly, at low consistencies (< 1.5 wt%), the apparent yield stress was the same for the MFC and the NFC suspensions. As the NFC suspensions contain more nano-sized elements than MFC suspensions, the main cause for their gel-like behaviour, one could assume a higher yield stress for the NFC suspensions when compared to the MFC suspension at equal consistency. However, as the manufacturing processes differ significantly and as the oxidation even leads to grafting with functional groups, a direct comparison remains hazardous (see chapter 2.2.1.5). Some consistent effects are related to the partial replacement of CMC to MFC or NFC, e.g. a reduced storage modulus for MFC and NFC containing formulations. In general, the identification of specific effects of e.g. MFC/NFC with CMC and/or the pigment particles is difficult because of missing information, e.g. reference formulations, and because of the high amounts of co-binders (15 parts latex compared to 0.4 parts CMC; respectively 0.1 part CMC plus 0.3 parts MFC or NFC) which have a complex rheological behaviour of their own.

In another publication, Dimic-Misic et al. (Dimic-Misic et al. 2014) investigated model coating colour compositions, i.e. dispersed, ground calcium carbonate, clay and styrene acrylic latex as a base, mixed with MFC or NFC and/or CMC to investigate the influence of those additives on the rheology and the dewatering behaviour of the resulting compositions. Based on rheological investigation, the authors argued that, contrary to CMC, MFC and NFC do not lead to particles agglomeration. Furthermore, they claimed that the pigment particles do not interact strongly with the NFC/MFC and they can move freely within the suspension. In addition to the mentioned agglomeration effect of CMC on the pigment particles and the latex, the CMC appears to disperse the NFC/MFC or at least the respective fine fraction of MFC. As the pigments are already carrying an anionic charge, it is unlikely that CMC adsorbs onto their surface. Nevertheless, due to pigment flocculation, probably some CMC is bound in the bridging between the particles and is therefore available for dispersing the NFC/MFC materials. An interesting follow-up experiment would therefore be to use a pigment where the CMC was pre-adsorbed.

Dimic-Misic et al. (Dimic-Misic et al. 2013c) further presented rheological studies of high consistency (5, 10 and 15 wt%) furnishes consisting of 70 wt% dry filler (precipitated

CaCO_3), MFC or NFC (20 or 30 wt%, dry), and pulp fibres (0 or 10 wt%, dry). They found that furnishes containing MFC had a higher storage modulus compared to furnishes containing NFC in the LVE region. Additionally, they found that samples contain additionally pulp fibre have slightly higher storage moduli than samples without pulp fibres. In a strain sweep experiment, beyond the LVE region, as the storage moduli decreased with increasing strain, the abovementioned differences in storage moduli became smaller. Rheological measurements were also performed while simultaneously dewatering the different suspensions using an immobilisation cell (IMC). The cell gap was recorded in order to indirectly characterise the dewatering process. However, by comparing these data with gravimetrically determined solids content of formed pads, they concluded that the gap position is not a suitable parameter to determine the dewatering process, i.e. the MFC samples showed a larger gap but a higher final solids content. A simple explanation might be related to NFC containing furnishes providing more compact filter pads as finer NFC fibrils would fill in the pad porous structures built by the pigment and eventually the pulp fibres. In addition, the dense pad structure would further densify under vacuum filtration as pad compression develops due to the permeability being reduced. However, even under strong compression, less and less water is removed from NFC system due to water being bound more strongly than in MFC containing systems. Intervals between the vacuum filtration and parallel oscillation increased the final solids content of a given furnish. Furthermore, high shear rates (rotational speeds) in the intervals led to high final solids contents. The relative change in the final solids content between the filtrations, with and without the rotational intervals, decreased with increasing initial furnish solids contents. However (not mentioned by the authors), the absolute final solids content values did in fact increase with an increasing initial furnish solids content. It is finally mentioned that the method (IMC) had its limitations because inhomogeneous effects may occur, for instance a solids content gradient during dewatering, or even the formation of “solid flocs” that may detach from the filter and move as consolidated entities in the cell. We conclude that separating the filtration and the rheology measurement steps are advantageous. Accordingly, the change of rheological properties can be measured accurately and, by analysing the filtrate accordingly, be related to the changed relative composition of the remaining suspension.

The specific interaction between NFC, MFC, or H-MNFC grades (H, for highly fibrillated) and undispersed nano-PCC and nano-clay was investigated by measuring the particle adsorption on NFC, or CMC adsorbed NFC, using a quartz crystal microbalance (Nypelö et al. 2012). It was shown that nano-PCC adsorption increased with increasing CaCl_2 concentration, but was low at low ion speciation. Furthermore, CMC was adsorbed on the NFC surface at increased ion speciation levels leading to a significant CMC adsorption (Liimatainen et al. 2009). It resulted in an increased nano-PCC adsorption; i.e. about the same amount of nano-PCC was adsorbed on the CMC treated NFC at 1 mM CaCl_2 as it was adsorbed on pure NFC at 10 mM CaCl_2 .

Potential adsorption of pigment particles on MNFC fibres or fibrils and weak interactions impact the rheological response of a suspension. It is therefore of interest to investigate the change in rheological behaviour of pure MNFC suspension upon filler addition and upon an increase of ion speciation. As a reference point, the pure MNFC suspension needs to be analysed for eventual rheological changes upon increased ion speciation. The same evaluation should then be performed in the presence of CMC, even though a change in ion speciation will inherently change the CMC adsorption on cellulosic species (Liimatainen et al. 2009), as well as the interaction between the pigment particles and cellulose/CMC –cellulose surfaces (Nypelö et al. 2012). Eventually, an irreversible pre-sorbing of CMC on pure MNFC and/or pigment particles could be a solution.

Additionally, anionically dispersed pigment particles could be used to investigate the influence of the pigment particle charge on the interaction mechanisms, for instance with nano-clay used as anionic pigment (Nypelö et al. 2012).

Recent work by Dimic-Misic et al. (Dimic-Misic et al. 2015b) reveals the need for in-depth analysis of time-depending rheological effects of MNFC suspensions, in particular at low shear rates, i.e. “large” time constants. They found that high consistency, MNFC/pigment suspensions exhibited a rheopectic behaviour at low ($< \text{ca. } 15 \text{ s}^{-1}$) shear rates (cf. Iotti et al. (Iotti et al. 2011)). While thixotropic behaviour was mainly found in the flow curve, also rheopectic behaviour was found in the shear rate decreasing sweep, at around the same shear rates (10 and 20 s^{-1}) (Iotti et al. 2011) as found by Dimic-Misic et al. (Dimic-Misic et al. 2015b). Based on these data, a characteristic time constant was calculated that describes the build-up of a low-strain induced structure.

Chapter 3 - Hypothesis and objectives

3.1 Original goal

The initial goal of this PhD work was to study the interaction mechanisms between different components in a complex MNFC suspension. Namely, between cellulose fibrils and fibres, pigment particles and dissolved (bio-)polymers. The material space (components of the complex MNFC suspension) was defined by industrially relevant manufacturing processes. By understanding the interactions, it was planned to determine the conditions under which an MNFC suspension is stable and homogeneous, or destabilised. Both situations also have a practical relevance, e.g. when it comes to storage, transportation and handling of such materials, but also in application-relevant processes like drying and consolidation. This knowledge also allows to hypothesise models, that hopefully allow to predict the material's behaviour under specific conditions, but also lay the basis, for example, for a reliable material characterisation. The key characterisation technique selected for this PhD study was rheometry, as it is able to characterise a material at different deformation situations. Even though only indirectly, rheological behaviour of suspensions can be used to derive morphological models, especially when coupled with additional characterisation techniques. This again is of high practical relevance for industrial scale applications.

A summary of the original work plan and proposed experimental techniques and conditions are presented in the next subsection. Then, in section 3.2, a chronological reasoning is provided about why the initial goals had to be refined during the course of this work. In section 3.3, the latest thesis objectives are then provided, finally.

3.1.1 Material space

The base material for the MNFC process is the pulp. As pulp is a natural product deriving from natural sources, mainly wood, and as pulp manufacturing processes are very different, very different pulp qualities are available. In order to have the least probability of having interference of other species than cellulose, like lignin and hemicellulose, with the other MNFC components, a sole bleached, wood-free eucalyptus pulp will be used in this work. The effect of naturally present species other than cellulose on pulps on an MNFC suspension's stability should not be neglected (Dimic-Misic et al. 2015a).

Although it would be of interest to investigate this point systematically, it has not been considered in the present work.

The co-processing of pigment filler in the MNFC manufacturing process is promising for the production of MNFC qualities. Consequently, the resulting suspensions contain a certain amount of pigment fillers, whereas the ratio between cellulosic and inorganic matter may be different for different products. The influence of the pigment filler on the MNFC suspension's stability is therefore of a major interest and will therefore be one important parameter to be investigated.

The main parameter of interest concerning the filler is the ratio in relation to cellulose. However, also the filler type (particle size distribution, surface treatment) may be interesting to investigate. In order to maintain a comparability potential throughout the work, the pigment filler will be limited to only one mineral that is calcium carbonate as obtained from marble stone via a mechanical grinding process.

In first pilot scale application trials performed at UQTR (Roussière et al. 2015) it was seen that it may be necessary or useful to add other biopolymers to the pigmented MNFC suspension to improve the application process. As carboxymethyl cellulose (CMC) already performed satisfyingly in the mentioned MNFC application processes, the addition of this biopolymer will be mainly investigated. The addition level of CMC will be of special interest in order to be able to eventually evaluate current hypotheses in the field (Charfeddine et al. 2015; Roussière et al. 2014). However, the CMC characteristics like molecular weight distribution and degree of substitution will not be changed.

Additionally, the effect of the charge nature will be investigated by using a cationic- and an amphoteric polymer as additive.

3.1.2 Properties and products characterisation

All the components used to manufacture a pigmented/complex MNFC based suspension have to be characterised considering the parameters that may influence the overall suspension properties.

The feed or input materials can be characterised individually. Whereas the characterisation of pigment particles and CMC are well established and standard procedures exist, the characterisation of MNFC is not yet standardised. Actually, modified standard procedures, typically used, e.g. for pulp characterisation, are under evaluation and/or discussion

concerning their validity (see chapter 2.4.1). Therefore, concerning the characterisation of MNFC, the recommendation of a recent publication by Kangas et al. (Kangas et al. 2014) will here be followed by assessing a set of key properties of the MNFC suspension that, when considered together, provide a relatively complete description of the product under investigation.

3.1.3 Stability and homogeneity assessment

Rheological measurements provide information about the interactions in complex systems. On the one hand, the response of the system to an applied force, typically shear force via a shear process, is measured to obtain information on the interaction potentials, e.g. strength of interaction or nature of interaction. On the other hand, time dependent effects are measured to get information on potential structural changes within the system like ordering or structuring and relaxation processes. Depending on the property of interest, different rheological measurements may be carried out.

However, one should keep in mind that rheological properties are but a macroscopic or averaged response related to the various components of the investigated system. This means that an observed behaviour may have different causes when evaluated or considered on the fundamental, localised interaction level. It is therefore important to measure different rheological properties that will provide insights to different aspects of an overall interaction in order to get a more differentiated and finer analysis, and therefore truly understand the fundamentals mechanisms controlling the flow behaviour of pigmented MNFC suspensions.

Furthermore, as pigmented MNFC suspensions are a heterogeneous system, special care has to be taken to avoid artefacts in measurements that may arise e.g. due to phase separation. Accordingly, an extensive and critical literature review with a focus on appropriate measuring conditions for MNFC suspensions will be carried out.

The main parameters of interest on the suspension stability will be the dilution, respectively the consistency, of the suspension, the degree of fibrillation of the MNFC, as well as the influence of the other components that are the pigment filler and the additive. A special focus will not only be placed on the nature and amount of filler pigment and the additive, but also on the “addition sequence”. The study of the addition sequence is related to the potential adsorption of the additive, at least for the CMC (Roussi re et al. 2014; Xu

2014) onto one or both other components. Indeed, we can surmise a preferential adsorption onto one of both other components. As a result, the distribution of the additive would be different whether it is added to a pre-mixed cellulose and filler suspension or to one component first, before the second component is added. Eventually, we hypothesise that a changed “additive-distribution” may have an influence on the rheological properties.

3.2 Refined goal

Following the initial phase of the work, a thorough literature survey, designed to focus more strongly on rheological characterisation of MNFC suspensions, was undertaken. Additionally, a good understanding of the different nanocellulose types, as well as the current hypotheses and work in the field of MNFC rheology, had to be established. As a pre-requisite for moving forward with the experimental work, adequate experimental techniques and parameters have to be defined, and, very importantly, qualified. The core of the experimental study was then set to investigate selected aspects of the material parameter space of a complex MNFC suspension, using a design of experiments (DoE) approach. The ad-hoc defined parameters of interest for this planned investigation were: suspension solids content, degree of fibrillation, different additives (anionic, cationic, neutral), pigment particles (added and/or coprocessed) and fixation of polymers on added or coprocessed pigment particles. A schematic summary of the original proposal can be found in Figure 3.1.

During the initial experimental work, two issues became apparent.

- The MNFC manufacturing process was not as stable as originally assumed, i.e., the process efficiency of the selected manufacturing route exhibits very high fluctuations between individual batches. As a consequence, two batches of the same composition and apparent equal process conditions can be of different quality, i.e. DoF (see section 6.1 for more information). So, a comparison between a pure MNFC and ones that were coprocessed with pigments and/or additives is not possible, as potential differences cannot be distinguished from those originating from the variable process efficiency.
- The selection of adequate rheological measurement conditions and parameters was not as straightforward as planned. On the one hand, published work sometimes

proposed contradictory setups, or were not fully conclusive. This topic is of special importance for complex suspensions like MNFC, because of their susceptibility for measurement artefacts leading to misinterpretation of the obtained data. On the other hand, a thorough assessment of rheological behaviour of namely MNFC suspensions was missing (as opposed to e.g. NFC suspensions). Also, it was found that rheological data often were not quantified when reported, or only very few properties like storage and loss moduli, and probably yield stress and some apparent viscosity numbers. This is especially a shortcoming in the case of a material that exhibits a very complex rheological behaviour, as a lot of information is not provided by just giving a few classically fitted parameters.

Topic	Parameter	Condition	Experiments
Pure MNFC	Suspension consistency	highest DoF	5
	DoF (medium and low)	0.5, 1 and 2 wt% s.c.	6
Additives	CMC (adsorption eq, higher lower)	highest DoF, 1 and 2 wt% s.c.	6
	CMC (adsorption eq, higher lower)	lowest DoF, 1 wt% s.c.	3
	Cationic polymer	highest DoF, 1 wt% s.c.	3
	Latex	highest DoF, 1 wt% s.c.	3
	Pigment (GCC)	highest and lowest DoF	2
	CMC (3 levels) plus pigment (one level)	highest DoF	3
Co-processed	Pigment (GCC)	highest DoF, 1 wt% s.c.	1
	CMC (3 levels)	highest DoF, 1 wt% s.c.	3
	Pigment and CMC (3 levels)	highest DoF, 1 wt% s.c.	3
Co-processed and added	Pigment (cp) + CMC (added, 3 levels)	highest DoF, 1 wt% s.c.	3
	CMC (cp, 3 levels) + Pigment added	highest DoF, 1 wt% s.c.	3
CMC on pigment	3 types (added)	highest DoF, 1 wt% s.c.	3
	3 types (cp)	highest DoF, 1 wt% s.c.	3
Dewatering	Depending on rheological data	highest DoF, 1 wt% s.c.	6
Total			56

Figure 3.1: Original DoE matrix proposal with targeted parameters and predefined conditions and an estimate of experiments needed.

In the light of the above, this work focuses on the rheological measurement itself, i.e. the introduction of new and useful flow curve and viscoelastic data descriptors, and the investigation of the influence of different measurement setups of shear rheometers on those properties. Due to this aspect, and the limitations caused by the MNFC manufacturing process, the original DoE matrix was reduced significantly. Keeping in

mind the relevance for industrial manufacturing and application of MNFC products, the parameters to be investigated were limited to solids content and DoF of the MNFC suspensions.

3.3 Objectives

The ultimate goals of this work are thus defined to be:

- Establish a good understanding of the influence of commonly used shear rheometer setups and measurement parameters on flow curve and viscoelastic data of MNFC suspensions.
- Parametrisation and quantification of rheological data of MNFC suspensions, with a special focus on the complex flow curve behaviour that is typically observed for these materials.
- Investigate the influence of the suspension solids content and the DoF on the observable rheological properties.
- Hypothesise morphological models and interaction mechanisms to explain the observed behaviour and test these against existing models.

Chapter 4 - Materials and Methods

As one part of this work was to establish a profound understanding of the rheological behaviour of MNFC suspensions, the development of reliable rheological measurement procedures was crucial (see section 3.2). Despite different procedures having their respective advantages or disadvantages or being proven to be more or less prone to side effects and erroneous interpretations, it may even be argued that side are an inherent component of how a suspension reacts to a shear situation and, as such, are teaching the observer something valuable about the material being studied. But in any case, one should at least be aware of the potential implications a certain measurement system and condition can have on the resulting interpretation. In order to gain this understanding, the experimental set-up was, and had to be, adjusted several times, and so the whole work has been a continued learning process. To visualise this process better, the following sections (especially section 4.2.1 and subsections) anticipate some of the results and data in the publications that follow.

4.1 Materials

4.1.1 MNFC

The following sections describe the general process used to manufacture the MNFC suspensions investigated in this work. Please note that the term *MFC* is used in this section as opposed to MNFC. However, this is only to be better in line with the terminology used in the later presented articles (Chapter 7 - , Chapter 8 - and Chapter 9 -); the material is still classified as MNFC (see section 1.1 for more information). The specific energy consumption numbers and process details only apply to the materials described in the above-mentioned articles. The specifics for the MFC suspensions investigated in earlier publications are detailed in the respective chapters, yet, the general process was the same in all cases (see, for example, sections 4.1.1.1 or 6.1 for more information).

The following sections describe the different manufacturing processes to transform a pulp suspension in MFC suspensions of different grades (Figure 4.1).



Figure 4.1: Photograph of the feed material (eucalyptus pulp), medium fibrillated- and highly fibrillated MFC suspension (left to right). All suspensions are at 2 wt% solids content.

4.1.1.1 Medium DoF MFC

Bleached eucalyptus pulp was chosen as the feed material for MFC manufacturing. The material was available in dry mats and all used material was from the same bale. So, a constant feed material quality is assured throughout this work. A grinding process using the Supermasscolloider (Figure 4.2) was chosen for manufacturing the MFC (see paragraph 2.2.1.1). The advantage of this process is the ability to produce at comparatively high solids contents, and the good practical handling at lab scale. Even though described in publications frequently (Josset et al. 2014; Kangas et al. 2014; Nogi et al. 2009; Subramanian et al. 2008), potential practical challenges in the manufacturing process are not mentioned. In order to achieve fibrillation at all, the grinding stones have to be in contact (typically referred as to *contact mode*, or to have a *negative gap setting* in practice). The suspension is forced through the grinding stones (upper is static, lower is rotating, see Figure 4.2) only by centrifugal force, typically in a batch mode. The resulting flow- or processing rate is then a combination of mainly the rpm of the rotating stone, the pressure on the stones and the suspension solids content. A typically chosen rotor speed is $1\,500\text{ min}^{-1}$ (rpm), yet, from own experience, it is believed that lower rotor speeds achieve a higher degree of fibrillation per pass (not supported by conclusive data though). For the settings chosen by this work, i.e. a gap of $-50\text{ }\mu\text{m}$ (that is rather low pressure, but increased the lifetime of the grinding stones significantly) and a solids content of 3 wt%, the residual time of the suspension in the feed hopper can be several minutes to hours per batch. As the starting material is unrefined pulp at 3 wt%, it has a strong tendency to

dewater, i.e. the suspension becomes filtrated in front of the grinding stones. So, if the residence time of the suspension in the hopper is too large because of low rpms of the rotor, the suspension becomes upconcentrated and ultimately will not pass anymore through the grinding stones. With an increasing degree of fibrillation, the water holding capacity of the pulp/MFC increases (Hii et al. 2012), so the suspension becomes more homogeneous, i.e. has a lesser tendency to dewater. Taking those effects into account, a rather unique process (not reported by anybody else to my knowledge) was developed that ensures practicability, stable runnability, reduced wear of grinding stones and process economy (with respect to manufacturing time and energy). In the beginning of the process, where dewatering is more severe, the rpm of the rotor is kept high, and then with progressing fibrillation and therefore a reduction in the dewatering tendency, the rpms are lowered progressively with the amount of passages to increase the fibrillation efficiency without risking to upconcentrate the suspension too much. The actual rotational speed sequence chosen for this work was 5 passes at 2 500 rpm, followed by two passes for each of the following speeds: 2 000, 1 500, 1 000, 750 and 500 rpm. The model used was a MKCA 6-2 grinder equipped with type E 46# grinding stones (all from Masuko Sangyo Co., Ltd., Japan).

During the initial phase of the work, it was recognised that the grinding efficiency can vary rather significantly, already from one batch to the next (see chapter 6.1 for more information on the learning process). No detailed study was carried out to investigate the reason behind this, yet some factors that may contribute to this variation may be: changing wear status of the grinding stones, no temperature control of the system and the *negative gap* setting is a rather inaccurate setting when actually the pressure on the stones is the critical parameter.

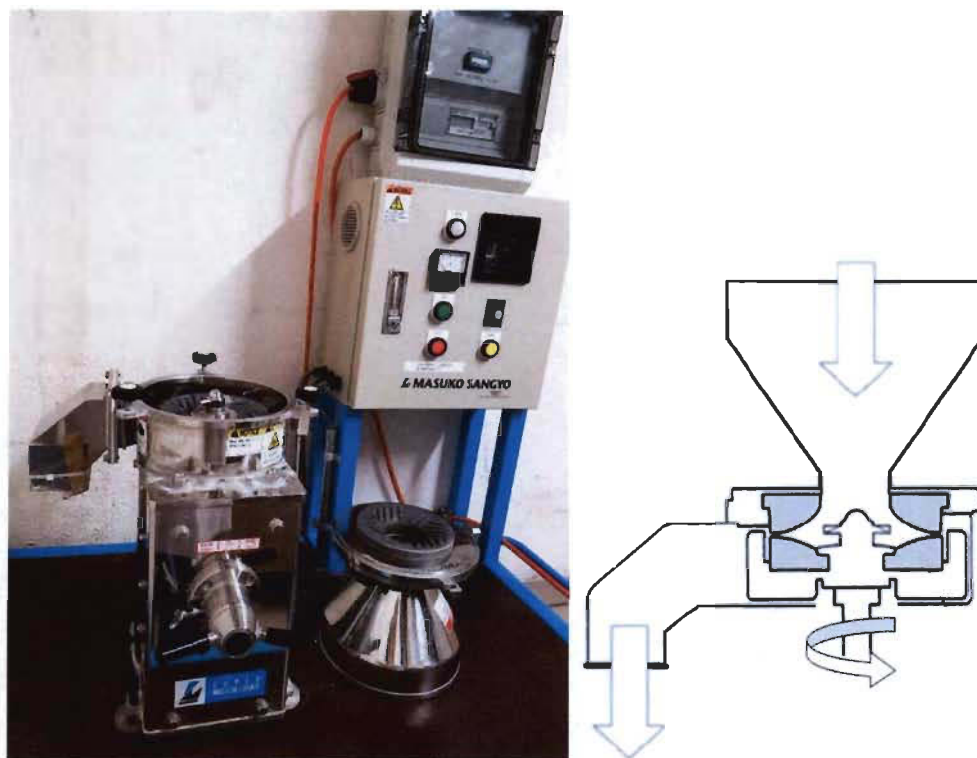


Figure 4.2: Photograph of the MKCA 6-2 Supermasscolloider used for the MFC manufacturing (left) and a schematic of the grinding stone (grey), feed system (hopper) and outlet system (right).

To have a consistent MFC suspension quality throughout the rest of the work, enough material was manufactured to not run out of it during the experimental studies. Therefore, 5 batches with 10 kg each were manufactured and mixed together after production. The final solids content was 3.2 wt%, and the average specific energy input (total electrical energy consumption normalised with dry amount MFC) was 7.2 MWh^{-1} .

4.1.1.2 High DoF MFC (H-MFC)

To achieve a higher degree of fibrillation MFC (H-MFC), an additional fibrillation process was employed to a part of the standard MFC. Here, a homogeniser based process was chosen, as it is thought to be a more efficient fibrillation process for higher DoFs. An NS 2006 L homogeniser (Niro Soavi) with a maximal pump capacity of $30 \text{ dm}^3\text{h}^{-1}$ was used (Figure 4.3). However, instead of the standard impact plate and ring type of

homogenisation chamber, an LPN60 module (Serendip AG, now Netzsch) was mounted. The principle of this module is that shear forces are introduced to the suspension in a small nozzle, and the generation of a large pressure drop between before and after the nozzle, that may lead also to cavitation. The typical operation pressure is 60 MPa, and it is achieved by the flow rate, the nozzle diameter and the back pressure that can be applied at the material outlet. For this type of homogeniser, two nozzle types with diameters of 80 and 120 μm can be used. It is known that homogeniser systems (independent of the homogenisation module type) of that size are prone to be clogged by inhomogeneous suspensions. It is therefore typical, that suspensions are diluted to very low solids, or to pre-refine the suspension in order to reduce the risk of clogging. As one of the goals of this work was to investigate MFC suspensions also at increased solids contents, too much of a dilution was not a viable option. Also, an additional up-concentration step would have added another unknown variable (e.g. by eliminating some fibril fractions or induced aggregation etc.). Therefore, the medium DoF MFC was subjected to another pass through the Supermasscolloider at -80 μm and 500 rpm, and was then diluted to 2 wt%. This suspension was then passed through the homogeniser in single passes, for ten passes with the 120 μm nozzle and two passes with the 80 μm nozzle. The pump speed was set to the maximum (30 dm^3h^{-1}), and the pressure was adjusted to 60 MPa using the back pressure screw for all passes. This process (including the additional Supermasscolloider pass) added additional 20.7 MWh^{-1} of specific process energy.

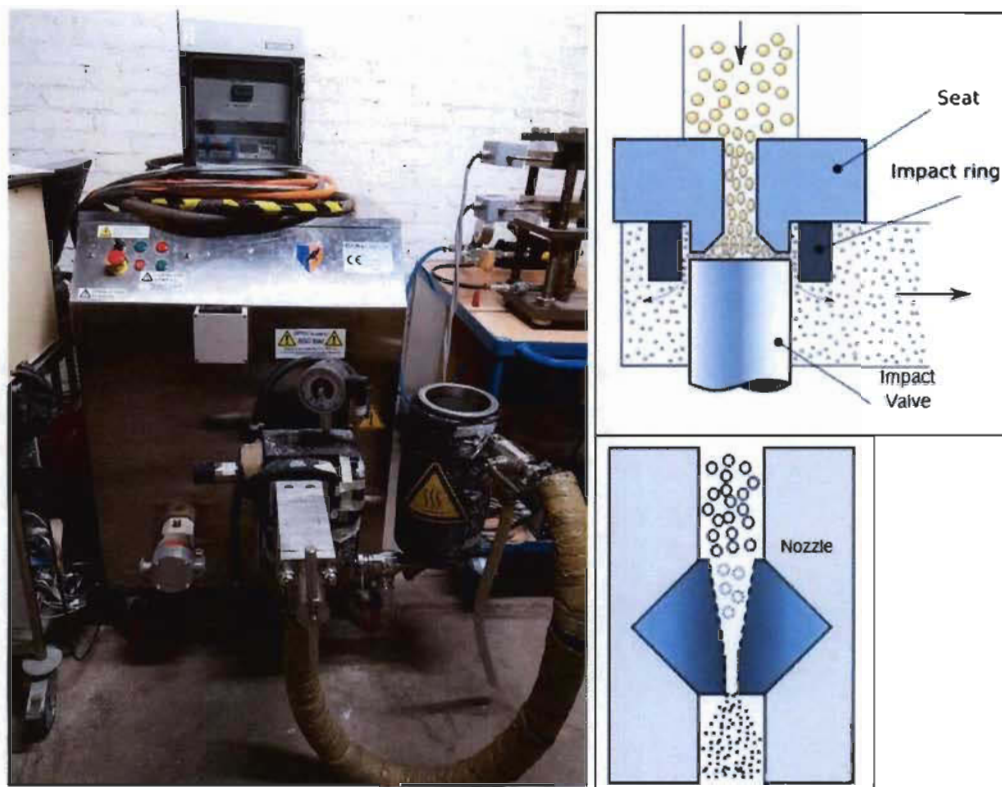


Figure 4.3: Photograph of the homogeniser used to manufacture the H-MFC (left) and schematics of the classical impact ring/-plate homogenisation setup (top right) and the here used nozzle setup (bottom right).

4.2 Methods

The following sections provide an overview on characterisation techniques used in this work and so obtained data. Details on specific aspects of certain techniques or evaluation methods can be found directly in the respective publication sections.

4.2.1 Rheology

All the rheological measurements performed in this work were carried out on an MCR 300 shear-rheometer from Anton Paar (Figure 4.4). A temperature controlled mount (TEZ 150P) is installed to house the different Couette-type measurement systems cups. The temperature control consists of a built in Peltier element for heating and a constant cooling loop, realised by an external thermostat (ministate 230, Huber). All the experiments were carried out at $20 (\pm 0.1) ^\circ\text{C}$, whereas the external thermostat set temperature was fixed at

15 °C. Please note that only the cup temperature is actively controlled and maintained, not the bob. Due to the relatively large amount of sample volume (compared, for example, to plate or cone setups) and the low measurement temperature, no special precautions were taken to reduce or prevent water evaporation from the measured suspension.

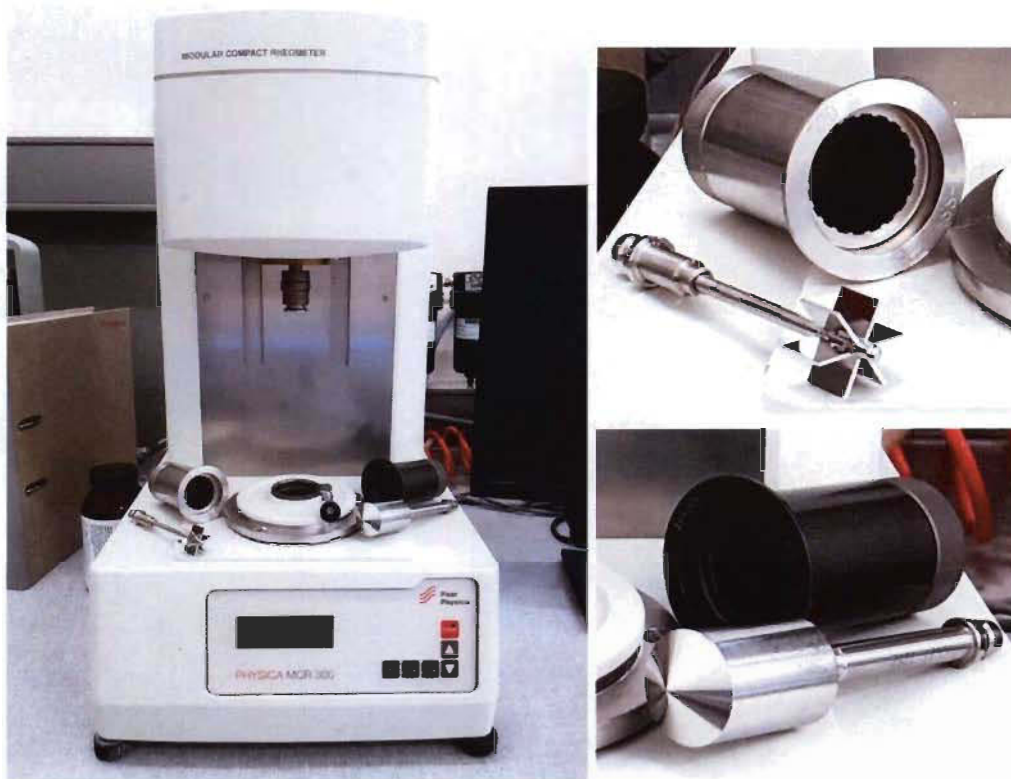


Figure 4.4: Photograph of the used MCR 300 rheometer (left) and the vane with serrated cup (top right) and the smooth CC27 (bottom right) measurement setup.

The selection of different measurement setups was limited to Couette-type systems (cylinder- or vane in cup). On the one hand, those set-ups have practical advantages compared to e.g. cone-plate or plate-plate systems, like lesser tendency for solvent evaporation and no issues with sample spillage for low viscosity materials and/or high shear rates (Mezger 2014). On the other hand, several researchers (Naderi and Lindström 2015; Nazari et al. 2016; Saarinen et al. 2009) have recommended the use of Couette type setups, as they have shown that cone-plate and plate-plate may promote (additional)

nonlinear effects in MFC suspension, leading to potential measurement artefacts. Details in the used measurement system components can be found in Table 4.1 or in the respective publications. All of the systems were used as supplied by Anton Paar, except for the roughened CC27 cup and bob. As described in section 7.4.3, a 100-grit abrasive sandpaper was used to roughen the surface of a smooth CC27 system. However, the roughening procedure lead to a wavy (circumferential grooves), rather than a randomly rough surface (Figure 4.5). The calculated waviness was $1.8 \pm 0.3 \mu\text{m}$.

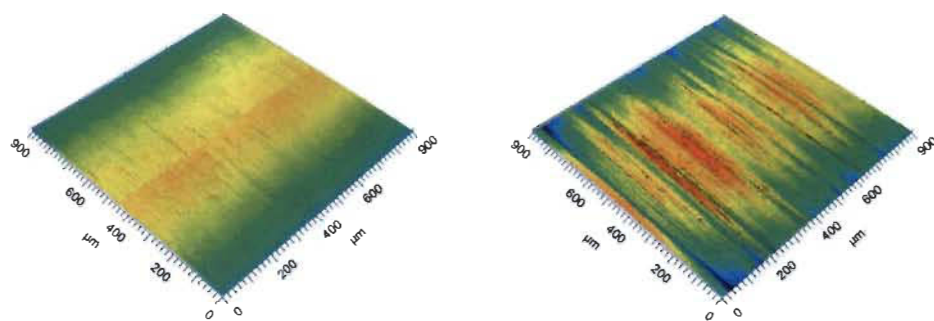


Figure 4.5: Confocal laser scanning microscopy images of a smooth (left) and roughened (right) CC27 bob.

The reason for using different measurement geometries, and comparing rheological properties that were measured with those different geometries, was the topic of the article presented in Chapter 7 - .

Table 4.1: Details of measurement system components used in this work. *Inner diameter for cups, outer diameter for bobs.

System element	Condition	Type	Diameter (mm)*	Abbreviation
Cup	Smooth	CC27	28.92	CC27
Bob	Smooth	CC27	26.66	CC27
Cup	Roughened	CC27	28.92	RR
Bob	Roughened	CC27	26.66	RR
Cup	Smooth	CC17	18.08	CC17
Bob	Smooth	CC17	16.66	CC17
Serrated Cup	Serrated (length profiled)	CC27-SS-P	28.88	S
Vane	6-bladed	ST-6V-16	22	V

4.2.1.1 Sample preparation

Respective amounts of pulp, MFC or H-MFC (and mixtures thereof) were diluted to the desired solids content (typically 0.5, 1, 1.5 and 2 wt%, but also 0.1 and 3 wt%) by adding tap water and a thorough mixing procedure. First, the diluted suspensions were treated with a rotor stator mixer (Polytron PT 3000, Kinematica) at $12\,000\text{ min}^{-1}$ for 2 minutes and put into an ultrasonication bath for 5 minutes. The suspensions were then let to rest for at least one hour before being measured. Directly before loading it to the measurement cell, the suspensions were shaken by hand. To ensure a thorough dispersion of all dilutions made from the stock MFC suspensions, the size per batch of a dilution was limited, mainly due to the size of the available rotor stator mixer. Typically, 250 or 500 cm³ plastic bottles were used and filled with 230, respectively 450 g of final suspension.

4.2.1.2 Viscoelasticity

As explained in section 2.4.2.4, oscillation experiments can be carried out to investigate a material's viscoelastic behaviour. The material's response to an oscillating movement is measured, typically either fixing the oscillation frequency and changing the amplitude, or

vice versa. In this work, the behaviour in dependence of strain, respectively stress was of interest, therefore, amplitude sweeps were performed. A frequency sweep was still performed, in order to define a suitable frequency for the amplitude sweep. A 1 wt% MFC suspension was measured with a CC27 setup, at a fixed amplitude of 0.1 % and by 50 log-equidistantly distributed point measurements (automated acquisition time) from 0.01 to 100 Hz. Figure 4.6 shows the storage-, loss modulus as well as the phase angle in dependence of the angular frequency. Please note that the x -axis is not in Hz, as the setting indicated above, but is presented like this for a better comparability with data from other work. It is apparent, that the storage modulus is increasing with the oscillation frequency whereas the loss modulus goes through a small local minimum before increasing again. This behaviour is typical and well reported by others (Charani et al. 2013; Taheri and Samyn 2016; Veen et al. 2015). The phase angle is rather stable in an extended frequency range, and so the frequency for amplitude sweep measurements was chosen to be about in the middle of this plateau (dotted line at 0.5 Hz, or 0.314 rads^{-1}). No further measurements at, for example, different solids contents and MFC types were carried out because the data of others (Charani et al. 2013; Taheri and Samyn 2016; Veen et al. 2015) indicate no changes to this general behaviour for different solids contents or DoFs.

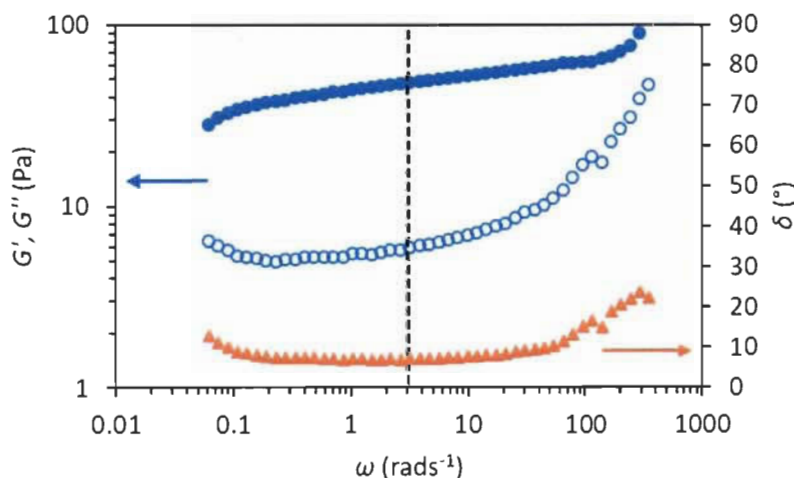


Figure 4.6: Storage (full circles) and loss modulus (hollow circles) data, as well as phase angle (full triangles) data of a frequency sweep experiment of a 1 wt% MFC suspension, measured with a CC27 geometry.

The general settings for amplitude sweep measurements was set to be 0.5 Hz, 60 log-equidistantly distributed amplitude values between 0.001 and 1 000 % with automated acquisition time mode and amplitude control (as opposed to shear stress control). Typical examples of amplitude sweep graphs are given in Figure 4.7 (1 wt% H-MFC suspension measured with VS system). In order to be able to quantitatively compare such data, properties and characteristic numbers have to be extracted. Details on these procedures are described in section 7.4.3. But in short, the maximal storage (G'_{\max}) and linear loss modulus (G''_{lin}), the minimal phase angle (δ_{\min}), the yield stress (τ_y) and the limit of linearity (*LoL*) were calculated. Both moduli properties (and therefore also the phase angle) describe the material behavior in the quasi linear viscoelastic regime, where the elastic part of the structure predominantly remains intact. The yield stress and the limit of linearity describe the onset of the structure breakdown, in terms of strain and stress respectively. Traditionally, those properties are derived from the onset of the decrease in the storage (=elastic) modulus of a material. However, in this work, the shear stress and the *LoL* were derived from the phase angle data to also take into account the inherent viscous behavior of MFC suspensions. In this work, the yield point was defined to be where the phase angle exceeded the minimal phase angle by 5 %, being a modified approach compared to the one used by (Moberg and Rigdahl 2012) where the *LoL* was defined as 90 % of the maximal storage modulus. The shear stress at the yield point was defined as the apparent yield stress, and the corresponding deformation to be the *LoL*. More detailed explanations on the viscoelastic properties can be found in section 7.4.3.

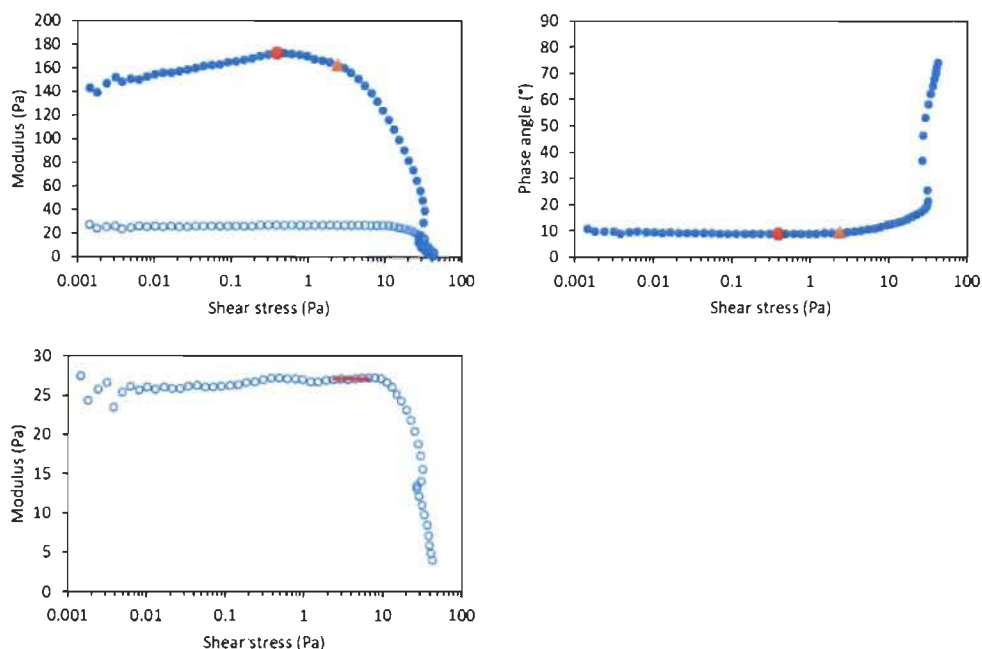


Figure 4.7: Storage-(full circles) and loss modulus (hollow circles) data (top and bottom left graphs) and phase angle data (top right graph) of a 1 wt% H-MFC suspension, measured with a VS geometry. The red points mark G'_{\max} , (top left) respectively δ_{\min} (top right), and the orange triangles mark the yield points (95 % of G'_{\max} , or 105 % of δ_{\min}). The bottom left graph shows the loss modulus only for better visibility, including the fit of the apparent linear region to determine G''_{lin} .

4.2.1.3 Flow curves

This section gives a brief overview on the complex flow curves typically measured for MFC suspensions and serves as a basis to explain the measurement settings that were chosen in this work. Also, the different flow curve properties and characteristics that help quantify the flow curve data are explained briefly. A detailed discussion of all the above-mentioned topics can be found in the respective articles (Chapter 7 - and Chapter 8 -).

In the beginning of this work, flow curves were measured with 30 equidistantly distributed points between 0 (effectively 0.1) and 1 000 s^{-1} , directly followed by the same sweep in reversed order (1 000 to 0.1 s^{-1}) with a fixed acquisition time of 10 s per point. A pre-shearing and rest interval were part of the procedure, as well as the repetition of the shear

rate sweep for a total of three times (details in section 5.4.1.5). However, after some more experimental work, and considering procedures described in the literature, the experimental conditions were changed. To begin with, the shear rate profile was changed to a log-equidistant distribution. The reason for this is well visualised in Figure 4.8, where a typical flow curve of a 1 wt% MFC suspension is shown (measured with a CC27 system). The triangles show the data that was obtained using a linear shear rate profile (data taken from Chapter 5 -) and the circles show data from a log-distributed profile (data taken from Chapter 7 -). The general offset between the two curves is most probably caused because the MFC was from two different batches (see section 4.1.1.1 for explanation). Otherwise, the trends are very alike. Yet, the assessment of the low to medium shear rate range (0.01 to 100 s^{-1}) reveals a behaviour that is overlooked completely by using the linear profile. So, it was rather obvious to change to the log distributed shear rate profile.

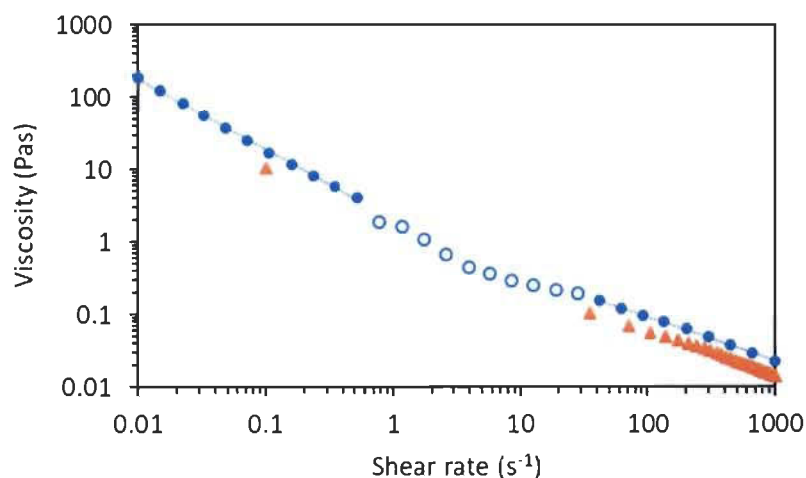


Figure 4.8: Comparison of flow curves obtained by different measurement protocols, i.e. log distributed shear rates (blue circles) and linearly distributed shear rates (orange triangles). The hollow circles indicate the transition region, only visualised by the log distributed shear rate protocol.

Details on the hypothesis of the morphological model for this three-zone behaviour can be found in Chapter 7 - , but in short, an aggregation of the MFC fibrils and formation of

water rich voids is likely to happen in the transition zone. By monitoring the viscosity acquisition times as defined by the software (upon reaching a stable viscosity value), it is apparently possible to visualise this transformation very well (Figure 4.9). The apparent start and end of the transition zone is sometimes shifted a bit compared to the indication from the acquisition time data (e.g. well visible in Figure 4.9 on the right graphs for the end of the transition). But in all cases, the acquisition time data is more conservative, compared to the apparent limits (i.e. indicates a lower shear rate for the start of the transition and a higher shear rate for the end of the transition). But it was also found, that the fit correlations for the two power law regions were typically better if done up to or from the shear rates indicated by the acquisition time data (see later or Chapter 7 -). Otherwise, this changed acquisition time setting does not seem to have any other impact on the flow curve (more information can be found in Chapter 6 -). So, the usefulness of these additional data has been shown, and therefore the automated acquisition time setting was kept from this point on.

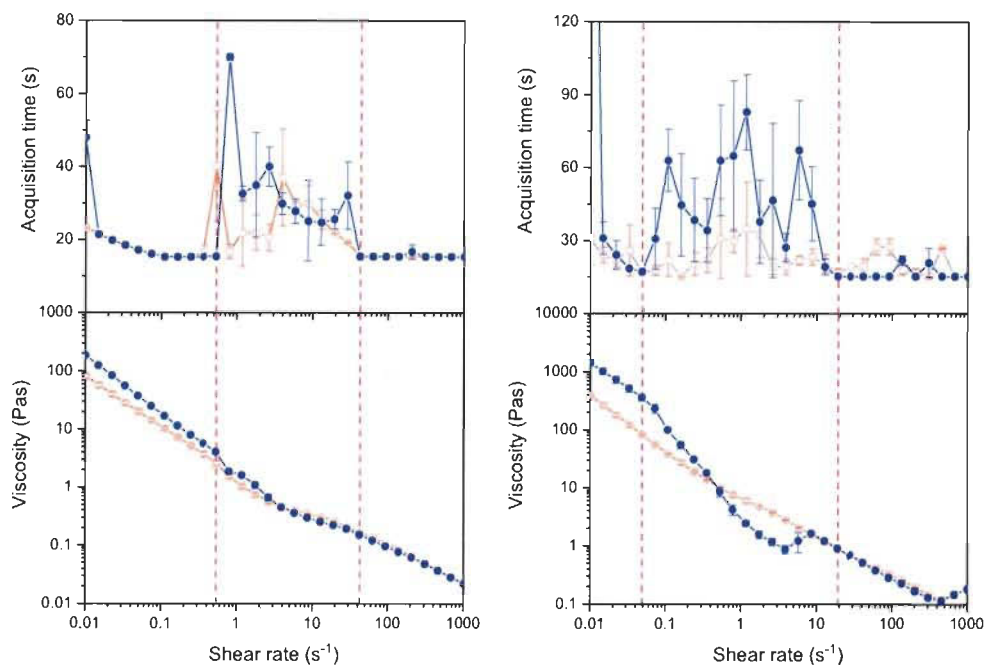


Figure 4.9: Stacked diagram of acquisition time and viscosity data in dependence of shear rate for a 1 wt% MFC suspension measured with the CC27 (left) and VS system (right). Blue circle points are from the shear rate increasing sweep and hollow orange square points are from the shear rate decreasing sweep. The red dashed lines indicate the shear rates before and after the transition as identified by the acquisition time data.

On the basis of flow curves looking like the ones presented in Figure 4.9 or, for example, Figure 7.15, they were divided in three regions, i.e. two power law following, apparent shear thinning zones 1 and 2, divided by the transition region. Each region is described by different properties and descriptors. This enables a quantitative comparison of different flow curves. Zone 1 and 2 (Figure 7.2) are described by their power law coefficients, i.e. the *consistency coefficient* (K) and the *flow index* (n), a characteristic viscosity that is calculated from those parameters at ad hoc defined shear rates ($\eta_{0.02}$ in zone 1 at 0.02 s^{-1} and η_{100} in zone 2 at 100 s^{-1}) and finally the end of zone 1 and the start of zone 2. The consistency coefficient describes the overall viscosity level and the flow index the shear thinning behaviour. Technically, the calculated viscosity values at 0.02 and 100 s^{-1} do not

add any additional information, however, MFC suspensions are frequently characterised by specific viscosity values, and so a certain, limited comparability is provided.

The transition region is of course already defined by the end of zone 1 and the start of zone 2, but in addition the local viscosity minimum is described in terms of depths and position. As mentioned earlier in this section, the transition zone is believed to be a formation of fibril aggregates and water rich voids. So, the depths can probably be linked to the extent that the suspension fibrils aggregate, respectively to how much water can be released and how well the aggregates can be surrounded thereby.

4.2.2 Data treatment and presentation

4.2.2.1 Data treatment

If not mentioned otherwise, all data presented in this work is based on triplicate measurements. Every single measurement within a triplicate was a new filling from a respective dilution makedown, as opposed to, for example, measuring one filling three times. This was done to avoid measuring a suspension that may have had a persisting changed morphology from a preceding measurement. As indicated in the sample preparation section (4.2.1.1), the amount of a given dilution that was made down from the stock MFC suspensions was limited, so typically several makedowns of a given dilution were necessary to carry out all rheological measurements. In the study presented in Chapter 8 - , this was even done intentionally, i.e. three separate makedowns for each tested dilution were made, and each makedown was measured three times. Additional control measurements were performed regularly, to ensure comparability between individual makedowns of a given mixture and solids content. Such measurements also confirmed that the MFC stock suspensions didn't change over time. Details of every single filling and makedown that was measured are recorded in respective protocols.

Except for the study presented in Chapter 8 - , the three individual measurements of a triplicate were first combined into one curve, i.e. the data of the three measurements at each shear rate, respectively amplitude was averaged to get one average set of data for the triplicate. This was then used to carry out the property determination described in the preceding sections.

As explained earlier, zone 1 and 2 were described i.a. by a power law describing the relationship between viscosity and shear rate, according to

$$\eta = K\dot{\gamma}^{n-1}$$

Equation 4.1

with η being the viscosity, K the consistency coefficient, $\dot{\gamma}$ the shear rate and n the flow index (further details can be found in section 7.4.3). Origin 2017 software was used to automatically fit the data (viscosity depending on shear rate). No weighting or parameter restrictions were applied. Generally, the datapoints that were used for the fit were selected using the information from the automated acquisition time data. Fits were only performed if at least 3 datapoints were available.

For certain data sets, statistical methods were employed to determine whether datasets were significantly different from each other or not. To do this, ANOVA (analysis of variance) tests were performed. Again, an automated method in the Origin 2017 software was used. As this test is intended only for normally distributed data, a built-in normality test (Shapiro-Wilk, $\alpha = 0.05$) was performed first. The ANOVA test probes the null hypothesis H_0 , that is that all means are the same at a chosen significance level α (that was 0.05 in all tests in this work). The significance level is the chance, that the test results in declining H_0 , even though it would be true. In some cases, also the test power β was evaluated, which is the likelihood that the test correctly rejects H_0 . Finally, also the strength of effect was determined by the software. Those additional parameters help to interpret the ANOVA test results as they are ratings for the reliability and “robustness” (in addition to α). If the software identified significant differences in a dataset, also a pair wise test was performed (Tukey test, $\alpha = 0.05$) to identify the different mean-pairs.

Some data obtained in this work was non-continuous, and so the ANOVA test should not be used. In this case, a non-parametric test was used instead (Kruskal-Wallis). The test was performed using Excel software, following the procedures described in (Chan and Walmsley 1997). More details on the statistical tests can be found specifically in Chapter 8 - .

4.2.2.2 Introduction to ternary diagrams

The extensive study on the influence of the DoF of MFC suspensions on their rheological properties (published in the article presented in Chapter 9 -) consisted also of binary and ternary mixtures of pulp, MFC and H-MFC suspensions. The total suspension solids content was kept at 0.5, 1, 1.5 and 2 wt% respectively, and the relative amounts of the single components were varied. Figure 4.10 shows the full matrix of mixtures that were manufactured at a given solids (blue circles), and the additional mixtures at 1.5 wt% (red triangles). Please note, that for solids below 2 wt%, several mixtures with a high pulp share were not manufactured or measured because of strong sedimentation that would have interfered with the rheological measurements.

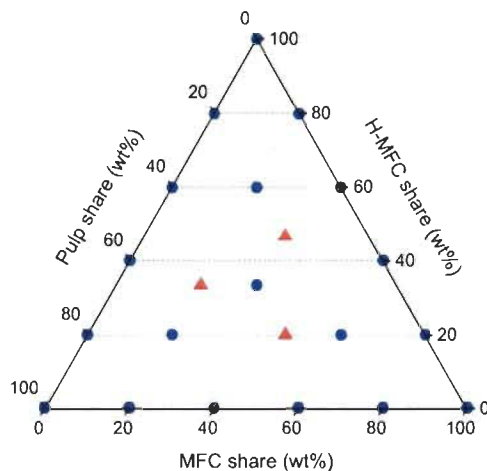


Figure 4.10: Ternary diagram of the planned mixtures for each of the total suspension solids contents (0.5, 1, 1.5 and 2 wt%) (blue circles) and the additional mixtures for 1.5 wt% total suspension solids content. Please note, that not all of these mixtures were realised in the actual study (especially for increasing pulp shares at decreasing solids content).

The concept of ternary diagrams may not be familiar to everyone, so this short introduction should help to understand them. Ternary mixture diagrams are used to visualise mixtures consisting of up to three components, whereas the sum of all three components has to be 100 % (or 1 when talking in terms of shares). So, this concept only

works when the total composition is the same for all mixtures displayed (in terms of, for example, volume, weight or number). In this work, and this particular experimental study, the mixtures were grouped in different solids content. So, all mixtures having the same solids content can be visualised in one ternary diagram. The property of interest can then be visualised for example as (colour) contour plot (like contour lines on a geographical map) or as a 3D plot with having the property as the z (height) value.

The general read out of such diagrams in terms of mixture composition is indicated in the left graph in Figure 4.11. Each vertex of the triangle represents 100 % of one component, and becomes less along the median until this component reached 0% at the opposing side. Note that constant shares of a component are lines that are parallel to their 0 wt% side (that is the side to the right of the respective component's scale side). In practice, the composition at a given point in the ternary diagram can be read out by drawing lines that are intersecting the point and parallel to the left side of the component of interest, as indicated in the right graph of Figure 4.11. Please note, that, if the scales are reversed (100 \rightarrow 0 %), then it would be lines parallel to the right side of the component of interest.

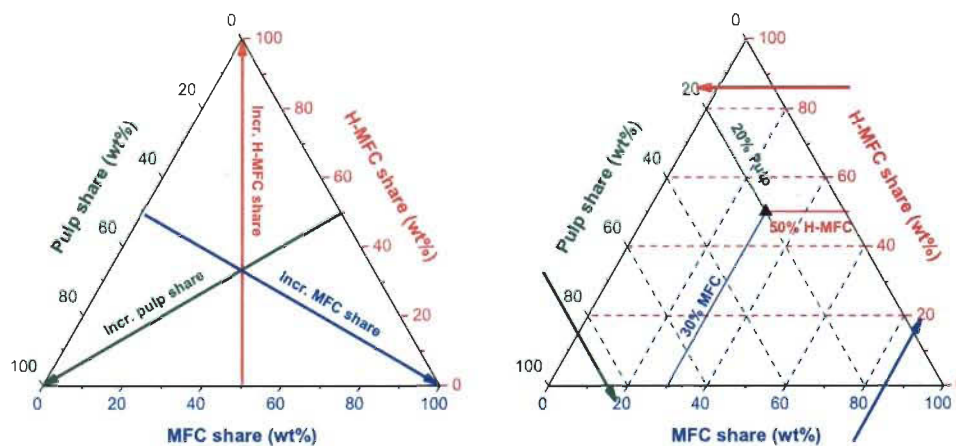


Figure 4.11: Example ternary diagrams with indications of general composition trends (left) and an example composition (30% MFC, 50% H-MFC and 20% pulp) with a visual read out guide.

Figure 4.12 shows some examples of how a final ternary contour plot could look for an arbitrary property, displayed as color contour profile in dependence of the mixture

composition. In this case, purple represents low values and red high values, following a rainbow scale. The solid lines within the plot are contour lines (lines of equal property values) and act only as additional visual guidelines. Those contour plots, or 3D versions of them can be used to qualitatively identify general trends. For instance, the left graph in Figure 4.12 indicates, that the property is only depending on the pulp share, i.e. decreases with increasing pulp share. This is apparent, because the contour lines follow the grid lines for constant pulp shares (left graph of Figure 4.11). In the case of the middle graph in Figure 4.12, all components seem to contribute to the property, yet still it appears that pulp is the weakest and H-MFC is the strongest contributor to the property. The overall trend in the right graph of Figure 4.12 is the same, yet, as the contour lines are closer to the grid lines for a constant H-MFC share, it can be assumed, that the H-MFC defines the property more strongly than the other components. Also, the shape and distance between contour lines can provide additional, qualitative information on potential trends.

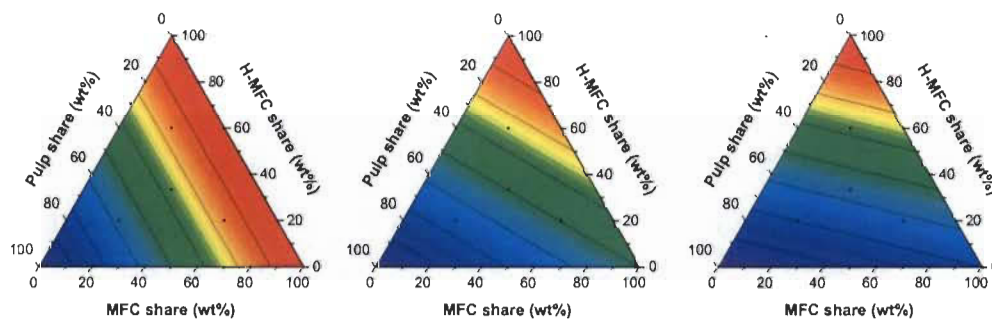


Figure 4.12: Example ternary contour plots with simulated property data. The linear scale is arbitrary, only indicating property values from low to high (purple to red), visualising different model trends. Left graph: property is only depending on pulp share (decreasing with increasing pulp share), middle graph: property is depending on all component shares, right graph: like middle graph, but the H-MFC share dependency is stronger compared to the other ones.

4.2.3 Particle size distribution analysis

Based on the argumentation provided in section 2.4.2.3, image analysis of optical and scanning electron micrographs was investigated to obtain a fibre/fibril width distribution. However, various attempts have failed, either because the images were not suitable for

image analysis, or the obtained fibril width distributions were apparently not representative. A detailed explanation can be found in the supporting information of Chapter 9 - .

Chapter 5 - Article 1: Rheological investigation of complex micro and nanofibrillated cellulose (MNFC) suspensions: discussion of flow curves and gel stability

Published article.

Michel Schenker, Joachim Schoelkopf, Patrice Mangin, Patrick Gane; Tappi Journal; 2016; 15(6); 405-416

5.1 Foreword

This article published the initial experimental work of this thesis. The aim of this part of the work was to explore the relevant boundary conditions of the material space parameters (section 3.1.1). The focus of the work was, therefore, put on measuring rheological properties of MNFC suspensions with changing the following parameters: solids content of the MNFC, degree of fibrillation, pigment to MNFC ratio and the influence of addition of CMC. Finally, also the effect of fixing the CMC on a pigment was investigated, as well as the effect of reducing the charge of such a CMC coated pigment. As will be shown in the following sections, this initial work enabled the creation of a hypothesis regarding the suspension morphologies depending on the different suspension composition parameters as well as on the shear condition. It was based and critically discussed with view on other researcher's work and hypotheses in the field of rheology of nanocelluloses.

5.2 Abstract

Micro and nanofibrillated cellulose in aqueous suspension presents many challenges when considering its use, for example, in forming nanocomposites. The inclusion of filler particles either as extender or as functional additive allows the range of strength and deformation properties to be extended. These properties, however, are linked in many cases to the rheological properties of the raw material mix. Interactions under dynamic shear or under controlled stress at low amplitude reveal the potential to generate functional interactions, not only between the cellulose components themselves but also between the cellulose, polymer additives, as well as surface modified pigment fillers. Examples are given demonstrating the action of adding cellulosic polymer in the form of carboxymethyl cellulose (CMC) to micro nanofibrillated cellulose (MNFC). Rheological studies show

how these combinations with CMC, added either in free form or preadsorbed onto calcium carbonate filler particles, leads to a variety of responses. Dispersability of the MNFC is increased by the use of free CMC polymer addition, and the usually expected flocculating action on added filler is seen not to occur. Alternatively, the preadsorbed CMC on the calcium carbonate pigment filler leads to an interaction between the fibrillar cellulose and the surface modified calcium carbonate pigment filler, to which incorporation of cationic polymer leads to a reduction of interaction, provided the addition level does not exceed the isoelectric point of the mix. The observations are viewed in the context of a combination of proposed physical contact dynamics in the form of disordered and ordered alignment.

5.2.1 Keywords

Micro- nanofibrillated cellulose, MNFC, rheology, flow curve, phase angle, pigment fillers, carboxymethyl cellulose

5.3 Introduction

Micro and nanofibrillated cellulose (MNFC) materials are very interesting for many different applications in various fields¹ due to their excellent mechanical and barrier properties². Even though these materials were reported already quite some time ago by Turbak, Snyder and Sandberg³, already pointing out the material's great potential in various applications, there are not yet well established, large, full scale applications of it. On the one hand, the originally very high energy consumption of the manufacturing process was a hindering factor to produce a cost efficient product. Intensive work has been carried out to overcome this hurdle, using different approaches like applying enzymatic⁴ or chemical pretreatments⁵, using alternative pulp sources⁶⁻⁸ or introducing grinding aids in the mechanical breakdown process^{9, 10}. These efforts led to the set-up of numerous pilot and (pre) commercial manufacturing plants for different kinds of MNFC products. On the other hand, the application of MNFC products in various applications remains challenging, especially on the large (industrial) scale where also economic factors come into play. One of the key factors that makes an application of MNFC in production challenging is the high water content and the strong associated interaction with water. In addition to the challenge of water removal, MNFC suspensions also show a complex, non-

Newtonian rheological behavior over a large span of shear rate- and time scales¹¹. The investigation of MNFC suspension rheology, and the influence of different material parameters on it, has, amongst others, two main benefits. Firstly, one is prepared for problems that may arise in large scale applications where different kinds of shear forces and shear rates may be introduced in MNFC, and MNFC containing, suspensions. Secondly, rheology allows the observer to hypothesise models describing the structure and interactions within MNFC suspensions, and subsequently to test these hypotheses accordingly. This in turn can be used, for instance, to predict potential shear force assisted dewatering^{12, 13}. This work investigates the influence of basic MNFC material parameters on the respective suspension rheological behavior, and thus set out to explain the effects seen using initially already proposed models by other reserachers^{14, 15} and then extending them suitably for application to as yet novel unreported effects.

A special focus is placed here on the effect of CMC and pigment particle addition on MNFC suspension rheology. A dry ground, chemical-free calcium carbonate was used as reference pigment particle filler. Furthermore, special surface modified pigment particle fillers, so-called pigment hydrocolloid hybrid pigments, were used as co-additives. CMC, and optionally additional polyDADMAC, is adsorbed on the pigment particle surface to form the pigment filler hydrocolloid hybrid. This localisation of CMC (and additional polyDADMAC) leads to previously unreported rheological changes in the MNFC suspension response, which in turn correlate with increased pigment filler-MNFC nanocomposite strength, previously reported in earlier work by the same authors⁹.

5.4 Experimental

5.4.1 Materials

5.4.1.1 Preparation of the Fillers

Two different types of pigment particle fillers were used, standard pigment filler and functional pigment filler, respectively: a fine, dry ground dispersant free calcium carbonate of marble source (fGCC), and functional surface modified calcium carbonate in the form of so-called filler pigment hydrocolloid hybrid (PHCH) in slurry suspension. The PHCH pigments are formed from dispersant free calcium carbonate, also of marble source,

that is surface modified by wet co-processing with 1.5 w/w% (based on dry pigment) carboxymethyl cellulose (CMC), either alone (PHCHa) or in the combination with 0.6 w/w% cationic polyDADMAC (PHCHb). To exclude potential filler particle size distribution (PSD) related effects on the composite suspension rheology, the particle size distribution (PSD) of the two filler types was carefully controlled to be closely similar (fGCC: volume based d_{50} of 1.7 μm , PHCHa and b: volume based d_{50} of 1.8 μm , measured by a static laser diffraction method, using a Mastersizer 2000 (Malvern Instruments Ltd., England)).

The CMC used had a degree of substitution of 0.8 and a molecular weight M_w of 60 kgmol^{-1} (Finnfix 10, CP Kelco, Finland) and the used polyDADMAC was Catiofast BP (BASF, Germany).

Surface charge of the pigments, manifest in the form of the zeta potential, was measured with a Zetasizer Nano ZS (Malvern Instruments Ltd., England) at 25 °C and a 0.1 w/w% solids content, using deionised water in a 10 mM NaCl salt solution for dilution. Three measurement runs were performed per sample with an automated determination of single point measurements per run using the Smoluchowski approximation to convert the electrophoretic mobility into zeta potential. The zeta potential for fGCC was -8.2 ± 0.9 mV, for PHCHa -33.7 ± 1.6 mV and for PHCHb -25.2 ± 0.8 mV.

5.4.1.2 Preparation of MNFC

Bleached eucalyptus pulp from a Swiss paper mill site (ex Sappi Biberist fine paper) in the form of once-dried mats was used as the cellulose basis material for all micro nanofibrillated (MNFC) products. Pulp lumps were mixed with tap water (45 ° fH) using a stirrer with a dissolver disc type of rotor for about 1 hour to have a pulp suspension of 3 w/w% consistency. This suspension was then run through an ultrafine friction Supermasscolloider MKCA 6-2 grinder equipped with type E 46# grinding stones (Masuko Sangyo Co., Ltd., Japan) at a contact/gap setting of “-50 μm ” in single passes. The following rotational speed sequence was used for the standard MNFC: 5 passes at 2 500 rpm, followed by two passes for each of the following speeds: 2 000, 1 500, 1 000, 750 and 500 rpm. Two additional passes at 500 rpm were conducted for a further “17 pass” MNFC and a contact/gap setting of “-80 μm ” with the standard rotational speed sequence form an “intensive treatment” MNFC.

It should be pointed out that the wear condition of the grinding stones of the ultrafine friction grinder can have a significant influence on the grinding efficiency. As a consequence, samples produced by the same procedure at different total operation times of the grinding stones may not be of the same degree of fibrillation. It is therefore important only to compare samples within a single manufacturing series, or samples from close manufacturing series, to ensure comparability. In this manner, relative comparison studies are still possible.

5.4.1.3 MNFC morphology

In order to assess the network structure of the fibrils in suspension, scanning electron microscopic (SEM) images of freeze dried MNFC suspensions were taken. The MNFC suspension was diluted to 0.5 w/w% using tap water and followed by rotor stator mixing (Polytron PT 3000, Kinematica AG, Switzerland) for 5 minutes. The suspension was then frozen by immersing it in liquid nitrogen and freeze dried (Alpha 1-2 LD Freeze Dryer, Martin Christ Gefriertrocknungsanlagen GmbH, Germany). A small piece was torn out of the dried structure and mounted on a support to be able to image the internal MNFC structure. The sample was sputtered with 50 nm gold before imaging using a LEO 435 VPi SEM (LEO Electron Microscopy Ltd, Cambridge, UK). Another sample was prepared where 5 w/w% (based on the cellulose dry content) CMC was added as 4 w/w% suspension (in tap water) to the MNFC suspension before dilution. The sample preparation otherwise was the same as described before.

5.4.1.4 Composite suspension preparation

The chosen amounts of additive components were added to the MNFC suspension, i.e. pigments as they were produced, freely added CMC as 4 w/w% solution in tap water and subsequently diluted further to the target solids content, defined in relation to the cellulose fraction only. The pigment ratios are thus based on the total dry amount of cellulose and pigment, and the CMC ratios are based on the addition in relation to cellulose dry amount only. For example, a sample at 2 w/w% dilution with 50 w/w% fGCC and 2 w/w% CMC is described as having the components added to 100 g of MNFC suspension, itself consisting of 2 g cellulose in 98 g water, in weight proportions of 2 g fGCC and 0.04 g CMC. This gives a total weight of 102.04 g, with a total solids content of 3.96 w/w%, but

a cellulose based solids content of 2 w/w% (2 g cellulose and 98 g water). This definition is chosen in order to keep the cellulose to water ratio constant throughout all samples, as the rheological behavior of MNFC suspensions is strongly depending on this ratio and the impact of adding the other components is then studied at constant MNFC levels. The additives alone do not exhibit a characteristic rheological behavior at such low relative ratios to water content. The samples then were stirred thoroughly using a stirrer with a dissolver disk type rotor at 750 min^{-1} for about 30 minutes.

5.4.1.5 Rheology measurements

All the rheological measurements were performed on an MCR 300 rheometer (Anton Paar GmbH, Austria) with a CC27 cylinder and cup geometry at 20°C . This measurement set-up was recommended by Saarinen *et al.*¹⁶. They also point out that wall slip (sometimes also referred to as lubrication flow), although likely to occur, will not dominate the rheological measurements. This statement requires qualification in practice as the colloidal stability of the mix certainly plays a dominating role, and can lead to phase separation with significant build-up of water at the boundary interface. However, as long as the system is continually sheared beyond the yield stress, the claim of Saarinen *et al.*¹⁶ can be supported. Although serrated surfaces in plate-plate geometry are frequently used to overcome wall-slip, they have been avoided here as they create non laminar flow close to the boundary¹⁷. The sample material was shaken before it was loaded to the measurement cell to avoid interim sedimentation of the suspension. In order to have the same shear-history for all the samples, a pre-conditioning was also performed before all measurements consisting of 2 minutes at 50 s^{-1} shear rate (rotation), followed by 5 minutes rest.

Flow curves of viscosity dependence on shear rate were obtained by performing a shear rate increase ramp (0 to $1\,000 \text{ s}^{-1}$ with 30 viscosity point measurements with 10 s per point measurement), followed by a shear rate decrease ramp ($1\,000$ to 0 s^{-1} with 30 viscosity point measurements at 10 s per point measurement). After 2 minutes rest, the same profile was applied again. In total three of these programs were applied, and the data of the two last shear rate increase ramps and all three decrease ramps were averaged to give the data for the ramp up and ramp down, respectively.

The flow curves provide information on the dynamic interaction of the suspension system as the structure is constantly in relative movement. Typically, strongly interacting systems including entanglements and attractive interactions exhibit higher viscosities due to the hindrance of relative movement of the involved entities. Systems having weak interactions or a collapsed structure typically exhibit low viscosities. Furthermore, systems with highly charged entities show low viscosities. The measurement of the viscosity as a function of decreasing shear rate gives further indicative information about the time dependence of recovery after a potential structural change.

In addition to dynamic shear, an oscillatory experiment was performed by fixing the frequency at 0.5 Hz and changing the oscillation amplitude (amplitude sweep). This was done by changing the response stress to the applied strain within the controlled region from 0.1 to 100 Pa with 50 point measurements made once a stable value reading was attained, followed by a controlled stress decrease ramp from 100 to 0.1 Pa, also with 50 point measurements.

The phase angle δ was chosen to be evaluated in more detail as it contains information on the relative effects of the elastic and gel-like structure and the viscous behavior of a viscoelastic material, as well as on the eventual breakdown of the gel-structure:

$$\delta = \tan^{-1} \frac{G''}{G'} \quad \text{Equation 5.1}$$

with G'' being the viscous loss modulus and G' being the elastic storage modulus, respectively. The advantage of using the phase angle is that it is a relative, normalised parameter compared with the absolute values of the moduli. The point of equality between the storage and loss moduli sometimes is referred to as the flow point¹⁷ and can easily be read out at $\delta = 45^\circ$. An amplitude sweep measurement can thus give a deeper insight into the ratio of the potential change from an elastic solid to a viscous liquid as a function of deformation leading to the resulting stress. It is recalled that, up to the point where the solid-like structure (also often referred to as gel structure) is broken down, the predominant interaction is of an elastic nature, i.e. existing bonds in the form of potential energy wells are not broken, so one can refer to it as a “static” structure, which can be contrasted to the purely dynamic situation in a flow curve experiment.

5.5 Results and Discussion

5.5.1 MNFC morphology

As can be seen in the SEM images in Figure 5.1a and b, the MNFC material is an entangled network of fibrils of different diameters. Whereas some individual fibrils of only some nanometers diameter can be seen, also larger fibrils and fibril aggregates are present. The overall network of the MNFC suspension (Figure 5.1) appears not to be completely homogeneous, as areas of higher and lower fibril density can be identified. The dispersing effect of CMC on MNFC fibrils and the resulting change of the suspension network are obvious when comparing Figure 5.1c and Figure 5.1a.

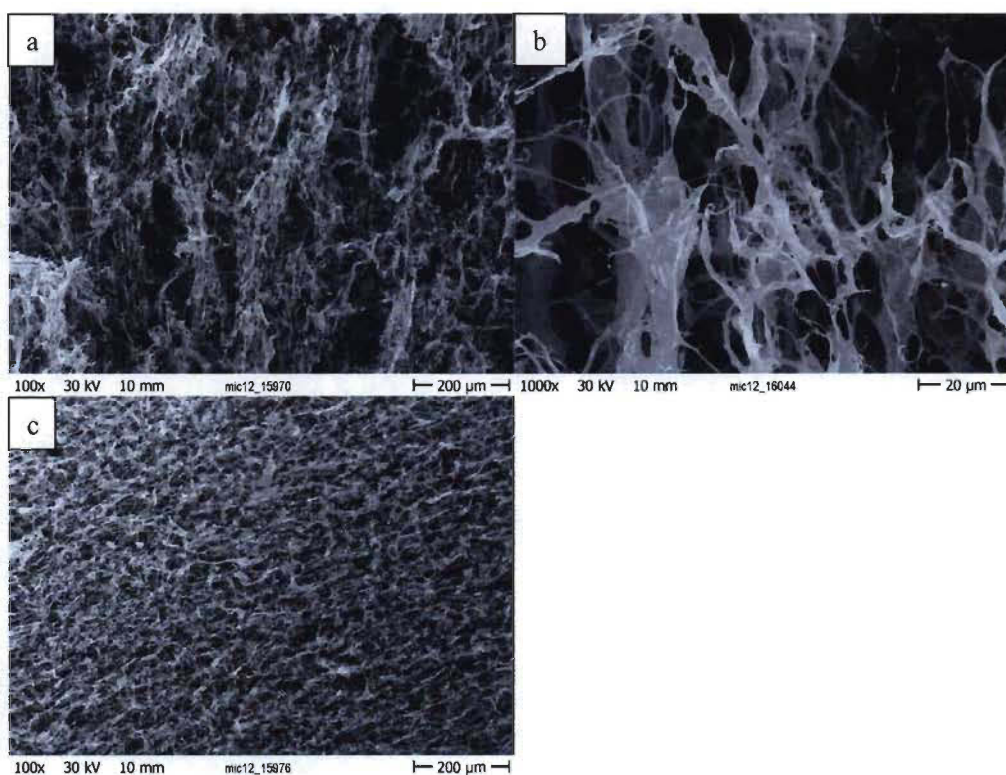


Figure 5.1: SEM images of freeze dried MNFC suspension (a, b) and MNFC + 5 w/w% CMC suspension (c).

5.5.2 Influence of solids content on MNFC rheology

Figure 5.2 shows the flow curves of the pure MNFC suspensions at different solids contents and of the tap water that was used to make the according dilutions. The well-

known shear thinning behavior of the MNFC suspensions^{3, 11, 18, 19} as well as the overall reduction of viscosity with decreasing solids content^{11, 19} are apparent. It also can be seen that if the dilution becomes too great, that the MNFC suspension exhibits the viscosity of water, indicating the loss of interaction between MNFC entities. Furthermore, one can clearly see the hysteresis between the shear rate increase and decrease ramps for the dilutions greater than 0.5 w/w%. This was also reported by Iotti *et al.*¹¹. However, by comparing the hysteresis of the 1 w/w% dilution with the ones from the 2 and 3 w/w% dilutions, a reverse of the hysteresis can be seen that was not reported by Iotti *et al.*¹¹. There also seems to be a trend that the hysteresis area becomes larger for higher solids contents, starting at 2 w/w%.

We hypothesise that shear leads to a structural change in the MNFC suspension with the two extreme conformations indicated in Figure 5.3 as highly entangled (low shear, Figure 5.1a) and highly oriented (high shear), and that these structures need a minimal recovery time, which is at least larger than the acquisition time for one measurement point, as also seen by Iotti *et al.*¹¹. In this way, we can interpret the predominant conformation in the shear rate increasing ramp as being the entangled one, whereas in the shear rate decreasing ramp it is the highly oriented one. In a more diluted system (low solids content (s.c.)), the high shear conformation leads to an overall reduced interaction, leading to a lower viscosity in the shear rate decreasing ramp at a given shear rate value. In the case of a less diluted system (high s.c.), however, the high shear conformation leads to an overall stronger interaction related to re-entanglement similarly compared with the low shear conformation, and therefore exhibits higher viscosity values at a given shear rate in the shear rate decreasing ramp. This model is generally in agreement with the one proposed by Horvath and Lindström¹⁴, and so their model can be used to identify the nature of the abovementioned interactions in the low shear conformation regime. In the case of low consistencies, the dominating interactions are of a colloidal nature, whereas in the case of high consistencies it is considered to be fiber interlocking.

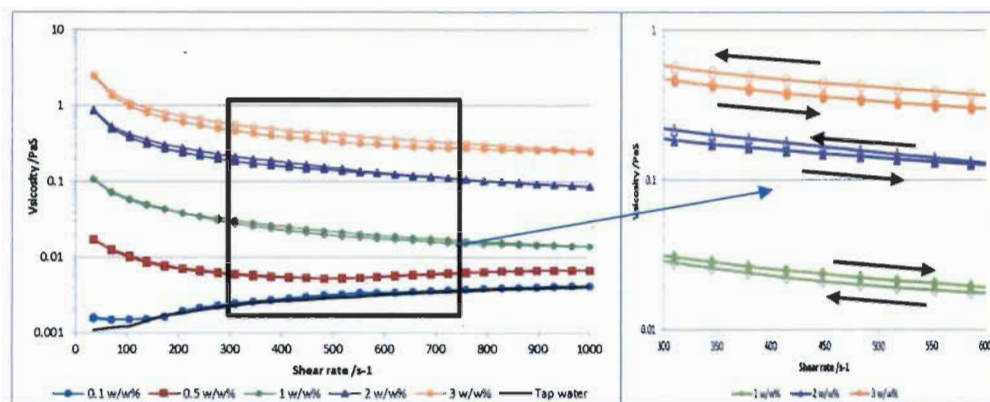


Figure 5.2: Flow curves of MNFC samples at different solids contents, and the tap water that was used to make the various dilutions. The filled symbols represent the measurement points of the shear rate increase ramp whereas the open symbols represent the measurement points of the shear rate decrease ramp. The extracted picture is the enlarged region indicated in the main plot, arrows indicating the shear rate increasing and decreasing ramps.

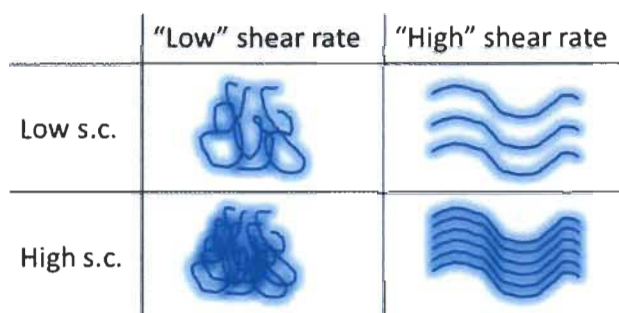


Figure 5.3: Schematic of the proposed conformations at high and low shear rate for higher and lower solids contents. The "halos" around the fibers indicate their interaction potential. At high enough solids concentration the aligned structure is suspected to transit into an entangled matrix, similar to the low shear rate state, but in this case induced by the forced proximity of the fibrils.

The amplitude sweep measurement shows that the yield point increases with increasing solids content of the MNFC suspension (Figure 5.4). It also seems that some secondary structure is formed temporarily as all curves show characteristic "shoulders" in the amplitude increase ramp.

It is not surprising that higher solids contents of MNFC suspensions lead to increased flow points as there are more cellulose entities that form interactional “bonds”, i.e. situated within a potential energy well, and therefore more force (shear stress) is required to break them. Again, also here, the observed data are in good agreement with the data presented by Horvath and Lindström¹⁴. Also note that the phase angle is the same (10°) for all solids contents before the gel structure breakdown.

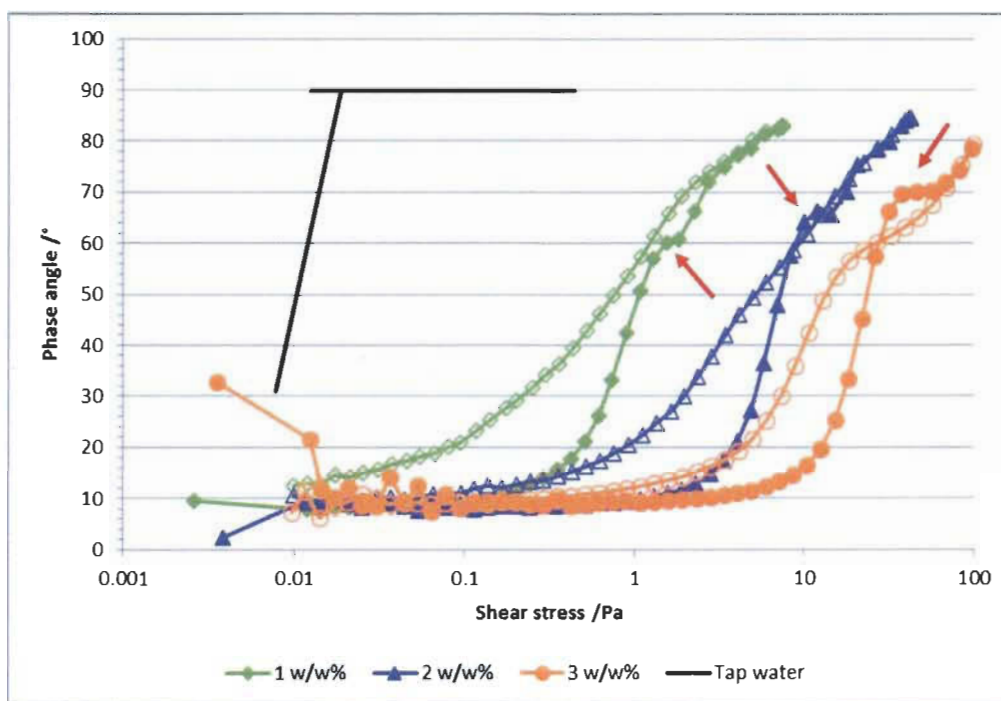


Figure 5.4: Amplitude sweep curves of MNFC samples at different solids contents, and the tap water that was used to make the different dilutions. The filled symbols represent the measurement points of the shear rate increase ramp whereas the open symbols represent the measurement points of the shear rate decrease ramp. The inconsistent starting phase angle is considered here to be an artefact of the measurement. The red arrows are marking the characteristic shoulders in the increasing shear stress ramp.

5.5.3 Influence of the degree of fibrillation on MNFC suspension rheology

As the degree of fibrillation increases, the overall viscosity becomes greater, as is apparent in Figure 5.5. An increasing degree of fibrillation (DoF) seems to have a like effect to that

of increasing solids content. However, apparently the hysteresis becomes smaller with the increasing degree of fibrillation as opposed to the trend with increasing solids content.

If we hypothesise again the same structural situation as described earlier, then the change of the hysteresis area can be explained accordingly: at low degrees of fibrillation (DoF), there is not much interaction between the cellulose entities as there are only few surface features and the main structural body is relatively stiff, so not many interaction points are present in the low shear conformation (Figure 5.6). In the high shear alignment conformation, however, there is much more interaction due to the alignment as long as the solids content is high enough. Therefore, a large hysteresis can be seen between the shear rate increasing and decreasing curves, that is, once again, assuming the already proposed predominant conformations in the respective sweeps. But if the degree of fibrillation is high, then there is already a high level of interaction in the low shear conformation because more individual entities are present that probably are more flexible compared with the dimensionally thicker less fibrillated entities. This leads overall to many more interaction points. The alignment in the high shear conformation does not lead in this case to substantially more interactions, so the difference in the viscosity curves for the increasing and decreasing shear rate ramps is small indicating only slight hysteresis. The overall increase of viscosity with increasing degree of fibrillation can probably be attributed to the lesser amount of free water. The increase of water retention by an increasing degree of fibrillation was already described by Herrick *et al.* using the water retention value as characteristic²⁰.

Alternatively, it could be assumed that the relaxation time is changing with the degree of fibrillation, in respect to the diameter of the cellulose entities: the smaller the diameters are, the faster a given conformation can rearrange, and therefore the hysteresis becomes smaller or disappears when the relaxation time becomes shorter than the point measurement time. This then would mean that the effect is no longer dependent on the predominant conformation as a function of the direction of the shear rate change, but just an equilibrium conformation that is only depending on the actual shear rate. Alternative time dependent measurements could reveal which hypothesis applies better to the current situation, or if it is probably a combination of many.

The trend of an increased overall viscosity with an increasing degree of fibrillation was also seen, for example, by Sneek²¹, who investigated the viscosity dependence of mechanically fibrillated MFC on the number of passes through an ultrafine friction grinder. However, one also finds publications where an opposite trend is seen, for example a finer (TEMPO oxidised) NFC having a lower viscosity than a coarser MFC^{15, 22}, or an increased number of passes through an ultrafine friction grinder led to an MFC with lower viscosity²³, or at least not to an increased viscosity as the difference was quite small. In the latter case it was argued that probably a cutting of the fibers/fibrils can lead to a reduced viscosity. In the other case, Horvath and Lindström's¹⁴ explanation can be applied, in respect to increased charge on the fibers leading to a decrease in internal friction, as the TEMPO oxidation typically leads to an increased surface charge density⁵. However, it cannot be attributed to the generally decreased fibril dimensions (increased DoF), as in this case it is not the surface charge density which is increased, but rather the overall charge in the system by exposing new charged surface. It is very probable that the overall viscosity of an MNFC suspension is the result of an interplay of different, opposing effects that are changed differently upon changing the degree of fibrillation.

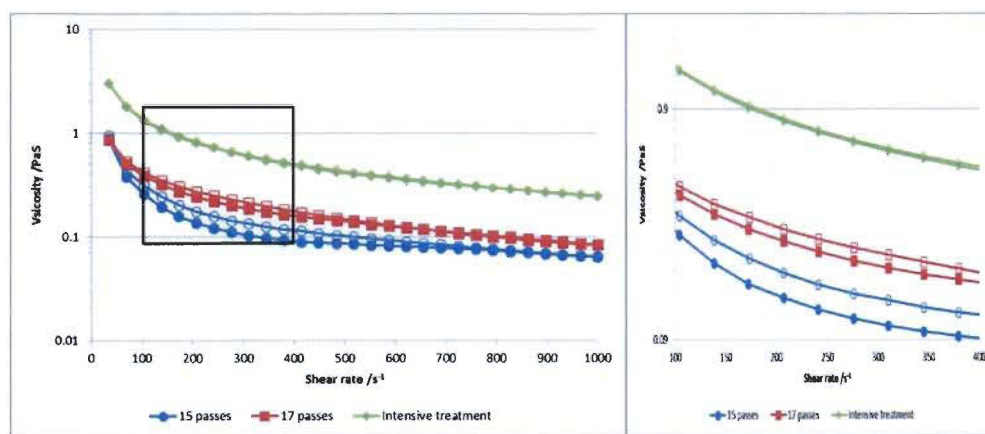


Figure 5.5: Flow curves of MNFC suspensions at different degrees of fibrillation. The dilution for these samples was set to 2 w/w%. The neighboring plot shows the enlarged region outlined in the main diagram.





	"Low" shear rate	"High" shear rate
Low DoF		
High DoF		

Figure 5.6: Schematic of the proposed conformations at high and low shear rate for greater and lesser degrees of fibrillation. The halos around the fibers indicate their interaction potential, which here is seen to have a greater penetration into the water phase than that shown in Fig. 5.3, due to the greater zeta potential, causing more interaction potential overlap.

The flow point also increases with increasing degree of fibrillation, as can be seen in Figure 5.7. The same explanation for the increasing flow point as was applied to increasing solids content can also be used here, i.e. increased degree of fibrillation results in a greater number of individual nanofibrillar entities, and thus more connection/interaction points per unit volume are present, and, therefore, more force (shear) is needed to break down the attendant gel structure.

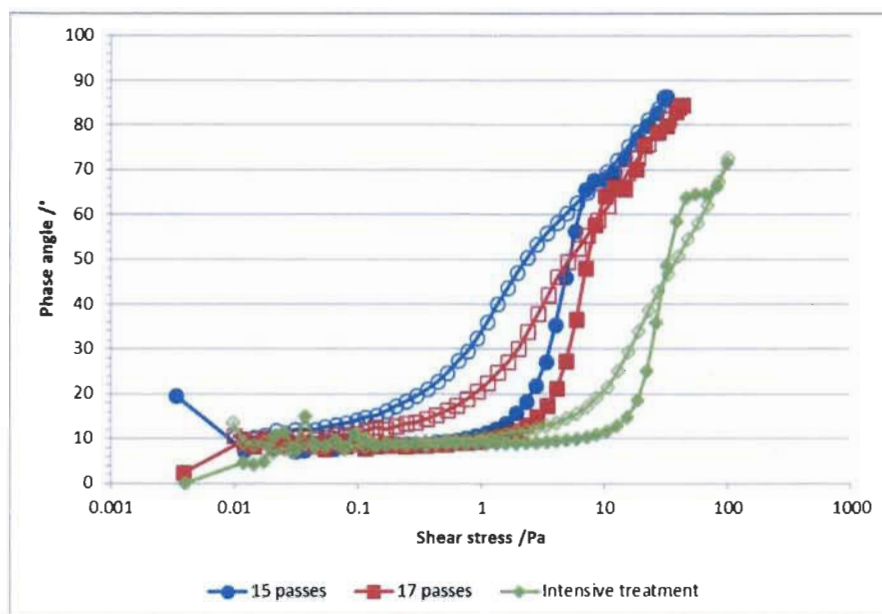


Figure 5.7: Amplitude sweep curves of MNFC suspensions at different degrees of fibrillation. The dilution for these samples was set to 2 w/w%.

5.5.4 Influence of additives on MNFC suspension rheology

As can be seen from the flow curves (Figure 5.8) and the amplitude sweep measurements (Figure 5.9), the addition of pigment filler, even at substantial amounts of 50 w/w% of the total dry mass (MNFC(fGCC50%)) does not have a strong influence on the rheological response of the MNFC suspension. There is only a small lift of the flow curve to higher viscosity values, but no change of the curve shape, and only a slight increase of the flow point seen in the amplitude sweep measurement. The absence of significant changes of the MNFC suspension rheology indicates that there is little to no interaction of the pigment particles with the MNFC entities. This may be attributed to the low surface charge and lack of reactivity of undispersed calcium carbonate pigment particles, with its ζ potential value of -8.2 mV. The relative inertness could perhaps already have been foreseen indirectly as it is known from traditional papermaking that untreated ground calcium carbonate particles behave relatively independently of the fibers in a paper sheet and during the forming process, albeit unless retention chemicals are used or the solids content has risen high enough to create enforced physical contact. Also Dimic-Misic *et al.*¹⁵ concluded in their investigation of different

coating color formulations, that the pigment they used, even though it was anionically dispersed and the system was more complex, did not effectively interact with the added MFC or NFC. In a later publication²², they also provide a schematic model and assign a more critical role to the addition of CMC to a system containing MFC or NFC and pigment particles and further coating color components. On the one hand it is mentioned that the CMC has a dispersing effect on the MFC or NFC material by reducing the cellulose particulate interactions, as indicated earlier, for example, by Vesterinen *et al.*²⁴, or shown visually by Xu and Roussi re in their work^{25, 26}. On the other hand, they also mention that in the presence of CMC, flocculation of the dispersed filler and the latex is induced in the case only where MFC/NFC is absent. The influence of CMC on the rheology of MNFC suspensions, and in those containing pigment filler, is hereby further investigated in this current work.

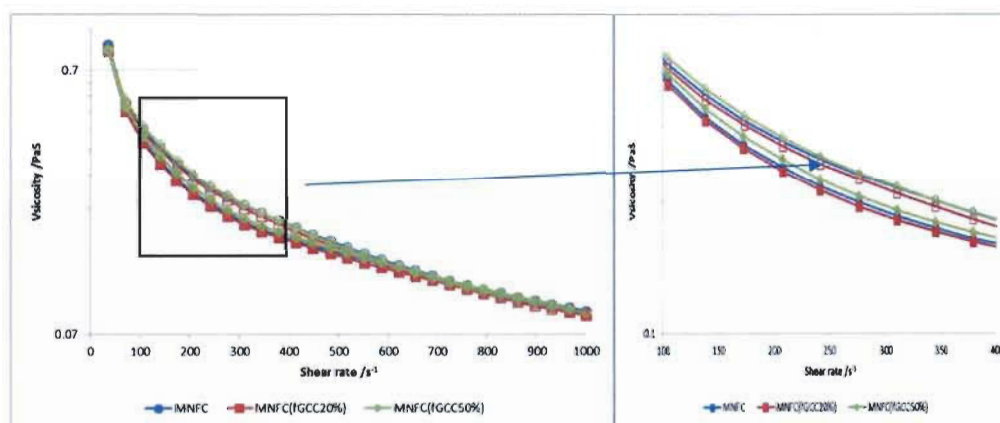


Figure 5.8: Flow curves of MNFC suspensions at different pigment filler loadings. The indicated filler levels are based on the total dry amounts. The cellulosic solids content was 2 w/w% for all samples. The neighboring plot shows the enlarged portion outlined in the main figure.

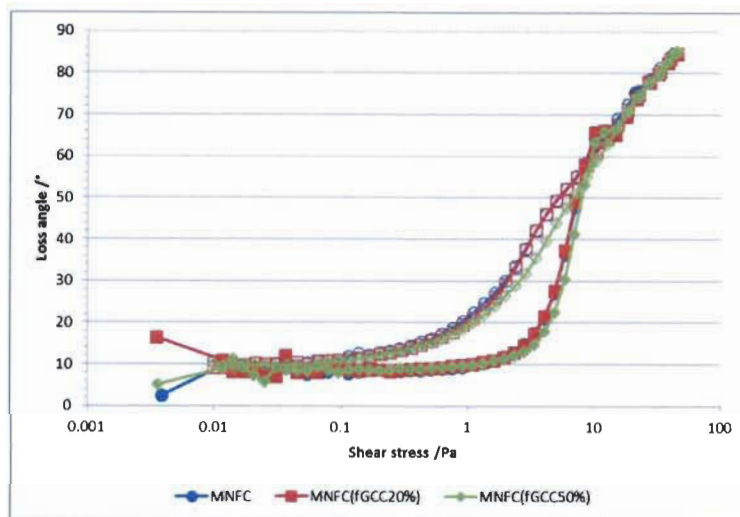


Figure 5.9: Amplitude sweep curves of MNFC suspensions at different pigment filler loadings. The indicated filler levels are based on the total dry amounts. The cellulosic solids content was 2 w/w% for all samples.

A reduced attractive interaction between the cellulose entities due to the addition of CMC can be observed as a reduction of the overall viscosity at increased shear rates in Figure 5.10. Apparently, the addition of only 0.5 w/w% CMC is enough to reduce the viscosity at increased shear rates (cf. MNFC vs. MNFC(CMC0.5%) above 600 s^{-1}). Interestingly, even higher amounts of CMC do not reduce the overall viscosity further, but reduce the hysteresis area, and also tend to inverse the hysteresis at increased shear rates (MNFC(CMC5%) above 500 s^{-1}). From the amplitude sweep curves one can see that the gel structure is broken down at slightly decreased shear stresses when CMC is added to the MNFC suspension (Figure 5.11), but independent of the CMC amount over this range of addition levels, as the measurements for 0.5, 2 and 5 w/w% CMC content are having an identical upsweep curve. However, as the hysteresis of the flow curves is becoming smaller and even inverted, the excess CMC has probably a more complex effect. Following the previously proposed argumentation, the effect of “excess” (=“free”) CMC might be explained by the dispersing effect of CMC: as more entities get dispersed, the MNFC suspension appears as a more fibrillated material, and therefore, as hypothesised previously, the low and high shear state do not differ that much in interaction. Therefore,

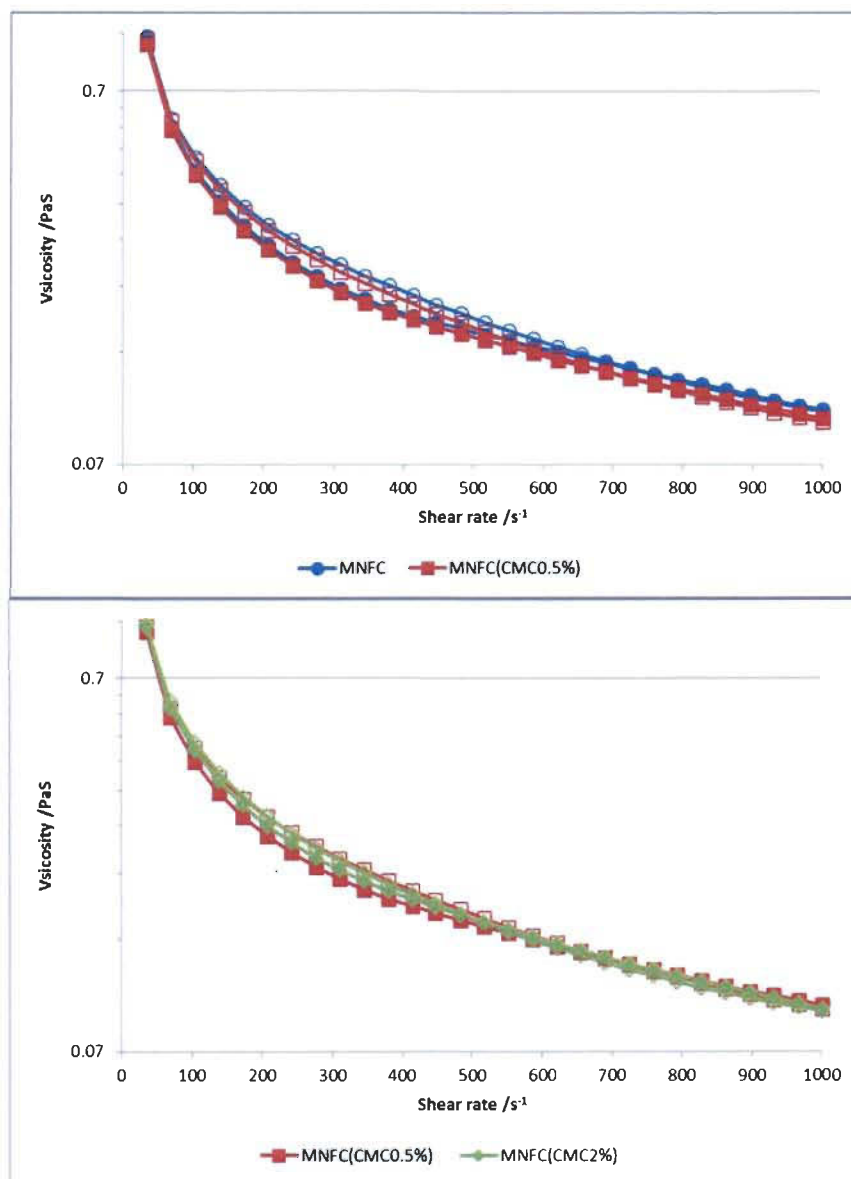
the hysteresis between the shear rate increasing and decreasing curves disappears. Alternatively, the hysteresis might be lost due to an increased mobility of the finer entities, effectively reducing the time constant of the structure reorganisation. These results clearly indicate that the state of CMC, either bound to the cellulose particulate surface, as described by Horvath and Lindström¹⁴, or present as free polymer, has an influence on the rheological response of the MNFC system. Whereas bound CMC reduces the flow point and the general viscosity by adding to the electrostatic repulsion, and thus reducing internal friction, free CMC on the other hand may change the apparent degree of fibrillation, thus reducing relaxation time of the MNFC suspension.

The decrease of yield stress of pulp suspensions due to addition of CMC was also reported by Liimatainen *et al.*²⁷. On the one hand they found that the yield stress keeps decreasing with increasing CMC amount, as opposed to the here presented data and to those of Horvath and Lindström¹⁴, and, on the other hand, they also saw that an increasing amount of non-adsorbed CMC led to a further reduction of the yield stress. It may be that the yield stress determination method used by Liimatainen *et al.*¹³ is confused by viscosity and time dependent effects that lead to a misinterpretation of the yield stress.

It is also worth noting, that the plateau phase angle before the gel structure breakdown is not changed upon the addition of CMC nor throughout the increasing addition levels. This indicates that the static interaction is still determined predominantly by the MNFC entities themselves. However, as the flow point is slightly reduced by the presence of CMC, the ultimate stress that can be borne by the system before losing the gel structure is reduced. It also should be mentioned that when pigment filler and CMC are both added together to an MNFC suspension, the property-determining component is clearly the CMC, as can be seen in Figure 5.12 and Figure 5.13, as the curves of the filler and CMC containing sample (MNFC(fGCC50%)(CMC2%)) are following the respective curves of the CMC-only containing sample (MNFC(CMC2%)).

The general effects of the above discussed additives are summarised in Figure 5.14. CMC (red) disperses the cellulose entities by being adsorbed initially on their surface, and, when in excess, remaining partly in solution. The pigment particles (orange) do not interact with the cellulose fibrils. A significant adsorption of CMC onto the pigment particles is not

expected, because of the low reactivity of their undispersed surface. The data presented in the following paragraph will support these conclusions.



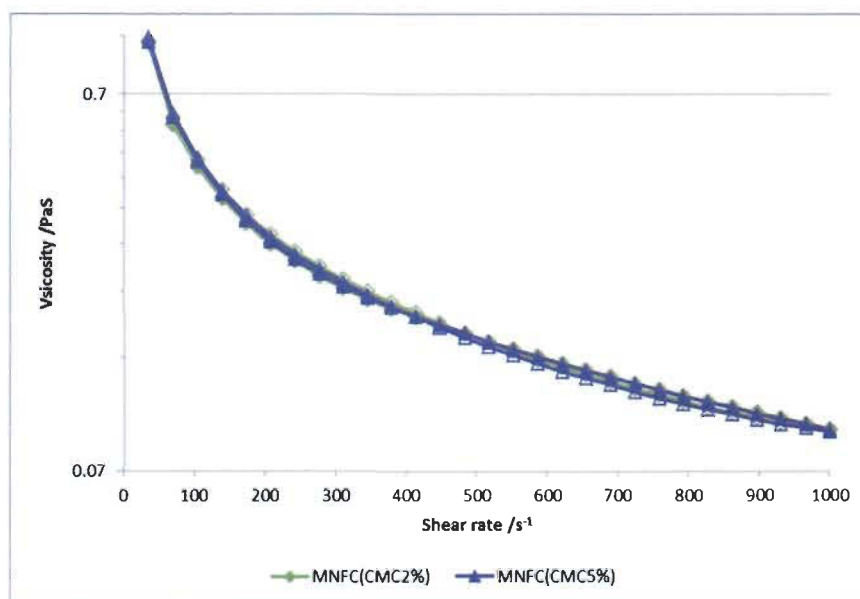


Figure 5.10: Flow curves of MNFC suspensions at different CMC loadings. The indicated addition levels are based on the cellulose dry amounts. The cellulosic solids content was 2 w/w% for all samples.

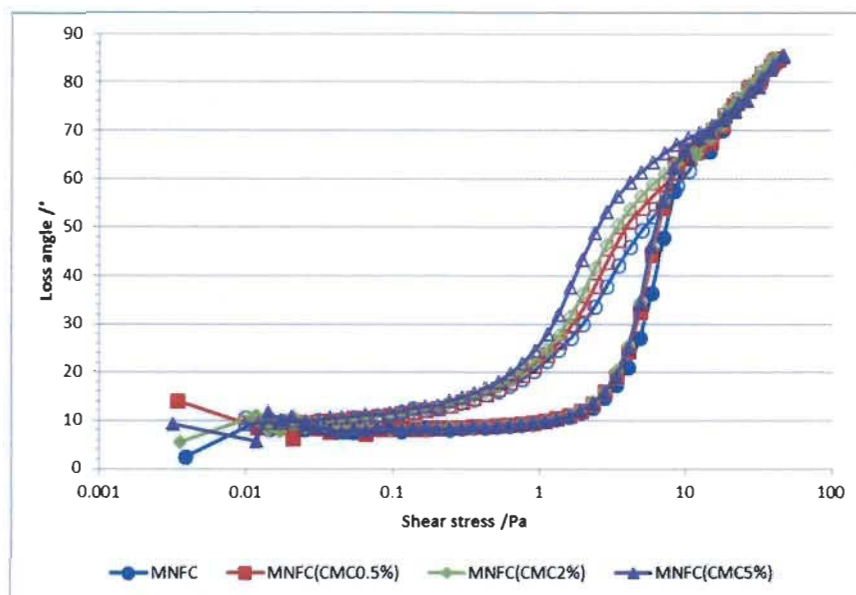


Figure 5.11: Amplitude sweep curves of MNFC suspensions at different CMC loadings. The indicated addition levels are based on the cellulose dry amounts. The cellulosic solids content was 2 w/w% for all samples.

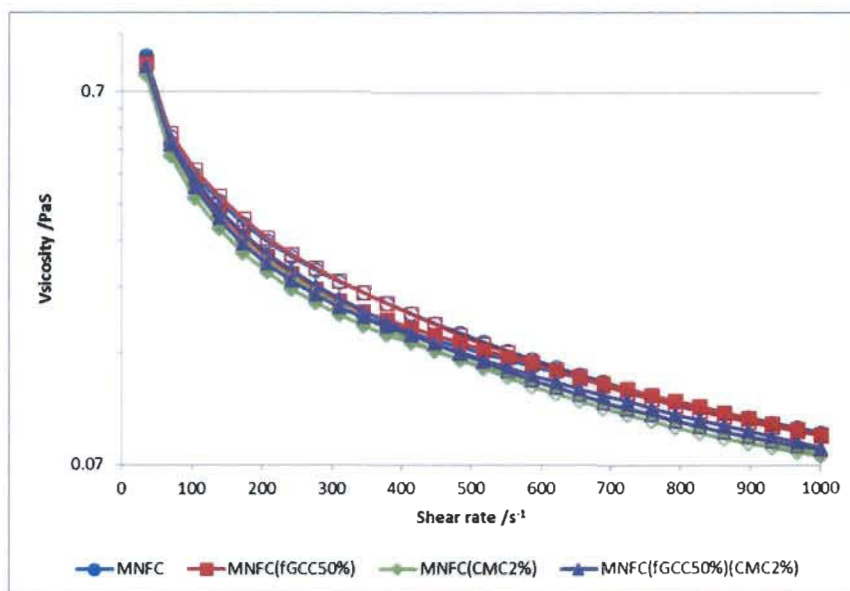


Figure 5.12: Flow curves of MNFC suspensions containing zero, one or two additives (CMC and/or fGCC). The indicated CMC addition levels are based on the cellulose dry amounts, whereas the filler levels are based on the total dry amount. The cellulosic solids content was 2 w/w% for all samples.

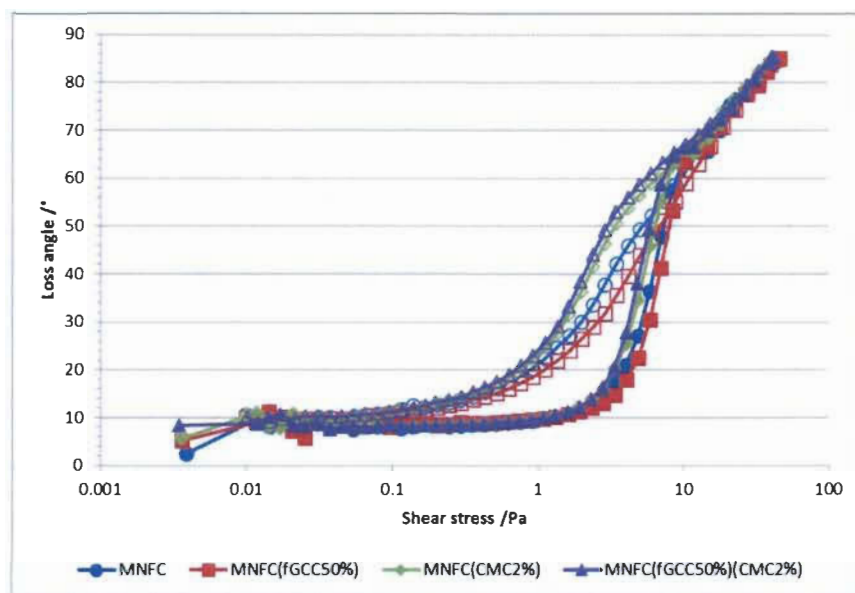


Figure 5.13: Amplitude sweep curves of MNFC suspensions containing zero, one or two additives (CMC and/or fGCC). The indicated CMC addition levels are based on the cellulose dry amounts, whereas the filler levels are based on the total dry amount. The cellulosic solids content was 2 w/w% for all samples.

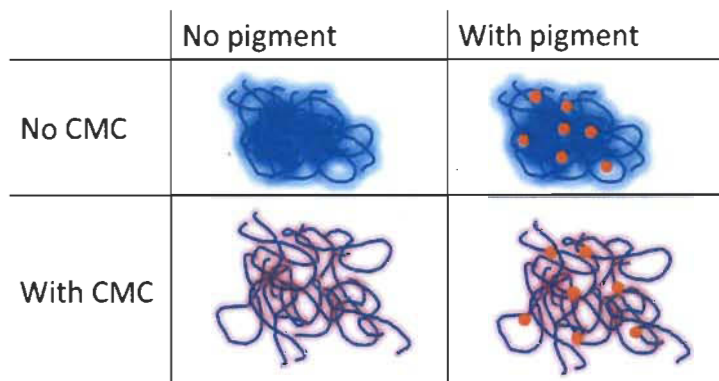


Figure 5.14: Schematic of the proposed conformations for MNFC suspensions with and without CMC and/or pigment. The blue halos around the fibers indicate their interaction potential and the red halos indicate the general altering of the fiber-fiber interaction potential related to the presence of CMC.

By co-grinding CMC with the calcium carbonate pigment filler (PHCHa), as also with further addition of cationic polymer (PHCHb), the CMC (and cationic polymer) is bound to the pigment filler surface. This “immobilisation” of the polymer(s) on the surface has an effect on the MNFC suspension rheological behavior when such pigment fillers are mixed into it. Looking at the flow curves (Figure 5.15) reveals that the CMC-only co-processed pigment filler (PHCHa) leads to a generally increased viscosity, a reduced hysteresis area and even a slight hysteresis reverse at increased shear rates ($> 650 \text{ s}^{-1}$). The additionally cationic polymer co-processed PHCH (PHCHb) pigment filler also leads to an increase of the viscosity, but less pronounced and only at lower shear rates ($< 700 \text{ s}^{-1}$). Interestingly, the gel structure breakdown (flow point) is affected (increased) only by the cationic polymer containing PHCH (PHCHb), as can be seen in Figure 5.16. This might be expected due to the Coulombic attraction of the anionic MNFC and partly amphoteric pigment.

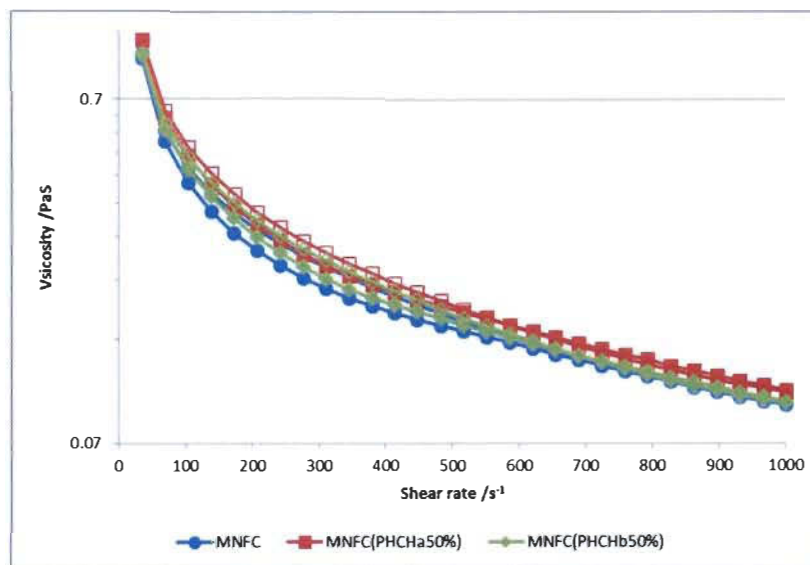


Figure 5.15: Flow curves of MNFC suspensions containing no and the two different PHCH filler pigments, PHCHa and PHCHb. The indicated filler levels are based on the total dry amount. The cellulosic solids content was 2 w/w% for all samples.

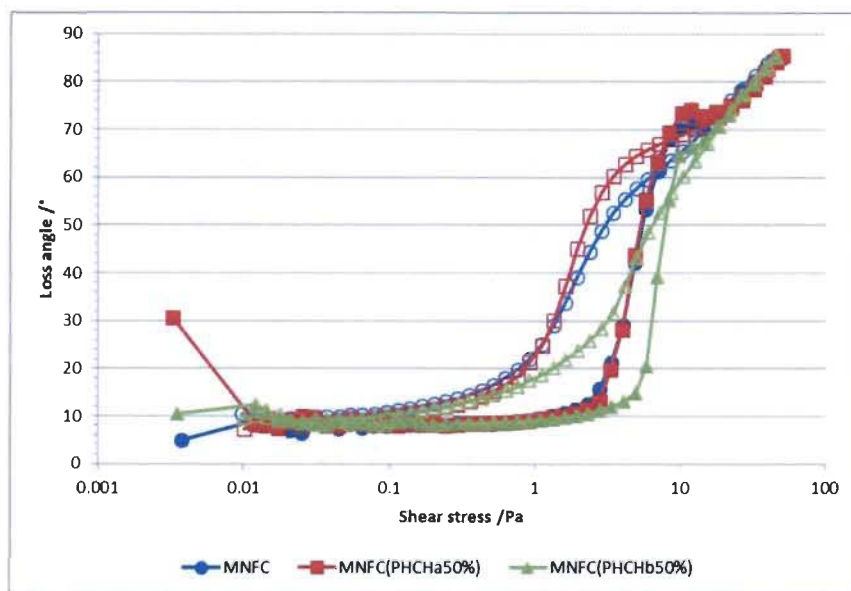


Figure 5.16: Amplitude sweep curves of MNFC suspensions containing no pigment additive versus the two different PHCH pigments. The indicated filler levels are based on the total dry amount. The cellulosic solids content was 2 w/w% for all samples.

As there is no reduction of the flow point in the PHCHa containing MNFC suspension, but the addition of CMC (as also together with fGCC) does reduce the yield point, it can be concluded that most of the CMC actually is bound to the pigment filler particles in this case of PHCH. Furthermore, it can be hypothesised that the static structure of the cellulose entities is not altered by the CMC covered particles, but, interestingly, those particles have an influence on the dynamic structure flow curve. Firstly, there is an increased viscosity, indicating a stronger interaction between the involved entities during initial collisions. As this was not seen for untreated calcium carbonate particles (fGCC), it can be assumed that a specific CMC-cellulose interaction may be attributed to the development of this stronger interaction. We hypothesise, that the increase of anionicity of the pigment filler particle seems not to be the reason for an increased viscosity, as this most probably would lead to overall less internal friction and therefore even lower viscosities. Secondly, the hysteresis becomes smaller, and this, then, may be attributed to free CMC (see above for explanation). This finding is contradictory to what is observed in the amplitude sweep

measurement, as in the case of free CMC, in that the flow point would be expected to decrease too. So it may be that the observed flow point is determined by several counter-acting effects. Further investigations are needed to clarify this situation.

As the flow curve is less changed when PHCHb is added compared to PHCHa, it can be concluded that there is less dynamic interaction. As the PHCHb pigment particles are also covered by cationic polymer, it might be concluded that there is less specific CMC-cellulose interaction as a part of the CMC is interacting with the cationic polymer. On the other hand, as the flow point is increased, the situation must be different in the static configuration. Probably a stable, but weak, (electrostatic) structure is formed between the cellulose entities and the PHCHb particles that is destroyed during shearing and they are not rapidly enough re-formed in the flow curve measurement. As a result, the cellulose entities and the pigment particles are not hindered anymore in their relative movement, and the viscosity is not much different from that of a pure MNFC suspension. Further (rheological) investigations are needed to test this hypothesis.

It was shown that the localisation of CMC (and polyDADMAC) on pigment fillers does have a significant influence on the rheological properties of MNFC suspensions compared with addition of those polymers directly to pigment filler containing MNFC suspensions. Earlier work in the field of MNFC-pigment nanocomposites already indicated that the localisation of CMC (and additional polyDADMAC) on the pigment filler surface leads to a beneficial behavior compared with their direct addition when fillers are used with MNFC⁹. It was shown specifically that such surface treated PHCH pigments lead to a significant increase in mechanical strength properties in an MNFC-pigment composite compared with when they contain non surface-treated pigment filler, with or without the free addition of CMC. The present work thus confirms the then proposed increased interactions of the PHCH pigment filler particles with the cellulose fibrils, as manifest here, for example, by the increased gel strength.

Further work needs to be done, but using this knowledge looks promising as a tool for tailoring MNFC suspension properties, as also for manufacturing economic and well performing pigmented MNFC composite materials.

5.6 Conclusions

The influence of MNFC suspension properties on its rheological behavior was investigated. The typical shear thinning behavior was observed, and existing mechanistic models were applied and extended for interpretation of the data. Apparently contradictory data were critically discussed in the light of competing mechanisms of charge repulsion, particle entanglement and gel formation, which highlights the need for further clarifying investigation. Also, the influence of additives on MNFC suspension rheology, namely CMC and pigment particles, was investigated. Also, here, some existing data could be confirmed and explained by mechanistic models. Finally, it was found that the localisation of CMC on pigment filler particles by adsorption during pigment co-processing produces pigment filler particles that change the MNFC suspension rheology in a way that so far has not been previously reported. Such pigment hydrocolloid hybrid (PHCH) particles can increase either the gel-strength or the apparent viscosity of an MNFC suspension, whereas regular pigment particles and CMC typically show no or opposite effects. The further development of such PHCH pigment particles may be a versatile tool specifically to influence the rheological behavior of an MNFC suspension, and thereby impact ultimately on the properties of composites made therefrom.

5.7 Acknowledgements

We would like to acknowledge Roman Lack and Christian Fritz (both Omya International AG) for the manufacturing of the PHCH pigment particles and the MNFC suspensions.

5.8 References

1. Hubbe, M. A., Rojas, O. J., Lucia, L. A., et al., Cellulosic Nanocomposites: A Review, *BioResources* 3(3):929(2008).
2. Lavoine, N., Desloges, I., Dufresne, A., et al., Microfibrillated cellulose - Its barrier properties and applications in cellulosic materials: A review, *Carbohydrate Polymers* 90:735(2012).
3. Turbak, A. F., Snyder, F. W., and Sandberg, K. R., Microfibrillated cellulose, a new cellulose product: properties, uses, and commercial potential, *Journal of Applied Polymer Science* 37:815(1983).

4. Ankerfors, M., "Microfibrillated cellulose: Energy-efficient preparation techniques and key properties," Licenciate, KTH Royal Institute of Technology, 2012.
5. Saito, T., Nishiyama, Y., Putaux, J. L., et al., Homogeneous Suspensions of Individualized Microfibrils from TEMPO-Catalyzed Oxidation of Native Cellulose, *Biomacromolecules* 7(6):1687(2006).
6. Moran, J. I., Alvarez, V. A., Cyras, V. P., et al., Extraction of cellulose and preparation of nanocellulose from sisal fibers, *Cellulose* 15(1):149(2008).
7. Alemdar, A. and Sain, M., Isolation and characterization of nanofibers from agricultural residues - Wheat straw and soy hulls, *Bioresource Technology* 99:1664(2008).
8. Josset, S., Orsolini, P., Siqueira, G., et al., Energy consumption of the nanofibrillation of bleached pulp, wheat straw and recycled newspaper through a grinding process, *Nordic Pulp and Paper Research Journal* 29(1):167(2014).
9. Schenker, M., Schoelkopf, J., Mangin, P. J., et al., *Pigmented Micro-Nanofibrillated Cellulose (MNFC) as packaging composite material: a first assessment*, paper presented at the PaperCon, Atlanta, 2015.
10. Svending, P., *Commercial Break-Through in MFC Processing*, paper presented at the Tappi International Conference on Nanotechnology for Renewable Materials, Vancouver, 2014.
11. Iotti, M., Gregersen, O. W., Moe, S., et al., Rheological Studies of Microfibrillar Cellulose Water Dispersions, *Journal of Polymers and the Environment* 19(1):137(2011).
12. Dimic-Misic, K., Puisto, A., Paltakari, J., et al., The influence of shear on the dewatering of high consistency nanofibrillated cellulose furnishes, *Cellulose* 20(4):1853(2013).
13. Dimic-Misic, K., Maloney, T. C., and Gane, P. A. C., Defining a strain-induced time constant for oriented low shear-induced structuring in high consistency MFC/NFC-filler composite suspensions, *Journal of Applied Polymer Science* 132(47)(2015).
14. Horvath, A. E. and Lindström, T., The influence of colloidal interactions on fiber network strength, *Journal of Colloid and Interface Science* 309:511(2007).

15. Dimic-Misic, K., Gane, P. A. C., and Paltakari, J., Micro- and nanofibrillated cellulose as a rheology modifier additive in CMC-containing pigment coating formulations, *Industrial and Engineering Chemistry Research* 52(45):16066(2013).
16. Saarinen, T., Lille, M., and Seppälä, J., Technical Aspects on Rheological Characterization of Microfibrillar Cellulose Water Suspensions, *Annual Transaction of the Nordic Rheology Society* 17:121(2009).
17. Mezger, T. G., *The Rheology Handbook, 4th Edition*, Vincentz Network, 2014.
18. Pahimanolis, N., Salminen, A., Penttilä, P. A., et al., Nanofibrillated cellulose/ carboxymethyl cellulose composite with improves wet strength, *Cellulose* 20(3):1459(2013).
19. Pääkkö, M., Ankerfors, M., Kosonen, H., et al., Enzymatic Hydrolysis Combined with Mechanical Shearing and High-Pressure Homogenization for Nanoscale Cellulose Fibrils and Strong Gels, *Biomacromolecules* 8(6):1934(2007).
20. Herrick, F. W., Casebier, R. L., Hamilton, J. K., et al., Microfibrillated cellulose: morphology and accessibility, *Journal of Applied Polymer Science* 37(9):797(1983).
21. Sneck, A., Pitkänen, M., Kangas, H., et al., *New approach to classification of cellulose fibrils and suitable methods for their characterization*, paper presented at the Tappi International Conference on Nanotechnology for Renewable Materials, Arlington, 2011.
22. Dimic-Misic, K., Salo, T., Paltakari, J., et al., Comparing the rheological properties of novel nanofibrillar cellulose-formulated pigment coating colours with those using traditional thickener, *Nordic Pulp and Paper Research Journal* 29(2):253(2014).
23. Kangas, H., Lahtinen, P., Sneck, A., et al., Characterization of fibrillated celluloses. A short review and evaluation of characteristics with a combination of methods, *Nordic Pulp and Paper Research Journal* 29(1):129(2014).
24. Vesterinen, A. H., Myllytie, P., Laine, J., et al., The effect of water-soluble polymers on rheology of microfibrillar cellulose suspension and dynamic mechanical properties of paper sheet, *Journal of Applied Polymer Science* 116(5):2990(2010).
25. Xu, X., "Study of the relationship between the dispersion of micro-nano-fibrillated-cellulose (MNFC) and their ability in curtain coating," MSc, University of Quebec in Trois-Rivieres, 2014.

26. Roussière, F., Xu, X., Dubé, M., et al., *Dispersion of Micro-Nano Fibrillated Cellulose (MNFC) by Carboxy Methyl Cellulose (CMC) and its characterization*, paper presented at the Tappi International Conference on Nanotechnology for Renewable Materials, Vancouver, 2014.
27. Liimatainen, H., Haavisto, S., Haapala, A., et al., Influence of adsorbed and dissolved carboxymethyl cellulose on fibre suspension dispersing, dewaterability, and fines retention, *BioResources* 4(1):321(2009).

Chapter 6 - Presentation 1: Rheological investigation of pigmented micro-nano-fibrillated cellulose (MNFC) suspensions: Discussion of flow curves

Oral presentation.

Michel Schenker, Joachim Schoelkopf, Patrice Mangin, Patrick Gane; 2016 International Conference on Nanotechnology for Renewable Materials, Grenoble.

6.1 Foreword

In the course of manufacturing the MNFC suspensions, it became very obvious, that the Supermasscolloider was not able deliver a consistent MNFC product quality, even though the manufacturing parameters were fixed. This was attributed to the changing wear situation of the grinding stones. Indications for this limitation were already identified and described to some extent in the previous publication. Yet, it was only in this subsequent experimental series, that the full severity of this drawback became apparent. As a consequence, firstly, it was decided to work only with one single batch of MNFC in order to rule out the influence of a changing manufacturing process. Secondly, the focus was set on a more in-depth investigation of an adequate rheological characterisation (revisiting the chosen measurement parameters and evaluation). Thirdly, the material property space investigation was limited to the degree of fibrillation.

As a pre-evaluation of the newly defined measurement protocols and material space focus, a short experimental study was carried out and published as a presentation.

6.2 Summary

In order to be able to better compare the of this work with data that is presented in the literature (e.g. (Agoda-Tandjawa et al. 2010; Iotti et al. 2011)), and also to be able to investigate the transition zone behaviour of MNFC suspension flow curves, according measurement parameters were adopted and expanded. Namely, the shear rate profile was changed to log-equidistantly distributed shear rates, and the acquisition time setting was changed from 10 s per point to automated. In the automated acquisition time setting, the software selects the point measurement time automatically, when reaching a stable reading. The minimum time was not less than 15.2 seconds. It is shown that this mode

provides very alike flow curves compared to when a constant acquisition time is selected (i.e. 10 s). However, by also monitoring the automated acquisition time, the typical transition zone within a flow curve can be visualised alternatively, as the acquisition times become larger and more unstable (higher standard deviations) in this area, as compared to the two shear thinning regions.

It is shown that an increased solids content not only increases the overall viscosity of an MNFC suspension, but also that the transition zone becomes smaller (reduced shear rate range) and less pronounced (smaller viscosity drop). In order to mimic a coarser MNFC, different shares of pulp fibres were added to the MFC, but keeping the overall solids content constant (1 wt%). The flow curves showed irregular behaviour for pulp shares of 50 wt% and higher, so only the flow curves with 40 wt% pulp or less were evaluated. With an increasing pulp share, the end of the transition zone was extended to higher shear rates, whereas the onset of the transition zone was not changed. Also, the overall viscosity in zone 1 and 2 did decrease with an increasing pulp share. Furthermore, CMC was added to the MFC suspension, with the intention to mimic a finer MNFC by getting better dispersed fibrils (Veen et al. 2015). Here it was found that the CMC shortens the transition zone, i.e. the onset of zone 2 happens at lower shear rates. The overall viscosity was not changed. As the CMC does not only change the state of dispersion, but also inherently changes the charge situation in the suspension, the observed effects cannot be attributed only to the presumed increased level of homogeneity.

This preliminary work did not discuss the potential morphological mechanisms causing the changed flow curves with respect to residual fibers or added CMC in detail, yet it showed the potential of the changed measurement protocol and the benefit of observing the automated acquisition time.

6.3 Presentation



Rheological investigation of pigmented micro-nano-fibrillated cellulose (MNFC) suspensions:

Discussion of flow curves

PRESENTED BY
Michel Schenker
 Senior Scientist
 Omya International AG / FiberLean / UQTR

Coauthors:
**Joachim Schoelkopf, Patrice Mangin
 and Patrick Gane**



Content overview

- **Introduction**
 - Micro-nanofibrillated cellulose (MNFC)
 - Review / refresher of last year's presentation
 - The challenge – "why the topic has changed"
- **Materials and Methods**
- **Results**
 - Comparison of flow curve measurement procedures
 - Production process instabilities
 - Influencing parameters: solids content
 - General profile
 - Influencing parameters: residual fibres
 - Influencing parameters: CMC / dispersion
- **Conclusions**

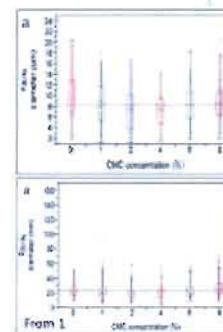
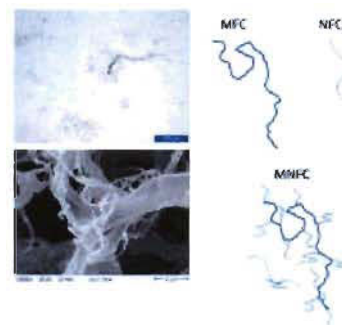


Introduction

Micro-nanofibrillated cellulose

Why Micro-Nanofibrillated Cellulose?

- Mechanical fibrillation process
 - broad size distribution
- Residual fibres, fibril aggregates, fibrils and nanofibrils
 - *nano fibrillation occurs on micro and nanofibres*
 - **MNFC**
 - **FiberLean MFC**
- Benefits
 - economical
 - improved self-retention and coating holdout
 - enlarged property-space



¹ Roussière, F. and Xu, X. et al., *Tappi International Conference on Nanotechnology for Renewable Materials*, Vancouver, 2014

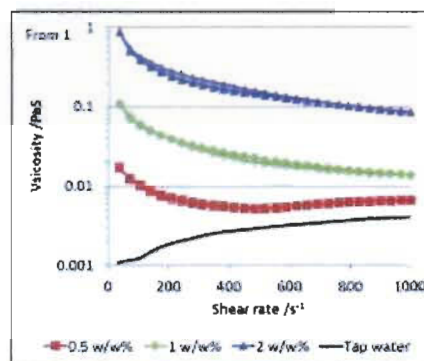
TAPPI

Introduction

Last year's presentation

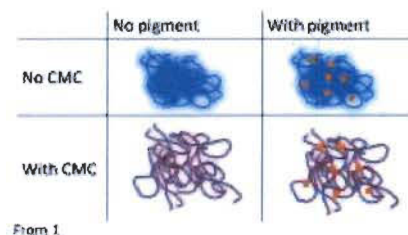
Flow curves

- Linear shear rate profile
- Hysteresis
- Influence of mixed additives



Proposed next steps

- Investigate the influence of coprocessing additives
- Investigate time depending effects



² Schenker, M. et al., *Tappi International Conference on Nanotechnology for Renewable Materials*, Atlanta, 2015

TAPPI

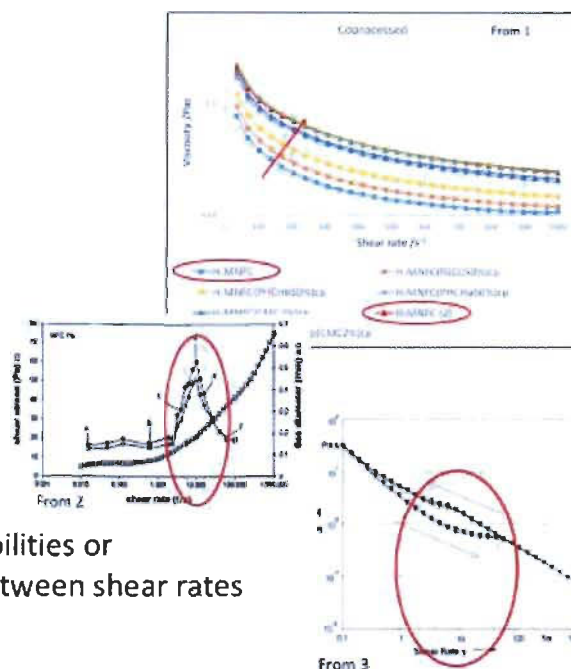
Introduction The challenge

Additive coprocessing

- Suspicious trend
 - Different behavior of reference material with equal composition
- Change of process efficiency

Literature

- Indication of flow instabilities or mechanistic changes between shear rates from 1 to 100 s^{-1}



¹ Schenker, M., et al., PaperCon, Cincinnati, 2016

² Karppinen, A., et al., Cellulose, 19(6), pp. 1807 (2012)

³ Iotti, M., et al., Journal of Polymers and the Environment, 19(1), pp. 137 (2011)

TAPPI

Materials and Methods

Materials used

- Pulp: bleached wood-free eucalyptus pulp

MNFC manufacturing

- Ultrafine friction grinder (Supermasscolloider)
 - Single pass mode, total of 15 passes, changing revolution speeds
 - 3 wt% cellulose consistency

Sample preparation

- Dilutions made from stock MNFC and tap water (same as for production, 45 °F)
 - consistency for cellulose is held constant at 1 w/w%

TAPPI

Materials and Methods

Rheological measurement parameters

- Paar Physica Rheometer MCR 300
 - single gap cylinder (CC27), 1.13 mm gap width
- Flow curve measurement
 - no pre-conditioning (no difference found to preconditioned samples)
 - $0.01 - 1\,000\text{ s}^{-1}$ shear rate with 30 points log-distributed, directly followed by $1\,000 - 0.01\text{ s}^{-1}$ shear rate with 30 points log-distributed
 - Automated acquisition time determination (standard) or constant acquisition time of 10 s
 - $20\text{ }^{\circ}\text{C}$
- Evaluation
 - Viscosity
 - Acquisition time

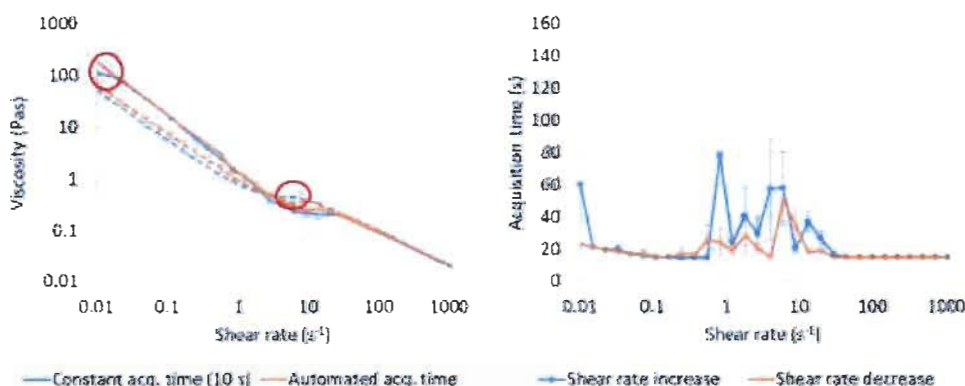


Results

Comparison of flow curve measurement procedures

Viscosity acquisition time mode

- Acquisition time of 10 s seems to be generally long enough for accurate viscosity read out

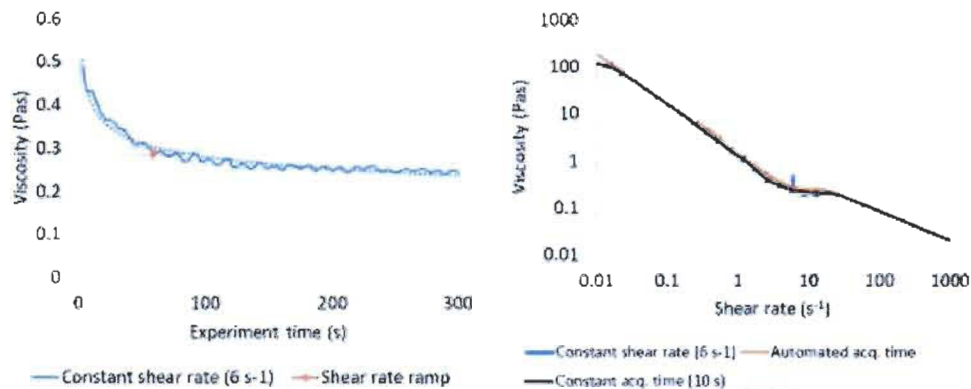


Results

Comparison of flow curve measurement procedures

Shear history

- Precedent shear history influences the actual shear rate reading → 10 s acquisition time enough after some points



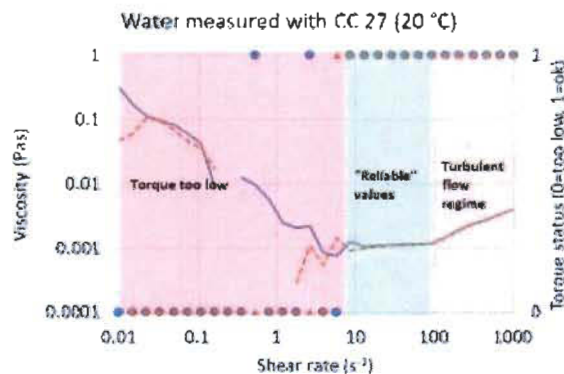
TAPPI

Results

Comparison of flow curve measurement procedures

Measurement set-up limitations

- "Wide" gap (CC 27) → not reliable for low viscosities at low shear rates, turbulent flow at high shear rates



TAPPI

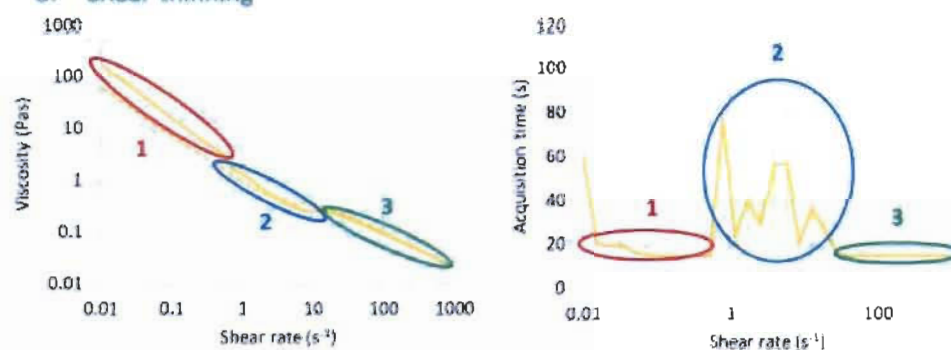
Results

General profile

Viscosity profile

1. Shear thinning
2. Transition zone
3. Shear thinning

- Reported by others, e.g. Iotti *et al.*¹ and Agoda-Tandjawa *et al.*²
- Attributed to flocculation by Karppinen *et al.*³



¹Iotti, M., *et al.*, *Journal of Polymers and the Environment*, 19(1), pp. 137 (2011)

²Agoda-Tandjawa, *et al.*, *Carbohydrate Polymers*, 80(3), pp. 677 (2010)

³Karppinen, A., *et al.*, *Cellulose*, 19(6), pp. 1807 (2012)

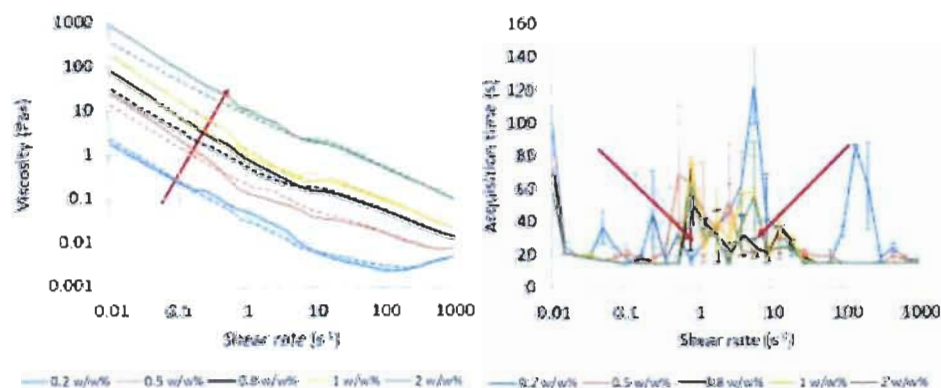
TAPPI

Results

Solids content

Solids content

- Increasing viscosity level with increasing solids
- Stabilisation of acquisition times



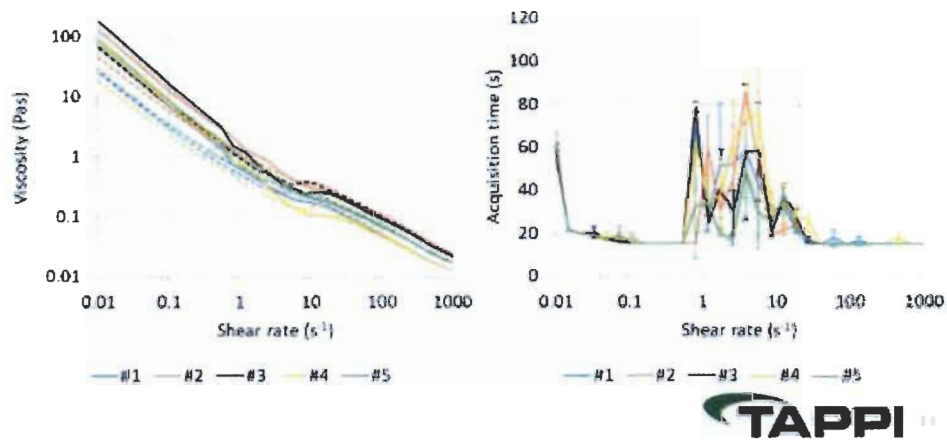
TAPPI

Results

Production process instabilities

Manufacturing sequence

- Overall viscosity level variation
- Slightly different transition zone endpoint

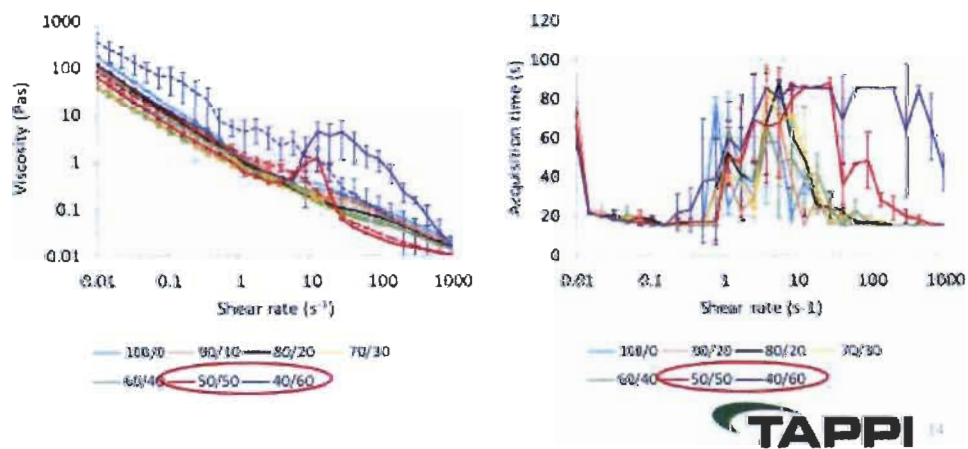


Results

Residual fibres

Coarse fibre share

- Irregularities starting at 50/50 coarse fibre ratio

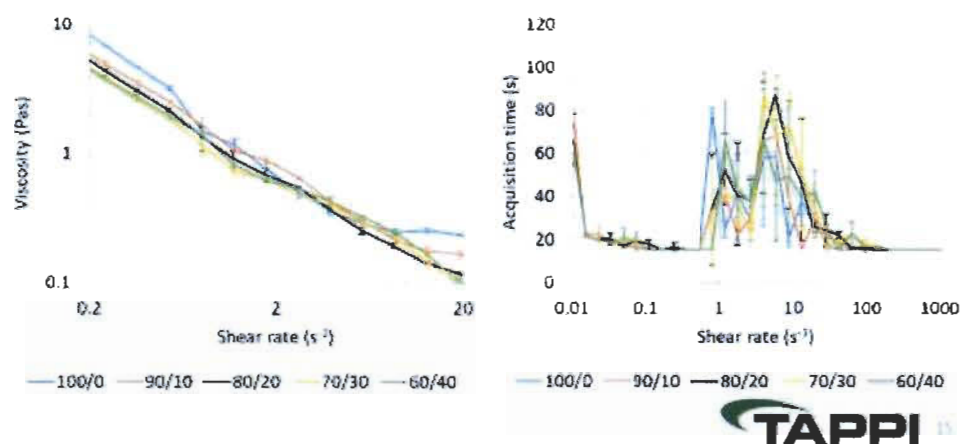


Results

Residual fibres

Coarse fibre share

- Transition zone extends with increasing share
- Viscosity within transition zone remains

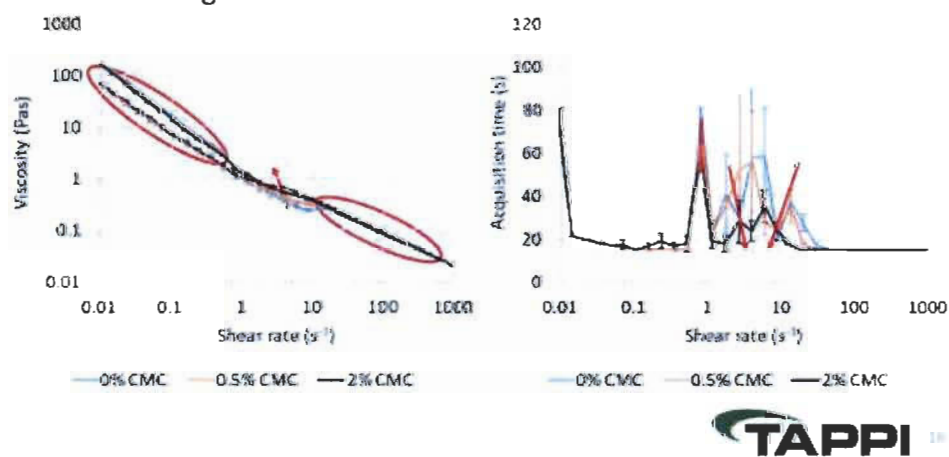


Results

CMC / dispersion

CMC (increasing state of dispersion)

- Viscosity level unchanged
- Shortening of transition zone
- Stabilisation of acquisition time



Conclusions

- Acquisition time monitoring helps in identifying transition zone
- Coarse fibres don't change onset of transition zone
 - induced aggregation doesn't depend on amount of residual fibres
 - probably depends on residual fibre size distribution (to be checked)
- Coarse fibres extend the transition zone
 - break down of aggregates does depend on amount of residual fibres
- CMC (state of dispersion) shortens transition zone
 - share of apparent large scale features (flocculated fibrils) is reduced
- Sample quality differences still not fully characterised

→ shows big potential to use flow curves for MNFC morphology characterisation



Thank you

PRESENTED BY

Michel Schenker

Senior Scientist

Omya International AG / FiberLean Technologies Ltd.

Michel.Schenker@omya.com



Chapter 7 - Article 2: Influence of shear rheometer measurement systems on the rheological properties of microfibrillated cellulose (MFC) suspensions

Published article.

Michel Schenker, Joachim Schoelkopf, Patrick Gane, Patrice Mangin; Cellulose; 2017; 25(2); 961-976; doi: 10.1007/s10570-017-1642-x

7.1 Foreword

As the preceding work has shown the potential of rheological measurements in providing information on the MNFC suspension morphology and potentially on the composition details (degree of fibrillation, amount of residual fibres), it was decided to carry out a more complete trial programme to investigate these initial observations in more detail. To be able also to develop morphological models, and/or to be able to compare own data with work done by other researchers, a solid understanding of the rheological measurements is necessary. This is especially highlighted because MNFC suspensions are known to exhibit a complex rheology and are very prone to measurement artefacts (Nechyporchuk et al. 2016). Even though described to be artefacts, most of these irregular suspension responses (with view to the underlying assumptions for rheological data interpretation), are inherent to MNFC suspensions, and can probably not be suppressed (Cloitre and Bonnecaze 2017). It also may not make sense to suppress them, as the same effects will be present in real applications, like being pumped through a pipe, and, therefore, such materials will behave the same way as in the rheometer. Nevertheless, in order to develop morphological models, it is necessary to be aware of these effects and how they are expressed in rheological measurements. So, on the one hand, viscoelasticity as well as flow curve data, was described with already known and newly introduced descriptors. The influence of four different shear rheometer set-ups on these properties was tested. To our knowledge, this was the first work that has investigated the influence of shear rheometer measurement setups on MNFC suspensions at such a detailed level.

This work, as well as the additional unpublished data, provided the basis for the decision to switch from the smooth CC27 system to the VS system for further rheological characterisations within this PhD work. Also, the importance and the potential benefits of carefully carried out data analysis and statistics became apparent while evaluating the unpublished data. This, in turn, created the motivation to have a closer look at the statistics of the flow curve hysteresis data that were presented in the subsequent publication (Chapter 8 -).

7.2 Abstract

Flow curve and viscoelastic measurements were performed on microfibrillated cellulose (MFC) suspensions of different solids content using both cylinder and cup (smooth and rough) as well as vane in cup geometries. To compare the data quantitatively from amplitude sweep measurements and dynamic flow curves several descriptors were newly introduced to parametrise the observed two-zone behaviour separated by a transition region. It was observed that the cylinder cup geometries are prone to erroneous effects like slip, wall depletion and/or shear banding. However, those effects were not observed when the MFC suspension was not stressed beyond the dynamic critical stress (yield) point, i.e. when still in the linear viscoelastic (LVE) regime. The vane in cup system on the other hand, seems to be less affected by flow inhomogeneities. By following the rheological properties as a function of the MFC suspension solids content, it could be shown that the global property trends remained alike for all investigated measurement systems, despite the presence of erroneous effects in some geometries. The observed effects were linked to recent model hypotheses in respect to the morphology of MFC suspensions under changing shear situations.

7.2.1 Keywords

Microfibrillated cellulose (MFC), rheology, vane, depletion layer, flow curve, viscoelasticity

7.3 Introduction

Since 1983, when microfibrillated cellulose (MFC) was introduced by Turbak et al. (Turbak et al. 1983), extensive work has been carried out on the manufacturing,

modification, application and metrology of this versatile material (Desmaisons et al. 2017; Kangas et al. 2014; Nechyporchuk et al. 2016a). The versatility originates from two main factors; on the one hand, various types of source materials can be used, including virtually all types of plants and even animals (tunicates), whilst on the other hand, there are several manufacturing processes, including diverse pre- and post-treatments that also lead to very different morphologies of the final product. Despite several attempts, there is still no unified nomenclature for all the different cellulose types, yet commonly used differentiations are fibrillated vs. crystalline (Nechyporchuk et al. 2016a) and nano- vs. micro-sized width (Moon et al. 2011). The differentiation between nanofibrillated- and microfibrillated cellulose (NFC and MFC, respectively) is not made very consistently in the literature, where the classical meaning of micro is re-emerging to cover the nano region. In this context, (Kangas et al. 2014) should be referenced as it provides a straightforward definition, stating that only materials containing solely nano-sized fibrils (related to fibril widths) should be called NFC. MFC materials may also contain nano-sized fibrils, yet they also contain larger fibrils or even fibres, so they have a broad particle width-distribution ranging up to the micrometre-scale. The material investigated in this work is therefore classified as MFC.

With the increasing level of commercialisation of MFC materials, the need increases also for meaningful methods of characterisation. On the one hand, they are needed for quality control, and, on the other hand, a good differentiation of various grades is needed to be able to select an optimal product for a specific application. Several attempts at classifying properties have been made lately (Desmaisons et al. 2017; Kangas et al. 2014), concluding that a combination of several different methods is needed. A rather direct characterisation is particle size analysis. However, due to the naturally high aspect ratio of cellulose fibrils, the broad distribution of length and widths and their tendency to coil, such analyses become rather challenging. The only direct method providing actual fibril dimensions, like width and length, is image analysis. The need for extensive sample preparation, long measurement times and the requirement for many counts to achieve statistical relevance, such characterisations are impractical. So, an easier characterisation method, that would still provide some information on the fibril morphology would be very interesting.

The rheology of suspensions is known to depend *inter alia* on the size features of the suspended phase, so it might be a good candidate. Also, it is comparatively fast and generally does not need large sample volumes for a measurement. Not surprisingly, quite some work on the rheological characterisation of various nano- and micro-cellulose suspensions has already been carried out. Very commonly, flow curves (viscosity as a function of shear rate) and viscoelastic properties are determined. Typically, rheology is often used as an additional characterisation, but without a specific property target discussion (Dimic-Misic et al. 2016; Naderi et al. 2016; Padberg et al. 2016; Pahimanolis et al. 2013). Yet still, and especially lately, more and more work can be found, that specifically investigates the rheology of nano- and micro-cellulose suspensions (Dimic-Misic et al. 2017; Dimic-Misic et al. 2015; Iotti et al. 2011; Martoia et al. 2016; Nazari et al. 2016; Nechyporchuk et al. 2016b). A major topic in this field is the presence of rheometric-induced artefacts (side-effects) like wall depletion (migration of the fibrils away from the measurement cell walls), shear banding and wall slip (Haavisto et al. 2011; Kumar et al. 2016; Naderi and Lindström 2016; Nechyporchuk et al. 2014; Nechyporchuk et al. 2016b; Saarinen et al. 2014). These effects can contribute significantly to the measurement data and, therefore, lead to misinterpretations. So, it is very important to minimise such effects as much as possible, or at least be aware and consider them in model developments. It was found that the type of rheometer and the type of measurement system can influence these perturbing effects, and, therefore, the resulting measured properties (Nechyporchuk et al. 2014; Saarinen et al. 2009). Nechyporchuk et al. (Nechyporchuk et al. 2014) have shown, that the side-effects also depend on the type of cellulose, i.e. that MFC types (named as “enzymatic-NFC” by the authors) are even more prone to side-effects. Several researchers concluded that parallel-plate and cone-plate setups of shear rheometers may lead to even more secondary effects (Naderi and Lindström 2015; Nazari et al. 2016; Saarinen et al. 2009), and so the use of wide gap concentric cylinder (CC) setups is recommended. Other counter measures include rough and serrated surfaces or vane in cup geometry. However, what is still missing even now is a direct comparison of the commonly mentioned counter-measures against these side-effects with view to the more susceptible MFC suspensions. The present work aims to fill this gap and to provide some insights on the efficiency of those counter measures, as well as relate the specific system

characteristics to prevailing hypothesised structural models of MFC suspensions (Karppinen et al. 2012; Saarikoski et al. 2012).

Several researchers also use pipe and/or slit rheometer setups to investigate the flow dynamics of MFC suspensions, often coupled with additional techniques that allow a tracking and/or visualisation of the fibril structures (Haavisto et al. 2011; Haavisto et al. 2015; Kataja et al. 2017; Kumar et al. 2016; Lauri et al. 2017). An *ad hoc* comparability of data obtained by shear and pipe/slit-rheometers is not to be expected as the deformation is initiated by mechanical shearing via two surfaces on the one hand, whereas on the other hand it is pressure driven. Yet, several authors were able to show that comparability of the different resulting datasets is given under some conditions (Haavisto et al. 2015), or through respective data handling/treatment (Haavisto et al. 2017). Using pipe/slit rheometers can have several advantages, for example the reduced likelihood of restricting flocculation, or the ability to add several different measurement techniques in parallel (Haavisto et al. 2015; Kataja et al. 2017). However, a rather large amount of sample material is necessary for such volumetric flow setups (typically $> 1 \text{ dm}^3$), and potentially changing suspension morphologies along the measurement tube due to extended residence time as a function of tube length (Haavisto et al. 2015).

Four different rheometer measurement systems are compared in this study, including two smooth CC set-ups with different measurement gaps, one rough surface CC setup and a vane in cup setup. A further aim of this work is to propose some new descriptors to classify the properties that can be gathered from flow curve and amplitude sweep data that allow a more quantitative analysis of the observations, in particular, the typically reported three-region shape of the flow curve (Iotti et al. 2011; Jia et al. 2014; Karppinen et al. 2012; Saarikoski et al. 2012; Shafiei-Sabet et al. 2012) is parametrised as two zones separated by a transition region.

7.4 Methods

7.4.1 Materials

MFC was manufactured by a purely mechanical process, described in detail elsewhere (Schenker et al. 2016). In short, bleached eucalyptus pulp was mechanically disintegrated as a 3 wt% aqueous suspension (tap water) using a Supermasscolloider MKCA 6-2

(Masuko Sangyo Co., Japan) in various single passes at different rotational speeds. The specific grinding energy, defined as the total electrical energy consumption normalised by the amount of dry cellulose matter, was 7.2 kWhkg^{-1} . This mechanical fibrillation process typically leads to a broad size distribution (Lauri et al. 2017), i.e. coarse fibres as well as individual fibrils are present in such a suspension (Figure 7.1). It is, therefore, classified as MFC, rather than NFC. Also, as there were no modifications made to the MFC, it should be classified additionally as a flocculated structure MFC according to Nechyporchuk et al. (Nechyporchuk et al. 2016b). Dilutions of 0.5, 1 and 2 wt% for further use were obtained by the addition of tap water, followed by 2 min of rotor stator mixing at $12\,000 \text{ min}^{-1}$ (rpm) (Polytron PT 3000, Kinematica, Switzerland) and 5 min exposure to an ultrasonic bath. Before further measurements, the dilutions were let to rest for at least one hour. As a reference for flow curve measurements, a standard oil was used (Brookfield, fluid 1000, 985 mPas at 25°C).

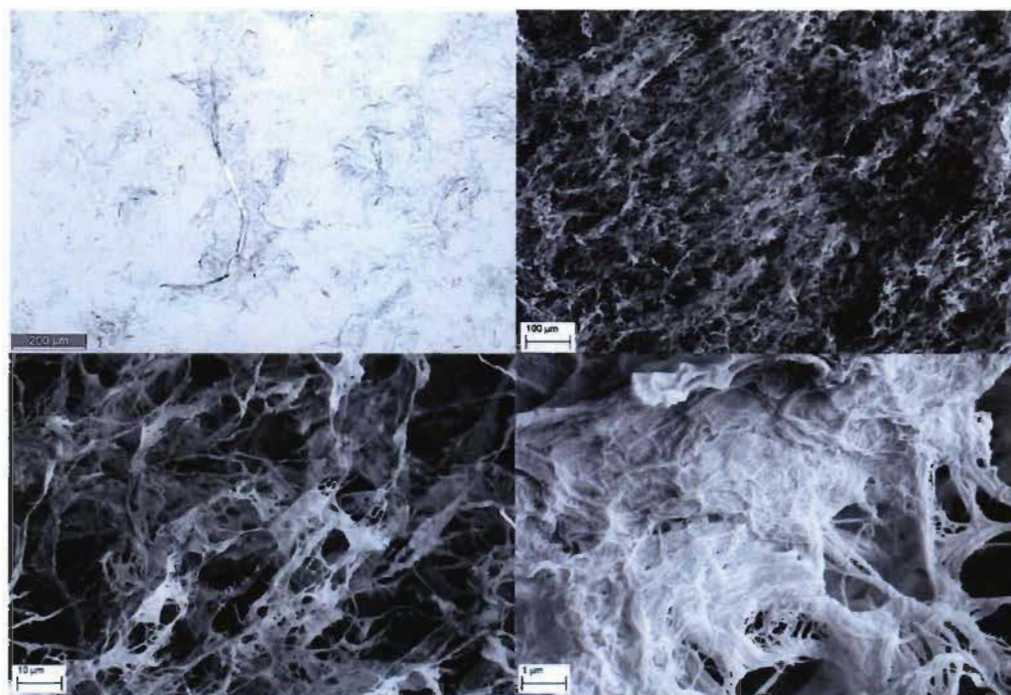


Figure 7.1: Optical microscopy image of MFC suspension at 0.5 wt% (top left), and SEM images of freeze-dried aerogels from 0.5 wt% suspensions at increasing magnifications (top right), (bottom left) and (bottom right). Some left over coarse fibres are apparent, as well as some individual and isolated fibrils.

7.4.2 Imaging

For imaging, the MFC suspension was diluted to 0.5 wt% and an equivalent of 5 wt%, based on dry weights, of carboxymethyl cellulose (Finnfix10, CP Kelco, Finland) was added as 1 wt% solution, prior to the above described mixing and ultrasonication. For optical microscopy (Axio Imager.M2m, Zeiss, Switzerland), one drop of suspension was placed between two glass slides. Another sample of this suspension was frozen in liquid nitrogen and then freeze dried using an automated system (Alpha 1-2 LD Freeze Dryer, Martin Christ Gefriertrocknungsanlagen GmbH, Germany). A piece was torn out of the aerogel and mounted on a support, so that the internal MFC aerogel structure could be imaged by SEM (Sigma VP, Zeiss, Switzerland) after being sputtered with gold (8 nm).

7.4.3 Rheological measurements

All the measurements were performed on an MCR 300 rheometer (Anton Paar, Austria) at 20 °C. Four different measurement systems were used, whereas all are based on a wide gap, cylinder and cup geometry. The first system is the CC27 ($d_{\text{cup}} = 28.92$ mm, $d_{\text{bob}} = 26.66$ mm), as it is supplied by the manufacturer (Anton Paar). The second system is also a CC27 system, but both cup and bob were roughened using a rough, 100 grit-class abrasive sandpaper (RR). The dimensions of the bob and cup as well as the moment of inertia of the bob were updated in the software accordingly. The roughening process led to a patterning on the surface, consisting predominantly of circular grooves around the geometrical rotation axis. So, waviness instead of roughness was calculated according to ISO 25178 for the bob from five different images recorded with a confocal laser scanning microscope (LSM 5 Pascal, Zeiss, Switzerland). The waviness was 1.8 ± 0.3 μm . The third system is the CC17 system ($d_{\text{cup}} = 18.08$ mm, $d_{\text{bob}} = 16.66$ mm) from Anton Paar. The fourth system is a vane (six blades) in serrated (length profiled) cup system (vane: ST22-6V-16, $d_{\text{vane}} = 22$ mm, cup: CC27-SS-P, $d_{\text{cup}} = 28.88$ mm, profile depths = 0.5 mm, profile widths = 1.65 mm), also supplied by Anton Paar (VS).

All the MFC suspensions, as well as the viscosity standard oil were measured as triplicates, whereas each measurement within a triplicate was a separate filling. For a given dilution, several dilution make-downs were used throughout the work presented here, whereas the repeatability was checked in all cases (data not shown). The data are presented as average values from the triplicate measurements, and respective standard deviations.

Flow curves (viscosity η in dependence of the shear rate $\dot{\gamma}$) were recorded by performing an automated shear rate increase ramp from 0.01 s^{-1} to $1\,000$ s^{-1} . 30 log- equidistant distributed point measurements were performed with automated acquisition time mode (minimal acquisition time is 15.2 s) and shear rate control.

As seen also by others, the flow curve of an MFC (or NFC and NCC) suspension typically consists of several, more or less distinct regions, showing different dependencies (Iotti et al. 2011; Jia et al. 2014; Karppinen et al. 2012; Shafiei-Sabet et al. 2012). Therefore, a focus of this work was put on a more effective description of these regions, to enable a comparison of such flow curves quantitatively. Figure 7.2 shows a typical flow curve with

two zones following a power law, divided by a transition showing a typical local minimum. At high shear rates, some measurements also showed an increase in viscosity with shear rate. This was attributed to non-laminar flow, observable as vortex in the cup. Such data points were omitted from the evaluation. Zone 1 and 2 are characterised by the two power law parameters of the Ostwald-de Waele fitting function according to

$$\eta_i = K_i \dot{\gamma}^{n_i-1} \quad \text{Equation 7.1}$$

where η_i is the viscosity, K_i is the consistency coefficient and n_i the flow index of zone i . Using the exponent $n - 1$ allows to compare it directly to data from other power law fluid descriptions based on stress, using the following form taken from the region beyond the yield stress τ_0 in the Herschel-Bulkley relation:

$$\tau = K \dot{\gamma}^n \quad \text{for} \quad \tau \gg \tau_0 \quad \text{Equation 7.2}$$

where τ is the shear stress (Lasseuguette et al. 2008). The data points for fitting in zone 1 were used up to shear rates at which a sudden increase of the acquisition time was seen. This increase in rheometer automated equilibrium acquisition time is believed to be a signal that the material is undergoing a transition in rheological state as the time required to achieve a steady measurement increases. Likewise, the data points for zone 2 were selected after the acquisition time dropped significantly once again at a shear rate after the transition zone. Zone 1 is additionally described with its apparent end and a viscosity value $\eta_{0.02}$ (low shear viscosity) that is obtained by solving the respective power law fit for a shear rate of 0.02 s^{-1} . Zone 2 is described additionally with the apparent start point and a viscosity value η_{100} (closely after the transition between low shear and high shear viscosity) that is obtained by solving the power law function for $\dot{\gamma} = 100 \text{ s}^{-1}$. The transition zone is characterised by the ratio of the low shear viscosity and the high shear viscosity and the comparative *relative depth of the local minimum* Δ_{\min} . The latter is a newly introduced parametrisation that is thought to be an indication of how strongly the suspension is aggregated (floculated) in the transition zone, e.g. previously reported, but not quantified accordingly, by Karppinen et al. (Karppinen et al. 2012). It is calculated by first fitting a power law function according to Equation 7.1 through $\eta_{0.02}$ and η_{100} and then interpolating it to the shear rate of the local minimum to get the *theoretical local minimum*

viscosity (Equation 7.4, Equation 7.5 and Equation 7.6). Δ_{\min} is then calculated as the difference between the theoretical local minimum viscosity and the actual viscosity at the local minimum, normalised by the local minimum viscosity (Equation 7.3),

$$\Delta_{\min} = \frac{\eta_{\min,th} - \eta_{\min}}{\eta_{\min,th}} \quad \text{Equation 7.3}$$

$$\eta_{\min,th} = K_{\text{int}} \dot{\gamma}_{\min}^{n_{\text{int}}-1} \quad \text{Equation 7.4}$$

$$n_{\text{int}} - 1 = \frac{\log(\eta_{100}/\eta_{0.02})}{\log(100/0.02)} \quad \text{Equation 7.5}$$

$$K_{\text{int}} = \frac{\eta_{0.02}}{0.02^{n_{\text{int}}-1}} \quad \text{Equation 7.6}$$

with $\eta_{\min,th}$ being the calculated viscosity at the shear rate of the local minimum $\dot{\gamma}_{\min}$ using the fitting function calculated from η_{100} and $\eta_{0.02}$ with the flow index n_{int} and consistency coefficient K_{int} at the zone interface of the transition, and η_{\min} being the local minimum viscosity.

It should be mentioned that the interpretation of Δ_{\min} has some limits. When η_{\min} is acquired in equilibrium (stable reading), then it may give a good indication of the aggregation in the suspension following the conclusions of Karppinen et al. (Karppinen et al. 2012). Yet, the acquisition times in the transition zone can exceed the maximal acquisition time set by the rheometer software under certain situations (data not shown). In this case, η_{\min} may be overestimated, and therefore Δ_{\min} underestimated.

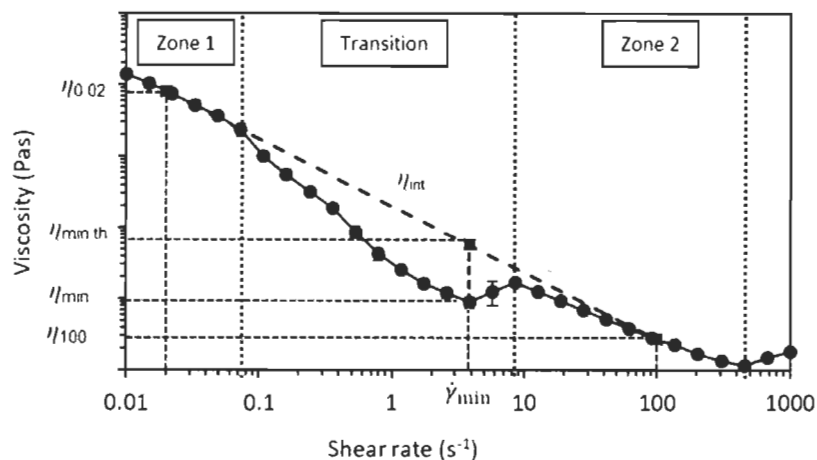


Figure 7.2: Typical flow curve of an MFC suspension characterised in this work. There are three distinct regions; zones 1 and 2 following a power law, being divided by a transition region. Some combinations of measurement setups and suspension solid contents also showed a fourth zone where the viscosity apparently seemed to increase. However, this was attributed to non-laminar flow, easily observable as vortex forming by the sample suspension in the cup. The parameters necessary for calculating the relative depth of the local minimum Δ_{min} , $\eta_{0.02}$ and η_{100} are indicated also.

Viscoelastic properties were determined by an amplitude sweep measurement at a frequency of 0.5 Hz. The automated, amplitude-controlled ramp was set from 0.001 % to 1 000 % with 60 log-equidistant distributed point measurements and automated acquisition time mode (in practice, the acquisition time was seen to be around 25.5 s for all points in all measurements).

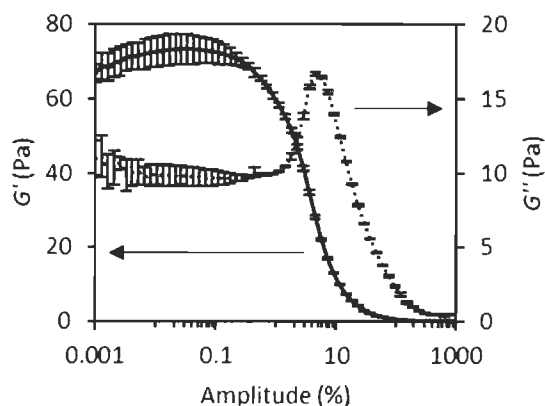


Figure 7.3: Storage and loss modulus (G' , G'') data of a 1 wt% MFC suspension measured with the CC27 geometry. The storage modulus data are represented with the full line on the left y -axis and the loss modulus data are represented with the dotted line on the right y -axis, respectively. Please note the different scales of both y -axis. The error bars indicate the standard deviation. It is apparent that the storage modulus is not linear, but goes through a maximum before the structure breakdown. The loss modulus is linear at low oscillation amplitudes and shows an increase before the structure breakdown.

It was found that there is only a very short linear regime for the storage modulus (G') at very low shear stresses, respectively extremely small amplitudes (Figure 7.3), so the maximal storage modulus G'_{\max} was evaluated in this work, rather than the typically used plateau value. Analogously, the minimum of the phase angle, δ_{\min} , was evaluated. As the loss modulus G'' typically showed some more extended linear regime (LV), the plateau value G''_{lin} was evaluated. MFC suspensions are known to behave like gels above certain concentrations, i.e. behaving like a viscoelastic solid ($G' > G''$) in a linear viscoelastic region (LVE), and after exceeding a critical shear stress, behaving like a viscoelastic liquid ($G' < G''$). Following (Moberg and Rigdahl 2012), the onset of the loss of linearity (Wu and Morbidelli 2001) was determined by the onset of the transformation from the viscoelastic solid to the viscoelastic liquid behaviour. Yet, in this work, the onset of the loss of linearity (LoL) was defined as the deformation at which the phase angle exceeded the minimal phase angle by 5 %. Selecting the phase angle instead of the storage modulus

to define the *LoL* was applied because the phase angle also includes the viscous behaviour of the material, i.e. the loss modulus:

$$\delta = \tan^{-1} \left(\frac{G''}{G'} \right) \quad \text{Equation 7.7}$$

The authors believe that in the case of a viscoelastic material, both moduli should be considered when discussing the structural response to a deformation, i.e. when undergoing shearing. Considering the storage modulus only may give an incomplete picture as the material naturally has a viscous response to the deformation, even at low deformations, i.e. in the LVE. It was, however, also found that there is a good correlation between the *LoL* determined as described above, and when determined using the onset of the loss of the storage modulus alone (data not shown). The dynamic yield stress in this work is defined as the stress at the *LoL*, $\tau_{y,\delta}$, as opposed to the static yield, τ_0 , shown in Equation 7.2.

7.5 Results

Graphs of the data that were used to derive the viscoelastic and flow curve parameters evaluated in this study, is provided in the Supplementary Information S1.

7.5.1 Viscoelastic properties

Figure 7.4a shows the evolution of the storage and loss moduli (G'_{max} and G''_{lin}) in the linear viscous regime (LV) as a function of the MFC suspension solids content for the different measurement systems. The storage modulus is significantly larger than the loss modulus under all geometric conditions, and the moduli increase with increasing solids content of the MFC suspension. This is typically seen throughout the literature, e.g. (Baati et al. 2017; Moberg et al. 2017; Nechyporchuk et al. 2016b; Pääkkö et al. 2007). Looking at an independent power law fitting, $y = ax^b$, of the moduli y against solids content x data (Table 7.1), it is apparent from the parameters a and b that the measurement system has only a small influence on the trends.

Only few authors have investigated the impact of different measurement systems on viscoelastic properties of MFC suspensions, e.g. (Naderi and Lindström 2015; Saarinen et al. 2009), whereas only Naderi and Lindström (Naderi and Lindström 2015) have directly compared different cylinder and cup setups (smooth and profiled). Saarinen et al.

(Saarinen et al. 2009) found that the cone-plate setup leads to a higher storage modulus plateau, compared to a plate-plate and a cylinder cone (CC27) system (all systems had a smooth surface). They argued that if wall slip (due to wall depletion) would be the dominant erroneous effect, then the data should be oppositely related to those observed. So, they attributed the observed effect to the gap size, whereby, in the cone-plate setup, the gap was too small in relation to residual fibres and/or fibril aggregates (“flocs”). In addition, Naderi and Lindström (Naderi and Lindström 2015) found that the storage as well as the loss moduli were smaller when measured with smooth CC surfaces compared to a profiled surface CC setup. This effect was attributed to the depletion layer. As the data in Figure 7.4a do not show any of those effects, it may be hypothesised, that the gap size is sufficiently large, so that no blocking of coarse aggregates occurs on the one hand, and that potential side-effects on the other hand contribute only slightly in the initial viscoelastic region.

Figure 7.4b reveals that the minimum in phase angle (δ_{\min}) is generally higher for the VS system compared to the CC27 and RR systems. As a higher phase angle means that the ratio of the loss and storage moduli is shifted more toward the loss modulus (Equation 7.7), the data indicate a more viscous, but still overall elastically dominated, behaviour of the MFC suspension when characterised by the VS system. Assuming the viscous behaviour to be a relative movement between fibres, i.e. a relocation of connection points (attractive inter-fibril interactions), and the elastic behaviour to be the stretching of the fibrils and/or fibrillar network, thus increasing the radius of gyration, the VS system seems to promote the relative movement of fibrils over that of distortion. This hypothesis remains, however, to be proven, e.g. by adding another measurement technique that allows high resolution (spatial and temporal) velocity profiling of the MFC suspension near the edges of the vane blades.

When the oscillation amplitude (strain) becomes large enough, then the structure breaks down and the viscoelastic properties of the suspension change. As explained earlier, this is characterised by the *LoL* and the yield stress ($\tau_{y,\delta}$) in this work (Figure 7.4c and d). For all systems, a trend is seen that higher solids contents decrease the *LoL* and increase $\tau_{y,\delta}$. Such a trend is also seen in the data presented by Jia et al. (Jia et al. 2014), yet the authors did not describe the effect. The increase of the shear stress with the increasing solids

content of the suspension can be explained easily by the increased number of fibrils and fibril contact points per unit volume of the suspension. However, the increased amount of fibril contact points also means that the length between the contact points becomes smaller. So, less strain is needed to create higher stress and such that the contacts break at lower strain and the system, therefore, starts to yield at a lower strain due to the greater induced stress.

A significantly increased limit of linearity and yield stress is seen for the VS system compared to the two others. Two reasons may be hypothesised for the later onset of the structure yielding for the VS systems. Either, the suspension structure actually collapses later as a function of strain in the VS system, or there is slip or a depletion layer effect occurring in the two other systems that is just wrongly interpreted as structure yielding. Figure 7.5 shows the typical phase angle data, exemplified by the 1 wt% MFC suspension. The higher value for δ in the LVE is apparent for the VS system, but also that the increase of δ as a function of strain is initially slower for the VS system. The very abrupt increase of the phase angle at lower deformation and assumed stress seen for the CC and RR system can indicate a slip, depletion layer or a shear banding effect. As there is no indication for such an effect within the LVE for the other systems, it may be hypothesised that one of the potential effects is induced in the CC and RR systems, or at least enhanced by the precedent deformation.

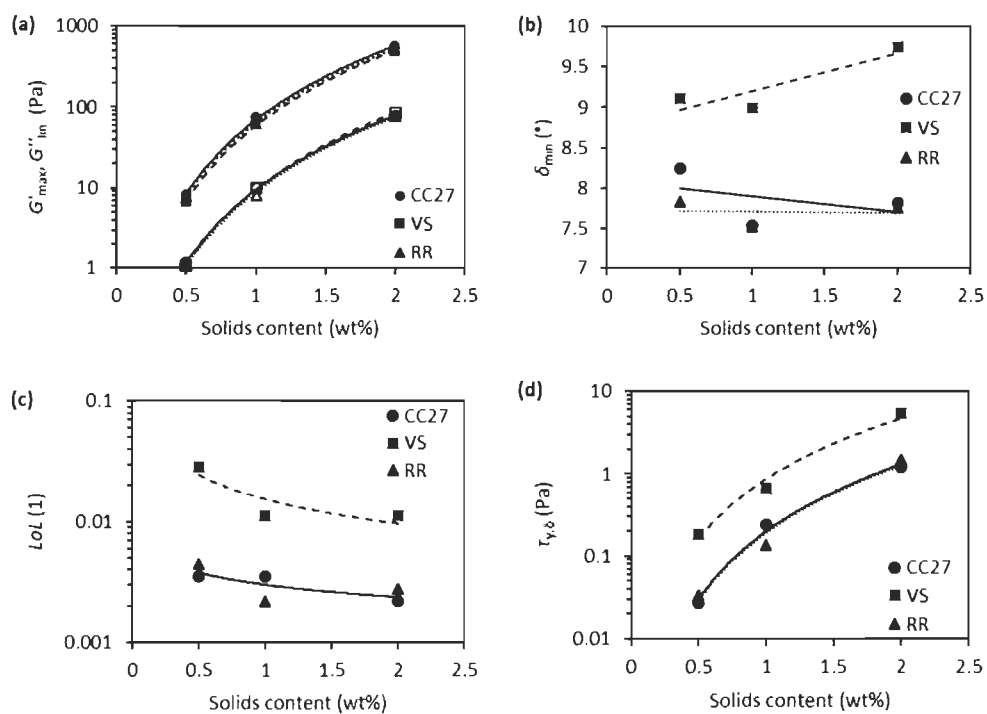


Figure 7.4: Viscoelastic properties in dependence of the suspension solids content for the different measurement systems CC27: smooth setup, VS: vane in serrated cup, RR: roughened cup and bob, as shown in (a)-(d). In graph (a), the maximum storage modulus data are represented with the filled symbols and the linear loss modulus data are represented with the hollow symbols, respectively.

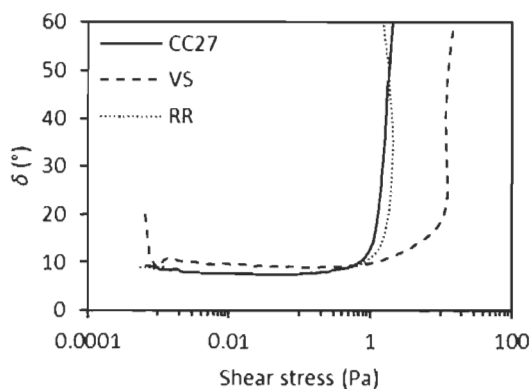


Figure 7.5: Phase angle (δ) as a function of the shear stress (τ), derived from an amplitude sweep measurement performed on a 1 wt% MFC suspension with different measurement systems. The higher phase angle in the initial viscoelastic region, as well as the later and prolonged onset of the increase of the phase angle for the VS system are apparent.

Table 7.1: Fitting function parameters of selected viscoelastic properties. The fitting function variable x is the solids content, and y is the fitted modulus property.

System	Property (y) (Pa)	$y = ax^b$	
		a (Pa)	b
CC27	G'_{\max}	73	2.9
VS	G'_{\max}	61	3.0
RR	G'_{\max}	63	3.1
CC27	G''_{in}	9.8	3.0
VS	G''_{lin}	9.8	3.1
RR	G''_{lin}	8.1	3.3

7.5.2 Flow curves

To verify that all measurement setups were initialised correctly, flow curves of a viscosity standard oil were recorded. Figure 7.6a shows the expected Newtonian behaviour and the viscosity value of about 1 Pas of the oil for all systems. This comparison is important, as it shows that, even though the VS and the RR systems are only relative systems, they

actually report the correct absolute viscosity values and trends. Having this information makes it possible to attribute differences seen later in this work to the different material responses to the measurement setups, and not the measurement system itself. Please note also the lower shear rate limits for reliable measurements for the respective systems, provided by the rheometer supplier (Figure 7.6a). Data of a given system that lie below the lower reliable detection limit on the curve should not be used. It is apparent, that the investigated measurement systems are not optimal for measuring low viscosity at low shear rates. Yet, as can be seen in Figure 7.6b, viscosities of the investigated MFC suspensions were several orders of magnitude larger than 1 Pas at low shear rates, and, thus, generally very well within the detection limits for reliable measurement.

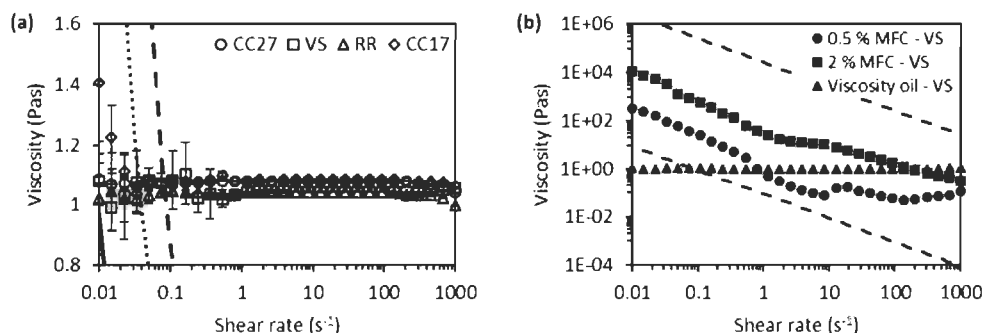


Figure 7.6: Flow curves of a viscosity standard oil measured with the different measurement setups (a). The error bars represent the standard deviations. The lines mark the limits for reliable measurements provided by the machine supplier for the used setups (full: CC27 and RR, dashed: VS and dotted: CC17). Flow curve values that are below or close to the lower limit of detection should not be interpreted. The MFC suspension viscosity was well above these minimal detection limits, exemplified here with 0.5 and 2 wt% MFC measured with the VS system (b).

Several articles describe, that flow curves of MFC suspensions consist of two or three distinct regions, and attribute those to different suspension morphologies, i.e. different status of flocculation (Karppinen et al. 2012; Martoia et al. 2015; Saarikoski et al. 2012; Saarinen et al. 2014). Some articles also describe such behaviour for NCC suspensions,

though it is attributed to the transformation from isotropic to chiral nematic liquid crystalline phases (Shafiei-Sabet et al. 2012). Flow curves of NFC suspensions also consist of different regions, yet it seems that there is much less or no flocculation (Nechyporchuk et al. 2014). However, to obtain a real NFC according to the earlier provided definition, chemical modifications have to be applied, which inherently increase the charge density on the fibrils. This, in itself, will also change the rheological response of the system (Veen et al. 2015). Further work is planned to investigate the influence of the fibril widths on the rheological properties of MFC suspensions, without having an additional influence of a changed surface charge. Karppinen et al. (Karppinen et al. 2012) and Saarikoski et al. (Saarikoski et al. 2012) show that, at rest and very low shear rates, the MFC suspension is a network of fibrils. Increasing the shear rate leads to a “flocculation” of the fibrils. Up to a maximum, the floc size increases with increasing shear rate and “voids” (depleted, water-rich areas) form and grow. After reaching the maximum, the floc size decreases again and the voids disappear. It should be noted here that the term “floc” is loosely used to refer to papermaking terminology where fibres are seen to clump together in a bulky cooperative structure. However, shear induced structure, such as that seen here is more likely to be due to physical entanglement, such as occurs in polymer systems, rather than a colloiddally defined floc. Martoia et al. (Martoia et al. 2015) confirmed this floc behaviour also for enzymatic NFC, and it can be attributed to a competition between attractive and repulsive surface forces (Chaouche and Koch 2001) that is influenced by the shear rate and stress condition. Saarinen et al. found additionally that there can be significant solids depletion at low shear rates (“below the yield stress”), dominating the flow curve. Naturally, this depleted layer also is seen in terms of rapid shear thinning. In all the aforementioned publications smooth cylinder cup setups were used, with gap widths ranging from 0.5 to 2 mm. Also, the investigated MFC or NFC suspensions were very probably similar to the MFC suspension that was used here in our work. In the following discussions of the flow curves, the same models are assumed because of these likely similarities between the materials and methods used and those applied in this work. It should be noted that comparing alike types of nanocelluloses is important, as different types behave differently in rheological measurements. It seems that three major types with different rheological behaviour can be distinguished: modified (e.g.

2,2,6,6-tetramethylpiperidinyloxy (TEMPO)-oxidised) and then fibrillated, mechanically fibrillated (including enzymatically pretreated) and crystalline cellulose. The main difference between the modified and the unmodified fibrillated materials is the increased surface charge, for example, due to the oxidation or the addition of polyelectrolytes. This increases the repulsive surface forces, and therefore works against flocculation (Martoia et al. 2015; Moberg et al. 2017; Naderi and Lindström 2016; Veen et al. 2015). Crystalline celluloses typically also carry more surface charges than fibril-derived materials, and have additionally a smaller aspect ratio and are stiff compared to fibrils, allowing them, for example, to form nematic structural phases (Shafiei-Sabet et al. 2012).

Figure 7.7 summarises the properties of zone 1 of the flow curves of the different measurement systems and as a function of the suspension solids contents. It is apparent, that the end of zone 1, or the beginning of the transition region, strongly depends on the measurement system (Figure 7.7a). Looking at the power law parameters (K_1 , n_1) and the related low shear viscosity ($\eta_{0.02}$) reveals that the material in the VS system leads to significantly different results compared to the other systems (Figure 7.7b-d). Also, the material in the RR system behaves differently, because the acquisition time data (not shown) indicate that there is no zone 1 in the RR setup measured flow curves, at least as we define it, i.e. no stabilised acquisition time. Due to this, no further evaluation of zone 1 properties according to the procedure described in the methods section was carried out using the RR system. However, it is apparent that the flow index n_1 would be negative before zone 2 starts for the RR system (n_1 would have been -0.13, -0.25 and -0.05 for 0.5, 1 and 2 wt%). A similar behaviour was described by Nechyporchuk et al. (Nechyporchuk et al. 2014), comparing smooth and rough surface cone-plate systems. Optical visualisation revealed that there was wall slip on the smooth moving surface geometry, and a significant solids depletion layer on the rough, moving surface. They attributed the depletion (“water release”) directly to the roughness and the deformation, since at the initial low shear rates, no water release was seen. This is in very good agreement with the data presented in this work. From the two smooth systems (CC27 and CC17), the smaller gap system CC17 shows slightly increased viscosity. This is initially unexpected because the depletion layer effect should become proportionally larger for a smaller gap (reducing the viscosity in the smaller gap), assuming a depletion layer thickness independent of the

gap (Barnes 1995; Yoshimura and Prud'homme 1988). It could, however, be hypothesised that the depletion layer could not stabilise in the presence of fibril flocs. In other words, the flocculated structures may have been so large in comparison to the measurement gap, that physical bridging occurred between the rotating and static geometry (alike the observations made by Saarinen et al. (Saarinen et al. 2009) in viscoelastic measurements). This then led to an apparently increased viscosity, compared to the larger gap system (CC27). Following the earlier reasoning, it may be concluded, that the viscosity ($\eta_{0.02}$) data in Figure 7.7d is a side-effect for the CC and RR systems, and less pronounced in the VS system. Haavisto et al. (Haavisto et al. 2015) find that flow indices close to 0 (and smaller than ca. 0.2) are a clear indication for slip induced by a depletion layer. So, following their argumentation, the here presented zone 1 data VS system with flow indices between 0.10 and 0.16 may still be dominated by the presence of a depletion layer. It should be kept in mind, however, that depletion on a vane geometry may have different consequences for the contribution to artefacts as there is significantly less tangential surface area compared to complete concentric cylinder setups. Also, additional side effects like suspension fracture at the edges of the blades (Nechyporchuk et al. 2015) may be present in the VS system. So, without a direct observation of the flow dynamics of an MFC suspension in a VS system, the degree of susceptibility and the nature of potential measurement artefacts of the VS system remain unclear. Also, the transition region starts earlier for the VS system (Figure 7.7a), indicating an earlier onset of flocculation because of a better shear transduction into the measurement gap, or a delay of the onset for the two CC systems due to slip, depletion or banding. As there is a constant, unidirectional shear in a flow curve experiment (strain deformation of the viscous suspension), the flow situation can be considered to be occurring outside the LVE, i.e. no longer dominated by elastic interactions. So, the conclusions drawn from the zone 1 flow curve behaviour (i.e. more pronounced side-effects for non-VS systems) are in good agreement with the observations made at the end of the LVE (onset of the increase of the phase angle).

With some exceptions, it seems that the end of zone 1 is shifted to higher shear rates when the solids content of the MFC suspension increases (Figure 7.7a). This indicates that the flocculation that is attributed to the transition region is hindered by a higher fibril concentration. In conjunction with the increase of viscosity ($\eta_{0.02}$) with the solids content

(Figure 7.7d), it can be concluded that reorganisation of the fibril network is hindered by a higher fibril concentration. This is rather straightforward, assuming that there are more connection points and more entanglements in a higher concentrated suspension (Iotti et al. 2011). Considering the standard deviations and the scatter of the flow indices (Figure 7.7c), no clear trend, however, can be identified.

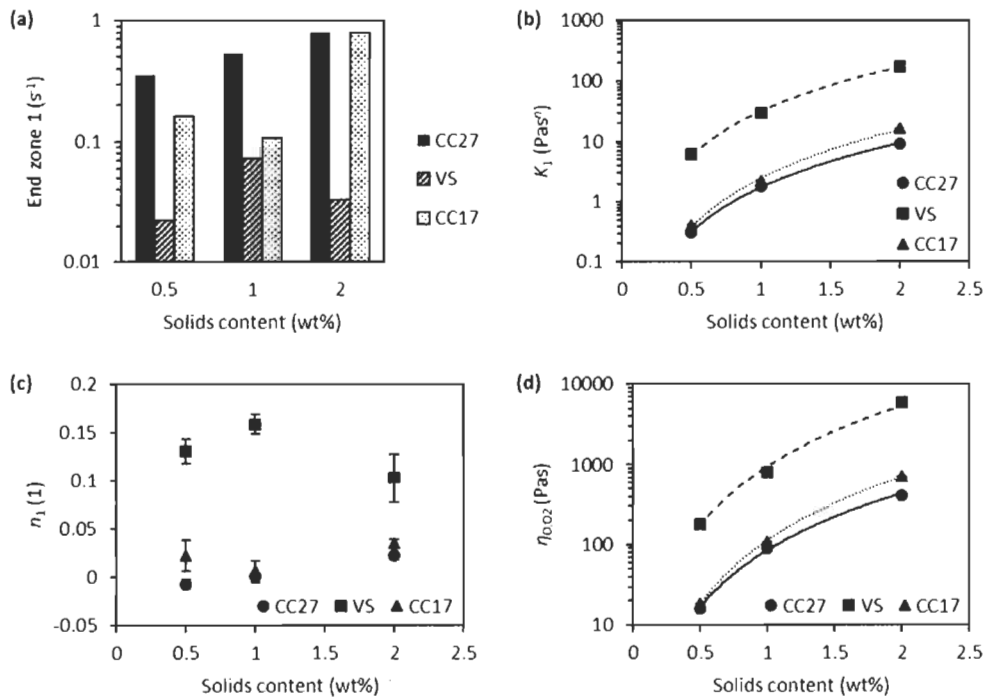


Figure 7.7: Description of zone 1 of the flow curve: end of zone 1 (a), power law parameters K_1 (b) and n_1 (c), and the interpolated viscosity at $0.02 s^{-1}$ for the different measurement systems (CC27: smooth setup, VS: vane in serrated cup, CC17: smooth setup) as a function of the suspension solids content.

The overall trends in zone 2 appear alike the ones seen for zone 1, when looking at Figure 7.8. The onset of zone 2 for the VS system happens at lower shear rates compared to all other systems (Figure 7.8a) and the consistency coefficient (K_2) as well as the high shear viscosity start point (η_{100}) are highest (Figure 7.8b and d). We can see that the relative difference between the VS and the other measurement systems is, however, smaller

compared to the differences in zone 1 (Figure 7.7b and d). The flow index of the VS system, though, is found to be smaller compared to the other systems (Figure 7.8c). As in zone 1, an earlier onset of zone 2 for the VS system may indicate a better transmission/carry-over of the shear across the measurement gap. As reported by others, it is likely that the whole material in the measurement gap is sheared homogeneously at high shear rates (Nechporchuk et al. 2014) with influences arising from depletion or other effects significantly suppressed. But apparently there are still some side-effects present overall as the zone 2 flow curves of the different systems are not identical. This is also supported by Kataja et al. (Kataja et al. 2017), who show that a depletion layer and/or solids content gradient layers remain present, even at high shear rates (volume flows). Interestingly, the start of zone 2, which is the change from a strongly flocculated system to a more homogeneous system (Karppinen et al. 2012), is shifted to lower shear rates for higher solids contents of the suspension (Figure 7.8a). Following the observation of Karppinen et al. 2012 (Karppinen et al. 2012), that “voids” (fibril-free, water-filled areas) are formed in the transition zone, it can be assumed that the size and volume fraction of these voids increase with decreasing solids content, as more water can be released from the gel structure in zone 1. This then leads to a delay of the reorganisation of the floc structure into the more homogeneous dispersion. In contrast to the flow indices of zone 1 (Figure 7.7c), the ones of zone 2 (n_2 , Figure 7.8c) follow a power law trend as a function of solids content (Table 7.2) and become smaller with increasing solids content of the suspension. This means that a higher solids content leads to a stronger shear thinning behaviour at increased shear rates. It is assumed that in zone 2, the suspension structure becomes more homogeneous (Haavisto et al. 2015; Karppinen et al. 2012) and/or more aligned (Iotti et al. 2011) with increasing shear rate. This will lead to less dynamic entanglements and therefore an eased flow. However, this does not preclude cooperative motion being considered to account for strong shear thinning, which has been seen and modelled in generalised particulate suspension systems (Toivakka and Eklund 1994; Toivakka and Eklund 1995). Assuming that entanglements are the major contribution to the dynamic viscosity of an MFC suspension, then this means that at very high shear rates (with respect to the shear rate range investigated in this study) the viscosity does not depend as strongly on the solids content, because the structure is less randomly entangled

anyway, though the cooperative motion hypothesis may well be stronger at higher solids content (Toivakka and Eklund 1994). However, at lower shear rates, still in zone 2, the viscosity is more strongly dependent on solids content because there are still entanglements undergoing dynamic formation and break-up, and their dynamic interaction rate depends on the particle-particle encounters, and so, inevitably, on solids content. This hypothesised mechanism would then explain the stronger shear thinning behaviour at higher solids contents as the change from dynamic contacts towards stabilised homogeneous or cooperative flow occurs rapidly. The increase of the overall viscosity in zone 2 (η_{100}) with the suspension solids content (Figure 7.8d) is still related to an increased amount of total contact points and entanglements (Iotti et al. 2011), and, thus, still increases with increasing solids content.

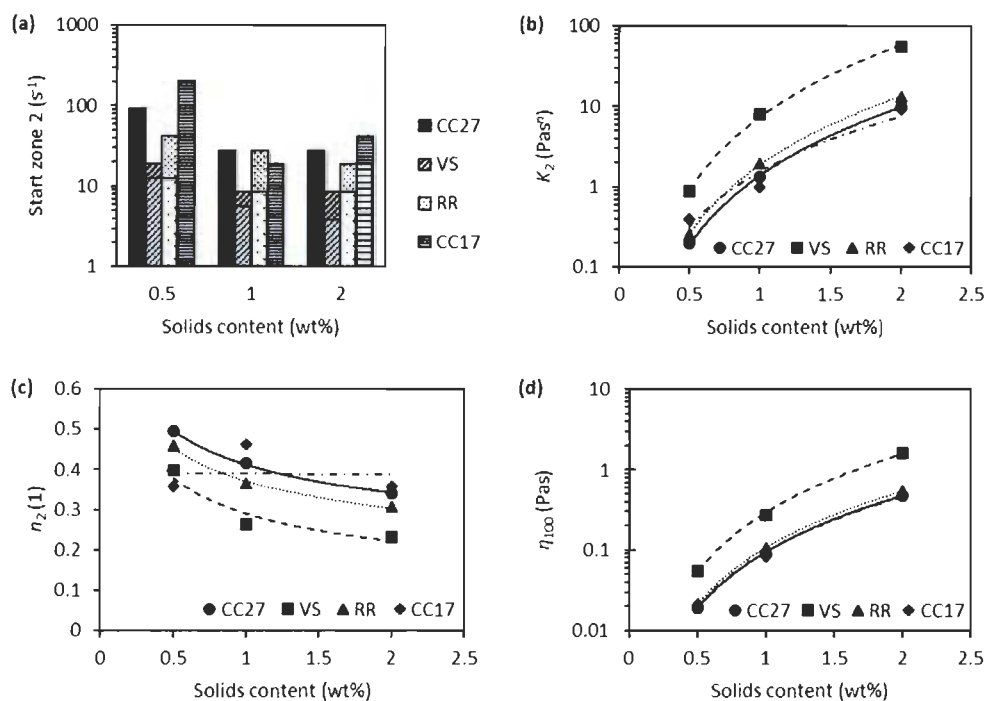


Figure 7.8: Description of zone 2 of the flow curve : start of zone 2 (a), power law parameters K_2 (b) and n_2 (c) and the interpolated viscosity at 0.02 s⁻¹. The lighter shaded bars in (a) show the earliest shear rate at which one of the triplicate measurements started the zone 2 power law behaviour. The difference of lighter and darker shaded bars of the same pattern is therefore a zone 2 onset deviation range.

Table 7.2: Fitting function parameters of selected flow curve properties. The fitting function variable x is the solids content, and y is the fitted modulus property.

System	Property (y)	$y = ax^b$	
		a	b
CC27	K_1	1.8	2.3
VS	K_1	30	2.5
CC17	K_1	2.2	2.9
CC27	$\eta_{0.02}$	90	2.2
VS	$\eta_{0.02}$	809	2.8
CC17	$\eta_{0.02}$	108	2.7
CC27	K_2	1.3	2.9
VS	K_2	8.0	2.8
RR	K_2	2.0	2.8
CC17	K_2	1.1	3.1
CC27	n_2	0.41	-0.27
VS	n_2	0.29	-0.43
RR	n_2	0.37	-0.30
CC17	n_2	0.39	0
CC27	η_{100}	0.09	2.4
VS	η_{100}	0.27	2.6
RR	η_{100}	0.11	2.4
CC17	η_{100}	0.09	2.5

The transition zone depth, Δ_{\min} , is about the same for all systems where a local minimum was identified (Figure 7.9a). This may indicate, that the same maximum degree of flocculation is achieved in all systems. However, depending on the measurement setup, this happens at different shear rates (local minimum, Figure 7.9b). The CC27 system did not show a clear minimum, even though the flow curve and the acquisition time data indicate a transition zone. It may be that the flocs in this system become as big as the measurement gap, or protrude into the transition wall and void regions, and therefore lead to blocking, interpreted as increased viscosity. The transition zone depth decreases with

the solids content of the MFC suspension. This is in good agreement with the observations made in zone 2, assuming bigger depleted voids and higher void shares also lead to a larger drop in viscosity.

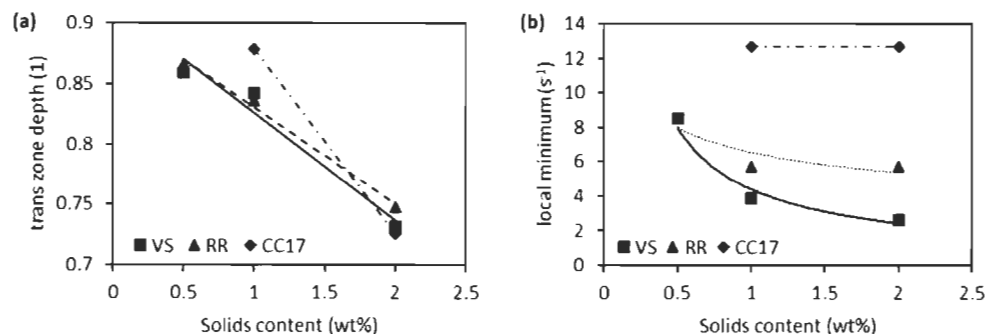


Figure 7.9: Description of transition zone properties: (a) normalised transition zone depth, and (b) the shear rate where the local viscosity minimum appears. The dotted lines are just for visual guidance and are not actual fits.

7.6 Conclusions

The aim of this work was to investigate the effects of different shear rheometer measurement setups on the observed rheological properties of MFC suspensions. Commonly used as well as newly proposed descriptors of viscoelastic and flow curve data were compared. Also, the potential mechanisms leading to the different results were proposed and discussed in relation to current morphological models of MFC suspensions. The viscoelastic measurements have shown that at very low deformations up to the elastic modulus maximum, where elastic interactions dominate the suspension response, commonly observed rheometric-induced side-effects (artefacts) like slip, solids depletion at the wall or shear banding only have a minor impact on the results. This finding of course may well be limited to the settings and conditions used in this study. It was seen that different commonly used measurement systems delivered very similar results. There is an indication, however, that the vane system with serrated wall cup (VS) is the least perturbation affected system. When the oscillation amplitude becomes larger, it seems that side-effects are induced in the smooth surface cylinder in cup (CC) and surface roughened (RR) setups, indicated by a very fast increase of the viscoelastic phase angle, and particularly an earlier onset of this increase compared to the VS system.

The flow curve data support the findings from the viscoelastic measurements. The lower viscosities and the later onsets of the transition region, respectively into zone 2, seen for the CC and RR systems compared to the VS system, indicate the presence of artefacts acting as side-effects. These observations are also well supported by recent publications where velocity profiling techniques reveal the flow dynamics of sheared MFC suspensions. The results presented here have shown that it is very likely that the VS system is much less susceptible to side-effects also in this shear regime, and therefore should be preferred when characterising MFC suspensions. Yet further studies, specifically on a wide range of MFC suspensions and a variety of vane-based setups, involving velocity profiling methods, would be needed for verification of this hypothesis before considering it a generalisation.

The trends of rheological parameters as a function of the MFC suspension solids content were also investigated. Despite the presence of side-effects that are suspected to be present in the CC and RR systems, most of the properties followed the same trends across the various geometries, independent of the measurement system used.

To be able to compare rheological data quantitatively, like the ones presented here, the obtained data need to be parameterised accordingly. The relevance in describing, for example, the onset points of different zones in the flow curves, or the limit of linearity in viscoelastic measurements, has been demonstrated here.

With this work as a basis, further investigations on the rheology of MFC suspensions as a function of MFC type and material properties are planned, providing further insight concerning the relationship between rheology and the morphology of MFC fibrillar material in suspension.

7.6.1 Acknowledgements

Omya International AG and FiberLean Technologies Ltd. are thanked for the support of this research. Silvan Fischer is also acknowledged for the microscopical characterisation of the MFC suspensions as well as Dr. Johannes Kritzing for very valuable discussions.

7.7 References

- Baati R, Magnin A, Boufi S (2017) High Solid Content Production of Nanofibrillar Cellulose via Continuous Extrusion. *ACS Sustainable Chemistry and Engineering* 5:2350-2359. doi:10.1021/acssuschemeng.6b02673
- Barnes HA (1995) A review of the slip (wall depletion) of polymer solutions, emulsions and particle suspensions in viscometers: its cause, character, and cure. *Journal of Non-Newtonian Fluid Mechanics* 56 doi:10.1016/0377-0257(94)01282-M
- Chaouche M, Koch DL (2001) Rheology of non-Brownian fibres with adhesive contacts. *Journal of Rheology* 42:369-382. doi:10.1122/1.1343876
- Desmaisons J, Boutonnet E, Rueff M, Dufresne A, Bras J (2017) A new quality index for benchmarking of different cellulose nanofibrils. *Carbohydrate Polymer* doi:10.1016/j.carbpol.2017.06.032
- Dimic-Misic K, Maloney T, Liu G, Gane P (2017) Micro nanofibrillated cellulose (MNFC) gel dewatering induced at ultralow-shear in presence of added colloiddally-unstable particles. *Cellulose* 24:1463-1481. doi:10.1007/s10570-016-1181-x
- Dimic-Misic K, Maloney TC, Gane PAC (2015) Defining a strain-induced time constant for oriented low shear-induced structuring in high consistency MFC/NFC-filler composite suspensions. *Journal of Applied Polymer Science* 132 doi:10.1002/app.42827
- Dimic-Misic K, Rantanen J, Maloney TC, Gane PA (2016) Gel structure phase behavior in micro nanofibrillated cellulose containing in situ precipitated calcium carbonate. *Journal of Applied Polymer Science* 133 doi:10.1002/app.43486
- Haavisto S, Cardona MJ, Salmela J, Powell RL, McCarthy MJ, Kataja M, Koponen AI (2017) Experimental investigation of the flow dynamics and rheology of complex fluids in pipe flow by hybrid multi-scale velocimetry. *Experiments in Fluids* 58 doi:10.1007/s00348-017-2440-9
- Haavisto S, Liukkonen J, Jäsberg A, Koponen A, Lille M, Salmela J Laboratory-Scale Pipe Rheometry: A Study of a Microfibrillated Cellulose Suspension. In: *PaperCon*, Covington, 2011.

- Haavisto S, Salmela J, Jäsberg A, Saarinen T, Karppinen A, Koponen A (2015) Rheological characterization of microfibrillated cellulose suspension using optical coherence tomography. *Tappi Journal* 14:291-302.
- Iotti M, Gregersen OW, Moe S, Lenes M (2011) Rheological Studies of Microfibrillar Cellulose Water Dispersions. *Journal of Polymers and the Environment* 19:137-145. doi:10.1007/s10924-010-0248-2
- Jia X et al. (2014) Rheological properties of an amorphous cellulose suspension. *Food Hydrocolloids* 39:27-33. doi:10.1016/j.foodhyd.2013.12.026
- Kangas H, Lahtinen P, Sneek A, Saariaho AM, Laitinen O, Hellén E (2014) Characterization of fibrillated celluloses. A short review and evaluation of characteristics with a combination of methods. *Nordic Pulp and Paper Research Journal* 29:129-143. doi:10.3183/NPPRJ-2014-29-01-p129-143
- Karppinen A, Saarinen T, Salmela J, Laukkanen A, Nuopponen M, Seppälä J (2012) Flocculation of microfibrillated cellulose in shear flow. *Cellulose* 19:1807-1819. doi:10.1007/s10570-012-9766-5
- Kataja M, Haavisto S, Salmela J, Lehto R, Koponen A (2017) Characterization of microfibrillated cellulose fiber suspension flow using multi scale velocity profile measurements. *Nordic Pulp & Paper Research Journal* 32:473-482. doi:10.3183/NPPRJ-2017-32-03-p473-482
- Kumar V, Nazari B, Bousfield D, Toivakka M (2016) Rheology of Microfibrillated Cellulose Suspensions in Pressure-Driven Flow. *Applied Rheology* 26:43534. doi:10.3933/ApplRheol-26-43534
- Lasseuguette E, Roux D, Nishiyama Y (2008) Rheological properties of microfibrillar suspension of TEMPO-oxidized pulp. *Cellulose* 15:425-433. doi:10-1007/s10570-007-9184-2
- Lauri J, Koponen A, Haavisto S, Czajkowski J, Fabritius T (2017) Analysis of rheology and wall depletion of microfibrillated cellulose suspension using optical coherence tomography. *Cellulose* doi:10.1007/s10570-017-1493-5
- Martoia F, Dumont PJJ, Orgéas L, Belgacem MN, Putaux JL (2016) Micro-mechanics of electrostatically stabilized suspensions of cellulose nanofibrils under steady state shear flow. *Soft Matter* 12:1721-1735. doi:10.1039/C5SM02310F

- Martoia F, Perge C, Dumont PJJ, Orgéas L, Fardin MA, Manneville S, Belgacem MN (2015) Heterogeneous flow kinematics of cellulose nanofibril suspensions under shear. *Soft Matter* 11:4742-4755. doi:10.1039/c5sm00530b
- Moberg T, Rigdahl M (2012) On the Viscoelastic Properties of Microfibrillated Cellulose (MFC) Suspension. *Annual Transactions of the Nordic Rheology Society* 20:123-130.
- Moberg T et al. (2017) Rheological properties of nanocellulose suspensions: effects of fibril/particle dimensions and surface characteristics. *Cellulose* 24:2499-2510. doi:10.1007/s10570-017-1283-0
- Moon RJ, Martini A, Nairn J, Simonsen J, Youngblood J (2011) Cellulose nanomaterials review: structure, properties and nanocomposites. *Chemical Society Reviews* 40:3941-3994. doi:10.1039/C0CS00108B
- Naderi A, J. E, Sundström J, Lindström T (2016) Enhancing the properties of carboxymethylated nanofibrillated cellulose by inclusion of water in the pre-treatment process. *Nordic Pulp & Paper Research Journal* 31:372-378. doi:10.3183/NPPRJ-2016-31-03-p372-378
- Naderi A, Lindström T (2015) Rheological Measurements on Nanofibrillated Cellulose Systems: A Science in Progress. In: Mondal MIH (ed) *Cellulose and Cellulose Derivatives*. Nova Science Publishers, Inc., pp 187-202
- Naderi A, Lindström T (2016) A comparative study of the rheological properties of three different nanofibrillated cellulose systems. *Nordic Pulp & Paper Research Journal* 31:354-363. doi:10.3183/NPPRJ-2016-31-03-p354-363
- Nazari N, Kumar V, Bousfield DW, Toivakka M (2016) Rheology of cellulose nanofibers suspensions: Boundary driven flow. *Journal of Rheology* 60:1151-1159.
- Nechyporchuk O, Belgacem MN, Bras J (2016a) Production of cellulose nanofibrils: A review of recent advances. *Industrial Crops and Products* 93:2-25. doi:10.1016/j.indcrop.2016.02.016
- Nechyporchuk O, Belgacem MN, Pignon F (2014) Rheological properties of micro-/nanofibrillated cellulose suspensions: Wall-slip and shear banding phenomena. *Carbohydrate Polymers* 112:432-439. doi:10.1016/j.carbpol.2014.05.092

- Nechyporchuk O, Belgacem MN, Pignon F (2015) Concentration effect of TEMPO-oxidized nanofibrillated cellulose aqueous suspensions on the flow instabilities and small-angle X-ray scattering structural characterization. *Cellulose* 22:2197-2210.
- Nechyporchuk O, Belgacem MN, Pignon F (2016b) Current progress in Rheology of Cellulose Nanofibril Suspensions. *Biomacromolecules* 17:2311-2320. doi:10.1021/acs.biomac.6b00668
- Pääkkö M et al. (2007) Enzymatic Hydrolysis Combined with Mechanical Shearing and High-Pressure Homogenization for Nanoscale Cellulose Fibrils and Strong Gels. *Biomacromolecules* 8:1934-1941. doi:10.1021/bm061215p
- Padberg J, Bauer W, Gliese T (2016) The influence of fibrillation on the oxygen barrier properties of films from microfibrillated cellulose. *Nordic Pulp & Paper Research Journal* 31:548-560. doi:10.3183/NPPRJ-2016-31-04-p548-560
- Pahimanolis N et al. (2013) Nanofibrillated cellulose/ carboxymethyl cellulose composite with improves wet strength. *Cellulose* 20:1459-1468.
- Saarikoski E, Saarinen T, Salmela J, Seppälä J (2012) Flocculated flow of microfibrillated cellulose water suspensions: an imaging approach for characterisation of rheological behaviour. *Cellulose* 19:647-659. doi:10.1007/s10570-012-9661-0
- Saarinen T, Haavisto S, Sorvari A, Salmela J, Seppälä J (2014) The effect of wall depletion on the rheology of microfibrillated cellulose water suspensions by optical coherence tomography. *Cellulose* 21:1261-1275. doi:10.1007/s10570-014-0187-5
- Saarinen T, Lille M, Seppälä J (2009) Technical Aspects on Rheological Characterization of Microfibrillar Cellulose Water Suspensions. *Annual Transaction of the Nordic Rheology Society* 17:121-128.
- Schenker M, Schoelkopf J, Mangin P, Gane P (2016) Rheological investigation of complex micro and nanofibrillated cellulose (MNFC) suspensions: Discussion of flow curves and gel stability. *Tappi Journal* 15:405-416.
- Shafiei-Sabet S, Hamad WY, Hatzikiriakos G (2012) Rheology of Nanocrystalline Cellulose Aqueous Suspensions. *Langmuir* 28:17124-17133. doi:10.1021/la303380v

- Toivakka M, Eklund D (1994) Particle movements during the coating process. *Nordic Pulp & Paper Research Journal* 9:143-149. doi:10.3183/NPPRJ-1994-09-03-p143-149
- Toivakka M, Eklund D Prediction of suspension rheology through particle motion simulation. In: *TAPPI Coating Fundamentals Symposium*, Atlanta, GA, 1995. TAPPI Press, pp 161-177
- Turbak AF, Snyder FW, Sandberg KR (1983) Microfibrillated cellulose, a new cellulose product: properties, uses, and commercial potential. *Journal of Applied Polymer Science* 37:815-827.
- Veen SJ, Versluis P, Kuijk A, Velikov KP (2015) Microstructure and rheology of microfibril-polymer networks. *Soft Matter* 11:8907-8912. doi:10.1039/C5SM02086G
- Wu H, Morbidelli M (2001) A model relating structure of colloidal gels to their elastic properties. *Langmuir* 17:1030-1036. doi:10.1021/la001121f
- Yoshimura A, Prud'homme RK (1988) Wall slip corrections for Couette and parallel disk viscometers. *Journal of Rheology* 32:53-67. doi:10.1122/1.549963

7.8 Supplementary information

7.8.1 Viscoelastic data

Storage- and loss modulus data of the 0.5 wt% (Figure 7.10), 1 wt% (Figure 7.11) and 2 wt% (Figure 7.12) suspensions obtained by the different measurement setups investigated in this study are presented here. Based on these datasets, the different viscoelastic properties were evaluated that are presented in Figure 7.4 and Figure 7.5, as well as in Table 7.1 in the main article.

It is apparent, that the VS system is not suitable for low modulus suspensions (0.5 wt% MFC suspension, Figure 7.10) at low shear stresses (small amplitudes), as the data is strongly fluctuating. These low shear rate data was omitted from the evaluation. The later onset of the decrease of both moduli (that is described by the increase of the phase angle in the main article) for the VS system is apparent for all suspension solids contents. The smooth CC27 system shows a characteristic increase of the loss modulus just before it

decreases for all solids contents. Also, the roughened CC27 system (RR) exhibits such a behaviour, yet less pronounced.

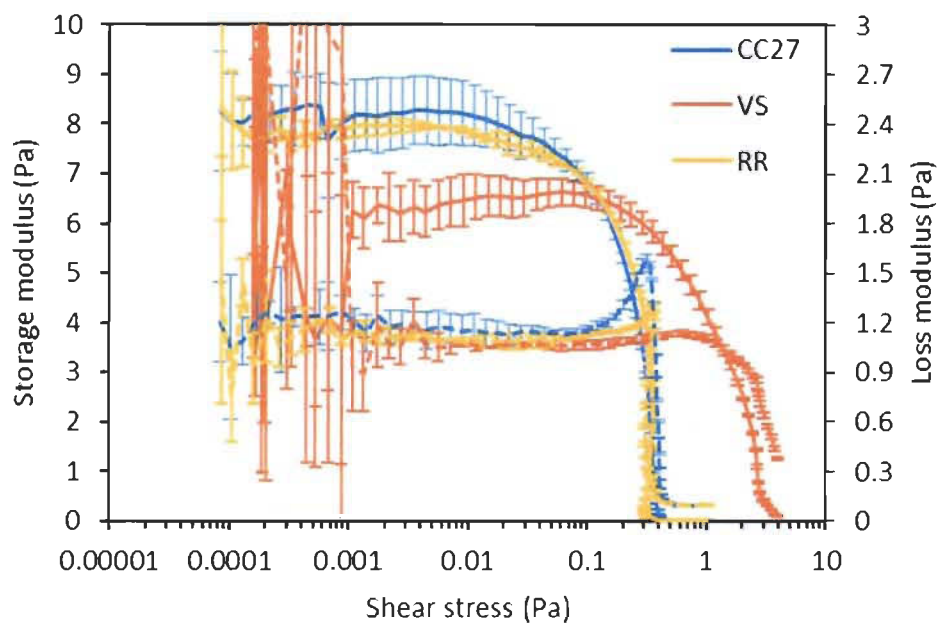


Figure 7.10: Amplitude sweep data of the 0.5 wt% for the different investigated measurement setups. The full lines represent storage modulus data (left y-axis) and the dashed lines represent loss modulus data (right y-axis). The error bars represent standard deviations.

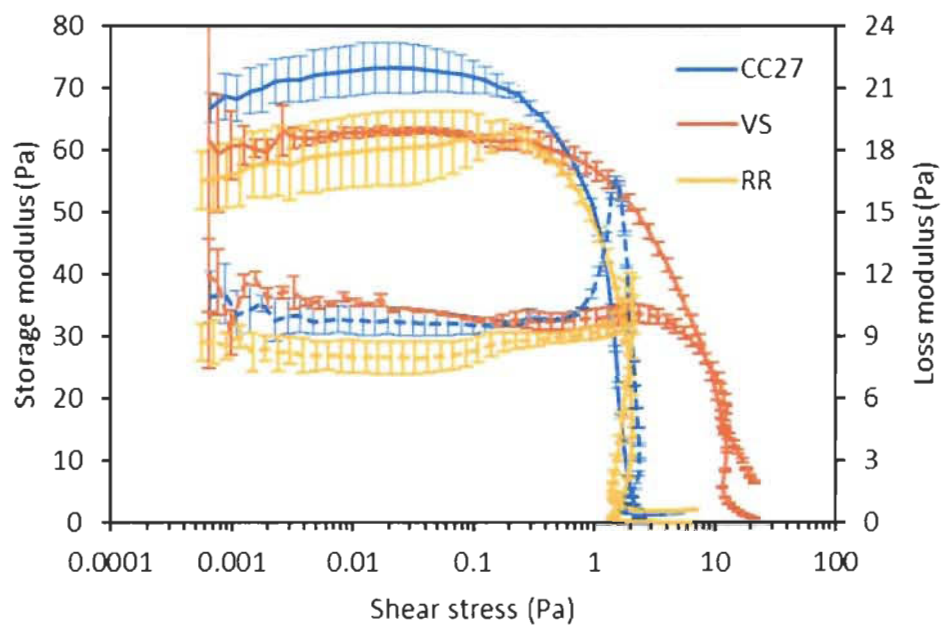


Figure 7.11: Amplitude sweep data of the 1 wt% for the different investigated measurement setups. The full lines represent storage modulus data (left y-axis) and the dashed lines represent loss modulus data (right y-axis). The error bars represent standard deviations.

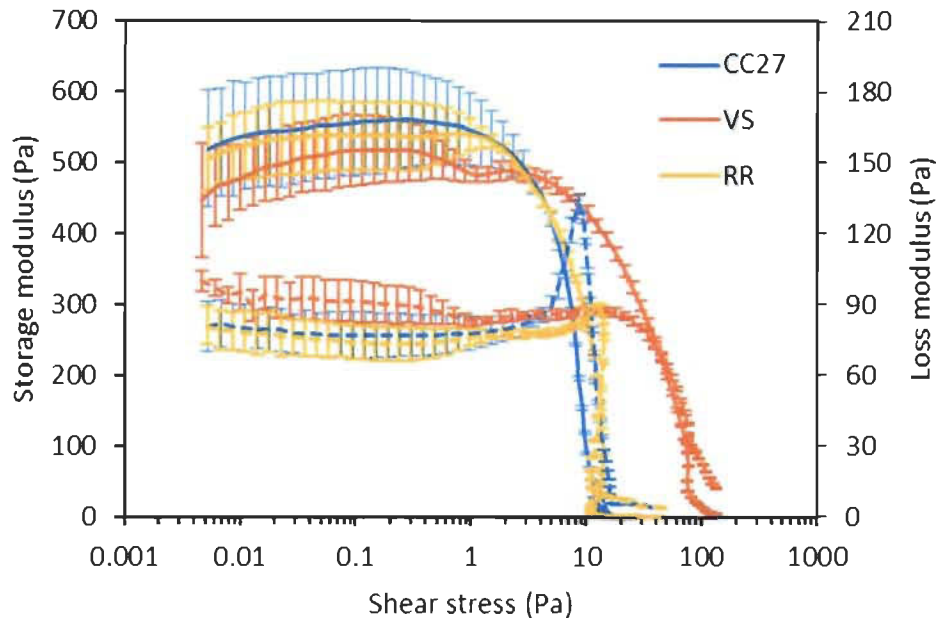


Figure 7.12: Amplitude sweep data of the 2 wt% for the different investigated measurement setups. The full lines represent storage modulus data (left y-axis) and the dashed lines represent loss modulus data (right y-axis). The error bars represent standard deviations.

7.8.2 Flow curve data

The individual flow curves of the 0.5 wt% (Figure 7.13), 1 wt% (Figure 7.14) and 2 wt% (Figure 7.15) obtained by the four different measurement systems used in this study are presented here. Based on these datasets, the different flow curve parameters were evaluated that are presented in Figure 7.7 to Figure 7.9 and Table 7.2 in the main article. The strongly changing overall viscosity in dependence of the solids content is very apparent. The change of the end of zone 1 and the increased overall viscosity level for the VS system at all solids contents is obvious as well. The apparent increase of viscosity for the VS system at increased shear rates and especially at lower suspension solids contents is attributed to turbulent flow (Nechyporchuk et al. 2015). This data was omitted from the calculations of the flow curve parameters.

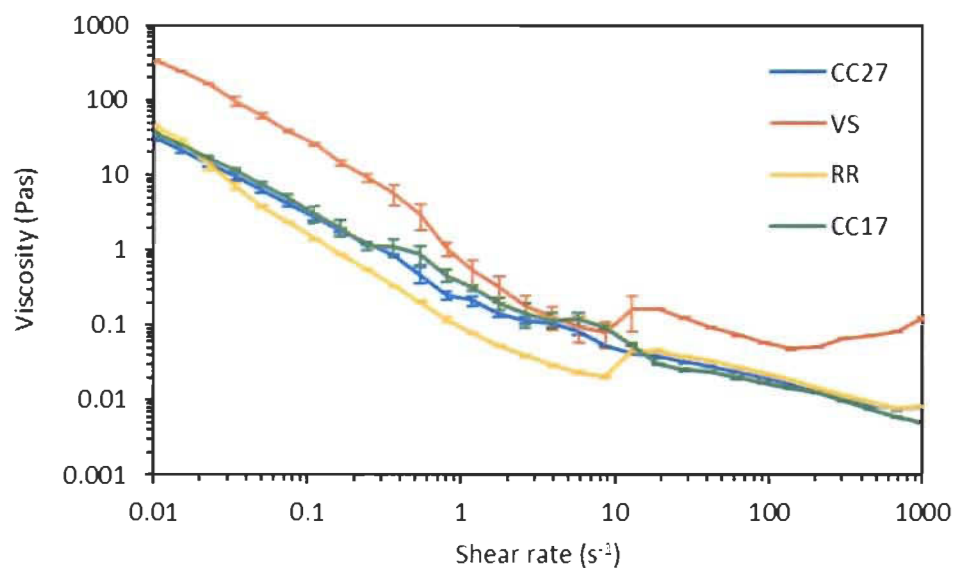


Figure 7.13: Flow curves of the 0.5 wt% MFC suspension for the different investigated measurement setups.

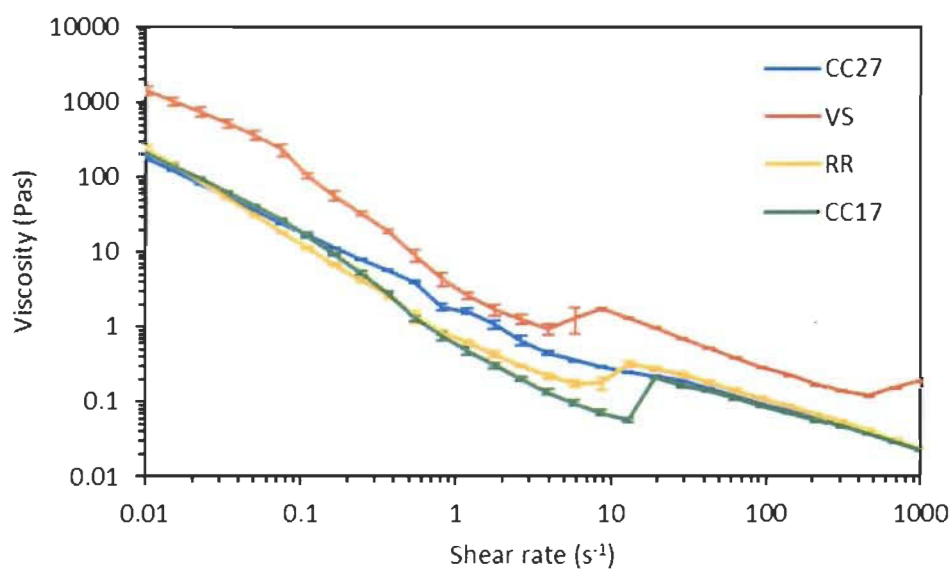


Figure 7.14: Flow curves of the 1 wt% MFC suspension for the different investigated measurement setups.

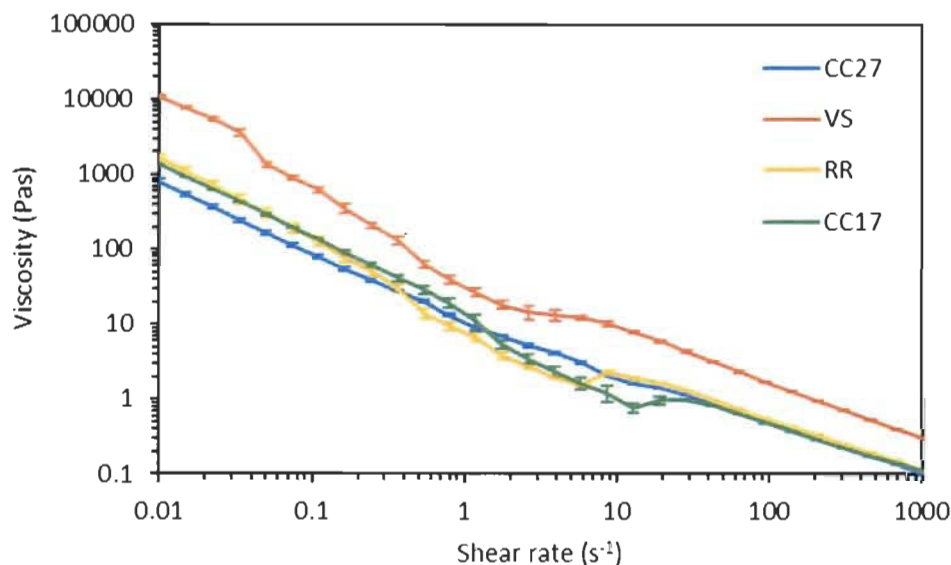


Figure 7.15: Flow curves of the 2 wt% MFC suspension for the different investigated measurement setups.

7.8.3 References

Nechyporchuk, O., Belgacem, M.N., Pignon, F. (2015) Concentration effect of TEMPO-oxidized nanofibrillated cellulose aqueous suspensions on the flow instabilities and small-angle X-ray scattering structural characterisation. *Cellulose* 22:2197-2210.

7.9 Additional, unpublished data

7.9.1 Influence of individual measurement setup geometries

In addition to using the different measurement setups, also only individual components of the measurement systems, i.e. cup or bob, were exchanged. Comparing data from such “mixed” systems (condition of bob and cup is different) with the respective “complete” systems (cup and bob are of the same condition) allows to identify what component of the measurement geometry (bob or cup) is dominating a certain property, or the rheological measurement in general.

To investigate this, the 1 wt% MFC suspension was measured additionally with combinations of either smooth or roughened CC27 geometries and combinations of smooth CC27 and vane, respectively serrated cup geometries. In all cases, the bob, respectively the vane is the moving geometry, whereas the cup is static.

7.9.1.1 Viscoelastic properties

As already mentioned in the publication, the measurement system does not seem to have an influence on the properties below the yield point, i.e. when still in the LVE regime. It is therefore not surprising that the storage- as well as the loss modulus (G'_{\max} and G''_{lin}) are about the same for all measurement systems, independent of their configurations (Figure 7.16 and Figure 7.17). This also applies generally to the smooth and roughened CC27 systems, where most of the properties were very alike, and so also for the mixed system, no significant differences are expected (Figure 7.17). However, for the *LoL* and the yield stress, a significant difference between the VS and the CC27 system was seen, and consequently, a difference is seen for the respective mixed systems (Figure 7.16). Like the VS system, the vane in smooth cup system provides increased *LoL* and $\tau_{y,\delta}$ values compared to the CC27 and the smooth bob in serrated cup system. The data furthermore suggests that the vane, respectively the smooth bob overall dominate the measured properties (as the absolute values of the respective systems are very alike). There seem to be minor deviations from those trends, e.g. for the phase angle data of the CC27 and the smooth bob in serrated cup systems or the *LoL* and yield stress data of the RR and the smooth cup and rough bob systems. However, considering the typically high standard deviations (see e.g. Figure 7.11) for this data, they probably can be neglected.

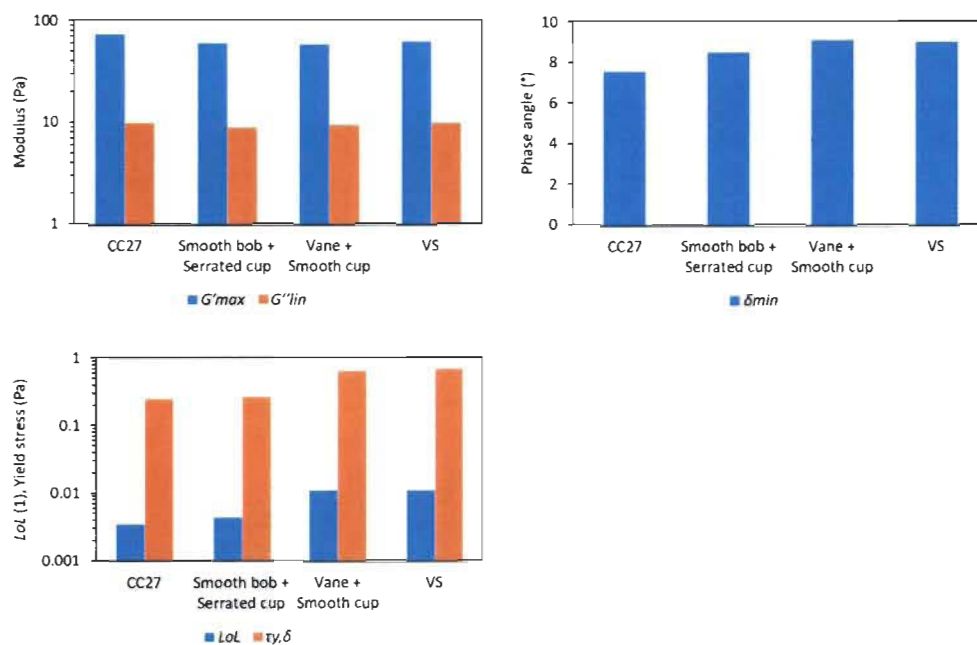


Figure 7.16: Viscoelastic properties of the 1 wt% MFC suspension, measured with the CC27 and the VS system, as well as with mixed setups, i.e. CC27 bob with serrated cup and vane with CC27 cup.

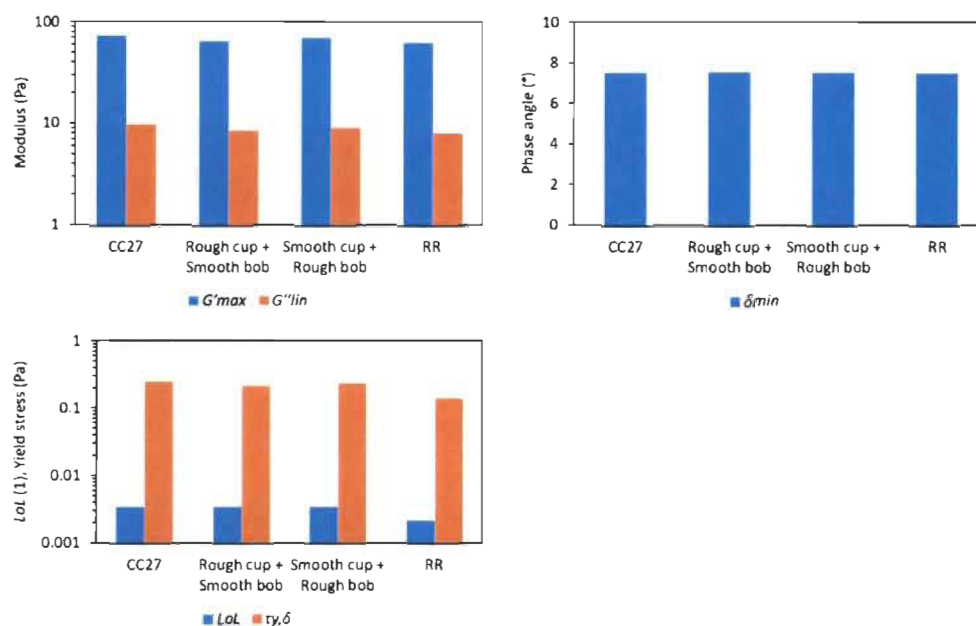


Figure 7.17: Viscoelastic properties of the 1 wt% MFC suspension, measured with the smooth and roughened CC27 system, as well as with mixed setups, i.e. smooth bob with roughened cup and roughened bob with smooth cup.

7.9.1.2 Flow curve properties

From the data presented in the publication (e.g. Figure 7.7 and Figure 7.8), it is apparent that the measurement system can lead to different values of most of the flow curve properties, especially the VS system in comparison with the other systems. Together with the data of the mixed systems, it is very apparent again, that the moving geometry is determining the properties (Figure 7.18 and Figure 7.19). There seems to be an additional difference between the power law coefficients of the VS, the CC27 and the respective mixed systems (Figure 7.18). However, without having standard deviations, a solid conclusion is not possible. Unfortunately, the data treatment procedure used for this experimental study, as explained in the publication, does not allow to calculate standard deviations (due to the averaging of the triplicate flow curve data). If all single data points are used for the fitting instead, respective standard errors for the fitted parameters can be calculated by the used software (Origin 2017). Figure 7.20 shows the recalculated data for

the power law parameters n and k for the zone 1 and 2 flow curve sections. It is very apparent, that the zone 1 properties have a higher standard deviation compared to the respective zone 2 properties. As a consequence, potential differences of zone 1 parameters between systems having the same bob (vane) condition become insignificant. However, all of the differences of the zone 2 properties in all different systems appear to be significant (not statistically tested though).

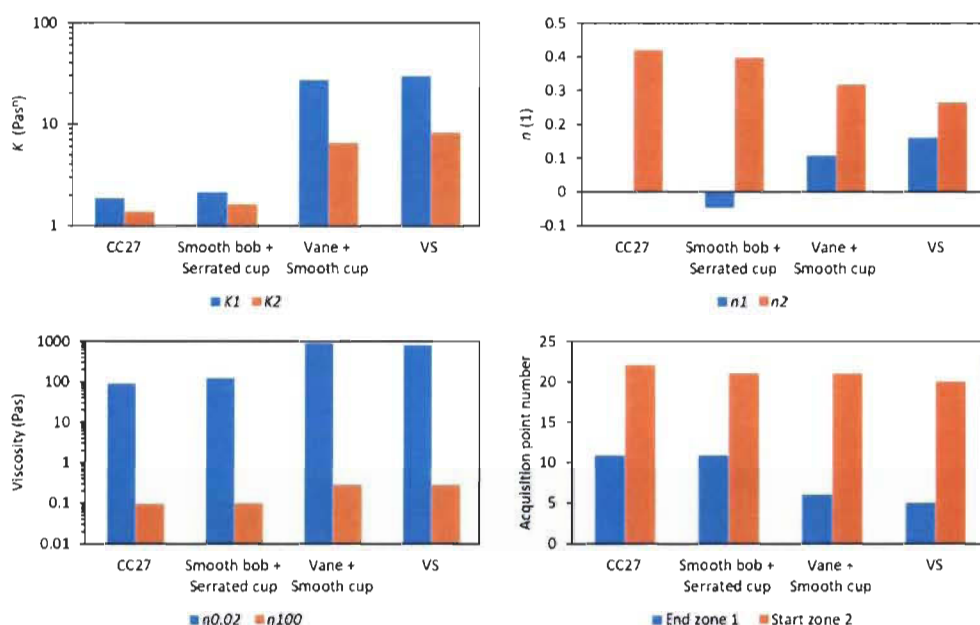


Figure 7.18: Flow curve properties of the 1 wt% MFC suspension, measured with the CC27 and the VS system, as well as with mixed setups, i.e. CC27 bob with serrated cup and vane with CC27 cup.

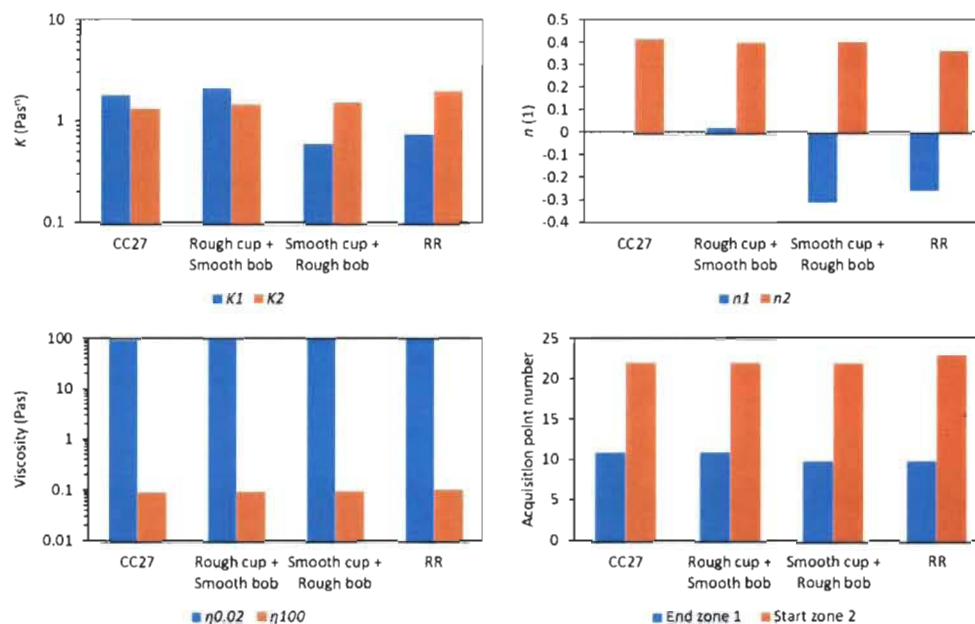


Figure 7.19: Flow curve properties of the 1 wt% MFC suspension, measured with the smooth and roughened CC27 system, as well as with mixed setups, i.e. smooth bob with roughened cup and roughened bob with smooth cup. Please note, that the K_1 and n_1 data of the RR and the Smooth cup with rough bob have to be taken with care (see main publication for further information).

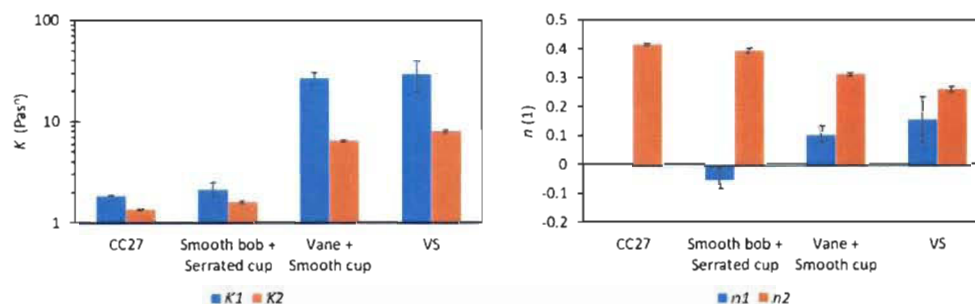


Figure 7.20: Power law fitting parameters of zone 1 and 2 flow curve sections of the 1 wt% MFC suspension, including the standard error of the respective parameters as calculated by the fitting software. Please note that the mean values are the same as presented in Figure 7.18

7.9.2 Conclusions

At small and slow deformations, i.e. at the end of the LVE range and at low shear rates, it seems reasonable to assume that the material's response is limited to the volume close to the moving geometry; especially when the measurement gap is rather large in comparison to the suspension's characteristic length scales (e.g. particle- or aggregate size) and the suspension exhibits a complex rheology. However, when the suspension is sheared over the complete gap, one would expect, that the condition of the static geometry also has an influence on the measurement values. The present data, where n_2 , K_2 , η_{100} and probably the start of zone 2 are properties where the complete gap is sheared, seems to support this partially (Figure 7.20). On the one hand, the zone 1 properties are the same (or at least not significantly different from each other due to strongly overlapping standard deviations) for a given moving geometry, i.e. vane vs. smooth bob. On the other hand, the zone 2 properties are different for each setup of geometry conditions. But again, it appears that the influence of the condition of the moving geometry is stronger compared to the condition of the static surface.

Despite the interesting evidences on the influence of respective measurement setup geometries on

certain flow curve properties, no further work was carried out in this area, e.g. not further data was recalculated to get an idea on standard deviations or -errors, or no further combinations of measurement system conditions were tested. On the one hand, additional characterisation methods that would allow to test morphological hypotheses would have been missing, and on the other hand, it was not the focus of this PhD work. Yet, this additional data supports the findings of the related publication and further justifies the decision to use the VS system for further rheological investigations of MFC suspensions.

Chapter 8 - Article 3: Quantification of flow curve hysteresis data – a novel tool for characterising microfibrillated cellulose (MFC) suspensions

Published article.

Michel Schenker, Joachim Schoelkopf, Patrick Gane, Patrice Mangin; Applied Rheology; 2018; 28(2); 22945; doi: 10.3933/ApplRheol-28-22945

8.1 Foreword

Firstly, this work can be considered as an extension of the previous work presented in Chapter 7 - as it presents yet another way of evaluating and quantifying rheological data. Secondly, a special focus was put on the statistical evaluation of the obtained data. The work resulted in a rather simple calculation procedure to obtain hysteresis data from flow curves. This protocol even allows one to compare directly the respective hysteresis data of MNFC suspensions having different solids contents, which is not straightforward because of the strong solids content dependency of the apparent viscosity. The further evaluation of the data obtained in this work (but which wasn't published) also has shown, that the general protocol of using triplicate measurements to evaluate the rheological behaviour of MNFC suspensions is generally sufficient to obtain reproducible data.

8.2 Abstract

A novel method is introduced to describe quantitatively hysteresis seen in flow curves of microfibrillated cellulose suspensions. Also, a data normalisation procedure is presented that allows a direct comparison of data from suspensions of different solids contents. The discussion of the flow curve hysteresis of an MFC suspension is proposed to provide a lot of information on the suspension morphology under flow. Such information is not only useful for process design, but also may serve as a quality control tool. Hysteresis data as a function of the suspension solids content are provided, and considered with reference to an overview made of peer work in the field. Two discrete hysteresis loop areas were found in the flow curves presented in this work, each associated with a distinct shear rate region, one where the viscosity of the flow curve during shear rate increase is higher than that of the shear rate flow curve at decreasing shear rate (named *positive hysteresis*) and another

where it is the opposite (named *negative hysteresis*). This behaviour seems to have been rarely reported, and where reported we offer an explanation, based on morphological models and rheometer measurement set up, as to why other researchers may find a variety of hysteresis forms. It is hypothesised that the *negative normalised hysteresis* is mainly depending on the excessive flocculation/structuration induced at intermediate shear rates during the shear rate increase, and that it is necessarily less with increasing solids content because of the reduced availability of free water. The *positive normalised hysteresis*, however, is considered to originate from the different morphologies at lower shear rates, i.e. the initial, homogeneous structure vs. the structure that was previously induced by the intermediate shear during shear rate decrease. The *positive normalised hysteresis* appears not to depend on the solids content, indicating a self-similarity or scaling behaviour of the structuring with respect to the underlying network structure.

8.2.1 Keywords

Microfibrillated cellulose, suspension, flow curve, hysteresis, morphology, quantification

8.3 Introduction

In recent years and currently, the potential for micro- and nanofibrillated cellulose materials (MFC, NFC) in various applications continues to be exploited intensively, not only by academia, but also by the industry [1-3]. The reason for this is the material's versatility, its interesting mechanical properties and of course the abundance and sustainability of its raw feed source [4]. The coarser MFC grades (referring to the nomenclature proposal by Kangas et al. [5], whereby the term NFC should be used for materials containing only fibrils with width on the nanometre scale), are especially interesting for high volume applications due to the lower production energy requirements that enable lower costs [6] and higher volume productions [7]. Whilst abiding by the definition of Kangas et al. [5], it is important to recognise that MFC itself will inevitably display nanofibrillation on the microfibre surface, leading on occasions to the term micro nanofibrillated cellulose (MNFC). As these grades naturally have a broad fibril size (widths) distribution, and may have different fibril morphologies depending on the fibrillation processes, individual products may exhibit differing sets of properties and each may be more, or less, suitable for a specific application.

To be able to select an adequate MFC product, a meaningful characterisation is necessary, and so lately also some effort is being put into developing procedures to classify the various MFC grades [5,8]. The common findings are typically that a single characterisation method is not sufficient and that even a set of properties provides limited comparability for MFC grades of different origin, e.g. from different raw materials and/or derived via different pre- and post-fibrillation treatments. By getting a better understanding of the MFC (suspension) morphology, data obtained from different characterisation techniques may be understood better and more detailed interpretation may be possible. Even though rather indirect, rheological investigations can, if applied judiciously, provide essential insights into the suspension morphology. Therefore, the combination of direct and/or indirect imaging techniques with rheology measurement techniques are very strong tools to test hypothesised mechanistic models [9-12]. Yet, to be able to compare data of different studies, it is necessary to quantify the observed data and describe the used measurement parameters with an adequate level of detail. The latter is of special importance for MFC suspensions as they exhibit a complex rheology, including shear rate- as well as time-dependencies. These inherent properties in connection to the fact that they are at least two-phase (heterogeneous) hydrocolloids can lead to many measurement-induced artefacts, that also can depend strongly on the measurement parameters [13-15].

Whereas it is very common to report different viscosity numbers and storage and loss moduli, it is rare that further rheological properties are reported for MFC suspensions. Flow curves (viscosity as a function of shear rate) as well as amplitude and frequency sweep graphs are also provided sometimes [16,17]. Several articles specifically investigate the rheology of MFC suspensions, commonly using shear rheometers [14,18-22], but also pipe rheometers are used [23,24], sometimes even coupled with additional techniques to get more direct information on the suspension morphology [10,11,22,25]. A comprehensive and extensive review on recent developments in measuring the rheology of micro- and nanofibrillated cellulose suspensions is provided by Nechyporchuk et al. [26]. Yet, especially the information within flow curve graphs is typically not quantified. This is unfortunate, especially for a material like an MFC suspension that exhibits a very distinct flow behaviour, e.g. a discontinuous power law shear thinning flow curve,

composed of different regions [17,19,27,28]. A recent study by Schenker et al. [13] proposed several descriptors to describe quantitatively amplitude sweep measurements and flow curves, yet, only the shear rate increasing ramp of the flow curve is evaluated. This is especially highlighted because it was shown before, that MFC suspensions have different flow curves, depending on the direction of the shear rate profile, i.e. from low to high and *vice versa*. This behaviour is expressed as the hysteresis areas between the two flow curves when they are overlaid [9,19,29]. As described by Martoia et al. [9] and Iotti et al. [19], this phenomenon can be attributed to different suspension morphologies, that originate from the different shear histories of the two flow curves. So, the hysteresis itself contains some information on the different morphologies at different shear rates, and therefore is a very promising property for deriving morphological models of MFC suspensions under flow.

The content of this work aims at comparing different approaches on how to describe the hysteresis in a useful way, and then to investigate those hysteresis derived properties in dependence of solids contents of the MFC suspension. The obtained data are tested statistically to identify whether potential trends are significant or not. Finally, the data are discussed with a view on existing morphological models of sheared MFC suspensions and a direct comparison made with hysteresis data seen from previous researchers' work. This work appears to be the first to propose the use of quantitative flow curve hysteresis data of MFC suspensions to derive mechanistic models. Further work is then carried out, to be reported in an upcoming study, to test the applicability of this promising characterisation method on different grades of MFC.

8.4 Experimental

8.4.1 Materials

The materials used in this work are the same as those studied previously by Schenker et al. [13,29]. As described previously, the MFC was manufactured by a purely mechanical process [29]. Briefly, bleached eucalyptus pulp was mechanically disintegrated as 3 wt% aqueous (tap water) suspension by means of an ultrafine friction grinder (Supermasscolloider MKCA 6-2, Masuko Sangyo Co., Japan). The method employs single passes at different grinder rotational speeds. The total electrical energy

consumption normalised by the amount of dry cellulose matter, defined as the specific grinding energy, was 7.2 kWhkg^{-1} . This process of mechanical fibrillation leads typically to a broad size distribution [10], i.e. containing both coarse fibres as well as individual fibrils (Figure 8.1). Thus, it is classified as MFC rather than NFC. In addition, since the MFC was not further modified, it forms a flocculated structure according to the description of Nechyporchuk et al. [26]. The starting suspension was diluted to 1, 1.5 and 2 wt% for use by further addition of tap water, followed by 2 min mixing at $12\,000 \text{ min}^{-1}$ (rpm) in a rotor stator mixer (Polytron PT 3000, Kinematica, Switzerland) followed by 5 min exposure in an ultrasonic bath. Prior to performing measurements, the diluted samples were left to stand for at least one hour.

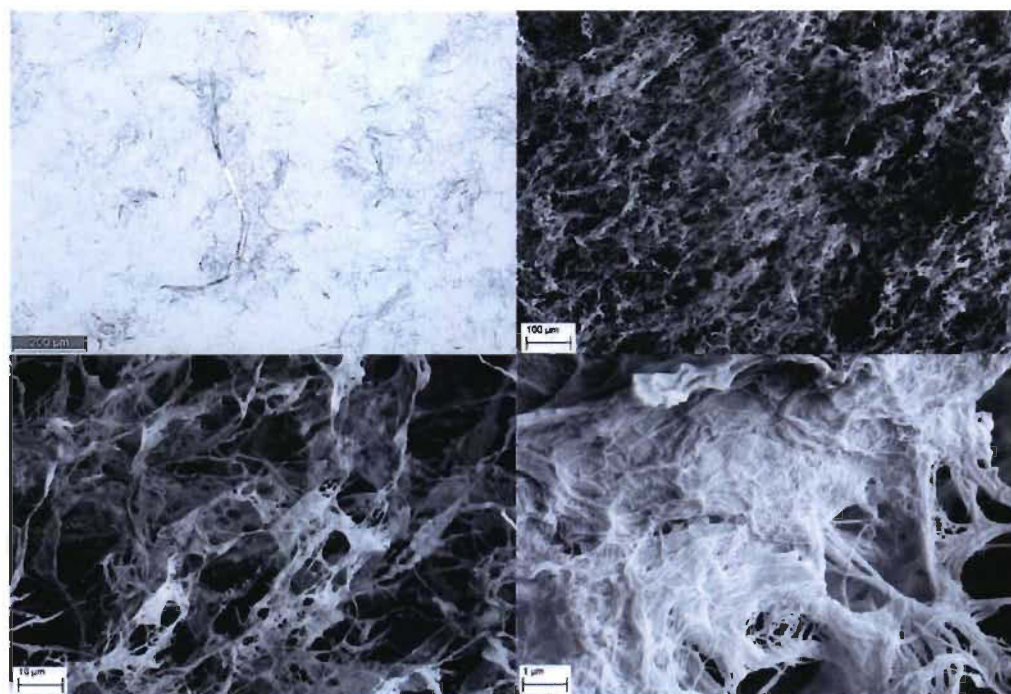


Figure 8.1: Optical microscopy image of MFC suspension at 0.5 wt% (top left), and SEM images of freeze-dried aerogels from 0.5 wt% suspensions at increasing magnifications (top right), (bottom left) and (bottom right). Some left over coarse fibres are apparent, as well as some individual and isolated fibrils. [Taken from Schenker et al. [13]]

8.4.2 Imaging

Optical microscopy was the prime method of imaging (Axio Imager.M2m, Zeiss, Switzerland). Sample preparation consisted of diluting the MFC suspension to 0.5 % (w/w) and then adding carboxymethyl cellulose (Finnfix10, CP Kelco, Finland), made down to 1 wt% solution as a dispersing agent, at an amount equivalent to 5 wt%, based on dry weight of MFC prior to mixing and ultrasonication.

One drop of the prepared MFC suspension was placed between two glass slides for examination in the optical microscope.

A second portion of the sample suspension was frozen in liquid nitrogen and freeze dried (Apha 1-2 LD Freeze Dryer, Martin Christ Gefriertrocknungsanlagen GmbH, Germany).

A piece of the resulting aerogel was broken away from the sample and mounted on a support and sputtered with gold (8 nm) to enable imaging of the internal MFC aerogel structure by scanning electron microscopy (SEM) (Sigma VP, Zeiss, Switzerland).

8.4.3 Rheological measurements

All the measurements were performed on an MCR 300 rheometer (Anton Paar, Austria) at 20 °C, equipped with a vane (six blades) in serrated (length profiled) cup system (vane: ST22-6V-16, diameter $d_{\text{vane}} = 22$ mm, cup: CC27-SS-P, diameter $d_{\text{cup}} = 28.88$ mm, profile depth = 0.5 mm, profile width = 1.65 mm), also supplied by Anton Paar (VS). This measurement system was selected because it appears to be less prone to produce measurement system-related artefacts, like shear banding or water depletion and connected apparent wall slip. In recent work, Schenker et al. [13] came to this conclusion by comparing different commonly used measurement systems and their influence on flow curve properties.

Flow curves (viscosity η in dependence of the shear rate $\dot{\gamma}$) were recorded by performing an automated shear rate increase ramp from 0.01 to 1 000 s⁻¹ directly followed by a shear rate decrease ramp from 1 000 to 0.01 s⁻¹. 30 log- equidistant distributed point measurements were performed for each ramp, all with automated acquisition time mode and shear rate control. Further information on the automated acquisition time setting can be found in [30]. The tested shear rate points $\dot{\gamma}_i$ can be calculated according to

$$\dot{\gamma}_i = 0.01 \cdot 10^{(5/29)^{i-1}} \text{ s}^{-1} \quad \text{Equation 8.1}$$

Minimal and maximal acquisition times are 15.2 and 500 s respectively, however, typically only the first measurement point (shear rate of 0.01 s^{-1}) shows acquisition times around and longer than 300 s. The automated acquisition time setting is chosen, in order to let the suspension equilibrate at a given shear rate before determining the viscosity. This is of special importance in the transition region (non-power law region of the shear rate increasing curve “1” in Figure 8.2), where it is hypothesised that a dynamic aggregation process is taking place. A respective, detailed discussion was provided recently by Schenker et al. [13,30].

For each of the 3 MFC suspension dilutions, 3 individual makedowns were produced, where each makedown was characterised from its own individual measurements which were repeated 3 times, creating 9 separate rheometer measurements per dilution.

Figure 8.2 shows a typical flow curve obtained in this work. The typical three region behaviour can be seen for the flow curve of the increasing shear rate (“1”) ramp-up [9,13,31], as well as the measurement set-up induced artefact at the very highest shear rates [13]. The flow curve of the decreasing shear rate (“2”) ramp-down does not exhibit such clearly defined regions, yet there are indications that also two different regions with different power law parameters can be found [19]. Very apparently, the two flow curves are not identical over the whole shear rate range, creating two separate hysteresis areas. At low shear rates, the viscosity of the increasing shear rate ramp-up is higher compared to the decreasing shear rate ramp-down at a given shear rate (+). The end of the positive hysteresis ($\dot{\gamma}_a$) is defined as the last shear rate where the viscosity of the increasing shear rate ramp η_1 is larger than the viscosity of the decreasing shear rate ramp η_2 . At intermediate shear rates, the opposite can be observed (-), and, at even higher shear rates, there is no or only an insignificant difference between the two flow curves. The end of the negative hysteresis ($\dot{\gamma}_b$) is defined as the first shear rate where the viscosities of both flow curves are again about the same. To characterise the hysteresis, the following approaches are introduced.

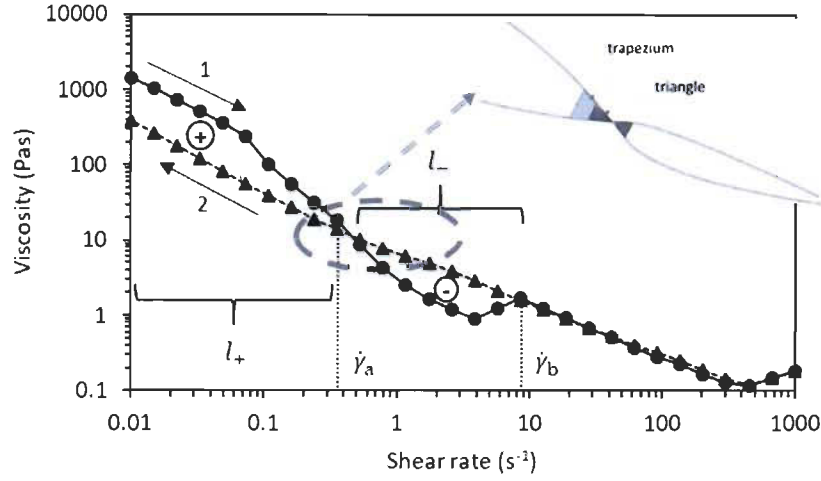


Figure 8.2: Typical flow curve of an MFC suspension characterised in this work, showing the positive (+) and negative (-) defined hystereses. The insert shows schematically the application of trapezia and triangles to determine the hysteresis area.

The *first method* aims to describe the actual hysteresis area, i.e. the actual area between the two flow curves. For the sake of simplicity, the area is not analytically integrated, but the trapezium rule approximation is employed, where the individual trapezia are made up from neighbouring viscosity curve differences and their shear rate differences, which are then summed discretely:

$$H_{A+}^* = \frac{1}{2} \sum_i \left((\dot{\gamma}_{i+1} - \dot{\gamma}_i) (\eta_1(\dot{\gamma}_i) - \eta_2(\dot{\gamma}_i) + \eta_1(\dot{\gamma}_{i+1}) - \eta_2(\dot{\gamma}_{i+1})) \right) \quad : \text{for } \dot{\gamma}_i < \dot{\gamma}_a$$

Equation 8.2

$$H_{A-}^* = \frac{1}{2} \left| \sum_i \left((\dot{\gamma}_{i+1} - \dot{\gamma}_i) (\eta_1(\dot{\gamma}_i) - \eta_2(\dot{\gamma}_i) + \eta_1(\dot{\gamma}_{i+1}) - \eta_2(\dot{\gamma}_{i+1})) \right) \right| \quad : \text{for } \dot{\gamma}_{a+1} < \dot{\gamma}_i < \dot{\gamma}_b$$

Equation 8.3

with H_{A+}^* and H_{A-}^* being the positive and negative absolute trapezia sum, respectively, and $\eta_1(\dot{\gamma}_i)$ and $\eta_2(\dot{\gamma}_i)$ being the viscosity of flow curve 1 and 2 at the shear rate $\dot{\gamma}_i$.

To capture also the rates of change of area at the crossing of the viscosity curves, the respective area adjoining either side the boundary with the crossing point, i.e. that spanned by the shear rates before and after the crossing point, can be expressed as two triangles

(each equivalent to a trapezium with one side zero length), and thus used to approximate the area growth each side of the crossing point as:

$$H_{A+}^{**} = \frac{\eta_1(\dot{\gamma}_a) - \eta_2(\dot{\gamma}_a)}{2} \cdot h \quad \text{Equation 8.4}$$

$$H_{A-}^{**} = \left| \frac{\eta_1(\dot{\gamma}_{a+1}) - \eta_2(\dot{\gamma}_{a+1})}{2} \cdot ((\dot{\gamma}_{a+1} - \dot{\gamma}_a) - h) \right| \quad \text{Equation 8.5}$$

$$h = \frac{(\dot{\gamma}_{a+1} - \dot{\gamma}_a)(\eta_1(\dot{\gamma}_a) - \eta_2(\dot{\gamma}_a))}{(\eta_1(\dot{\gamma}_a) - \eta_2(\dot{\gamma}_a)) + (\eta_2(\dot{\gamma}_{a+1}) - \eta_1(\dot{\gamma}_{a+1}))} \quad \text{Equation 8.6}$$

with H_{A+}^{**} and H_{A-}^{**} being the positive and negative absolute triangle and h being the height of the positive triangle.

The respective trapezia sum and triangle are summed together to get the positive (H_{A+}) and negative (H_{A-}) *absolute hysteresis*, respectively:

$$H_{A+} = H_{A+}^* + H_{A+}^{**} \quad \text{Equation 8.7}$$

$$H_{A-} = H_{A-}^* + H_{A-}^{**} \quad \text{Equation 8.8}$$

The *second method* uses the same approach as used for the absolute hysteresis, but the trapezium areas are normalised by the mean viscosity that is defined by the two viscosity pairs (the two parallel sides of the trapezia):

$$H_{N+}^* = 2 \sum_i \left(\frac{(\dot{\gamma}_{i+1} - \dot{\gamma}_i)(\eta_1(\dot{\gamma}_i) - \eta_2(\dot{\gamma}_i) + \eta_1(\dot{\gamma}_{i+1}) - \eta_2(\dot{\gamma}_{i+1}))}{\eta_1(\dot{\gamma}_i) + \eta_2(\dot{\gamma}_i) + \eta_1(\dot{\gamma}_{i+1}) + \eta_2(\dot{\gamma}_{i+1})} \right) : \text{for } \dot{\gamma}_i < \dot{\gamma}_a \quad \text{Equation 8.9}$$

$$H_{N-}^* = 2 \left| \sum_i \left(\frac{(\dot{\gamma}_{i+1} - \dot{\gamma}_i)(\eta_1(\dot{\gamma}_i) - \eta_2(\dot{\gamma}_i) + \eta_1(\dot{\gamma}_{i+1}) - \eta_2(\dot{\gamma}_{i+1}))}{\eta_1(\dot{\gamma}_i) + \eta_2(\dot{\gamma}_i) + \eta_1(\dot{\gamma}_{i+1}) + \eta_2(\dot{\gamma}_{i+1})} \right) \right| : \text{for } \dot{\gamma}_{a+1} < \dot{\gamma}_i < \dot{\gamma}_b$$

$$\quad \text{Equation 8.10}$$

with H_{N+}^* and H_{N-}^* being the positive and negative normalised trapezia sum, respectively. Also, the triangle areas, as before, representing the area growth behaviour either side of the crossing point are normalised using the following formulae:

$$H_{N+}^{**} = \frac{2H_{A+}^{**}}{\frac{\eta_1(\dot{\gamma}_a) + \eta_2(\dot{\gamma}_a)}{2} + \left(\eta_1(\dot{\gamma}_a) + h \frac{\eta_1(\dot{\gamma}_{a+1}) + \eta_1(\dot{\gamma}_a)}{\dot{\gamma}_{a+1} - \dot{\gamma}_a} \right)}$$

Equation 8.11

$$H_{N-}^{**} = \left| \frac{2H_{A-}^{**}}{\frac{\eta_1(\dot{\gamma}_{a+1}) + \eta_2(\dot{\gamma}_{a+1})}{2} + \left(\eta_1(\dot{\gamma}_a) + h \frac{\eta_1(\dot{\gamma}_{a+1}) + \eta_1(\dot{\gamma}_a)}{\dot{\gamma}_{a+1} - \dot{\gamma}_a} \right)} \right|$$

Equation 8.12

with H_{N+}^{**} and H_{N-}^{**} being the positive and negative normalised triangle hysteresis area. The trapezia and triangle areas are again summed up to give:

$$H_{N+} = H_{N+}^* + H_{N+}^{**} \quad \text{Equation 8.13}$$

$$H_{N-} = H_{N-}^* + H_{N-}^{**} \quad \text{Equation 8.14}$$

with H_{N+} and H_{N-} being the positive and negative *normalised hysteresis*, respectively. The *third method* aims to describe the data as it is presented in a log-log plot (Figure 7.2), so instead of looking at viscosity differences, the viscosity ratios are evaluated. As for the previously described methods, the hystereses are calculated by summing up trapezia and triangle areas. The calculation for this approach is simplified because the height of the trapezia is constant. To ease the calculations further, the constant length was set to 1, and the respective term for the height was removed completely from the calculations:

$$H_{R+}^* = \frac{1}{2} \sum_i \left(\log \frac{\eta_1(\dot{\gamma}_i)}{\eta_2(\dot{\gamma}_i)} + \log \frac{\eta_1(\dot{\gamma}_{i+1})}{\eta_2(\dot{\gamma}_{i+1})} \right) : \text{for } \dot{\gamma}_i < \dot{\gamma}_a \quad \text{Equation 8.15}$$

$$H_{R-}^* = \frac{1}{2} \left| \sum_i \left(\log \frac{\eta_1(\dot{\gamma}_i)}{\eta_2(\dot{\gamma}_i)} + \log \frac{\eta_1(\dot{\gamma}_{i+1})}{\eta_2(\dot{\gamma}_{i+1})} \right) \right| : \text{for } \dot{\gamma}_{a+1} < \dot{\gamma}_i < \dot{\gamma}_b$$

Equation 8.16

with H_{R+}^* and H_{R-}^* being the positive and negative relative trapezia sum, respectively. The positive and negative relative triangle areas (H_{R+}^{**} , H_{R-}^{**}), as well as the positive and negative relative hystereses (H_{R+} , H_{R-}) were then calculated as follows:

$$H_{R+}^{**} = \frac{\log \frac{\eta_1(\dot{\gamma}_a)}{\eta_2(\dot{\gamma}_a)}}{2} \cdot \frac{\log \frac{\eta_1(\dot{\gamma}_a)}{\eta_2(\dot{\gamma}_a)}}{\log \frac{\eta_1(\dot{\gamma}_a)}{\eta_2(\dot{\gamma}_a)} - \log \frac{\eta_1(\dot{\gamma}_{a+1})}{\eta_2(\dot{\gamma}_{a+1})}} \quad \text{Equation 8.17}$$

$$H_{R-}^{**} = \frac{\log \frac{\eta_1(\dot{\gamma}_{a+1})}{\eta_2(\dot{\gamma}_{a+1})}}{2} \cdot \left(1 - \frac{\log \frac{\eta_1(\dot{\gamma}_a)}{\eta_2(\dot{\gamma}_a)}}{\log \frac{\eta_1(\dot{\gamma}_a)}{\eta_2(\dot{\gamma}_a)} - \log \frac{\eta_1(\dot{\gamma}_{a+1})}{\eta_2(\dot{\gamma}_{a+1})}} \right)$$

Equation 8.18

$$H_{R+} = H_{R+}^* + H_{R+}^{**} \quad \text{Equation 8.19}$$

$$H_{R-} = H_{R-}^* + H_{R-}^{**} \quad \text{Equation 8.20}$$

The *fourth method* is a very simple alternative to calculate the relative hysteresis. Hence, instead of calculating the hysteresis areas, only the viscosity ratios are summed up (that is the same as summing up the log quotient of the viscosities):

$$H_{RS+} = \sum_i \left(\log \frac{\eta_1(\dot{\gamma}_i)}{\eta_2(\dot{\gamma}_i)} \right) : \text{for } \dot{\gamma}_i \leq \dot{\gamma}_a \quad \text{Equation 8.21}$$

$$H_{RS-} = \left| \sum_i \left(\log \frac{\eta_1(\dot{\gamma}_i)}{\eta_2(\dot{\gamma}_i)} \right) \right| : \text{for } \dot{\gamma}_{a+1} < \dot{\gamma}_i < \dot{\gamma}_b \quad \text{Equation 8.22}$$

with H_{RS+} and H_{RS-} being the positive and negative *relative hysteresis* calculated by the simplified method, respectively.

For all the different hysteresis types, a total hysteresis was calculated (sum of the magnitudes of the respective positive and negative hysteresis, H_A , H_R , H_{RS+} and H_{RS-}), as well as the positive share in % of the total hysteresis (H_{A+}/H_A , H_{R+}/H_R , H_{RS+}/H_{RS+} and H_{N+}/H_N).

Finally, also the “positioning” of the two different hystereses is characterised: the end of the positive hysteresis ($\dot{\gamma}_a$) is defined as the last shear rate where $\eta_1 > \eta_2$ and the end of the negative hysteresis ($\dot{\gamma}_b$) is defined where $\eta_1 \cong \eta_2$ for the first time after $\eta_1 < \eta_2$. Also, the respective “length” of the hysteresis is described by summing up the log-equidistantly distributed number of point measurements i (for the similarly defined point separation) within a respective hysteresis (l_+ , l_-). Please note that this method leads to a value depending on the acquisition settings of the rheometer. However, as long as the settings are consistently the same within a study, the thus obtained length data can be compared without any problems.

The hysteresis parameterising data described above, consisting of nine individual measurements per dilution, are presented in box charts (see e.g. Figure 8.4a) containing the data median (line), mean (triangle), 25 to 75 percentile (box) and minimum to maximum range (whiskers). The hysteresis position properties data are presented differently because box charts are not suitable. Here, the individual values are shown (hollow diamonds) instead of the percentile box. The mean and median data are presented the same way as described for the other hysteresis data.

Firstly, a normality test (Shapiro-Wilk, 0.05 significance level, Origin 2017) was carried out on the data points within each dilution and given property in order to identify potential grouping effects. Secondly, an analysis of variance test (ANOVA, 0.05 significance level, Origin 2017) was carried out among the different levels of dilution within each property separately. The test not only reveals whether different dilutions (mean values) at a given property are significantly different from each other, but also provides the strength of effect and the test power. For data where a significant difference was identified, a mean comparison test (Tukey, 0.05 significance level, Origin 2017) was carried out additionally to identify which combination of datasets were different. As the hysteresis position

properties (end and length of positive and negative hysteresis) appear to be not normally distributed and have discrete values, a Kruskal-Wallis test was carried out for these data instead [32].

8.5 Results and discussion

8.5.1 Morphological model

The presence of the so called “rheological hysteresis” in complex fluids is well known and attributed to the time-dependence of their viscosity, i.e. their thixotropy [33]. The reason for thixotropic behaviour is very often a morphological change of the fluid that is induced by deformation (shear), e.g. orientation of macromolecules, phase separation or other structural reorganisations. MFC suspensions are well known also to undergo morphological changes under flow, leading for instance to the typical discontinuous shear thinning behaviour [13,31,34], but also to hysteresis [9,17,19,35]. The hysteresis between the increasing shear rate viscosity curve and the decreasing shear rate viscosity curve is typically explained by different structures that depend on the shear history and the characteristically long relaxation times (= the time needed for a non-equilibrium structure induced at a given shear rate to transform back to its equilibrium structure). For the following discussions, it should be noted that the mechanistic model of Martoia et al. [9] is followed, and that this is well supported by, for example, Karppinen et al. [31] and Schenker et al. [13] for the shear rate increase part of the flow curve. In short, they explain the observed *positive hysteresis* (present at lower shear rates, as seen in this work, Figure 8.2) as originating because the initial structure (low shear rates of the increasing shear rate curve) is homogeneous, and has, therefore, a higher viscosity compared to the more flocculated structure that was induced by intermediate shear rates (on the decreasing shear rate ramp). It is apparent that the *negative hysteresis* is mainly caused by the “dip” of the increasing shear rate flow curve (Figure 8.2). Following the argumentation of Schenker et al. [13], based on findings of Karppinen et al. [31], this behaviour is related to the formation of loosely bound flocs and water-rich voids, reducing overall viscosity. It is interesting to note, that there is no such dip (or a lot less pronounced one) at the same shear rates in the decreasing shear rate ramp. So, it is possible to assume that the

flocculated structure that is induced by the high shear rates differs from the (flocculated) structure at the lower shear rates.

8.5.2 Flow curves

Figure 8.3 shows the averaged flow curves of the 1, 1.5 and 2 wt% MFC suspensions investigated in this work. *Positive* as well as *negative hysteresis* areas can be seen in all curves, and it is apparent that the *negative hysteresis* becomes smaller with increasing solids content. As is to be expected, the overall viscosity levels increase with the solids content. The quantitative evaluation of the hysteresis of these flow curves, as well as the potential underlying morphological reason will be discussed in the next section.

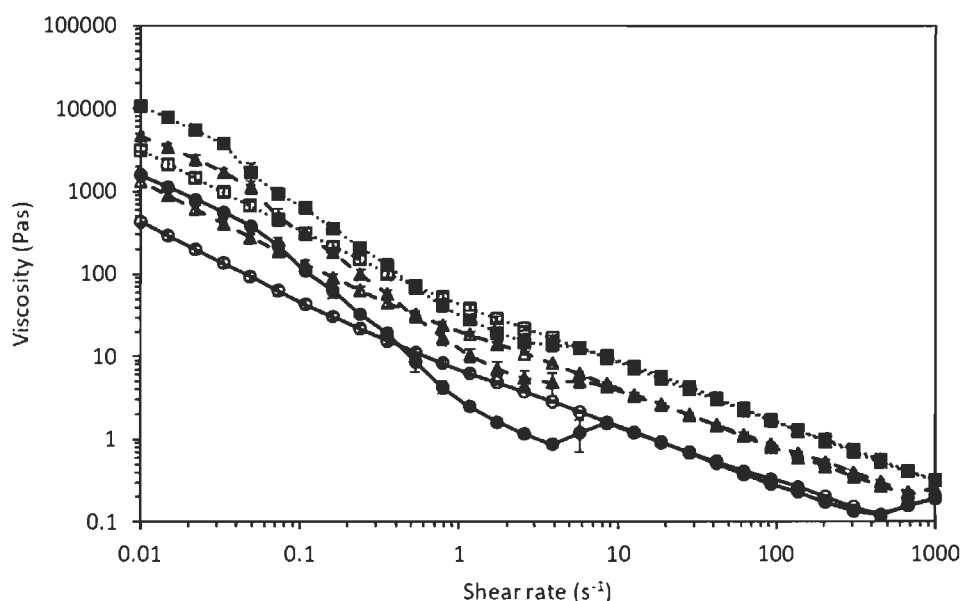


Figure 8.3: Flow curves of averaged data for 1 (circles), 1.5 (triangles) and 2 wt% (squares) MFC suspensions including standard deviations (error bars). The full symbols represent the data during shear rate increase and the hollow symbols represent the data during shear rate decrease, respectively.

8.5.3 Influence of solids content on hysteresis properties

When comparing the data spread in the following Figures (Figure 8.4 to Figure 8.6) with the standard deviations shown in Figure 8.3, they may at first sight appear inconsistent.

However, it should be kept in mind that the standard deviation is inversely scaled with the square root of the number of sample points, n , so becoming smaller with an increasing number of data points. Thus, the data in the following graphs do not show a standard deviation, but quantiles, and maximum and minimum values (so the complete data spread).

It is very apparent from the data in Figure 8.4a that the *positive absolute hysteresis* (H_{A+}) increases significantly (Table 8.1) with the solids content, keeping in mind the logarithmic scale. This is not surprising if one considers the overall viscosity increase with the solids content (Figure 8.3) and that H_{A+} is calculated from absolute viscosity values without any normalisation (Equation 8.2 to Equation 8.8). Keeping this in mind, at first the trend observed for the negative absolute hysteresis H_{A-} appears counterintuitive, cf. Figure 8.3 and Figure 8.4b. This can, however, be explained straightforwardly, once again, in terms of the strongly changing overall viscosities. Also for the same reason, the *total absolute hysteresis* H_A , Figure 8.4c, as well as the positive share H_{A+}/H_A , Figure 8.4d, are basically just depending on the *positive absolute hysteresis*. To undertake a separate evaluation of these properties is, therefore, questionable.

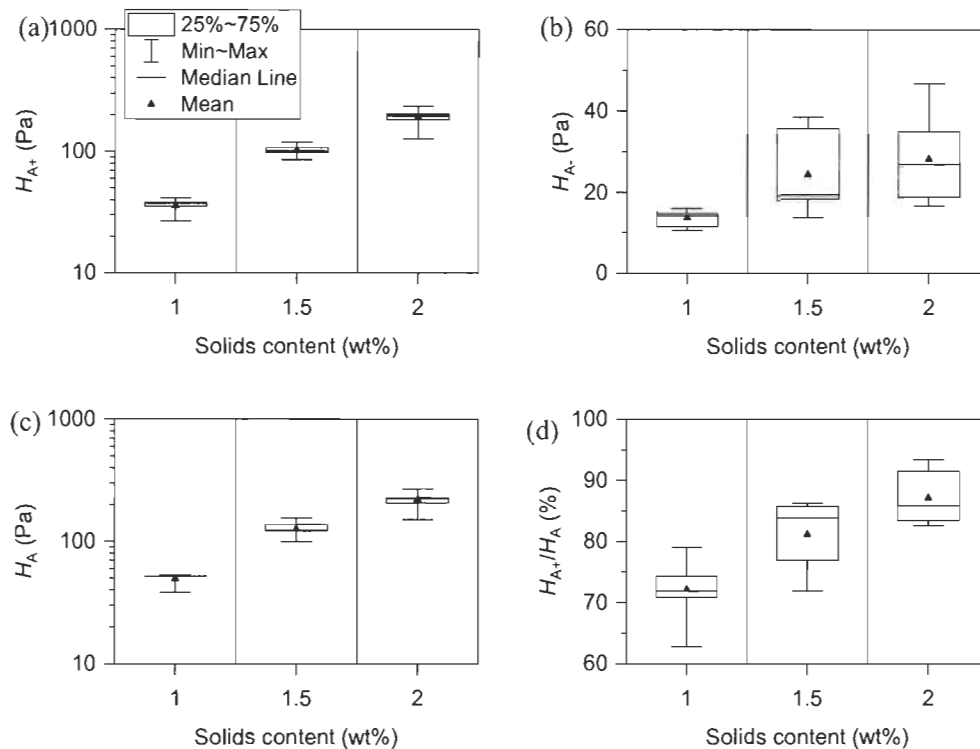


Figure 8.4: Box charts of absolute hysteresis data: (a) positive absolute hysteresis (H_{A+}), (b) negative absolute hysteresis (H_{A-}), (c) total absolute hysteresis (H_A) and (d) positive absolute hysteresis in respect to the total absolute hysteresis (H_{A+}/H_A). Please note that the scales for H_{A+} and H_A are logarithmic.

As seen in the discussion before, the absolute hysteresis data are very strongly dominated by the initial, low shear rate data due to the strongly shear thinning- and solid content-dependent nature of MFC suspensions. To be able to decouple this effect, the normalisation was introduced according to **Error! Reference source not found.** to Equation 8.14. These data are presented in Figure 8.5. The dependency of the positive normalised hysteresis H_{N+} on the solids content seems to have vanished (there was no significant difference found by the ANOVA test, Table 8.1). This contrasts with the H_{A+} data, yet it reflects directly the situation seen in the log-log flow curve diagram (Figure 8.3). Furthermore, the normalised data show clear trends (statistically significant, Table 8.1) that an increase in solids content leads to a decrease in the negative and total

normalised hystereses H_{N-} and H_N (Figure 8.5b and c) and an increased share of the positive normalised hysteresis H_{N+}/H_N (Figure 8.5d). The normalisation proves to be very useful with respect to making the hysteresis data of different dilutions directly comparable.

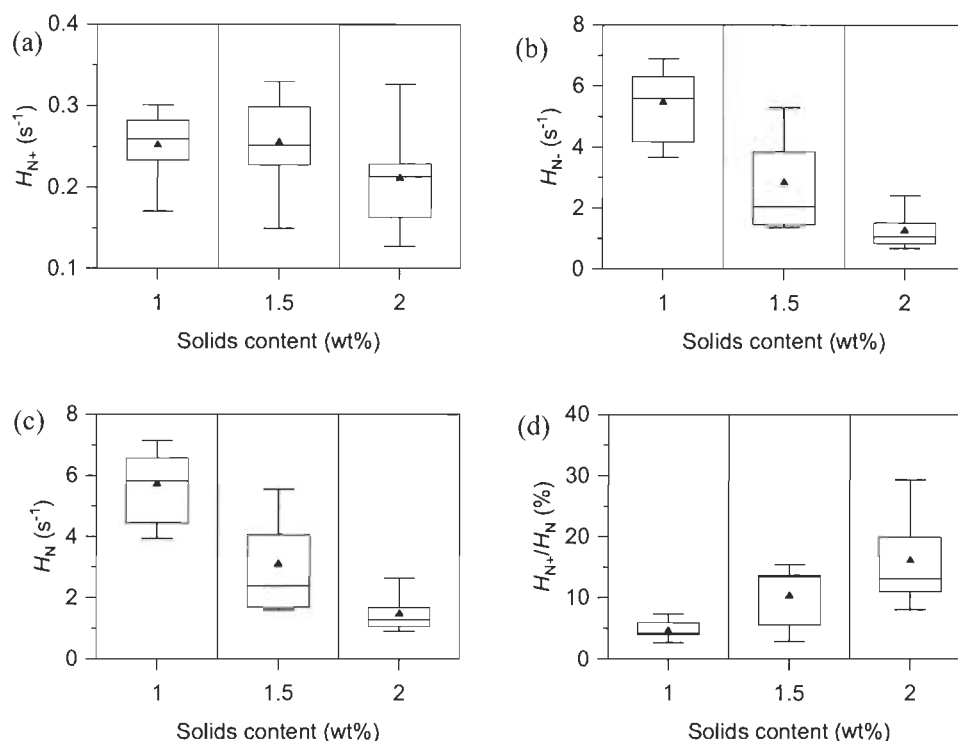


Figure 8.5: Box charts of normalised hysteresis data: (a) positive normalised hysteresis (H_{N+}), (b) negative normalised hysteresis (H_{N-}), (c) total normalised hysteresis (H_N), and (d) fraction of positive normalised hysteresis in respect to the total normalised hysteresis (H_{N+}/H_N).

It is apparent, that the normalised hysteresis data (Figure 8.5) and the relative hysteresis data (Figure 8.6) have very alike trends. This is supported by the statistical test data (Table 8.1), except for the positive hysteresis where the normalised data show no trend with the suspension solids content, but the relative data do. However, the low power of the ANOVA test for H_{N+} already indicates that the chance is high, that a significant difference is not found by the test. Furthermore, the strength of effect for the positive relative and

normalised hysteresis is small (in general, but also compared to the rest of the tested data). This indicates that even if there is a trend, the dependency of H_{N+} and H_{R+} on the suspension solids content will be small. As is to be expected, the relative hysteresis data, like the normalised hysteresis data, are not affected by the overall viscosity levels, because of their relative character.

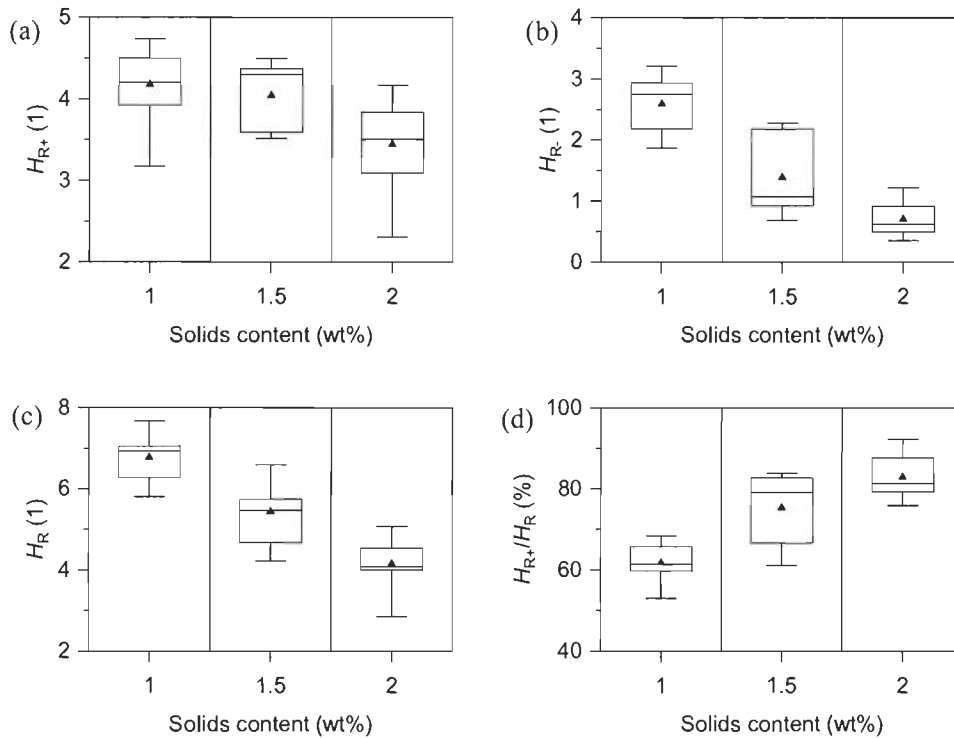


Figure 8.6: Box charts of relative hysteresis data: (a) positive relative hysteresis (H_{R+}), (b) negative relative hysteresis (H_{R-}), (c) total relative hysteresis (H_R), and (d) fraction of positive relative hysteresis in respect to the total relative hysteresis (H_{R+}/H_R).

It was found that the relative hysteresis data obtained by the simplified method (line summation) correlate very well ($r^2 > 0.99$ for all data sets) with the relative hysteresis data obtained by the extensive procedure (Figure 8.7), so no box charts are provided. The ANOVA test results are almost identical for both approaches (Table 8.1) as well, legitimising the simplified procedure.

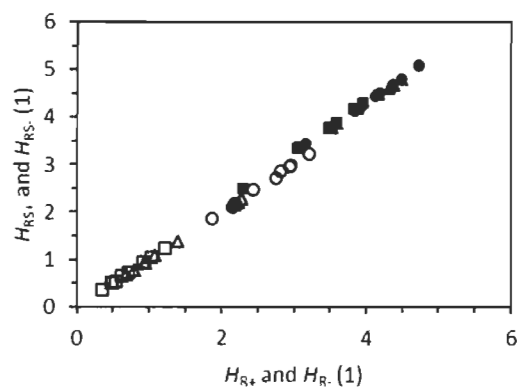


Figure 8.7: Comparison of positive (full symbols) and negative (hollow symbols) relative hysteresis data obtained by the regular method (H_{R+} and H_{R-}) and the simplified method (H_{RS+} and H_{RS-}). Circles represent the 1 wt% suspension data, triangles the 1.5 wt% data and the squares the 2 wt% data.

Table 8.1: Statistical test decisions including the ANOVA test power and strength of effect for hysteresis data.

Property	ANOVA result ($\alpha = 0.05$)	Test power	Effect strength	Significant pair-wise comparisons ($\alpha = 0.05$)
H_{A+}	Significantly different	1	0.92	All
H_{A-}	Significantly different	0.89	0.37	1 – 1.5 wt%, 1 – 2 wt%
H_A	Significantly different	1	0.92	All
H_{A+}/H_A	Significantly different	1	0.63	All
H_{N+}	Not significantly different	0.35	0.13	
H_{N-}	Significantly different	1	0.70	All
H_N	Significantly different	1	0.71	All
H_{N+}/H_N	Significantly different	0.98	0.48	1-2
H_{R+}	Significantly different	0.9	0.32	1 – 2 wt%, 1.5 – 2 wt%
H_{R-}	Significantly different	1	0.74	All
H_R	Significantly different	1	0.72	All
H_{R+}/H_R	Significantly different	1	0.66	1 – 1.5 wt%, 1 – 2 wt%
H_{RS+}	Significantly different	0.78	0.30	1 – 2 wt%
H_{RS-}	Significantly different	1	0.74	All
H_{RS}	Significantly different	1	0.70	All
H_{RS+}/H_{RS}	Significantly different	1	0.66	1 – 1.5 wt%, 1 – 2 wt%

As mentioned in the methods section, the data of the hysteresis positioning were not normally distributed (non-Gaussian), and, therefore, not presented as box charts (Figure 8.8). As all these data are based on shear rate values that are predefined by the rheometer software and the measurement settings, they are discrete. The different data groups that are apparent next to each other in Figure 8.8a and b, for instance, represent data of adjacent pre-set measurement shear rates ($0.24, 0.36$ and 0.53 s^{-1} for $\dot{\gamma}_a$, respectively, $3.86, 5.74$ and 8.53 s^{-1} for $\dot{\gamma}_b$). For all properties except the end of the positive hysteresis, and corresponding hysteresis length ($\dot{\gamma}_a, l_+$), both of which must have the same test results anyway in a parametrised test, a significant difference was found for the different solids contents (Table 8.2). The pair-wise test only identified a difference between 1 and 2 wt% for all these properties. Looking at the data directly then shows, that the median values of those data-pairs are just one value apart from each other, so the effect strength is low. Due to the nature of the present data, as discussed above, it is difficult to identify a potential trend. Yet, with some caution, it may be hypothesised that the end and the length of the negative hysteresis ($\dot{\gamma}_b, l_-$) as well as the total hysteresis length (l) decrease with increasing solids content, provided the increase in solids content is large enough.

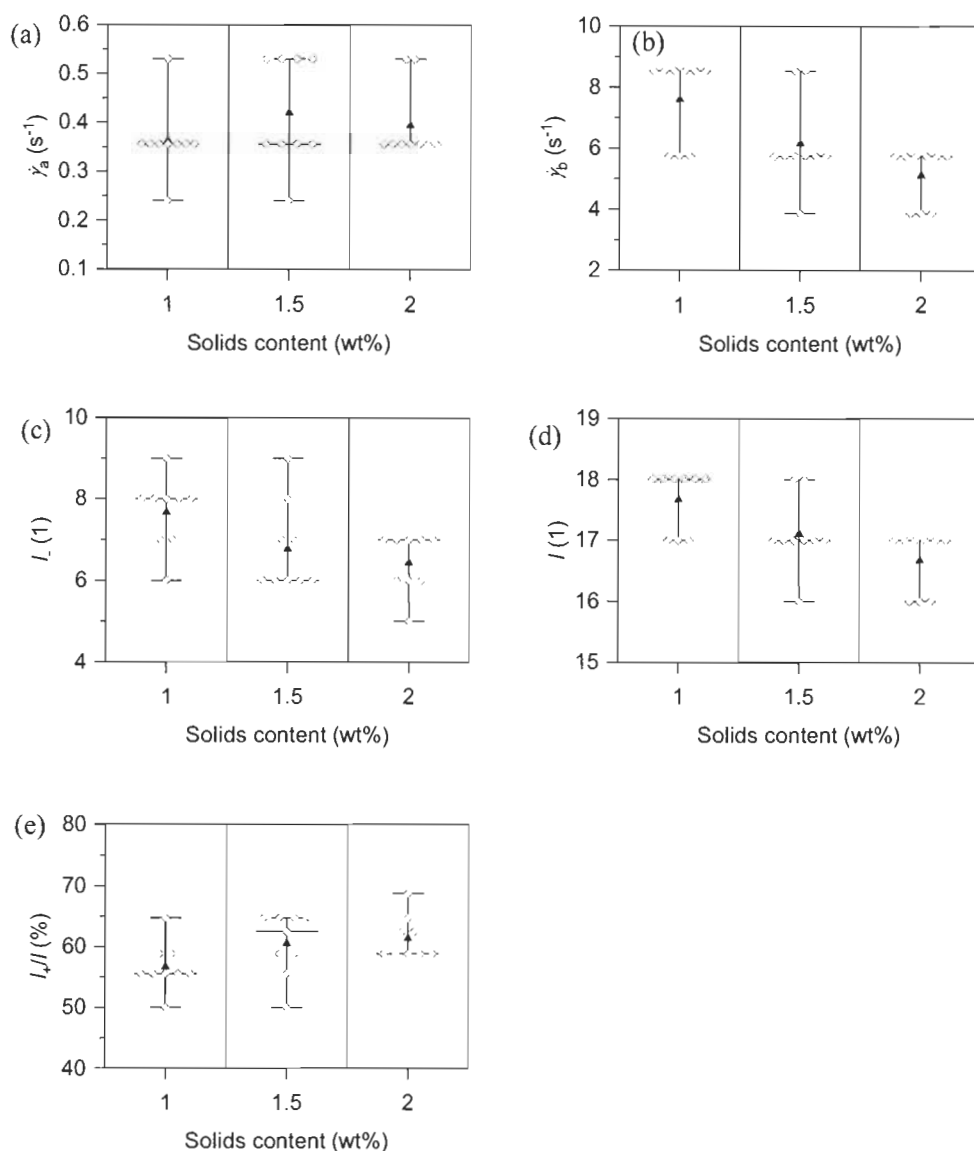


Figure 8.8: Hysteresis positioning data: (a) end of positive hysteresis ($\dot{\gamma}_a$), (b) end of negative hysteresis ($\dot{\gamma}_b$), (c) length of negative hysteresis (L_-) and total hysteresis length (L), and (e) fraction of positive hysteresis in relation to the total hysteresis length (L_+/L). The positive length data (L_+) are not presented because the distribution is identical to $\dot{\gamma}_a$.

Table 8.2: Statistical test decisions for the hysteresis positioning data. Even though the test for the fractional contribution of the positive length in respect to total hysteresis length (l_+/l) has provided a decision in favour that there is a significant difference among the data sets for the different solids contents, the pair-wise test, however, did not identify a significantly different dataset.

Property	Kruskal-Wallis result ($\alpha = 0.05$)	Significant pair-wise comparisons ($\alpha = 0.05$)
$\dot{\gamma}_a$	Not significantly different	
l_+	Not significantly different	
$\dot{\gamma}_b$	Significantly different	1 – 2 wt%
L	Significantly different	1 – 2 wt%
l	Significantly different	1 – 2 wt%
l_+/l	Significantly different	none

8.5.4 Learnings

Due to its strong dependency on the suspension solids content, the absolute hysteresis properties may be impractical for hysteresis discussions. Due to the strongly shear thinning nature of MFC suspensions, the hysteresis data at low shear rates are dominating the overall properties. On the one hand, comparisons between positive and negative hysteresis become bypassed, and on the other hand even within the positive hysteresis, the overall properties are mostly dominant within the very low shear rate region. Due to the high sensitivity, the absolute hysteresis may probably be used to differentiate between different solids contents. However, there are other more direct and equally sensitive rheological properties providing the same information [13].

The normalisation of the hysteresis data was successful in describing the data accurately from the point of view of their expression on the log-log flow-curve graphs. This is not only supported by visual observation, but also indirectly evidenced by the very good correlation between the relative hysteresis data and the actual quantified log-log plot data.

The simplified calculation of the relative hysteresis has shown to be accurate enough, so presents a legitimate way of obtaining the relative hysteresis data with less effort.

If one compares the normalised hysteresis with the relative hysteresis data, exemplified here with the positive hysteresis (Figure 8.9), it is apparent that the correlation is not very good. The reason for this can be expected from the hysteresis calculation procedures: for both the absolute and normalised hysteresis, trapezia and triangles are used as approximations to the real area between the curves. However, as the flow curves mostly follow power laws, there will be inherent errors arising from this approximation. As the log data are used for the relative hysteresis calculation, the power law behaviour is transformed to linear functions, and so trapezia and triangles become better approximations for the data. Therefore, it can be expected, that the relative hysteresis data are more accurate than the absolute and normalised data, and should be used in preference.

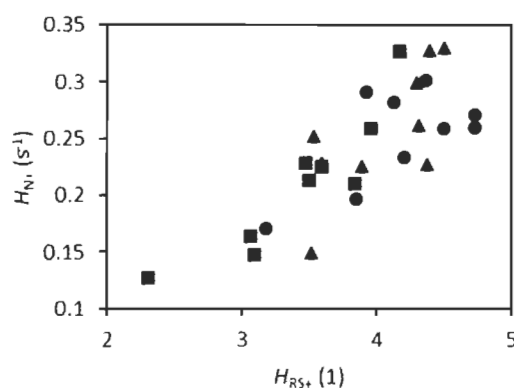


Figure 8.9: Comparison of positive normalised hysteresis and positive relative hysteresis data (obtained by the simplified calculation) of 1 wt% (circles), 1.5 wt% (triangles) and 2 wt% suspensions (squares).

Having a small data variation in respect to the hysteresis positioning may indicate that the number of contributing point measurements within the flow curves are too few. With the settings used in this work, each successive measured shear rate is about 150 % of the previous one. So, the span may be indeed too large to get a sufficiently closely stepped distribution. If enough points would be added, the length data should then follow a normal distribution, as it is based on logarithmic shear rate data. As the number of point

measurements is determined by the flow curve parameters, it may easily be increased by just changing those parameters adequately. If the span of shear rates should remain the same, this, of course, also means a significantly increased experimental data collection time.

8.5.5 Hysteresis properties dependence on solids content

As the positive relative hysteresis apparently does not change strongly with solids content, it may be hypothesised that the morphology at the end of the decreasing shear rate ramp-down is homomorphic with its structure at the beginning of the increasing shear rate ramp at low shear rates. The self-similarity in this case is interpreted in such a way that the amount and types of interactions between the fibrils in the primary shear state and within the structure at the end of the second flow curve scale with each other, independent of the solids content. This would also imply, that there is only a minor release of free water in the structure at the end of the second flow curve, because otherwise it could be expected that the positive hysteresis is increased more pronouncedly with a decrease of the solids content (higher potential availability of water). Since precisely this free water behaviour is seen for the negative relative hysteresis, it is likely that there is a significant water release in the transition zone during the increasing shear rate ramp-up, probably originating from a very pronounced flocculation as seen by Karppinen et al. [31]. As a lower solids content means more water to be freed, the negative relative hysteresis increases with decreasing suspension solids content. Following the proposed mechanistic model by Martoia et al. [9], the positive hysteresis is attributed to the difference between the initial structure and the finally flocculated structure that is induced and recovering at the end of the decreasing shear rate ramp-down. However, since the applicability of the morphological models proposed by Martoia et al. and Karppinen et al. to the experimental setup discussed here cannot be taken for granted *ad hoc*, the above discussion remains speculative and requires further proof, e.g. by rheo-optical measurements.

8.5.6 Comparison with other MFC suspension hysteresis data

Comparing a typical hysteresis obtained in this work, characterised by a positive and negative contribution ($\eta_1(\dot{\gamma}_i) > \eta_2(\dot{\gamma}_i)$ and $\eta_1(\dot{\gamma}_i) < \eta_2(\dot{\gamma}_i)$), respectively, with examples reported by others [9,17,19,35], reveals some significant differences. Very apparently, all

of them only report one type of hysteresis, either positive or negative according to our here-used definition. Whereas it is not clear if it is positive or negative in the works by Jia et al. and Agoda-Tandjawa et al. [17,35], it is reported to be positive by Martoia et al. [9] and to be negative in the work by Iotti et al. [19]. A direct comparison may be somewhat critical, as the MFC suspensions were manufactured differently (here: grinding; Iotti et al.: homogenised; and Martoia et al.: enzymatic pre-treatment and grinding) and, therefore, may inherently have a different flow curve profile. Nonetheless, all those different hystereses seem to be strikingly similar when the dilutions and measurement conditions are considered in addition, and a qualitative comparison should be possible. The following apparent differences should be especially highlighted:

- The MFC suspensions were pre-sheared in the cited experiments and was not pre-sheared in the current work (Martoia et al.: $1\,000\text{ s}^{-1}$ for 60 s, no mentioning of rest time; Iotti et al.: 50 s^{-1} for 120 s and 600 s rest time)
- The measurement systems were different (Couette in Martoia et al.'s work, parallel plate in Iotti et al.'s work and vane in serrated cup in our work)
- The solids contents (1 to 4 wt% in Iotti et al.'s work, even though only the 1 wt% flow curve was discussed in detail, and only 2 wt% in Martoia et al.'s work)
- The acquisition times were fixed in the cited works (Iotti et al.: 10 s, Martoia et al.: 50 s) and was automated in this work (min. of 15.2 s)
- The shear rate ranges were different (0.1 to $1\,000\text{ s}^{-1}$ and *vice versa* in Iotti et al.'s setup, 0.001 to $1\,000\text{ s}^{-1}$ and *vice versa* in Martoia et al.'s work and we used 0.01 to $1\,000\text{ s}^{-1}$ and *vice versa*).

Based on those differences, the absence of the positive hysteresis in Iotti et al.'s data may be explained by the pre-shearing. This may already have introduced a flocculated structure, which did not relax to recover the homogeneous structure during the rest phase, and therefore, the low shear viscosity during the shear rate ramp-up was already low (equal to the low shear viscosity of the shear rate ramp-down), and so no positive hysteresis is seen. The absence of the negative hysteresis in Martoia et al.'s work may have several reasons. Firstly, as shown in the work of Schenker et al. [13], the vane spindle (VS) system appears to lead to a stronger flocculation at intermediate shear rates, leading to a deeper

viscosity drop during the shear rate ramp-up compared to smooth cylinder roughened cup systems as used by Martoia et al. When comparing the flow curves obtained by different measuring systems through Schenker et al.'s work, the smooth system should be considered for Martoia et al.'s data. This is based on observations (unpublished), that the condition of the moving geometry (typically the inner part in modern shear rheometers using Couette type cells) is the main contributor to the overall flow curve. Secondly, as shown in this work, the negative hysteresis seems to become smaller with increasing solids contents, and as Martoia et al. only provided data at 2 wt% that can be considered as "high" solids content only, and so only a small hysteresis would be expected anyway.

The above comparison shows the critical influence of the rheometer set-up and measurement parameters. Yet, still, qualitative comparisons, like the one above, can be made when these conditions are fully considered. To do so, it is of critical importance to know all the relevant measurement parameters, as they strongly affect the obtained data. We, therefore, would highly encourage peers to provide such parameters when publishing rheological data in the context of similar systems, especially those including micro and nanofibrillated cellulose suspensions.

8.6 Conclusions

In this paper, we have set out to provide a procedure to quantify the hysteresis data of flow curves that are typically observed in MFC suspensions. At low shear rates (0.01 up to about 1 s^{-1}), a "positive hysteresis" area was found where the viscosity of the initial, shear rate increasing flow curve is higher than the viscosity of the following, shear rate decreasing curve. At further increasing shear rates up to about 10 s^{-1} , a "negative hysteresis" area was found, having a reversed order of the viscosities compared to the positive hysteresis. It was shown that a viscosity depending normalisation of the data is necessary to be able to compare directly data of MFC suspensions of different solids content. Whereas the positive normalised hysteresis decreased only slightly with an increasing suspension solids content, the negative normalised hysteresis decreased very strongly, as supported by statistical test results. These data show, that MFC suspensions exhibit different morphologies, not only depending on the shear rate, but also on the direction of the shear rate ramp, and, under some conditions, also on the suspension solids

content. Finally, hypothetical mechanistic models of the MFC suspensions as a function of shear rate were suggested, based on prior models proposed by other researchers, but remain to be proven.

The need to define both measurement geometry and data collection parameters in detail, including collecting sufficient measurement points, is emphasised by the uncertainty identified by statistically relevance testing. However, the same statistical rigour clearly provides confidence the principles applied.

Further work is carried out to investigate the influence of the degree of fibrillation of an MFC suspension on this and other rheological properties, to further demonstrate the usefulness of this novel characterisation method.

8.6.1 Acknowledgements

Elias Niklaus and Dr. Johannes Kritzinger are acknowledged for their valuable inputs on statistics and supporting discussions. Omya International AG and FiberLean Technologies Ltd. are thanked for their funding.

8.7 References

- [1] Hubbe MA, Ferrer A, Tyagi P, Yin Y, Salas C, Pal L and Rojas OJ: Nanocellulose in thin film, coatings, and plies for packaging applications: A review, *BioResources* 12 (2017) 2143-2233.
- [2] Oksman K, Y. A, Mathew AP, Siqueira G, Zhou Q, Butylina S, Tanpichai S, Zhou X and Hooshmand S: Review of the recent developments in cellulose nanocomposite processing, *Composites Part A: Applied Science and Manufacturing* 83 (2016) 2-18.
- [3] Boufi S, González I, Delgado-Aguilar M, Tarrès Q, Pèlach MA and Mutjé P: Nanofibrillated cellulose as an additive in papermaking process: A review, *Carbohydrate Polymers* 154 (2016) 151-166.
- [4] Nechyporchuk O, Belgacem MN and Bras J: Production of cellulose nanofibrils: A review of recent advances, *Industrial Crops and Products* 93 (2016) 2-25.
- [5] Kangas H, Lahtinen P, Sneek A, Saariaho AM, Laitinen O and Hellén E: Characterization of fibrillated celluloses. A short review and evaluation of

- characteristics with a combination of methods, *Nordic Pulp and Paper Research Journal* 29 (2014) 129-143.
- [6] Spence KL, Venditti RA, Rojas OJ, Habibi Y and Pawlak JJ: A comparative study of energy consumption and physical properties of microfibrillated cellulose produced by different processing methods, *Cellulose* 18 (2011) 1097-1111.
- [7] Svending P, Skuse D and Phipps J: Micro fibrillated cellulose - a new dimension in paper making in *Specialty Papers EU*, Manchester UK (2016).
- [8] Desmaisons J, Boutonnet E, Rueff M, Dufresne A and Bras J: A new quality index for benchmarking of different cellulose nanofibrils, *Carbohydrate Polymer* 174 (2017) 318-329.
- [9] Martoia F, Perge C, Dumont PJJ, Orgéas L, Fardin MA, Manneville S and Belgacem MN: Heterogeneous flow kinematics of cellulose nanofibril suspensions under shear, *Soft Matter* 11 (2015) 4742-4755.
- [10] Lauri J, Koponen A, Haavisto S, Czajkowski J and Fabritius T: Analysis of rheology and wall depletion of microfibrillated cellulose suspension using optical coherence tomography, *Cellulose* 24 (2017) 4715-4728
- [11] Haavisto S, Cardona MJ, Salmela J, Powell RL, McCarthy MJ, Kataja M and Koponen AI: Experimental investigation of the flow dynamics and rheology of complex fluids in pipe flow by hybrid multi-scale velocimetry, *Experiments in Fluids* 58 (2017) 158
- [12] De Kort DW, Veen SJ, Van As H, Bonn D, Velikov KP and Van Duynhoven PM: Yielding and flow of cellulose microfibril dispersions in the presence of a charged polymer, *Soft Matter* 12 (2016) 4739-4744.
- [13] Schenker M, Schoelkopf J, Mangin P and Gane PAC: Influence of shear rheometer measurement system selection on rheological properties of microfibrillated cellulose (MFC) suspensions, *Cellulose* 25 (2017) 961-976.
- [14] Nechyporchuk O, Belgacem MN and Pignon F: Rheological properties of micro-/nanofibrillated cellulose suspensions: Wall-slip and shear banding phenomena, *Carbohydrate Polymers* 112 (2014) 432-439.

- [15] Saarinen T, Lille M and Seppälä J: Technical aspects on rheological characterization of microfibrillar cellulose water suspensions, *Annual Transaction of the Nordic Rheology Society* 17 (2009) 121-128.
- [16] Pääkkö M, Ankerfors M, Kosonen H, Nykänen A, Ahola S, Österberg M, Ruokolainen J, Laine J, Larsson PT, Ikkala O and Lindström T: Enzymatic hydrolysis combined with mechanical shearing and high-pressure homogenization for nanoscale cellulose fibrils and strong gels, *Biomacromolecules* 8 (2007) 1934-1941.
- [17] Agoda-Tandjawa G, Durand S, Berot S, Blassel C, Gaillard C, Garnier C and J.L. D: Rheological characterization of microfibrillated cellulose suspensions after freezing, *Carbohydrate Polymers* 80 (2010) 677-686.
- [18] Dimic-Misic K, Nieminen K, Gane P, Maloney T, Sixta H and Paltakari J: Deriving a process viscosity for complex particulate nanofibrillar cellulose gel-containing suspensions, *Applied Rheology* 24 (2014) 35616
- [19] Iotti M, Gregersen OW, Moe S and Lenes M: Rheological studies of microfibrillar cellulose water dispersions, *Journal of Polymers and the Environment* 19 (2011) 137-145.
- [20] Moberg T, Sahlin K, Yao K, Geng S, Westman G, Zhou Q, Oksman K and Rigdahl M: Rheological properties of nanocellulose suspensions: Effects of fibril/particle dimensions and surface characteristics, *Cellulose* 24 (2017) 2499-2510.
- [21] Debon SJJ, Wallecan J and Mazoyer J: A rapid rheological method for the assessment of the high pressure homogenization of citrus pulp fibres, *Applied Rheology* 22 (2012) 63919.
- [22] Haavisto S, Salmela J, Jäsberg A, Saarinen T, Karppinen A and Koponen A: Rheological characterization of microfibrillated cellulose suspension using optical coherence tomography, *Tappi Journal* 14 (2015) 291-302.
- [23] Nazari N, Kumar V, Bousfield DW and Toivakka M: Rheology of cellulose nanofibers suspensions: Boundary driven flow, *Journal of Rheology* 60 (2016) 1151-1159.
- [24] Kumar V, Nazari B, Bousfield D and Toivakka M: Rheology of microfibrillated cellulose suspensions in pressure-driven flow, *Applied Rheology* 26 (2016) 43534.

- [25] Kataja M, Haavisto S, Salmela J, Lehto R and Koponen A: Characterization of microfibrillated cellulose fiber suspension flow using multi scale velocity profile measurements, *NORDIC PULP & PAPER RESEARCH JOURNAL* 32 (2017) 473-482.
- [26] Nechyporchuk O, Belgacem MN and Pignon F: Current progress in rheology of cellulose nanofibril suspensions, *Biomacromolecules* 17 (2016) 2311-2320.
- [27] Saarinen T, Haavisto S, Sorvari A, Salmela J and Seppälä J: The effect of wall depletion on the rheology of microfibrillated cellulose water suspensions by optical coherence tomography, *Cellulose* 21 (2014) 1261-1275.
- [28] Li M-C, Wu Q, Song K, Lee S, Qing Y and Wu Y: Cellulose nanoparticles: Structure-morphology-rheology relationships, *ACS Sustainable Chemistry and Engineering* 3 (2015) 821-832.
- [29] Schenker M, Schoelkopf J, Mangin P and Gane P: Rheological investigation of complex micro and nanofibrillated cellulose (MNFC) suspensions: Discussion of flow curves and gel stability, *Tappi Journal* 15 (2016) 405-416.
- [30] Schenker M, Schoelkopf J, Mangin P and Gane P: Rheological investigation of pigmented micro-nano-fibrillated cellulose (MNFC) suspensions: Discussion of flow curves in Tappi International Conference on Nanotechnology for Renewable Materials, Grenoble (2016).
- [31] Karppinen A, Saarinen T, Salmela J, Laukkanen A, Nuopponen M and Seppälä J: Flocculation of microfibrillated cellulose in shear flow, *Cellulose* 19 (2012) 1807-1819.
- [32] Chan Y and Walmsley RP: Learning and understanding the kruskal-wallis one-way analysis-of-variance-by-ranks test for differences among three or more independent groups, *Physical Therapy* 77 (1997) 1755-1761.
- [33] Mewis J and Wagner NJ: Thixotropy, *Advances in Colloid and Interface Science* 147 (2009) 214-227.
- [34] Saarikoski E, Saarinen T, Salmela J and Seppälä J: Flocculated flow of microfibrillated cellulose water suspensions: An imaging approach for characterisation of rheological behaviour, *Cellulose* 19 (2012) 647-659.

- [35] Jia X, Chen Y, Shi C, Ye Y, Abid M, Jabbar S, Wang P, Zeng X and Wu T: Rheological properties of an amorphous cellulose suspension, Food Hydrocolloids 39 (2014) 27-33.

8.8 Unpublished data

8.8.1 Introduction

Based on the flow curve data presented in the article above, a statistical investigation on the other flow curve properties was carried out. As pointed out in section 4.2.2.1, those properties typically are evaluated on averaged flow curves derived from the three individual measurements. On the one hand, this approach saves time, but, unfortunately, no standard deviation can be calculated, and so the information on variability is lost. Still, to have an idea on the data variability, this additional investigation was, nonetheless, carried out, using a dataset that consists of 9 single flow curve measurements per MFC suspension dilution, grouped in three sets of triplicates. The mean and standard deviation of flow curve properties were evaluated, and an ANOVA analysis was carried out to investigate if the suspension solids content has a significant influence on the investigated parameters. In addition, the respective triplicate sets within a dilution were compared and tested for repeatability using an ANOVA test.

All the flow curve properties were evaluated according to the procedures described in section 7.4.3, also using Origin 2017 for curve fittings (i.e. zone 1 and 2 power law fits). To test whether the compared datasets were different from each other, an ANOVA test was carried out, including a pairwise Tukey test to identify different dataset pairs (details in section 8.4.3). No ANOVA test was carried out on the *end of zone 1*, *start of zone 2* and the *local minimum* data because they are not continuous (section 8.4.3).

8.8.2 Results

The average and standard deviations of the properties in dependence of the suspension solids content can be found in Table 8.3. Those values are derived from the individual parameter values of the 9 individual flow curves per dilution. The respective distributions are shown in Figure 8.10. It is rather apparent, that the low and high shear viscosity ($\eta_{0.02}$, η_{100}), as well as the respective consistency coefficients (K_1 , K_2) strongly depend on the

suspension solids content (increase with increasing solids content). This was confirmed by the ANOVA tests that found significant differences among the solids contents for all these properties. An opposite trend was found for the relative transition zone depths (Δ_{bin}), and also confirmed by the ANOVA test to be significant. Then again, no significant change of n_1 with the solids content was identified. A weaker trend was found for n_2 as well, expressed by a significant difference between 1 and 2 wt%, but no other significant differences among the other suspension solids contents pairs.

A detailed discussion on the trends of these properties, and the potential implications on the suspension particulate morphology are presented in Chapter 9 - .

Table 8.3: Average values and standard deviations of flow curve properties of the 9 individually evaluated flow curves per dilution.

	K_1 (Pas ⁿ)		n_1 (1)		$\eta_{0.02}$ (Pas)	
	AV	SD	AV	SD	AV	SD
MFC 1 wt%	29	4	0.131	0.026	862	101
MFC 1.5 wt%	94	18	0.147	0.026	2613	276
MFC 2 wt%	200	51	0.130	0.035	5909	661

	K_2 (Pas ⁿ)		n_2 (1)		η_{100} (Pas)		Δ_{min} (1)	
	AV	SD	AV	SD	AV	SD	AV	SD
MFC 1 wt%	7	1.1	0.289	0.036	0.274	0.007	0.838	0.032
MFC 1.5 wt%	22	2.4	0.274	0.025	0.773	0.017	0.764	0.052
MFC 2 wt%	54	4.2	0.242	0.011	1.631	0.086	0.699	0.044

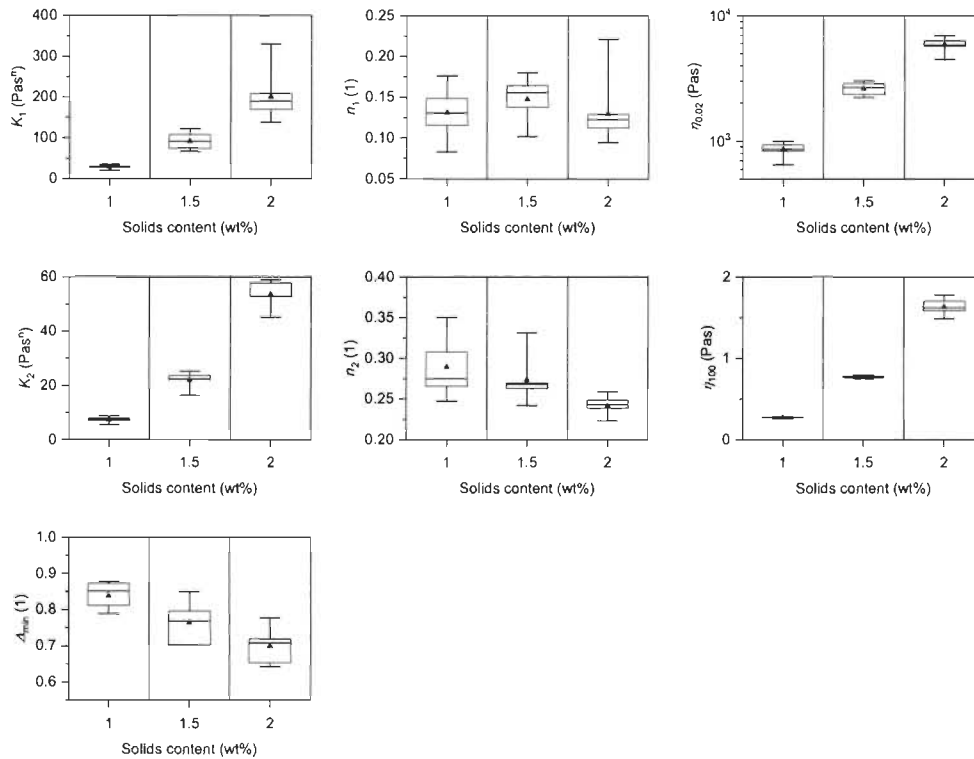


Figure 8.10: Box plots of the flow curve properties of the 9 individually evaluated flow curves per dilution. The set-up of the box-plots is the same as in the main article. The span gives the minimal and maximal values, the bow represents the 25 to 75 % data range, the line within the bow is the median and the triangle is the data mean.

The parameters with non-continuous values are presented in Figure 8.11. As mentioned in section 8.4.3, those values are determined by the predefined measurement protocol, and the granularity may be too low to reliably identify trends. No statistical tests were therefore applied on these datasets. Still, some (weak) trends can be identified visually, but also, that the data-scatter is typically \pm one tested shear rate for most properties and solids contents. A detailed discussion can be found in Chapter 9 - as well.

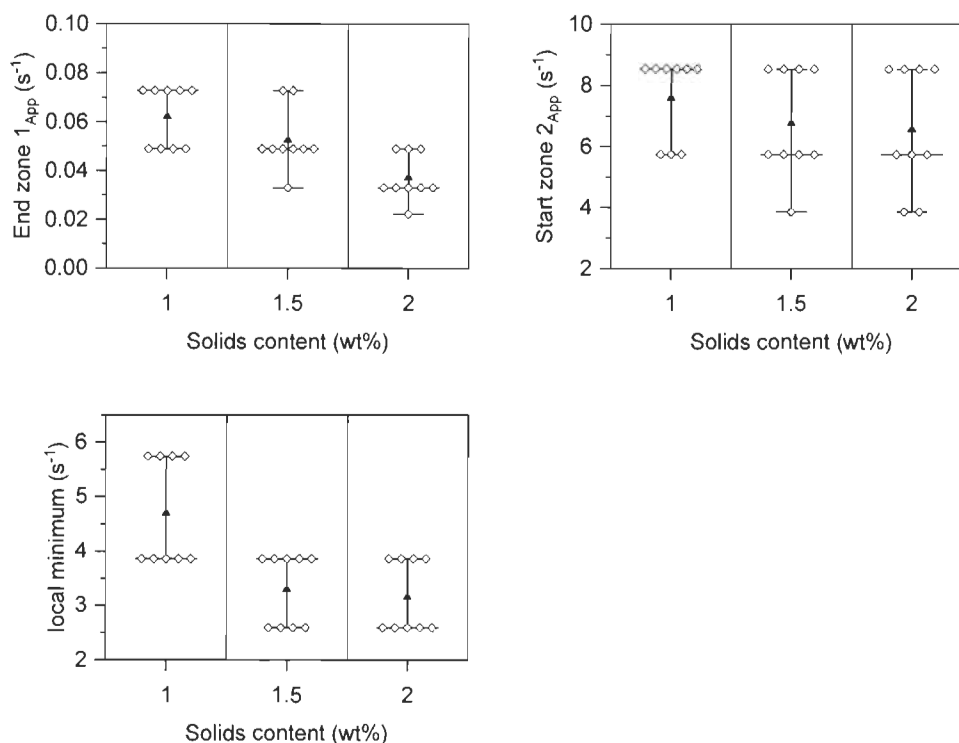


Figure 8.11: Box plots of the flow curve properties with non-continuous values. The hollow diamonds represent the single values, the triangle the mean value and the middle line is the median.

To see, whether the data of a triplicate set is able to deliver meaningful enough results for further analysis, the three triplicates within a solids content were compared using an ANOVA test as well. Table 8.4 summarizes the results obtained by the ANOVA test. As can be seen, the test resulted in most cases in accepting the null hypothesis (marked with “0”), meaning that the means are equal for the three triplicates of a given dilution (for $\alpha = 0.05$). In two cases, one of the triplicates was significantly different from the two others (marked with “1(2)”), and in two other cases, it was only one triplicate combination that was significantly different (marked with “1(1)”).

Table 8.4 Summary of the ANOVA test for the three triplicates within a dilution for the tested flow curve properties. “0” indicates that the data means were not significantly different for the three triplicates, “1(1)” indicates that one mean-pair was different and “1(2)” that two mean-pairs were different (indicating one set being an outlier).

	K_1	n_1	$\eta_{0.02}$	K_2	n_2	η_{100}	Δ_{\min}
MFC 1 wt%	0	0	0	1 (1)	1 (2)	1 (1)	0
MFC 1.5 wt%	0	0	1 (2)	0	0	0	0
MFC 2 wt%	0	0	0	0	0	0	0

8.8.3 Conclusions

The additional statistical investigation of the flow curve data indicates that a certain data scatter is to be expected for all of the evaluated rheological properties. However, apparent trends (as a function of the suspension solids content) are likely to be significant, despite the data scatter. Finally, also the use of the mean data of triplicated flow curves appears to deliver mostly reproducible results. These findings provide a basis for the identification of trends within the extensive study on the influence of the degree of fibrillation on the rheological properties of MFC suspensions, presented in the next chapter (Chapter 9 -).

Chapter 9 - Article 4: Rheology of microfibrillated cellulose (MFC) suspensions – influence of the degree of fibrillation and residual fibre content on flow and viscoelastic properties

Published article.

Michel Schenker, Joachim Schoelkopf, Patrick Gane, Patrice Mangin; Cellulose; 2018; doi: 10.1007/s10570-018-2117-4

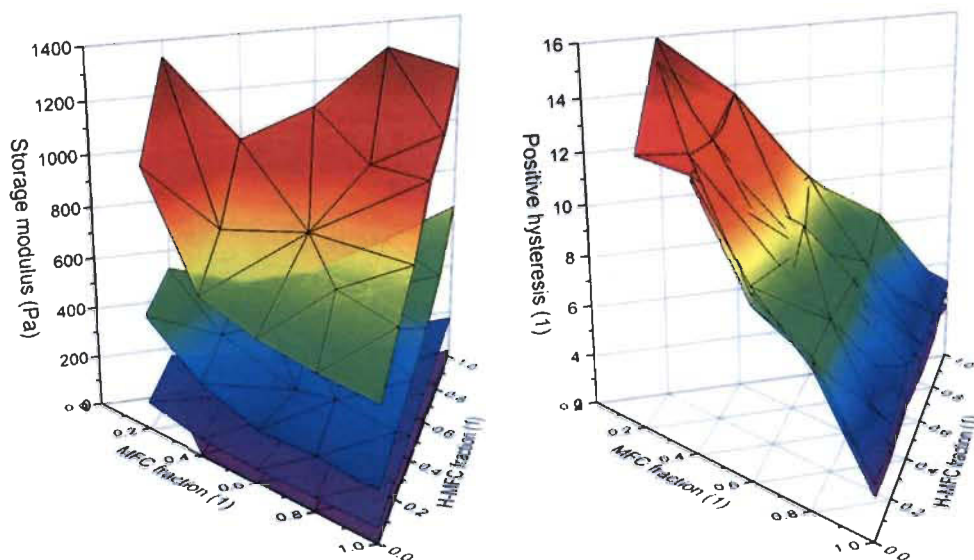
9.1 Foreword

The article presents the findings of an extensive experimental study (ca. 660 single rheometer measurements), investigating the effect of the DoF on the rheological properties of MNFC suspensions using mixtures of different DoF starting materials. This work represents the idea of the initial intention of this work, i.e. to investigate the rheological properties of MNFC suspensions in dependence of various aspects of the envisaged material space (section 3.1.1). Like studies for further suspension properties, such as added pigment particles or polymers can be seen as potential for further work. It is very apparent, that the experimental effort is very high, and so, here, only one aspect, the DoF, is investigated. To mitigate the experimental effort in the future, a design of experiment (DoE) approach should be considered. This could also have been employed here, yet, it was a conscious decision to test a complete mixture design so as to lay the groundwork and to build confidence in the procedures as works of this type were not reported before, and there was no experience or knowledge on the level of variation and significance of the rheological properties in dependence of the DoF. Having a thorough investigation like this as a basis, may provide more confidence in undertaking potential further similar studies.

This work combines learnings from all previous parts of this PhD work. For example, the experimental set-up chosen here is based on and reasoned based on the findings concerning the flow curve measurement protocol, as well as on the work on the influence of the measurement systems on rheological data. Furthermore, the newly introduced quantification procedures of the rheological data have together enabled this type of very compact data presentation and straightforward recognition of trends. Also, the confidence

in the obtained data obtained by looking at their statistics contributed to the findings in this final article. Then, finally, the findings of this work may help to understand and investigate the effects causing variations in MNFC qualities in a given production process, exemplified here by the ultrafine friction grinder.

9.2 Graphical abstract



9.3 Highlights

- Extensive investigation of the influence of the degree of fibrillation of MFC suspensions on their rheological properties.
- Quantification of flow curve and viscoelastic data.
- Comprehensive data presentation using ternary mixture contour diagrams.
- Discussion of findings with recent literature.

9.4 Abstract

The influence of the degree of fibrillation (*DoF*), i.e. the fibril width distribution, on the rheological properties of microfibrilated cellulose (MFC) suspensions was investigated. To extend the understanding of the dominating effect of either fibril diameter alone or diameter size distribution, flow curves (viscosity against shear rate) and viscoelastic measurements were performed on single, double and ternary component mixtures of

medium and highly fibrillated MFCs and pulp fibres across a range of solids content. The data were quantified using classical and recently introduced descriptors, and presented in comprehensive 3D/ternary contour plots to identify qualitative trends. It was found that several rheological properties followed the trends that are generally described in the literature, i.e. that an increasing DoF increases the MFC suspension network strength. It was, however, also found that coarse pulp fibres can have additional effects that cannot be explained by the increased fibril widths alone. It is hypothesised that the increased stiffness (directly caused by the larger fibril width) as well as the reduced mobility of the pulp fibres are additional contributors. The data are discussed in relation to recent findings in the field of rheology and related morphological models of MFC suspension flow behaviour.

9.4.1 Keywords

Microfibrillated cellulose (MFC), Rheology, Vane, Degree of fibrillation (DoF), Flow curve, Viscoelasticity

9.5 Introduction

The nanocellulose (NC) material-space contains a wide variety of different products with unique properties, despite their same underlying chemistry. The grades are ranging from fibrillated over crystalline to bacterial cellulose, and they have characteristic widths in the micrometre as well as in the nanometre range, they have medium to very high aspect ratios and can be manufactured from very different source materials (Nechyporchuk et al. 2016a). Chemical modifications of the surface hydroxyl groups widen the property- and application-space even more (Missoum et al. 2013; Stenstad et al. 2008). The classification of such a versatile material class is challenging, and still not completely aligned. Yet, a common strategy is to differentiate between bacterial, fibrillated and crystalline grades. Within the latter two, another classification regarding their characteristic size, i.e. fibril diameter or width for fibrillated grades, or crystallite size (width and length), is applied (Kangas et al. 2014). Typical examples of fibrillated grades are microfibrillated cellulose (MFC) or nanofibrillated cellulose (NFC), both of which having different names like cellulose filaments (CF) or cellulose nanofibrils (CNF).

Due to their chemistry, but also due to their shape and mechanical properties, fibrillated cellulose materials yield high viscous aqueous suspensions, already at low solids contents (Herrick et al. 1983; Pääkkö et al. 2007). The ability of the fibrils to form networks and aggregates, to entangle and to align, as well as their flexibility leads to a complex rheological behaviour (Hubbe et al. 2017). The same applies for crystalline cellulose suspensions, where the typically platelet shaped crystallites can organise in different phases, and, due to their crystalline nature, specifically interact with visible light (Shafiei-Sabet et al. 2012). There seems to be an increasing interest, not only in NC materials in general, but also in investigating their complex aqueous suspension rheology, as is apparent, for example, from two recent review articles in the field (Hubbe et al. 2017; Nechyporchuk et al. 2016b). On the one hand, it is necessary to know the rheology of these materials in practical applications, e.g. during pumping, extrusion or casting processes to make them processable. On the other hand, an understanding of the rheology with respect to the underlying suspension particulate morphology and chemistry enables researchers to design products for very specific needs.

A major challenge in MFC rheology measurements is the non-linear behaviour, and the heterogeneous, at least two-phase, composition. Related effects include complete or partial phase-segregation (depleted, water rich layers or voids), related apparent wall slip, and shear banding (Haavisto et al. 2015; Nazari et al. 2016; Nechyporchuk et al. 2014). The presence and the intensity of such effects do not only depend on the shear conditions, but also on the measurement system and protocol (Schenker et al. 2017). Not taking such effects into account, may lead to contradictory results, not infrequent in the literature, and probably wrong model hypotheses. Quite some effort is put into quantifying these effects (Yoshimura and Prud'homme 1988), mathematically correcting them (Mohtaschemi et al. 2014a, 2014b), and in developing protocols on how to avoid or suppress them (Barnes 2000). Cloitre and Bonnecaze (2017) pointed out in a recent review on wall slip of high solids dispersions, that such mechanisms are often considered as a nuisance because they violate assumptions and boundary conditions of the measurement method, yet it should be understood, that those mechanisms are fundamental components of how the material responds to the deformation. This valid comment highlights that it is as important to be at

least aware of such effects, ideally quantify and describe them, rather than trying to suppress them.

Occasionally, complementary measurement techniques are used to quantify directly or indirectly such non-linear effects, though they can also be used to study the suspension morphology under different shear conditions. Such complementary techniques include optical imaging (Saarikoski et al. 2012), velocity profiling using, e.g. ultrasound and/or tomography techniques (Kataja et al. 2017), and structural investigations like small angle neutron scattering (Orts et al. 1998) or x-ray scattering (Nechyporchuk et al. 2015). Such work has revealed, for instance, the tendency of unmodified MFC and NFC suspensions to aggregate (flocculate) at intermediate shear rates in constant shear experiments (Martoia et al. 2015), or the presence of a water (-rich) film close to measurement boundary geometries, as well as concentration gradient development and plug flow under certain shear conditions (Kataja et al. 2017).

It is well known that various suspension and cellulose fibril/crystallite conditions have an influence on the nanocellulose suspension rheology. Prominent conditions are the suspensions solids content, pH, salinity or temperature (Agoda-Tandjawa et al. 2010; Pääkkö et al. 2007). To a lesser extent, also the influences of the fibril dimensions, aspect ratio (the degree of fibrillation, short *DoF*) and surface charge (Besbes et al. 2011), and their respective probability and spatial distributions (Colson et al. 2016; Moberg et al. 2017), on the suspension rheology are investigated. In the case of mechanically produced (with or without enzymatic pre-treatments) MFC materials, the sign of the specific surface charge and the total surface charge is given by the feed pulp, and predominantly the *DoF* is changed during processing. Yet, processing towards increased *DoF* may still potentially change the surface charge density of the fibrils due to a potential release of solubles, hemicellulose and/or lignin from the original fibre structure into the suspension, though the process per se, being purely mechanical, does not add or subtract charge. Depending on the process and the process conditions, very different fibril width and length distributions, as well as residual fibre content may result. With a view, for example, on qualifying rheological measurements as quality control tools, or manufacturing a product with a dedicated rheology profile (rheological property profile is tailored to fit a specific

application), the understanding of the influence of the *DoF* on the rheological behaviour of the suspension can be very beneficial.

The aim of this work was to investigate the influence of the *DoF*, including the impact of residual, coarse fibres on rheological properties of MFC suspensions. Of particular interest were industrial type of MFC suspensions, typically characterised to have a broad size distribution, i.e. containing residual fibres and nanometre sized fibrils together with the main body of micrometre sized fibrils. In contrast to other works in this area, we chose to use only mechanical fibrillation processes to obtain different *DoF* MFC suspensions in order to exclude surface charge related effects (Moberg et al. 2017). To obtain a wide variety of different *DoFs*, but without changing other aspects of the fibrils, an extensive ternary mixture trial matrix was set-up. To be able to identify potential trends, the data were quantified using previously introduced techniques and descriptors (Schenker et al. 2018, 2017). Finally, the findings are discussed phenomenologically with a view on potential suspension morphologies, based on recent models obtained from rheo-optical studies of MFC suspensions (Haavisto et al. 2015; Karppinen et al. 2012; Martoia et al. 2015). The work presented here is intended not only to motivate other researchers in the field to consider thorough quantification of their rheological data, but also to propose some interesting aspects to investigate further the use of optical, or other, structure revealing techniques in combination with rheological studies of MFC suspensions.

9.6 Methods

9.6.1 Materials

To obtain samples made up of fibrillated cellulose material having three different degrees of fibrillation (*DoF*) whilst trying to avoid changing other material characteristics, like surface chemistry and charge, only mechanical fibrillation processes of increasing intensity were applied to a starting batch of a eucalyptus pulp suspension made down in tap water from dry pulp mats. The lowest *DoF* material in this study, representing residual fibres, was the eucalyptus pulp itself, denoted as *pulp*. Respective concentrations of *pulp* suspension were manufactured by adding according amounts of dry mat pulp to water under stirring using a dissolver disc type impeller.

The manufacturing process of the intermediate *DoF* material, denoted in this work simply as *MFC*, is described in detail elsewhere (Schenker et al. 2016a) and was the same as in recent works also reported by Schenker et al. (2018, 2017). In short, the eucalyptus pulp was mechanically disintegrated at 3 wt% in tap water using an ultrafine friction grinder under a varying chosen number of single passes, each at a different rotational speed. The specific grinding energy, is defined as the total electrical energy consumption normalised by the amount of dry cellulose matter was 7.2 kWhkg^{-1} .

To achieve a higher *DoF* *MFC* (short *H-MFC*) an additional fibrillation process was applied to the previously described *MFC* suspension, namely an homogenisation process. To avoid having to undergo a subsequent concentration of the short *H-MFC* suspensions for the following rheological characterisation, the solids content for the homogenisation process was set to 2 wt%. This is a rather high solids content for homogenisation in laboratory scale, so, to avoid blockages or other process failures, the starting *MFC* suspension was subjected again to an ultrafine friction grinder pass at 500 min^{-1} (rpm) and a gap setting of “-80 μm ”, maintaining the solids concentration still at 3 wt%. The process was carried out on an NS 2006 L homogeniser (Niro Soavi), equipped with an LPN60 dispersion module (formerly Serendip AG, now Netzsch-Gruppe, Germany). The suspension was then subjected to single passes, with a throughput pump setting of $30 \text{ dm}^3\text{h}^{-1}$ and a pressure of 600 bar for all passes, achieved by adjusting the back-pressure handle accordingly. For the first ten passes, a 120 μm diameter nozzle was used to avoid clogging. To intensify the fibrillation process, an 80 μm diameter nozzle was used for two additional passes. The specific energy input of these additional process steps was 20.7 kWhkg^{-1} .

Mixtures of the three materials, *pulp*, *MFC* and *H-MFC* were realised by adding the respective amounts of the suspensions and diluting the combination by the addition of tap water. The realised dilutions were 0.5, 1, 1.5 and 2 wt% and the mixture matrix can be found in Figure 2 of the supplementary information. The mixtures, as well as the pure *MFC* and *H-MFC* suspensions were treated by 2 min of rotor stator mixing at $12\,000 \text{ min}^{-1}$ (rpm) (Polytron PT 3000, Kinematica, Switzerland) and 5 min exposure to an ultrasonic bath (Transsonic T 890, Elma, Switzerland). Before further measurements, the dilutions were let to rest for at least one hour.

9.6.2 Data presentation

The rheological data are presented in ternary contour plots, one for each solids content. For a complementary visualisation, the contour surfaces are overlaid using a rainbow-type colour gradient, starting from purple at low values and ending at red for high values. The scale among the different ternary plots within one property is the same, so also the dependence on the solids content is directly visible. Instead of providing a separate colour scale, several contour lines within a ternary diagram are labelled with their respective values. A detailed introduction on the interpretation of ternary diagrams is provided in the supplementary information, but, generally speaking, the diagrams describe the composition of a ternary mixture, always adding up to 100%. Each vertex of the triangle represents 100% of one of the three components. The share of this component decreases constantly along the bisector of this vertex perpendicular to the opposite edge until it reaches that opposing side, where the share of this component is 0%. In the present work, the left vertex represents 100% *pulp*, the right vertex 100% *MFC* and the top vertex (apex) 100% *H-MFC*. Missing data points in the ternary graph mean that the specific mixture at the respective dilution was not evaluated because it was disturbed by irreproducible or other physical effects. An example of such an effect is the observation of sedimentation after high shear under decreasing shear rate at low solids content (0.5 wt% suspensions) due to structure breakdown.

Alternatively set-up ternary diagrams can be found in the supplementary information document. Also, animated 3D ternary diagrams where the different solids content data were stacked can be found in the online repository. Each solids content dataset is represented as individual surface. The grid line colour indicates the solids content (purple: 0.5 wt%, blue: 1 wt%, green: 1.5 wt% and red: 2 wt%).

9.6.3 Degree of fibrillation analysis

Several attempts were made to determine the fibre and fibril width distributions of the sample materials using image analysis methods. Due to the anticipated high polydispersity of the materials, SEM-image based techniques were evaluated rather than AFM or TEM based ones in an attempt to give visual confirmation and sufficient statistical relevance. Namely, two approaches described by Onyianta and Williams (2018) and Pyrgiotakis et al. (2018) were reproduced, including modifications in the sample preparations.

Unfortunately, either the obtained images were not suitable for image analysis (overlapping and confused configuration), or the obtained distribution histograms did not represent the apparent full width distributions (insufficient statistical relevance), i.e. they were not able to account for the coarser fibril/fibre fraction, like described for instance by Colson et al. (2016). Additional details on the apparent width distribution discrepancy can be found in the supplementary information. However, the exercise enabled us to identify the tendency of fibrils to aggregate at rest, even under very dilute regimes (perhaps meniscus force), as being one of the major challenges here. Common strategies to improve the level of dispersion, like adding carboxymethyl cellulose (Veen et al. 2015), were not sufficient (probably again related to the high levels of dilution).

The evolution of the degree of fibrillation (DoF) in this work is therefore indicated by qualitative and indirect data, namely by optical and scanning electron microscopy images and specific surface area (BET) measurements. For this, 0.5 wt% suspensions of pulp, *MFC* and *H-MFC* were frozen by immersion into liquid nitrogen directly after the ultrasonication step of the makedown procedure. The frozen samples were then subjected to freeze-drying (Alpha 1-2LD Freeze Dryer, Martin Christ GmbH, Germany). The specific surface area was measured using the Brunauer-Emmett-Teller (BET) method on torn out pieces of the resulting aerogels, sampled in duplicate (Tristar, Micromeritics, Germany). SEM images (Sigma VP, Zeiss, Switzerland) were taken as well from such torn-out pieces after being sputtered with gold (8 nm). For optical microscopy (Axio Imager.M2m, Zeiss, Switzerland), one drop of the respective 0.5 wt% suspension was placed between two glass slides.

9.6.4 Rheological measurements

All the rheological measurements were performed on an MCR 300 rheometer (Anton Paar, Austria) at 20 °C, equipped with a vane (six blades) in serrated (length profiled) cup system (vane: ST22-6V-16, $d_{\text{vane}} = 22$ mm, cup: CC27-SS-P, $d_{\text{cup}} = 28.88$ mm, profile depths = 0.5 mm, profile widths = 1.65 mm), also supplied by Anton Paar. The vane system was used because it is less prone to depletion at the wall and related apparent slip effects, as described, for example, by Mohtaschemi et al. (2014a) and Schenker et al. (2017).

All the suspensions were measured as triplicates, and each measurement within a triplicate was obtained from a separate filling of the measurement system. For a given dilution, several dilution makedowns were used throughout the work presented here, and the repeatability was checked in all cases (data not shown). The data are presented as average values from the triplicate measurements. Individual standard deviations are not presented, however, typical maximal standard deviations are provided for a given property as per cent of the average property values. Further standard deviation data can also be found in preceding work (Schenker et al. 2017, 2018). After loading the samples and immersing the vane, the system was let to rest for about two minutes before the measurement protocols were started. No pre-shearing protocol was applied in order to induce as little morphological changes to the suspension as possible.

Flow curves (viscosity η in dependence of the shear rate $\dot{\gamma}$) were recorded by performing an automated shear rate increase ramp from 0.01 s^{-1} to $1\,000 \text{ s}^{-1}$, directly followed by a ramp with reversed direction. 30 log-equidistant distributed point measurements were performed per ramp with automated acquisition time mode (minimal acquisition time is 15.2 s) and shear rate control. The automated acquisition time mode should ensure a steady state situation when acquiring a measurement (Schenker et al. 2016b). Having a steady state situation is important for the data interpretation with view on suspension morphology as it reduces the likelihood of time-dependent or start-up effects interferences (Puisto et al. 2015; Korhonen et al. 2017). Preliminary experiments have shown that the same flow curves can be obtained with different amounts of point measurements (data not shown). The typically obtained three region flow curve, exemplified with a 1 wt% *MFC* suspension flow curve in Figure 9.1, was quantified using the descriptors introduced by Schenker et al. (2018, 2017). In short, zone 1 is described by the power law parameters K_1 (consistency coefficient) and n_1 (flow index), the low shear viscosity $\eta_{0.02}$, where the subscript refers to the shear rate which the viscosity is quoted, and its end (*end of zone 1*). The transition region is characterised by the *position of the local minimum* and its relative depth (Δ_{\min}). Zone 2 is again described by its onset (*start of zone 2*), the power law parameters K_2 and n_2 and the representative high shear viscosity η_{100} . Finally, also the hysteresis between the shear rate increasing and shear rate decreasing curve is described with the positive and

negative relative hysteresis H_{RS+} and H_{RS-} respectively, using the simplified calculation according to Schenker et al. (2018).

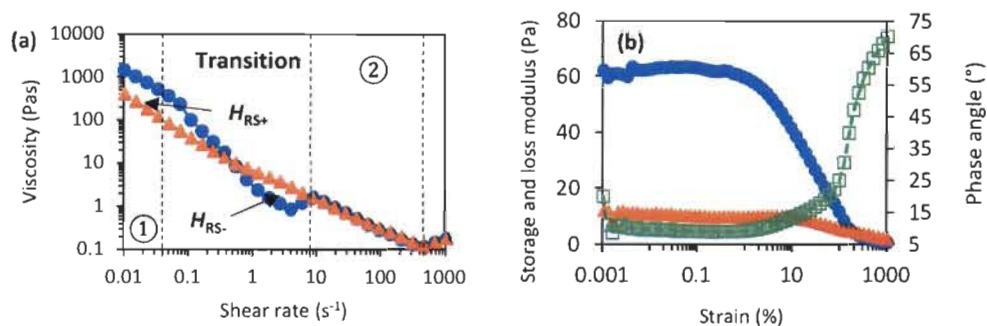


Figure 9.1: Flow curve (a) and amplitude sweep (b) measurement data of a 1 wt% MFC suspension. In the flow curve, the blue circles represent shear rate increase data and the orange triangles represent shear rate decrease data. In the amplitude sweep graph, the blue circles and the orange triangles represent the storage and loss moduli, respectively, and the hollow squares represent the phase angle.

Viscoelastic properties were determined by an amplitude sweep measurement at a frequency of 0.5 Hz. The automated, strain amplitude-controlled ramp was set from 0.001 % to 1 000 % with 60 log-equidistant distributed point measurements and automated acquisition time mode. In practice, the acquisition time was seen to be around 25.5 s for all points in all measurements. As for the flow curves, preliminary experiments have shown that the same rheograms can be obtained with different amounts of point measurements (data not shown). Here also, the descriptors introduced by Schenker et al. (2017) are evaluated, namely storage and loss moduli in the linear regime (G'_{\max} , G''_{lin}), as well as the limit of linearity (LoL) and the yield stress ($\tau_{Y,\delta}$), both determined via the phase angle data. Typically, the plateau values for the storage and loss modulus in the linear viscoelastic (LVE) regime are reported. In the present and precedent work (Schenker et al. 2017) it was however found, that only the loss modulus shows this plateau characteristic, whereas the storage modulus goes through a local maximum before it decreases with increasing strain. It was therefore decided to evaluate the maximal storage

modulus (G'_{\max}), and as commonly done, the plateau value of the loss modulus (G''_{lin}). Especially at lower solids content and low strain values, the moduli data tend to be noisy, such data was omitted from evaluation. The yield point, defined by the *LoL* (or strain at yield) and the yield stress ($\tau_{Y,\delta}$) was determined using the phase angle data, rather than the storage modulus data (Schenker et al. 2017). As a consequence of the behaviour of the moduli as a function of strain, the phase angle typically shows a local minimum. The yield point was defined to be where the phase angle deviates (increases) more than 5% from its minimal value, adapted from Moberg and Rigdahl (2012) and further described by Schenker et al (2017).

9.7 Results

9.7.1 Degree of fibrillation

The increase of the DoF from the *pulp*, through the *MFC* and to the *H-MFC* materials is apparent from the microscopy images (Figure 9.2). On the one hand, the amount of clearly visible fibres and fibrils in the optical microscopy images decreases with increasing treatment intensity. On the other hand, SEM images reveal an increasing amount of fine fibrils. This qualitative observation is well supported by the surface area data presented in Table 9.1 It is likely, that the *MFC* material has the broadest fibril width distribution among the investigated materials, as residual fibres are present as well as isolated fibrils, whereas the other two materials contain predominantly one or the other. The role of the *pulp* material in this work is to investigate the influence of residual fibres on the suspension rheology. The hypothesised (as there is no quantitative data to proof this) differences between the *MFC* and *H-MFC* materials are the absence of residual fibres in the *H-MFC* material, together with its narrower size distribution, also resulting in a smaller median width.

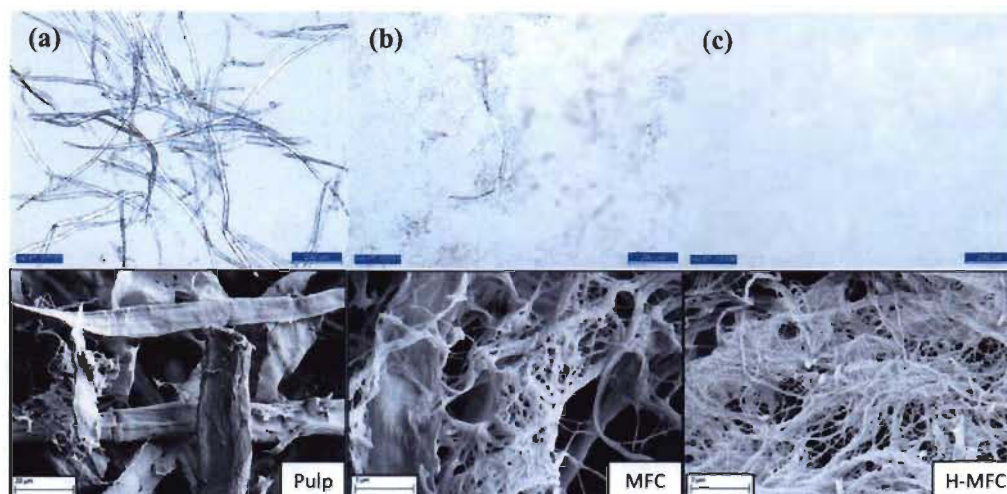


Figure 9.2: Optical (top) and SEM images (bottom) of the pulp (a), MFC (b) and H-MFC materials (c). The scale bars in the optical microscopy images are 200 μm .

Table 9.1: Specific surface area data of the pulp, MFC and H-MFC materials, including the standard deviations for the MFC and H-MFC materials.

Material	BET surface area (m^2g^{-1})
<i>Pulp</i>	0.4 *
<i>MFC</i>	7.7 ± 1.1
<i>H-MFC</i>	19.6 ± 1.2

*Only one valid measurement was obtained for the *pulp* material, hence no standard deviation is provided.

9.7.2 Suspension particulate morphology hypothesis

As described in previous publications (Schenker et al. 2018; Schenker et al. 2017), we place our interpretations and discussions of the present rheological data in the light of findings from other researchers. In those works, flow curves very alike the ones reported here were described, and in parallel the solid phase morphology was visualised (Haavisto et al. 2015; Karppinen et al. 2012; Martoia et al. 2015), confirming the aggregation behaviour in the transition region. Furthermore, a theoretical work, supported by

experimental evidence, on concentrated rigid fibre suspensions containing adhesive contacts (Bounoua et al. 2016) describes the present flow curves and trends very well.

9.7.3 Influence of DoF on static structure morphology

Figure 9.3 shows the storage modulus (G'_{\max}) data of the investigated mixtures. The strong dependence on the solids content is very apparent and is expected and well reported (Jia et al. 2014; Pääkkö et al. 2007; Shafiei-Sabet et al. 2012). Among the different dilutions, a very alike trend is observed. The storage modulus is highest at 100 wt% *H-MFC*, but also as high or only slightly reduced at increased *pulp* shares along and close to the 0 wt% *MFC* line. Furthermore, it increases monotonically from *MFC* to *H-MFC*. The loss modulus G''_{lin} follows the same trends (data not shown) and was lower by about one order of magnitude for all conditions. An increase of G'_{\max} with an increasing DoF is expected and is reported frequently (Moberg and Rigdahl 2012; Shafiei-Sabet et al. 2016; Taheri and Samyn 2016), so the trends seen for *MFC* to *H-MFC* are expected as well. Yet, there is also work showing different trends, e.g. Shogren et al. (2011) found a maximum of moduli (and viscosity) in dependence of the amount of homogeniser passes for a corn cob based cellulose gel, or work by Saarinen et al. (2009) showed a constant decrease of G' with increasing number of passes through a fluidiser. Nechyporchuk et al. (2016b) discussed these discrepancies recently with a view on the used measurement geometries and procedures and related the opposing trends to potential measurement artefacts and pre-treatment protocols. The measurement system and procedures used in this work are in line with the recommendations to obtain reliable data given by the cited authors. The present data indicate that coarse residual fibres can have a significant influence on the storage modulus of an *MFC* suspension by providing a high modulus that is also observed for highly fibrillated *MFCs*. This previously unreported finding may be useful to consider when comparing *MFC* suspensions that are manufactured with different processes, as they may lead to different polydispersities and/or residual fibre contents.

The storage modulus is a measure that describes a system's ability to store elastic energy, and its increase with an increasing DoF is typically reasoned to be caused by a stronger, more homogeneous network due to the reduced fibril size (Moberg and Rigdahl 2012; Shafiei-Sabet et al. 2016). So, the observed modulus increasing effect of the *pulp* fibres is somewhat contradictory, as a more open, less connected network is present. A potential

explanation may be found by considering the flexibility of the network elements, and not only the inter-fibril distances. If it is assumed that thicker fibres are more rigid compared to finer fibrils (as bending stiffness scales with the feature dimensions), then it may well be that they also can contribute strongly to the overall observed storage modulus.

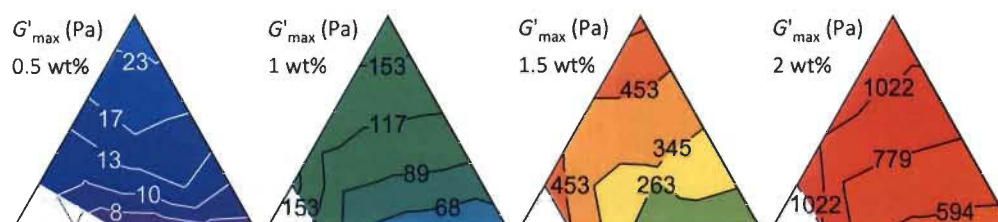


Figure 9.3: Storage modulus (G'_{\max}) data presented in ternary mixture contour plots for the different total solids contents of the mixtures, standard deviation was typically $\leq 10\%$. High storage modulus values are apparent for the left and top corner regions, representing high pulp and H-MFC shares respectively. Increasing MFC shares at the expense of H-MFC and pulp (moving toward right corner) reduces the storage modulus. A comprehensive instruction on how to interpret the ternary diagrams can be found in the supplementary information.

9.7.4 Influence of DoF on yielding behaviour

With increasing strain amplitude, γ , the suspensions start to yield and their behaviour begins to be determined as well by the ability of their interacting network to deform plastically (viscous dissipation). This transformation is characterised by the force (shear stress) that is needed to initiate it, and at which deformation it happens. In this work, the yield stress, $\tau_{\gamma, \delta}$ and the limit of linearity (LoL), both determined from phase angle data, δ , describe these parameters. From Figure 9.4, it is apparent on the one hand, that the yield stress increases with increasing solids content (as also seen, for example, by Mohtaschemi et al. (2014a)). On the other hand, higher DoF materials lead to increased yield stress, and residual fibres do not have an additional effect. As the yield stress will be strongly determined by the breaking of adhesive contacts and/or overcoming steric hindrances (Nechyporchuk et al. 2016b), the amount of contact points between fibrils/fibres is a determining factor for this property. The present data support this well, as increasing solids content, as well as increasing DoF (and a lower amount of residual fibres), results

in a higher contact point density, and this is also supported by data from other researchers (Moberg and Rigdahl 2012; Taheri and Samyn 2016).

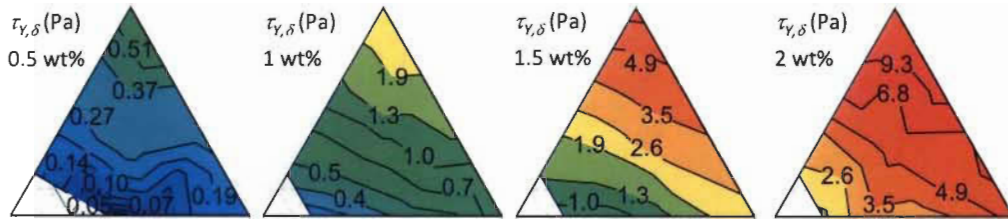


Figure 9.4: Yield stress determined from the amplitude sweep measurements using the phase angle approach ($\tau_{Y,\delta}$), standard deviation was typically $\leq 5\%$. The yield stress increases with increasing DoF, i.e. low values are obtained for increased pulp shares (left corner), intermediate values for high MFC shares (right corner) and high values for high H-MFC shares (top corner). Exchanging shares leads to monotonically changing yield stresses.

The corresponding limit of linearity in the data is presented in Figure 9.5. Especially for solids contents ≥ 1 wt%, it is obvious that the *LoL* is strongly defined by the amount of residual fibres. The 0.5 wt% data show the same general trend, yet there is somewhat more variation. Furthermore, the *LoL* generally decreases with an increasing solids content, similarly to that shown in work by Jia et al. (2014). As reasoned in an earlier work (Schenker et al. 2017), this trend can be explained by a stiffening of the network with increasing solids content due to the reduction of the distance between the connection points. Using the same reasoning, residual fibres would have an opposite effect, as less connection points are present. Yet, the present data show the opposite. So, it seems more likely that the number of coarse fibres per unit component solids content is less than the fine fibres they accompany, and the additional rigidity of the coarse fibres is reducing static entanglement. Coarse fibre involvement in flocculation, due to the lower charge density compared with fines, if present, therefore, is too weak to generate a strong elastic structure at high deformation.

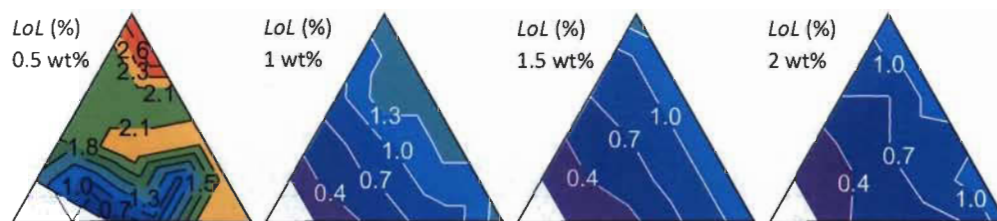


Figure 9.5: Limit of linearity (*LoL*) data. For solids contents ≥ 1 wt%, the *LoL* is decreasing with an increasing pulp content, apparent as the contour lines are parallel to the 0 wt% pulp line (right triangle side). As the *LoL* was obtained from averaged amplitude sweep rheograms, no standard deviation can be calculated.

To investigate the suspension behaviour further beyond the yield region, the constant shear experiments (flow curves) are now examined. It should be mentioned at this point, that viscosity measurements at low shear rates are very likely to be dominated by side effects. On the one hand, there is evidence for depletion near the measurement geometry boundary, leading to a water (-rich) layer (Kumar et al. 2016; Lauri et al. 2017) when smooth surfaces are used, and on the other hand, especially for larger gap settings, shear banding is likely to occur (Kumar et al. 2016; Mohtaschemi et al. 2014b). The use of serrated and/or rough surfaces or vane geometries (as in this work) are typically employed to prevent or reduce the solid depletion effects, commonly also referred to as apparent slip (Buscall 2010; Mohtaschemi et al. 2014b; Schenker et al. 2017). However, the shear banding cannot be prevented under uniform planar or axial flow, unless the measurement gap would be very small. But a small gap may lead to even more severe side effects for a heterogeneous suspension like MFC (Barnes 2000). When a critical shear stress and/or shear rate is overcome, however, the banding disappears, and so the interpretation of the results without an according correction is less critical (Martoia et al. 2015; Mohtaschemi et al. 2014b; Servais et al. 2003). This critical shear rate or stress is very likely depending on the MFC suspension properties, but is also likely to be in zone 1 and close to the transition region for the data presented in this work (Martoia et al. 2015; Mohtaschemi et al. 2014b; Servais et al. 2003). As we did not apply a correction to account for the shear banding, our zone 1 data have to be understood as apparent data only, yet the relative

trends are likely not to be influenced by omitting to make correction(s) (Mohtaschemi et al. 2014a).

Comparing the apparent low shear viscosity data ($\eta_{0.02}$) shown in Figure 9.6 with the storage modulus data (Figure 9.3) reveals striking similarities, i.e. the general increase with solids content, as well as the trend for increased values at increased *H-MFC* and *pulp* shares. Even though an evaluation of the shear thinning power law behaviour may be critical with shear banding being likely, it may be worth mentioning that the flow index n_1 was basically independent of solids content and composition, fluctuating around a value of 0.13 (data not shown). If one includes the assumption of Karppinen et al. (2012), that the reforming of new contacts within the network was fast enough to compensate the breaking induced by the shear in this region of the flow curve, one may hypothesise that the viscosity in zone 1 is determined by the network-induced elastic and viscous moduli. This could explain the likeness between the apparent low shear viscosity data with the moduli data, which is often the case in complex suspensions, yet remains purely speculative.

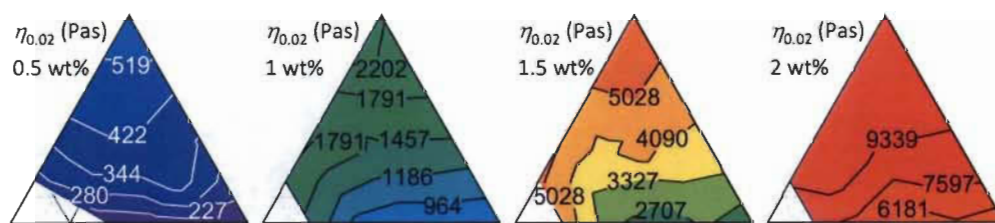


Figure 9.6: Apparent low shear viscosity ($\eta_{0.02}$) data, standard deviation was typically $\leq 10\%$. The trends resemble the ones described for the storage modulus data in Figure 9.3, i.e. the highest values are present at either high pulp (left corner) or high *H-MFC* shares (top corner).

9.7.5 Influence of DoF on aggregation behaviour

When increasing the shear rate further beyond a certain point it is hypothesised that the here-used MFC suspensions start to segregate into fibril rich-regions (aggregates or strong flocs) and water rich voids between them, as described in earlier work (Schenker et al. 2018; Schenker et al. 2017) and based on findings of, for example, Karppinen et al. (2012) and Martoia et al. (2015). This transition region is defined here by the end of zone 1 (onset of aggregation), the position of the local (viscosity) minimum, where the aggregation is

believed to be maximal, and the start of zone 2, where a homogeneous structure is reinstalled/resumed. Figure 9.7 shows the data for the position of the local minimum and are exemplary for the end of zone 1 as well as the start of zone 2 data, as these properties follow the same general trend. It is apparent that the position of the local minimum is shifted to higher shear rates for an increased *pulp* fibre share. The data may also indicate that the shift to higher shear rates is more pronounced for a combination of *pulp* and *H-MFC* shares. Yet, the distance from one to the next contour plot value is just one shear rate point measurement, and typically the data variation within a triplicate is ± 1 measurement point for this type of data. So, the significance between two neighbouring values may not be a given in every case. Therefore, this discussion should be considered from a more generalised point of view. Namely, the end of zone 1 (not shown), the position of the local minimum and the start of zone 2 (not shown), becomes shifted to higher shear rates, and the overall span of the transition is increased (not shown) for increased *pulp* shares. This behaviour appears to be stronger at increased solids content, though more so only when sufficient *pulp* fibres are present in the mixture. It may be hypothesised, that the coarse *pulp* fibres and/or a sufficiently high polydispersity generally hinder a structural reorganisation.

As described earlier, the relative transition zone depth (Δ_{\min}) additionally characterises the degree of aggregation (Schenker et al. 2017). However, no conclusive trends with regards to the DoF were found here, yet, nonetheless, the previously found trend of increasing relative transition zone depth with decreasing solids content (Schenker et al. 2017) was reproduced (data not shown).

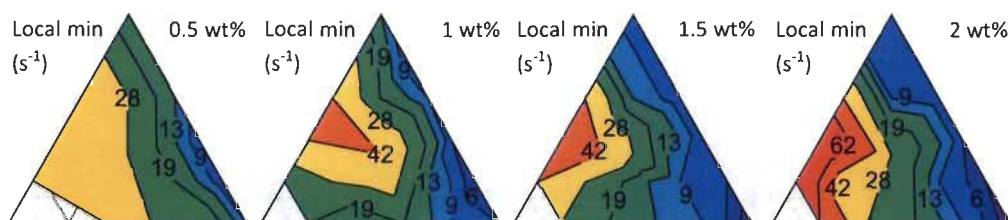


Figure 9.7: Position of the local minimum data. Generally, the position of the local minimum is at lower shear rates for low pulp contents (right triangle side) and increases with an increasing pulp share (moving towards the left corner). The contour lines represent actually probed shear rate values (measurement points). As the data are discrete, no standard deviation can be provided, however, a typical variation observed was ± 1 measurement point.

When a complete shear rate loop (shear rate increase ramp followed by shear rate decrease ramp) is performed, a difference between the two viscosities at a given shear rate can be seen (Figure 9.1). This hysteresis was observed before and generally a difference in the suspended material morphology, caused by the respective shear history, is held responsible (Iotti et al. 2011; Martoia et al. 2015). A recent publication by Schenker et al. (2018) discussed the potential origin of different hysteresis behaviours observed in the literature, and introduced a novel quantification approach that is applied also now in this present work. In short, two different types of hysteresis are identified: one where the viscosity of the shear rate increasing ramp is higher than the viscosity of the shear rate decreasing ramp, called positive hysteresis, and the other one, the negative hysteresis, where it is vice versa. The positive hysteresis (H_{RS+}) is attributed to the difference between the initial, homogeneous structure and the moderately aggregated structure after a full shear rate loop (Martoia et al. 2015; Schenker et al. 2018). The negative hysteresis (H_{RS-}) appears to be mainly dominated by the viscosity drop under the level of the shear rate increasing ramp at the transition zone, and therefore related to the degree and span of aggregation during this flow curve.

Figure 9.8 shows the results for the positive hysteresis. Please note that the data of the 0.5 wt% suspensions (and some points of the 1 and 1.5 wt% suspensions) are not shown, because those suspensions typically showed sedimentation, starting shortly after the shear

rate decrease ramp started. It is apparent that the positive hysteresis is independent of the solids content for all mixture ratios, confirming earlier findings (Schenker et al. 2018). Furthermore, there is a clear trend of higher positive hysteresis values for increased *pulp* shares. Following the above described reasoning, this may indicate a larger difference in suspension morphology between the unsheared and the pre-sheared (through the shear rate loop) state, induced by coarse fibres. It may be hypothesised again, that the coarser fibres may hinder structural rearrangements due to their stiffness compared to finer fibrils. The addition of visualisation, or other structure revealing techniques to such flow curve measurements would be of high value and could test this hypothesis. The negative hysteresis generally increases with a decreasing solids content (data not shown), that was also observed previously and attributed to a higher amount of available free water at decreased solids content (Schenker et al. 2018). Trends with the DoF are not very apparent, but a general reduction of the negative hysteresis with high *pulp* share is likely, as well as that the highest values are typically found at a combination of 20 to 40 % *pulp* with low to no *MFC* share. These general trends are somewhat unexpected, yet may be explained again by the stiffness of coarse fibres hindering a dense aggregate formation, for instance, (Bounoua et al. 2016), and a tendency for rather fine, easily entangling fibrils to aggregate more strongly (Naderi and Lindström 2015; Taheri and Samyn 2016). However, again, without any additional direct or indirect visualisation of the aggregated structure, such models remain hypothetical.

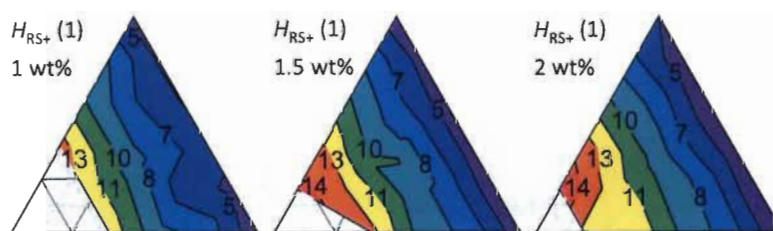


Figure 9.8: Positive hysteresis data, standard deviation was typically $\leq 15\%$. The decrease of the positive hysteresis with a decreasing pulp share is apparent, as the contour lines are parallel to the 0 wt% pulp line (right triangle side).

9.7.6 Influence of component mix on high shear behaviour

When the shear rate is high enough, the aggregated structure that formed in the transition region starts to break down again and the second, power law shear thinning zone starts (Bounoua et al. 2016; Karppinen et al. 2012; Martoia et al. 2015). Here, this zone is described by the apparent high shear viscosity η_{100} , and the respective data can be found in Figure 9.9. The typical increase of viscosity with solids content is clearly apparent, as well as that a higher DoF increases the high shear viscosity. This is in good agreement with the literature, consolidated in a recent review by Nechyporchuk et al. (2016b). It may be worthwhile to recall the different trend that is observed for the low shear viscosity. This difference indicates that the suspension morphologies, defining the apparent viscosities in zone 1 and 2, are different, i.e., the morphology of the sheared suspension material in zone 1 is supported by coarse, presumably stiff, fibres, whereas the morphology at increased shear rates (zone 2) is not affected by such fibres.

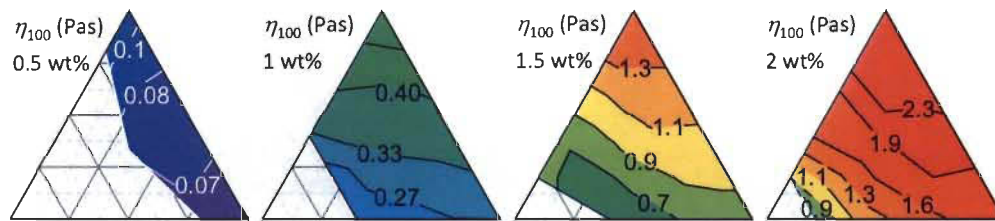


Figure 9.9: High shear viscosity (η_{100}) data, standard deviation was typically $\leq 10\%$. The high shear viscosity generally increases monotonically with the DoF, i.e. it is low towards the left corner (high pulp shares), intermediate towards the right corner (high MFC shares) and high towards the top corner (high H-MFC shares).

Further insight can be obtained by looking at the shear thinning behavior of zone 2, i.e. by looking at the consistency coefficient K_2 and the flow index n_2 . While K_2 basically shows the same trend (not shown) as the apparent high shear viscosity, the flow index appears to change strongly as a function of *pulp* content at low *pulp* contents, following also a function of solids content (Figure 9.10). It should be noted also, that the flow index was the highest at the maximal possible *pulp* content before sedimentation occurred within the flow shear cycle, at each given solids content, and its absolute value was almost the same

(0.64 ± 0.04) under this condition. The increase of shear thinning tendency (decrease of the flow index) with an increasing solids content was reported before for MFC suspensions (Bounoua et al. 2016; Lasseuguette et al. 2008; Schenker et al. 2017), and for pulp suspensions as well (Chaouche and Koch 2001). Bounoua et al. (2016) attributed this effect to the increasing role of attractive interactions at increased solids contents. Likewise, we (Schenker et al. 2017) attributed this effect to the increased importance of entanglements at lower shear rates of zone 2 for increased solids content. Extending those hypotheses may also explain the observed effect of a reduced shear thinning behaviour with an increased *pulp* share. As the coarser fibres lead to less entanglements and/or less attractive interactions (compared to the same mass/volume of fine fibrils), their presence resembles the effect of an increased dilution.

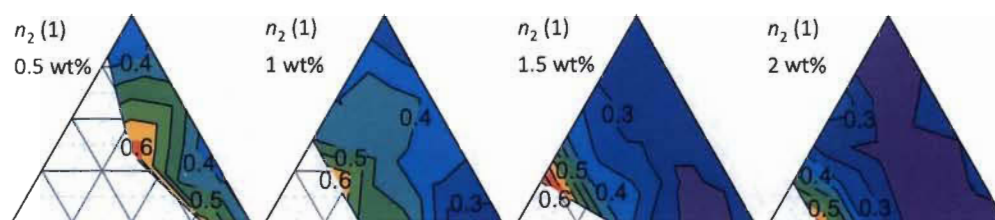


Figure 9.10: Flow index of zone 2 (n_2) data, standard deviation was typically $\leq 13\%$. The general trend of n_2 appears to follow the pulp share, becoming higher (lesser shear thinning tendency) with an increasing pulp share. The maximum value is very similar for all solids content and is found at the maximal pulp share in the mixture.

9.8 Conclusions

The present work investigates the rheological behaviour of suspensions containing MFC suspensions of different *DoFs*, as well as *pulp* fibres that mimic residual, unfibrillated fibres. The results follow the well-known properties of multimodal (and polydisperse) dispersions of particles in general, i.e. interactions at a distance and upon close approach (colloidal) are important flow controlling factors. The exception here is the extra factor that the fibrils are flexible to varying degree and become entangled, whereas round colloidal particles do not.

Given the above conclusion, refinements can be made in the way the flow response of complex shaped solids can be parameterised, including particle properties such as

flexibility and entangled aggregate formation. It appears that the present set of data enable us to split the structure and flow behaviour into three categories with view to the observed trends as a function of the suspension composition. The first category contains the properties that are trending with the fibre/fibril widths (*DoF*) only. The second set of properties is characterised by a discontinuous behaviour, i.e. the coarse *pulp* fibres lead to the same or alike level of property effect as the highly fibrillated *H-MFC*. The third category seems to depend mainly on the *pulp* share.

The behaviour observed in the first category applies for the following properties: yield stress ($\tau_{y,0}$, Figure 9.4), high shear viscosity (η_{100} , Figure 9.9) and the consistency coefficient in zone 2 (K_2 , not shown). In all these properties, the values are increasing with an increasing *DoF*, considering the *pulp* as being equivalent to a low *DoF* component, and are also strongly increasing with the suspension solids content. Such behaviour was described before in the literature. It is typically hypothesised that the increasing amount of fibrils (due to the increased *DoF* and/or the increased solids content) is responsible for the respective property increase. It is reasoned, that the relative movement between fibrils is hindered by the increased amount of physical interactions and entanglements. The present work supports those hypotheses, also for highly polydisperse MFC suspensions.

The second category, where the *pulp* share leads to a discontinuous behaviour includes specific changes in the following parameters: storage modulus (G'_{\max} , Figure 9.3), loss modulus (G''_{lin} , not shown) and the low shear viscosity ($\eta_{0.02}$, Figure 9.6). As mentioned in the results section, the interpretation of the low shear viscosity may be critical, though, because of potentially dominating shear banding. The trend in this category is that the unfibrillated *pulp* fibres and the highly fibrillated *H-MFC* lead to high parameter values. Alike behaviour was reported before (even though not specifically for materials containing residual fibres), yet the observed effects were attributed either to measurement artefacts related to the measurement geometries, or inadequate sample pre-treatment. It seems justifiable to assume that those artefacts were not present in this work, so it appears that this behaviour was not observed before. It is concluded that the *pulp* fibres contribute to the network strength by their stiffness, which is a direct cause of their width, whereas highly fibrillated systems gain their network strength from an increased network density and entanglement.

The properties that mainly depend on the *pulp* share include the limit of linearity (*LoL*, Figure 9.5), the positive hysteresis (H_{RS+} , Figure 9.8) and probably the flow index of zone 2 (n_2 , Figure 9.10). The reduction of the *LoL* with an increasing *pulp* share may be explained by the combined effect of the *pulp* fibres to increase the network stiffness, but also to lead to a smaller network density (less physical interactions). In turn, the lower amount of physical interactions caused by the coarser fibres may also explain the reduced shear thinning tendencies in zone 2 for higher *pulp* shares.

The trends for the aggregation descriptors with the *DoF* are not so clear, yet it appears that the coarse *pulp* fibres also influence the aggregation behaviour in the transition region, probably caused by a reduced mobility of the fibres compared to the finer fibrils. This is at least partially supported by the positive hysteresis data. The addition of rheo-optical measurement techniques to such measurements could be very insightful and probably help to reveal the mechanisms and contributions of the individual components.

In conclusion it can be stated that (residual) coarse fibres can influence the rheological properties of MFC suspensions, not always following trends that are typically observed for changing *DoFs*. We further conclude, that it is not only the increased width that leads to a lower network density (compared to fibrils) causing these differences, but also their increased stiffness and lower mobility. To confirm this conclusion, rheo-optical investigations could be envisaged. Additionally, the impact of a polydisperse system with improved packing and smoother transitions plays a distinct role. From an application point of view, this work also has shown that it is possible to obtain MFC suspensions with specific sets of rheological properties by combining different *DoF* MFCs and pulp fibres, potentially opening up an even wider application space.

As shown by other researchers, and summarized for instance by Nechyporchuk et al. (2016b), there seem to be two different types of fibrillated cellulose types with view on their rheological behaviour and respective suspension morphology under flow. The primary difference between the two types is the surface charge, being typically low for unmodified grades and high for chemically modified grades. The latter grades typically are relatively stable colloidal suspensions due to the increased electrostatic repulsion. As this repulsion alters e.g. the frictional interactions between the fibrils, the here-presented

findings cannot be transferred ad hoc to modified fibrillated cellulose grades. Additional experimental work would be needed to check the transferability.

9.8.1 Acknowledgements

Omya International AG and FiberLean Technologies Ltd. are acknowledged for their financial and in-kind support of this work. Dr. Johannes Kritzing (FiberLean Technologies Ltd.) is thanked for his valuable inputs on image analysis and data presentation as well as Silvan Fischer (Omya International AG) for the microscopical imaging work. We would like to also acknowledge Dr. Antti Puisto for helpful discussions.

9.9 References

- Agoda-Tandjawa G, Durand S, Berot S, Blassel C, Gaillard C, Garnier C, Doublier J.L. (2010) Rheological characterization of microfibrillated cellulose suspensions after freezing. *Carbohydrate Polymers* 80:677-686. doi:10.1016/j.carbpol.2009.11.045
- Barnes HA (2000) Measuring the viscosity of large-particle (and flocculated) suspensions - a note on the necessary gap size of rotational viscometers. *Journal of Non-Newtonian Fluid Mechanics* 94:213-217. doi:10.1016/S0377-0257(00)00162-2
- Besbes I, Alila S, Boufi S (2011) Nanofibrillated cellulose from TEMPO-oxidized eucalyptus fibres: Effect of the carboxyl content. *Carbohydrate Polymers* 84:975-983. doi:10.1016/j.carbpol.2010.12.052
- Bounoua S, Lemaire E, Férec J, Ausias G, Kuzhir P (2016) Shear-thinning in concentrated rigid fiber suspensions: Aggregation induced by adhesive interactions. *Journal of Rheology* 60:1279-1300. doi:10.1122/1.4965431
- Buscall R (2010) Letter to the Editor: Wall slip in dispersion rheometry. *Journal of Rheology* 54:1177-1183. doi:10.1122/1.3495981
- Chaouche M, Koch DL (2001) Rheology of non-Brownian fibres with adhesive contacts. *Journal of Rheology* 42:369-382. doi:10.1122/1.1343876
- Cloitre M, Bonnecaze RT (2017) A review on wall slip in high solid dispersions. *Rheologica Acta* 56:283-305. doi:10.1007/s00397-017-1002-7

- Colson J, Bauer W, Mayr M, Fischer W, Gindl-Altmutter W (2016) Morphology and rheology of cellulose nanofibrils derived from mixtures of pulp fibres and papermaking fines. *Cellulose* 23:2439-2448. doi:10.1007/s10570-016-0987-x
- Haavisto S, Salmela J, Jäsberg A, Saarinen T, Karppinen A, Koponen A (2015) Rheological characterization of microfibrillated cellulose suspension using optical coherence tomography. *Tappi Journal* 14:291-302.
- Herrick FW, Casebier RL, Hamilton JK, Sandberg KR (1983) Microfibrillated cellulose: morphology and accessibility. *Journal of Applied Polymer Science* 37:797-813.
- Hubbe MA, Tayeb P, Joyce M, Tyagi P, Kehoe M, Dimic-Misic K, Pal L (2017) Rheology of Nanocellulose-rich Aqueous Suspensions: A Review. *BioResources* 12:9556-9661.
- Iotti M, Gregersen OW, Moe S, Lenes M (2011) Rheological Studies of Microfibrillar Cellulose Water Dispersions. *Journal of Polymers and the Environment* 19:137-145. doi:10.1007/s10924-010-0248-2
- Jia X et al. (2014) Rheological properties of an amorphous cellulose suspension. *Food Hydrocolloids* 39:27-33. doi:10.1016/j.foodhyd.2013.12.026
- Kangas H, Lahtinen P, Sneek A, Saariaho AM, Laitinen O, Hellén E (2014) Characterization of fibrillated celluloses. A short review and evaluation of characteristics with a combination of methods. *Nordic Pulp and Paper Research Journal* 29:129-143. doi:10.3183/NPPRJ-2014-29-01-p129-143
- Karppinen A, Saarinen T, Salmela J, Laukkanen A, Nuopponen M, Seppälä J (2012) Flocculation of microfibrillated cellulose in shear flow. *Cellulose* 19:1807-1819. doi:10.1007/s10570-012-9766-5
- Kataja M, Haavisto S, Salmela J, Lehto R, Koponen A (2017) Characterization of microfibrillated cellulose fiber suspension flow using multi scale velocity profile measurements. *Nordic Pulp & Paper Research Journal* 32:473-482. doi:10.3183/NPPRJ-2017-32-03-p473-482
- Korhonen M, Mohtaschemi M, Puisto A, Illa X, Alava MJ (2017) Start-up inertia as an origin for heterogeneous flow. *Physical Review E* 95:022608. doi:10.1103/PhysRevE.95.022608

- Kumar V, Nazari B, Bousfield D, Toivakka M (2016) Rheology of Microfibrillated Cellulose Suspensions in Pressure-Driven Flow. *Applied Rheology* 26:43534. doi:10.3933/ApplRheol-26-43534
- Lasseuguette E, Roux D, Nishiyama Y (2008) Rheological properties of microfibrillar suspension of TEMPO-oxidized pulp. *Cellulose* 15:425-433. doi:10.1007/s10570-007-9184-2
- Lauri J, Koponen A, Haavisto S, Czajkowski J, Fabritius T (2017) Analysis of rheology and wall depletion of microfibrillated cellulose suspension using optical coherence tomography. *Cellulose* 24:4715-4728. doi:10.1007/s10570-017-1493-5
- Martoia F, Perge C, Dumont PJJ, Orgéas L, Fardin MA, Manneville S, Belgacem MN (2015) Heterogeneous flow kinematics of cellulose nanofibril suspensions under shear. *Soft Matter* 11:4742-4755. doi:10.1039/c5sm00530b
- Missoum K, Belgacem MN, Bras J (2013) Nanofibrillated Cellulose Surface Modification: A Review. *Materials* 6:1745-1766. doi:10.3390/ma6051745
- Moberg T, Rigdahl M (2012) On the Viscoelastic Properties of Microfibrillated Cellulose (MFC) Suspension. *Annual Transactions of the Nordic Rheology Society* 20:123-130.
- Moberg T et al. (2017) Rheological properties of nanocellulose suspensions: effects of fibril/particle dimensions and surface characteristics. *Cellulose* 24:2499-2510. doi:10.1007/s10570-017-1283-0
- Mohtaschemi M, Dimic-Misic K, Puisto A, Korhonen M, Maloney T, Paltakari J, Alava MJ (2014a) Rheological characterization of fibrillated cellulose suspensions via bucket vane viscosimeter. *Cellulose* 21:1305-1312. doi:10.1007/s10570-014-0235-1
- Mohtaschemi M, Sorvari A, Puisto A, Nuopponen M, Seppälä J, Alava MJ (2014b) The vane method and kinetic modeling: shear rheology of nanofibrillated cellulose suspensions. *Cellulose* 21:3913-3925. doi:10.1007/s10570-014-0409-x
- Naderi A, Lindström T (2015) Rheological Measurements on Nanofibrillated Cellulose Systems: A Science in Progress. In: Mondal MIH (ed) *Cellulose and Cellulose Derivatives*. Nova Science Publishers, Inc., pp 187-202

- Nazari N, Kumar V, Bousfield DW, Toivakka M (2016) Rheology of cellulose nanofibers suspensions: Boundary driven flow. *Journal of Rheology* 60:1151-1159. doi:10.1122/1.4960336
- Nechyporchuk O, Belgacem MN, Bras J (2016a) Production of cellulose nanofibrils: A review of recent advances. *Industrial Crops and Products* 93:2-25. doi:10.1016/j.indcrop.2016.02.016
- Nechyporchuk O, Belgacem MN, Pignon F (2014) Rheological properties of micro-/nanofibrillated cellulose suspensions: Wall-slip and shear banding phenomena. *Carbohydrate Polymers* 112:432-439. doi:10.1016/j.carbpol.2014.05.092
- Nechyporchuk O, Belgacem MN, Pignon F (2015) Concentration effect of TEMPO-oxidized nanofibrillated cellulose aqueous suspensions on the flow instabilities and small-angle X-ray scattering structural characterization. *Cellulose* 22:2197-2210. doi:10.1007/s10570-015-0640-0
- Nechyporchuk O, Belgacem MN, Pignon F (2016b) Current progress in Rheology of Cellulose Nanofibril Suspensions. *Biomacromolecules* 17:2311-2320. doi:10.1021/acs.biomac.6b00668
- Onyianta AJ, Williams R (2018) The Use of Sedimentation for the Estimation of Aspect Ratios of Charged Cellulose Nanofibrils. In: Fangueiro R, Rana S (eds) *Advances in Natural Fibre Composites*. Springer, Cham, pp 195-203. doi:10.1007/978-3-319-64641-1_17
- Orts WJ, Godbout L, Marchessault RH, Revol J-F (1998) Enhanced Ordering of Liquid Crystalline Suspensions of Cellulose Microfibrils: A Small Angle Neutron Scattering Study. *Macromolecules* 31:5717-5725. doi:10.1021/ma9711452
- Pääkkö M et al. (2007) Enzymatic Hydrolysis Combined with Mechanical Shearing and High-Pressure Homogenization for Nanoscale Cellulose Fibrils and Strong Gels. *Biomacromolecules* 8:1934-1941. doi:10.1021/bm061215p
- Puisto A, Mohtaschemi M, Alava MJ (2015) Dynamic hysteresis in the rheology of complex fluids. *Physical Review E* 91:042314. doi:10.1103/PhysRevE.91.042314
- Pyrgiotakis G et al. (2018) Development of high throughput, high precision synthesis platforms and characterization methodologies for toxicological studies of nanocellulose. *Cellulose* 25:2303-2319. doi:10.1007/s10570-018-1718-2

- Saarikoski E, Saarinen T, Salmela J, Seppälä J (2012) Flocculated flow of microfibrillated cellulose water suspensions: an imaging approach for characterisation of rheological behaviour. *Cellulose* 19:647-659. doi:10.1007/s10570-012-9661-0
- Saarinen T, Lille M, Seppälä J (2009) Technical Aspects on Rheological Characterization of Microfibrillar Cellulose Water Suspensions. *Annual Transaction of the Nordic Rheology Society* 17:121-128.
- Schenker M, Schoelkopf J, Mangin P, Gane P (2016a) Rheological investigation of complex micro and nanofibrillated cellulose (MNFC) suspensions: Discussion of flow curves and gel stability. *Tappi Journal* 15:405-416.
- Schenker M, Schoelkopf J, Mangin P, Gane P (2016b) Rheological investigation of pigmented micro-nano-fibrillated cellulose (MNFC) suspensions: Discussion of flow curves. *Tappi International Conference on Nanotechnology for Renewable Materials, Grenoble*
- Schenker M, Schoelkopf J, Mangin P, Gane P (2018) Quantification of flow curve hysteresis data – a novel tool for characterising microfibrillated cellulose (MFC) suspensions. *Applied Rheology* 28:22945. doi:10.3933/ApplRheol-28-22945
- Schenker M, Schoelkopf J, Mangin P, Gane PAC (2017) Influence of shear rheometer measurement system selection on rheological properties of microfibrillated cellulose (MFC) suspensions. *Cellulose* 25:961-976. doi:10.1007/s10570-017-1642-x
- Servais C, Ranc H, Sansonnens C, Ravji S, Romoscanu A, Burbidge A. Rheological methods for multiphase materials. In: *International Symposium on Food Rheology and Structure, Zürich, 2003*.
- Shafiei-Sabet S, Hamad WY, Hatzikiriakos G (2012) Rheology of Nanocrystalline Cellulose Aqueous Suspensions. *Langmuir* 28:17124-17133. doi:10.1021/la303380v
- Shafiei-Sabet S, Martinez M, Olson J (2016) Shear rheology of micro-fibrillar cellulose aqueous suspensions. *Cellulose* 23:2943-2953. doi:10.1007/s10570-016-1040-9
- Shogren RL, Peterson SC, Evans KO, Kenar JA (2011) Preparation and characterization of cellulose gels from corn cobs. *Carbohydrate Polymer* 86:1351-1357. doi:10.1016/j.carbpol.2011.06.035

- Stenstad P, Andresen M, Steiner TB, Stenius P (2008) Chemical surface modifications of microfibrillated cellulose. *Cellulose* 15:35-45. doi:10.1007/s10570-007-9143-y
- Taheri H, Samyn P (2016) Effect of homogenization (microfluidization) process parameters in mechanical production of micro- and nanofibrillated cellulose on its rheological and morphological properties. *Cellulose* 23:1221-1238. doi:10.1007/s10570-016-0866-5
- Veen SJ, Versluis P, Kuijk A, Velikov KP (2015) Microstructure and rheology of microfibril-polymer networks. *Soft Matter* 11:8907-8912. doi:10.1039/C5SM02086G
- Yoshimura A, Prud'homme RK (1988) Wall slip corrections for Couette and parallel disk viscometers. *Journal of Rheology* 32:53-67. doi:10.1122/1.549963

9.10 Supplementary information

9.10.1 Width distribution analysis

As mentioned in the main article, the image analysis approach we employed was apparently not successful in capturing the actual fibril width distribution, especially for the *MFC* material, due to inconsistencies in dispersion.

9.10.1.1 Method

The sample preparation method described by (Pyrgiotakis et al. 2018) was used as a basis. However, the MFC deposition was slightly altered as described method failed to produce micrographs that were suitable for SEM image analysis. Instead of depositing a drop of MFC suspension on the poly-L-lysine treated mica substrate for a certain time, we immersed the treated mica platelet in the stirred MFC suspension for one minute. The intention was to reduce the aggregation tendency of the fibrils in the highly diluted MFC suspension. The rinsed and dried platelets were mounted on sample holders and sputtered with gold before being imaged with SEM (Sigma VP, Zeiss, Switzerland). Images of the pulp suspensions were taken with an optical microscope (Axio Imager.M2 m, Zeiss, Switzerland) of a 0.1 wt% suspension that was kept between two microscopy glass slides. ImageJ (NIH) software was used to measure the fibril widths. At least 200 fibres or fibrils were measured, each at three locations along the length, whereas the respective average

value per fibre was used for the distribution generation. Origin 2017 software was used to calculate the median as well as the modulus of the distribution curves.

9.10.1.2 Results

The fibre and fibril width distributions obtained from the image analysis are presented in Figure 9.11. The trends of the distributions appear to make sense at first, i.e. distributions are shifted to smaller dimensions with increasing processing intensity and the distribution of the *MFC* material (b) is broader and has some residual coarser fibrils compared to the *H-MFC* (c) material. However, when compared to the optical and SEM images taken of the suspensions, respectively freeze-dried materials (Figure 9.2 of the main article), it is apparent that, for example, the coarse fraction (residual fibres in the range of 10s of μm or partially fibrillated fibres in the range of several μm) of the *MFC* material was not captured in the image analysis. Due to this very apparent discrepancy, the here presented width distribution data were not used in this work.

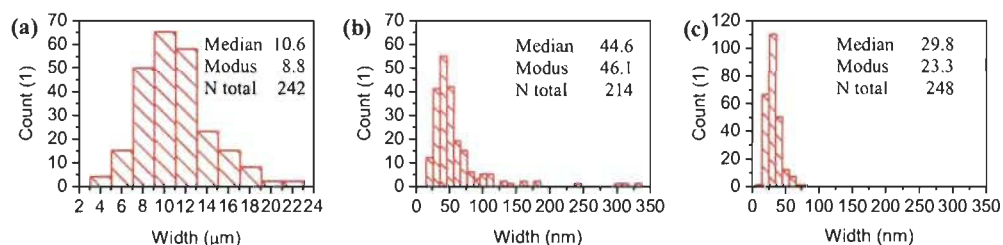


Figure 9.11: Fibre/fibril width histograms of pulp (a), MFC (b) and H-MFC (c), including the distribution median and mode values (units are the same as the respective x-axis).

9.10.2 Ternary diagrams

9.10.2.1 Ternary mixture matrix

Figure 9.12 shows a ternary diagram including all mixture ratios that were intended to be manufactured and characterised. The blue circle points were intended to be produced for all solids contents (0.5, 1, 1.5 and 2 wt%) and the red triangular points were additionally realised at 1.5 wt%. Please note that finally not all mixture ratios were characterised (completely) because of apparent sedimentation prior to, or during the rheological measurements.

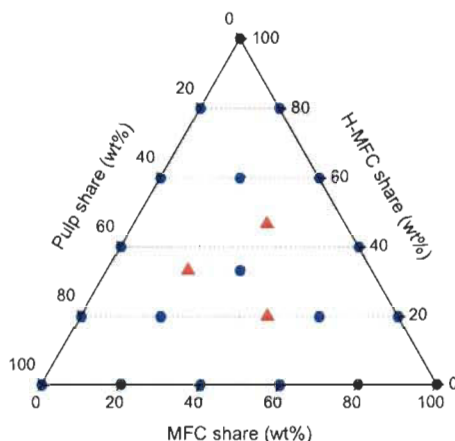


Figure 9.12: Ternary mixture diagram including investigated mixture ratios at all solids contents (blue circles) and additional ratios at 1.5 wt% (red triangles).

9.10.2.2 Introduction to ternary diagrams

In this work, we use ternary diagrams to present the rheological data in dependence of the suspension composition (Figure 9.13). The suspension can be composed of one, two or all three materials (pulp, MFC and H-MFC), whereas all components sum up to 100 % based on the solids content (that is 0.5, 1, 1.5 and 2 wt%). Each material share is displayed on one of the triangle's sides with an increasing share in counter-clockwise direction. The specific share of one component can be read out by following a parallel line of this component's 0 wt% line (indicated with the arrows in Figure 9.13, left image). A more general and simplified interpretation of the diagram is presented in the right image of Figure 9.13. The share of a component increases towards its 100 wt% vertex when moving along the perpendicular bisector of that vertex starting from the opposing triangle side.

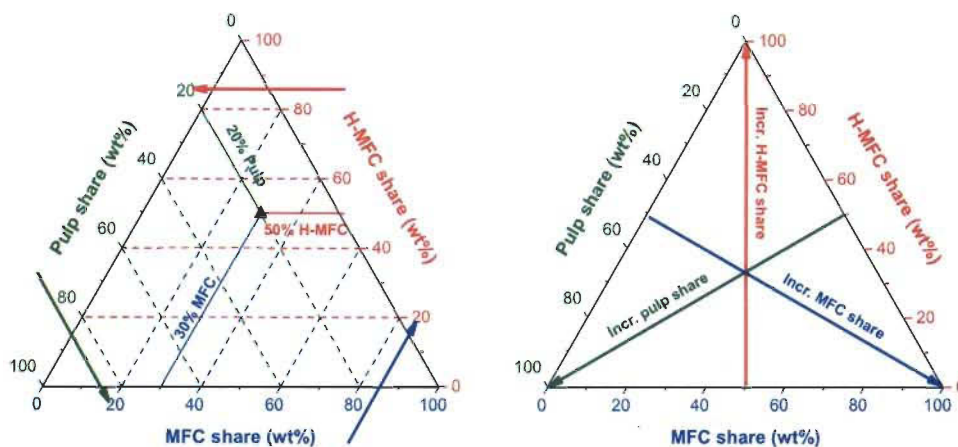


Figure 9.13: Visual guide for reading out the composition from a ternary mixture diagram (left) and a visual guide for a simplified, general read out of the composition trends (right).

The values of the investigated rheological properties are displayed in the ternary diagram by using contour colourmaps. Example diagrams containing generic data are shown in Figure 9.14. In this work, a rainbow spectrum colourmap is used to visualise the values of a property, ranging from purple for low values to red for high values. Such colourmaps allow a relatively fast read-out of general trends. For example, the left image of Figure 9.14 indicates that the property is solely depending on the *pulp* share and that it is decreasing with an increasing *pulp* share. The right image of Figure 9.14 on the other hand shows, that the property is depending on all three components whereas *pulp* leads to low, *MFC* to intermediate and *H-MFC* to high values.

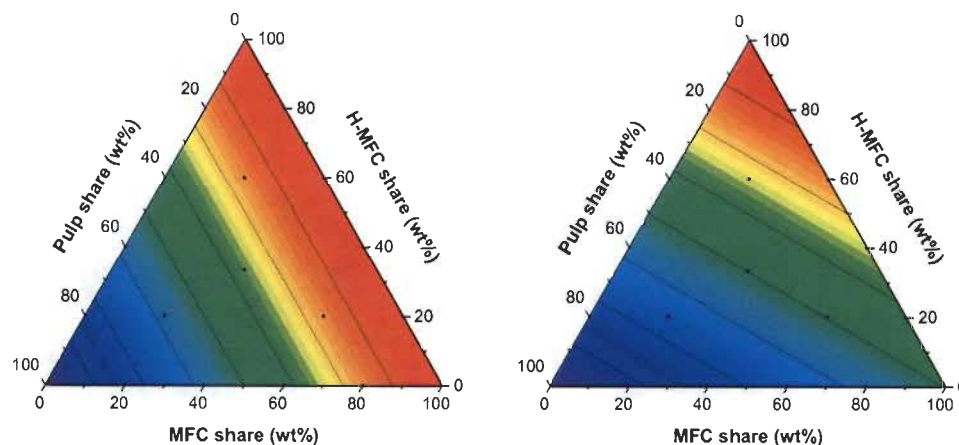


Figure 9.14: Example of colourmap contour ternary diagrams. The colour scale goes from low values (purple) to high values (red) following a rainbow spectrum. The left image shows a situation where the property is depending only on the pulp share, leading to low values. The right image shows a situation where a property is depending on all three components, where pulp leads to low, MFC to intermediate and H-MFC to highest values.

9.10.2.3 Alternative data representation

In the main article, the data of one property shares the same scale for all different solids contents, for better visualisation and more compact presentation. In this section, the same data are presented in a more detailed form, i.e. each diagram of a specific solids content within one rheological property has its own scale. Each of the following figures (Figure 9.15 to Figure 9.22) contains the data of one rheological property described in the main article, divided into the four solids contents (0.5 wt% top left, 1 wt% top right, 1.5 wt% bottom left and 2 wt% bottom right).

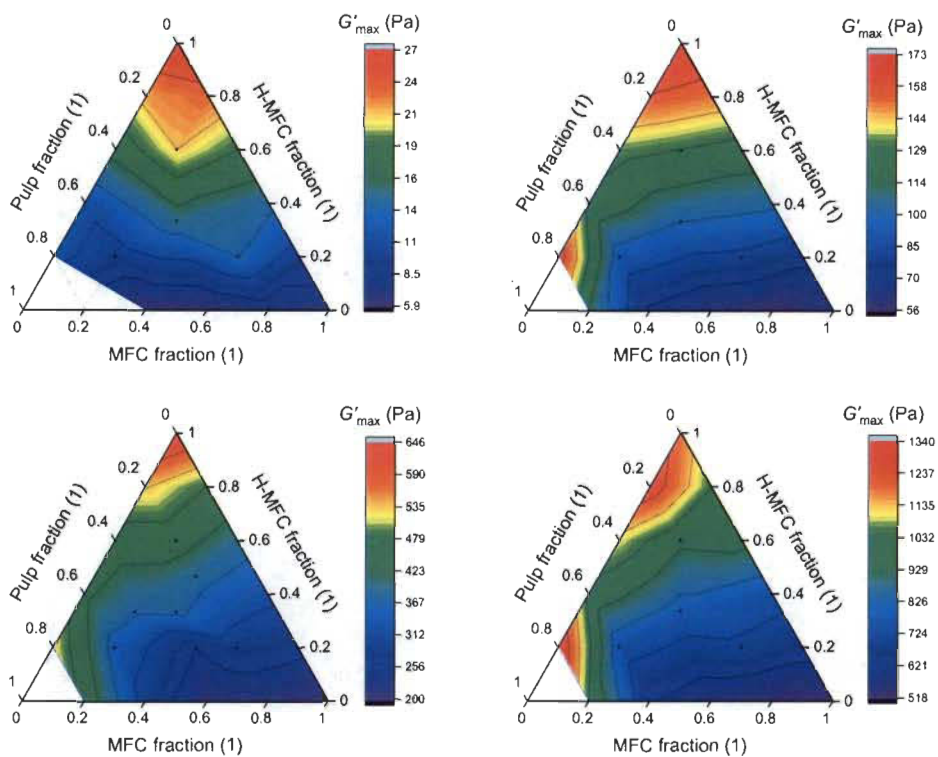


Figure 9.15: G'_{\max} data with individual scale bars for the single dilutions, 0.5 wt% (top left), 1 wt% (top right), 1.5 wt% (bottom left) and 2 wt% (bottom right). The scales are linear.

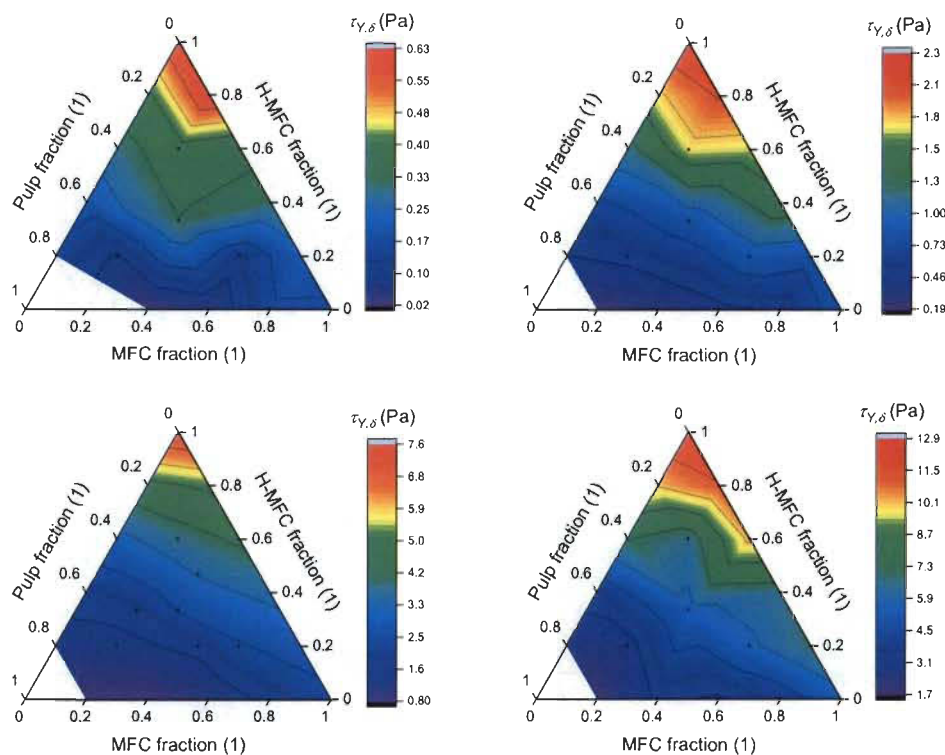


Figure 9.16: $\tau_{Y,\delta}$ data with individual scale bars for the single dilutions, 0.5 wt% (top left), 1 wt% (top right), 1.5 wt% (bottom left) and 2 wt% (bottom right). The scales are linear.

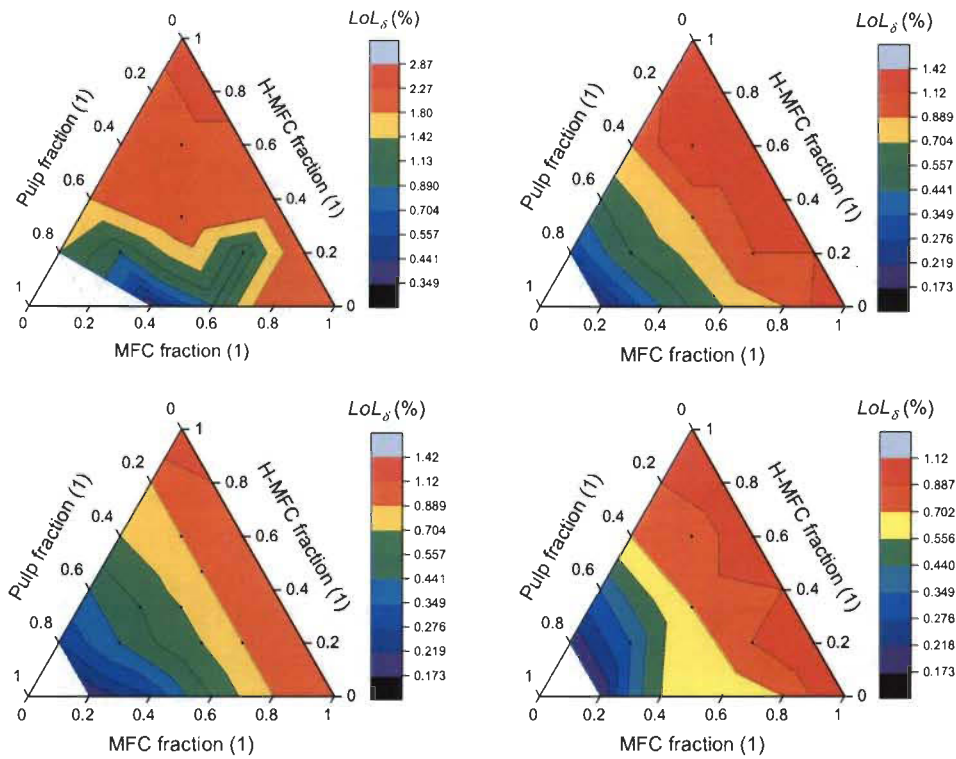


Figure 9.17: LoL data with individual scale bars for the single dilutions, 0.5 wt% (top left), 1 wt% (top right), 1.5 wt% (bottom left) and 2 wt% (bottom right). The scales are logarithmic and the values represent the actually set deformations.

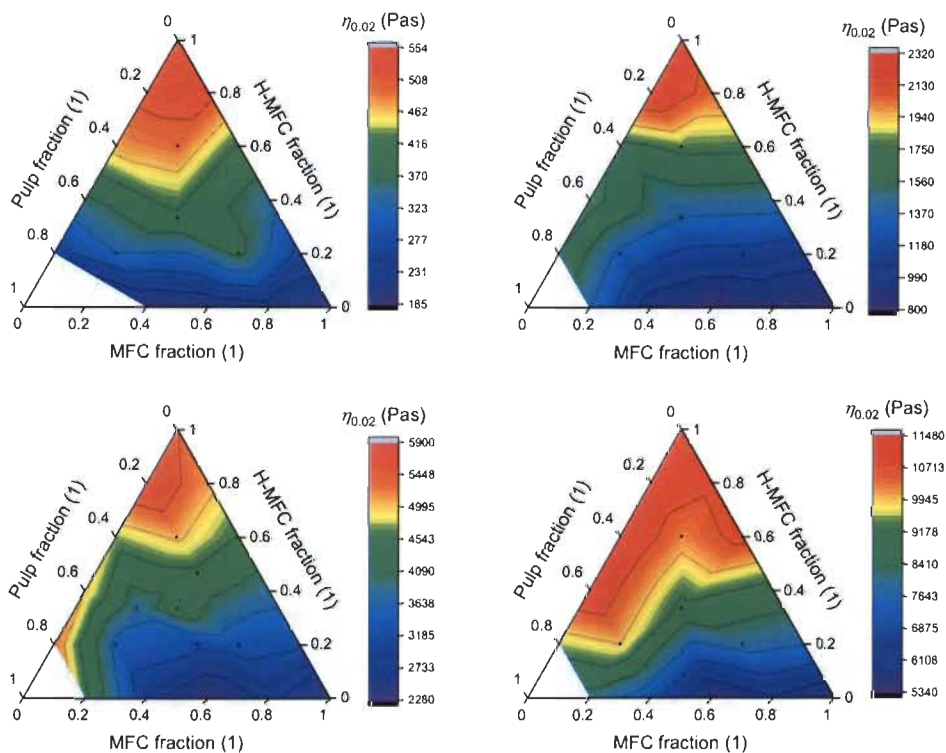


Figure 9.18: $\eta_{0.02}$ data with individual scale bars for the single dilutions, 0.5 wt% (top left), 1 wt% (top right), 1.5 wt% (bottom left) and 2 wt% (bottom right). The scales are linear.

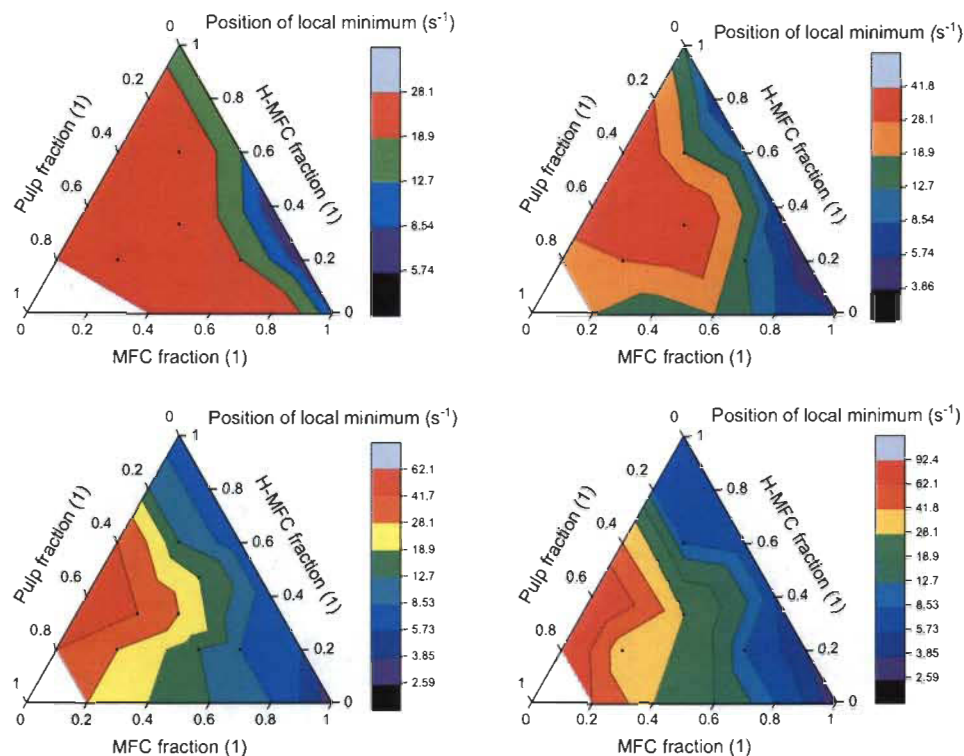


Figure 9.19: Position of the local minimum data with individual scale bars for the single dilutions, 0.5 wt% (top left), 1 wt% (top right), 1.5 wt% (bottom left) and 2 wt% (bottom right). The scales are logarithmic and the values represent the actually set shear rates.

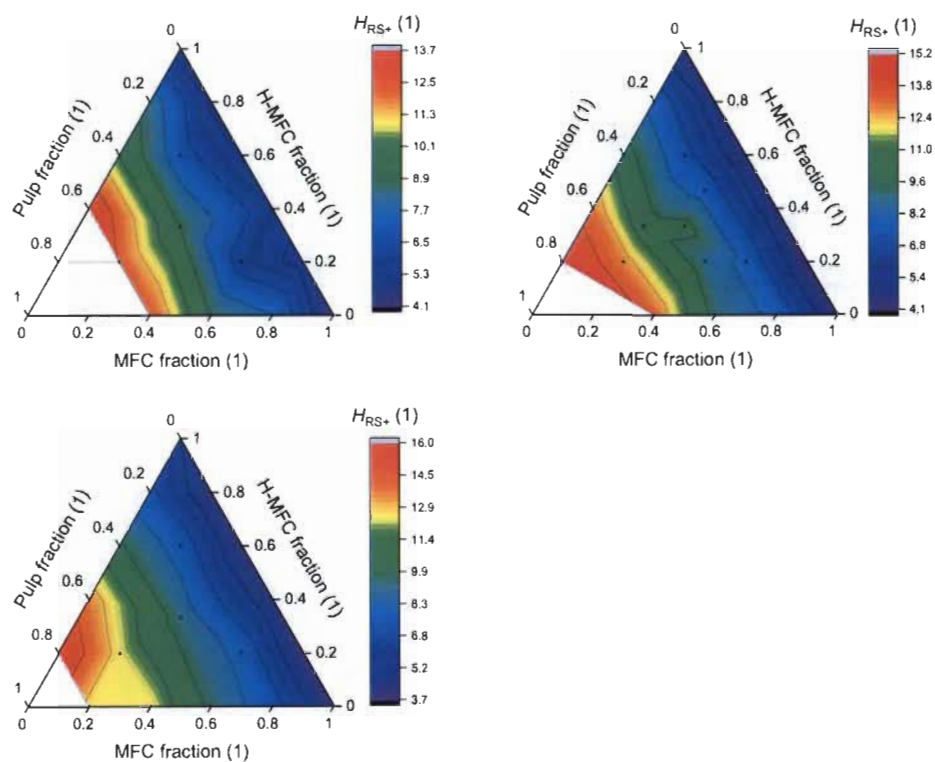


Figure 9.20: H_{RS+} data with individual scale bars for the single dilutions, 1 wt% (top left), 1.5 wt% (top right) and 2 wt% (bottom left). The scales are linear.

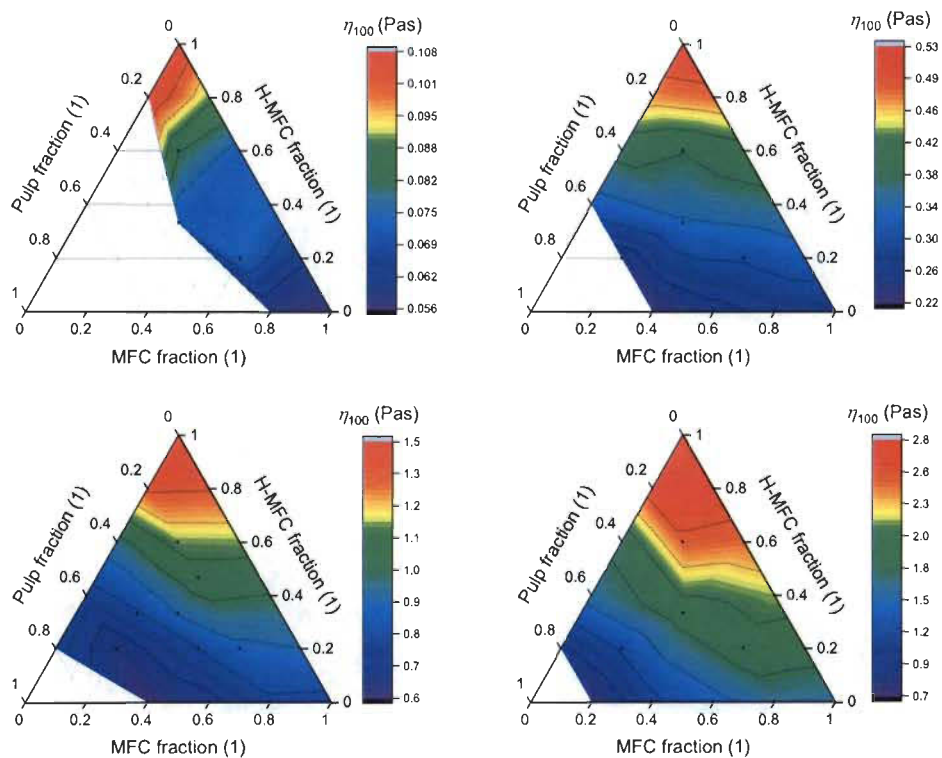


Figure 9.21: η_{100} data with individual scale bars for the single dilutions, 0.5 wt% (top left), 1 wt% (top right), 1.5 wt% (bottom left) and 2 wt% (bottom right). The scales are linear.

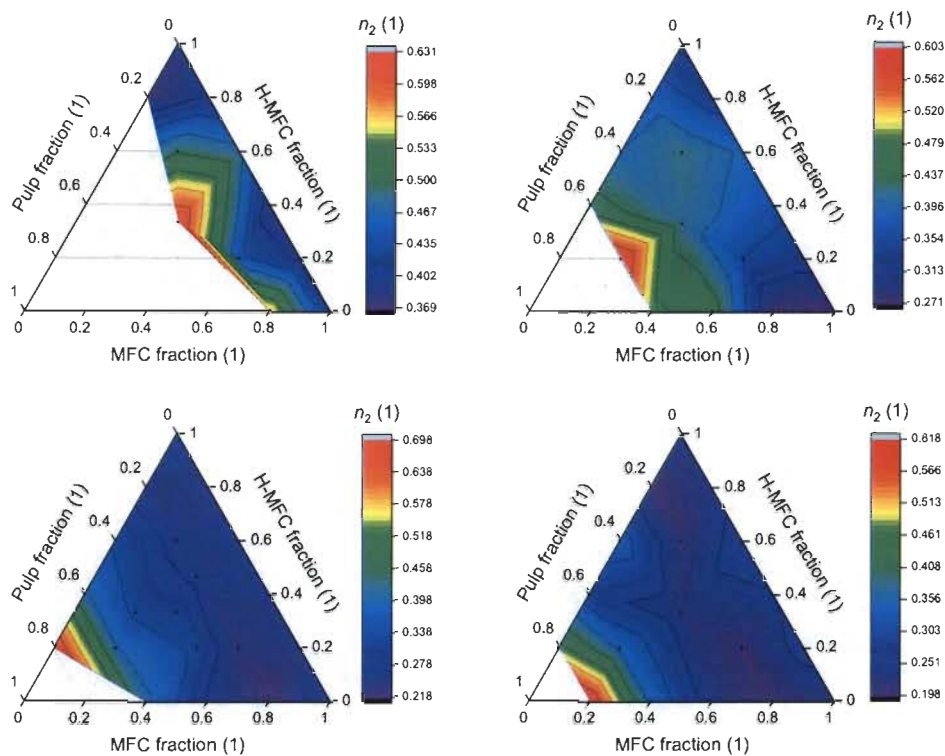


Figure 9.22: n_2 data with individual scale bars for the single dilutions, 0.5 wt% (top left), 1 wt% (top right), 1.5 wt% (bottom left) and 2 wt% (bottom right). The scales are linear.

9.11 References

Pyrgiotakis, G., Luu, W., Zhang, Z., Vaze, N., DeLoid, G., Rubio, L., Graham, W.A.C., Bell, D.C., Bousfield, D., Demokritou, P. (2018) Development of high throughput, high precision synthesis platforms and characterization methodologies for toxicological studies of nanocellulose. *Cellulose* 25:2303-2319. doi: 10.1007/s10570-018-1718-2

9.12 Unpublished data

This section contains the data sets (Figure 9.23 to Figure 9.31) that were referred to, but not shown in the main article of this chapter.

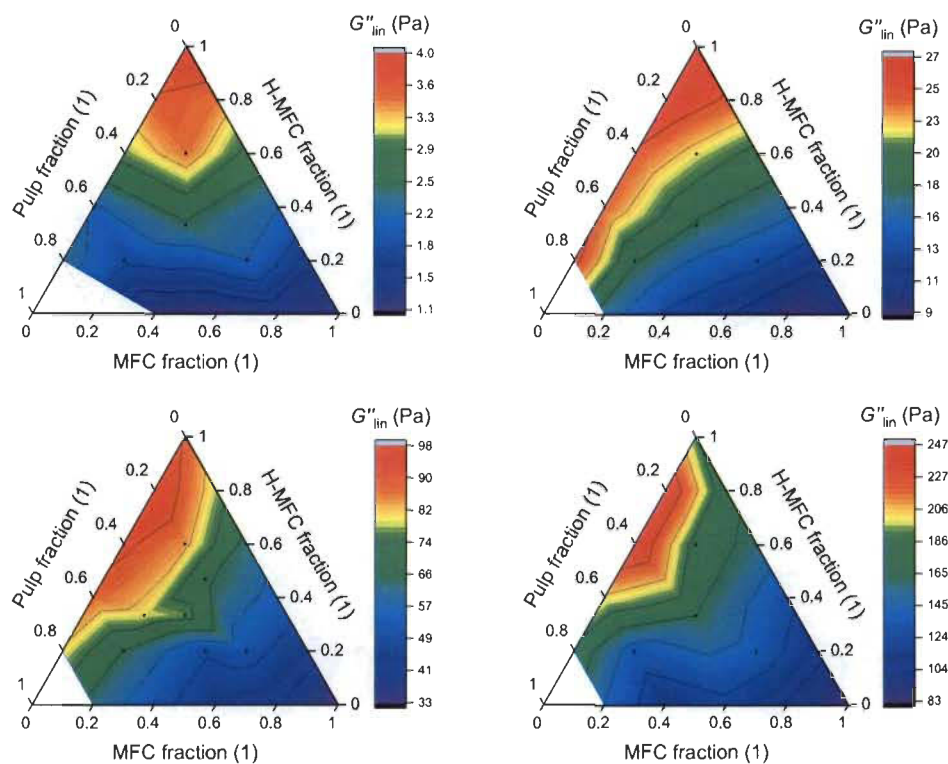


Figure 9.23: Loss modulus data with individual scale bars for the single dilutions, 0.5 wt% (top left), 1 wt% (top right), 1.5 wt% (bottom left) and 2 wt% (bottom right). The scales are linear.

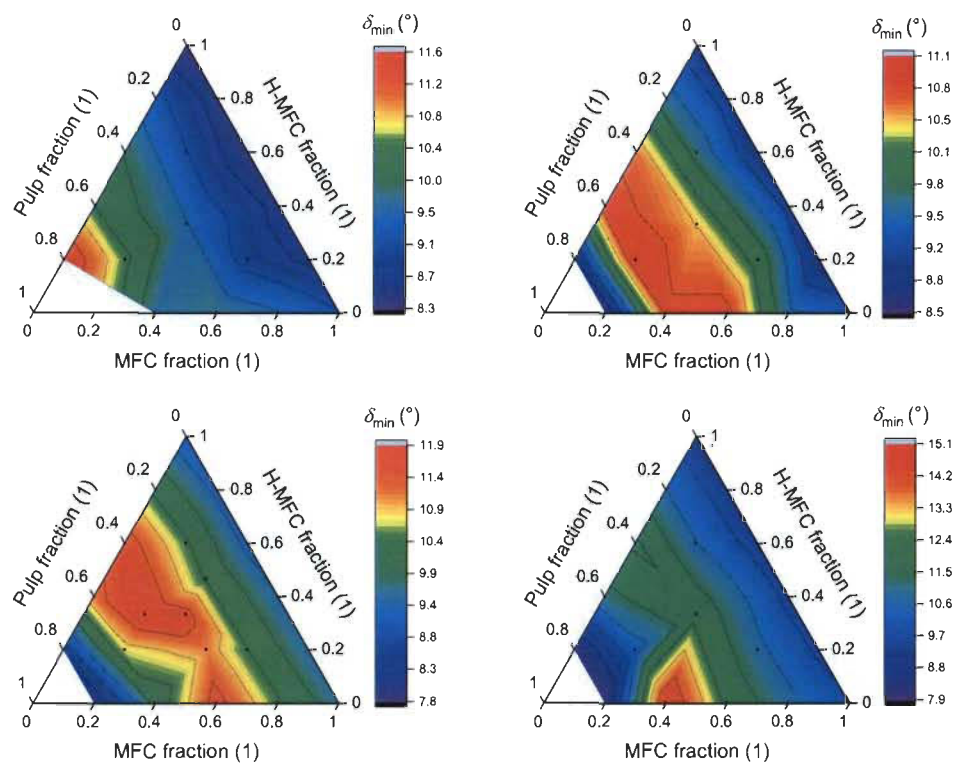


Figure 9.24: Phase angle data with individual scale bars for the single dilutions, 0.5 wt% (top left), 1 wt% (top right), 1.5 wt% (bottom left) and 2 wt% (bottom right). The scales are linear.

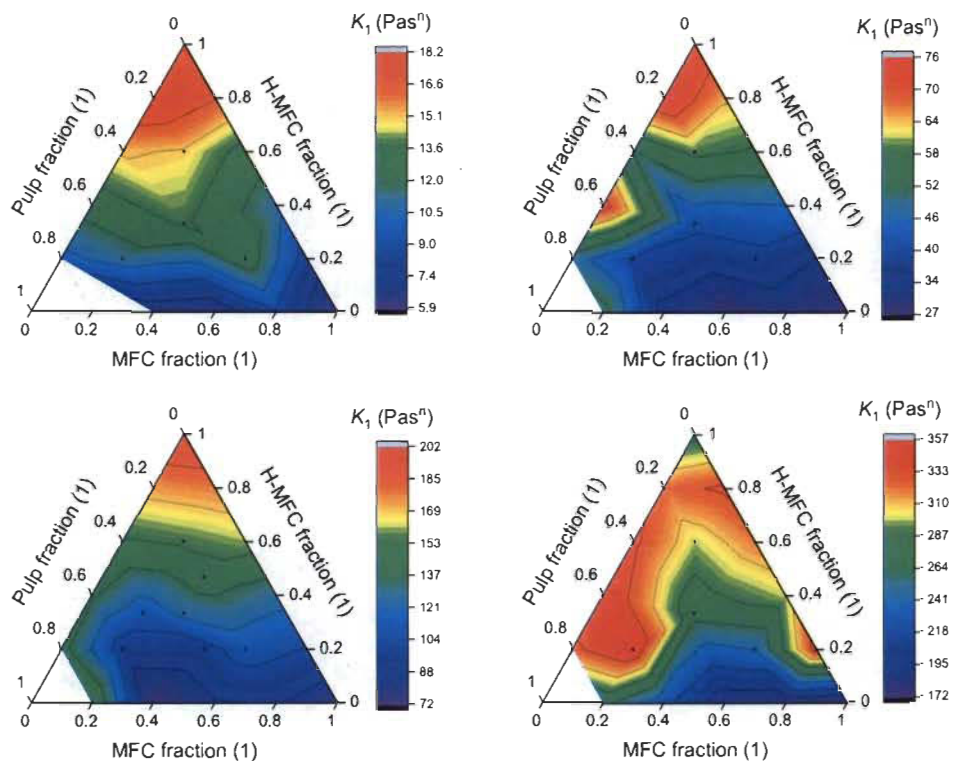


Figure 9.25: K_1 data with individual scale bars for the single dilutions, 0.5 wt% (top left), 1 wt% (top right), 1.5 wt% (bottom left) and 2 wt% (bottom right). The scales are linear.

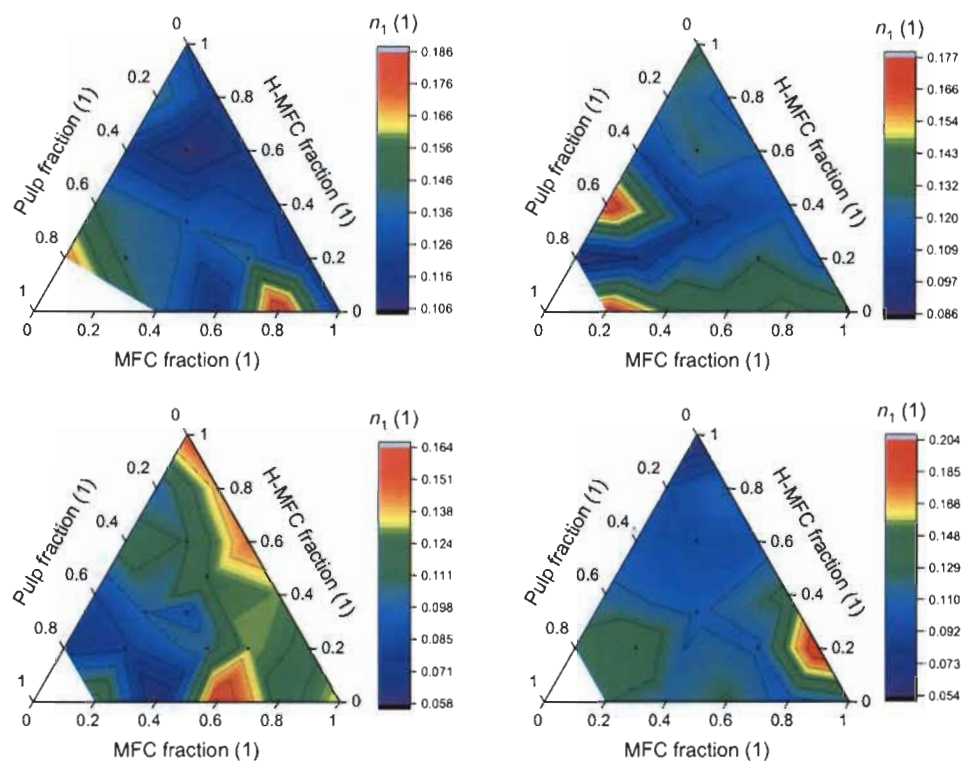


Figure 9.26: n_1 data with individual scale bars for the single dilutions, 0.5 wt% (top left), 1 wt% (top right), 1.5 wt% (bottom left) and 2 wt% (bottom right). The scales are linear.

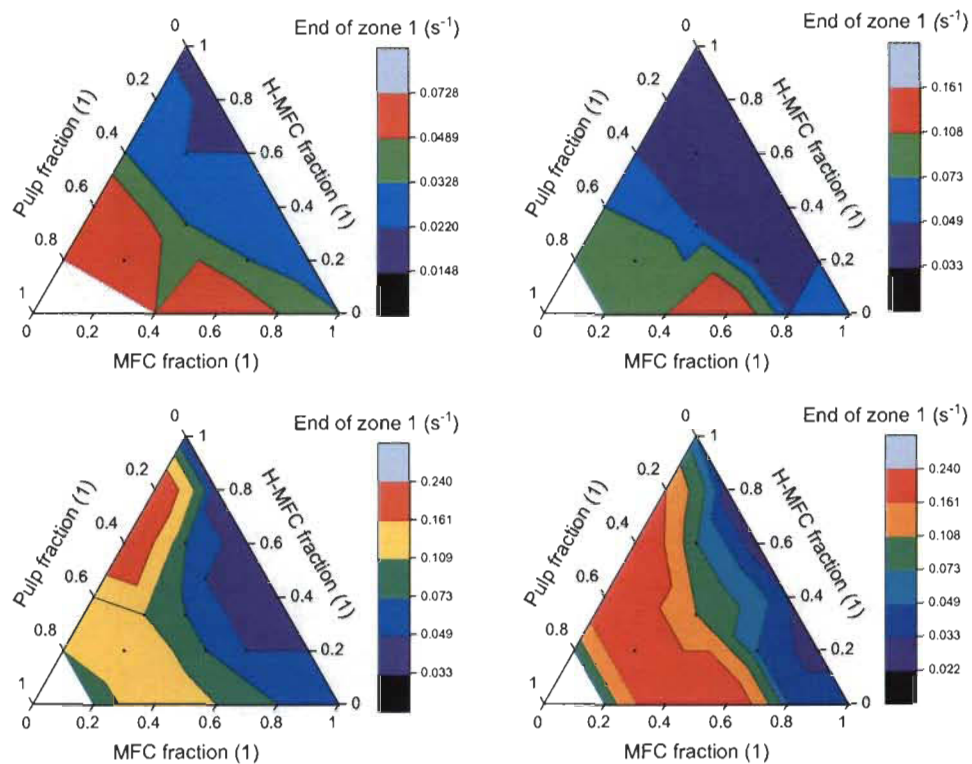


Figure 9.27: End of zone 1 data with individual scale bars for the single dilutions, 0.5 wt% (top left), 1 wt% (top right), 1.5 wt% (bottom left) and 2 wt% (bottom right). The scales are logarithmic and represent the actually set shear rates.

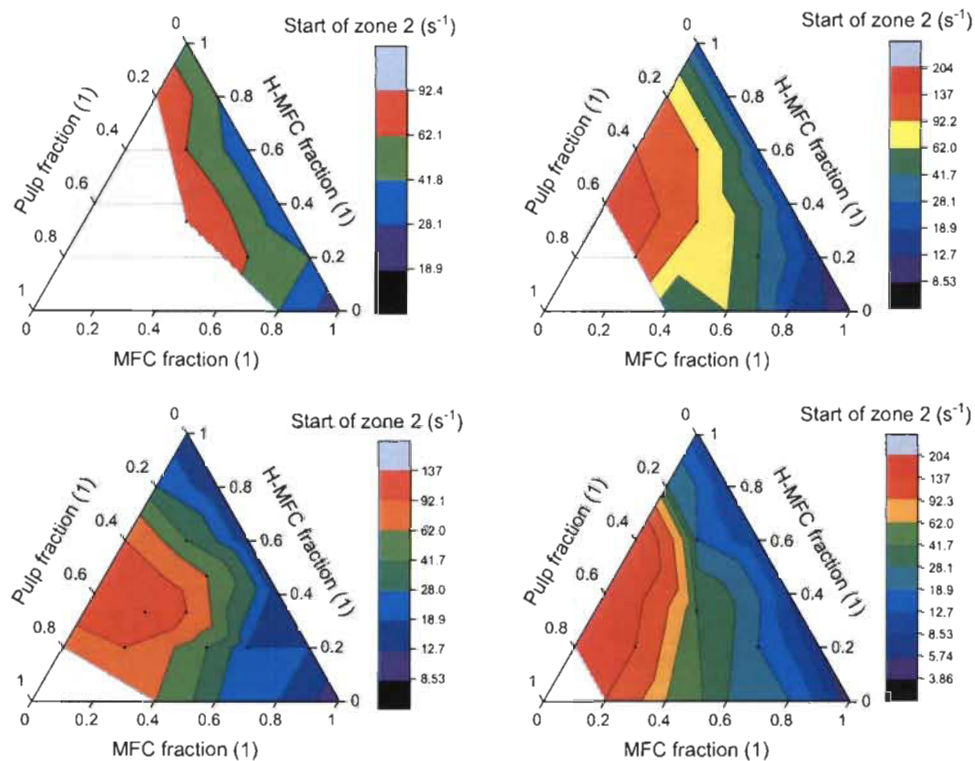


Figure 9.28: Start of zone 2 data with individual scale bars for the single dilutions, 0.5 wt% (top left), 1 wt% (top right), 1.5 wt% (bottom left) and 2 wt% (bottom right). The scales are logarithmic and represent the actually set shear rates.

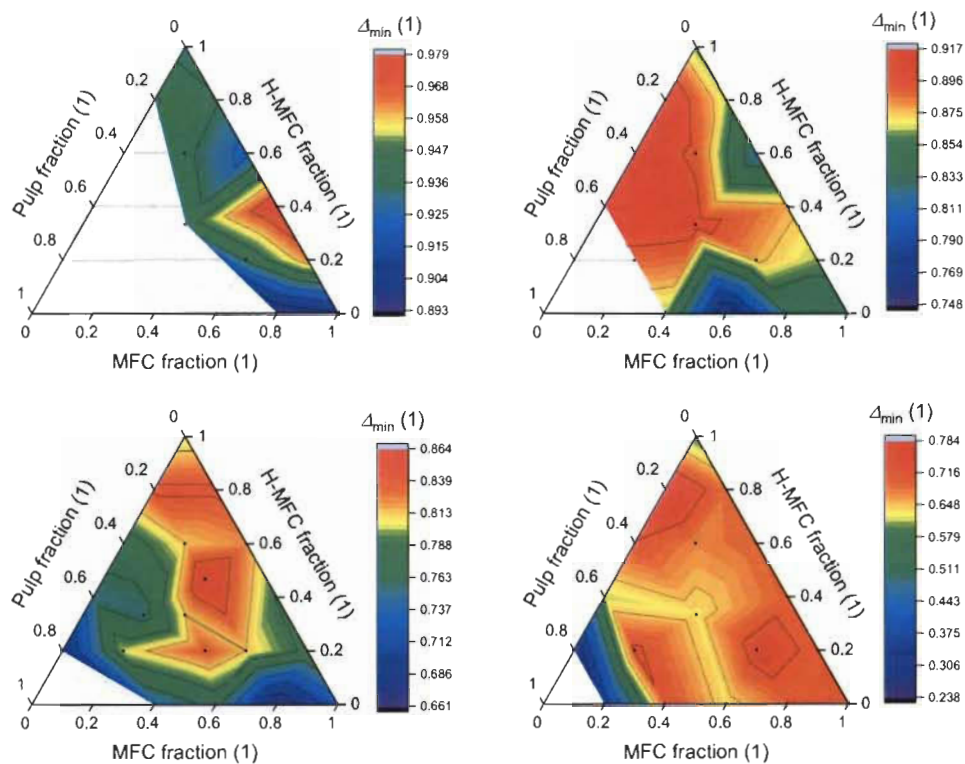


Figure 9.29: Relative transition zone depth data with individual scale bars for the single dilutions, 0.5 wt% (top left), 1 wt% (top right), 1.5 wt% (bottom left) and 2 wt% (bottom right). The scales are linear.

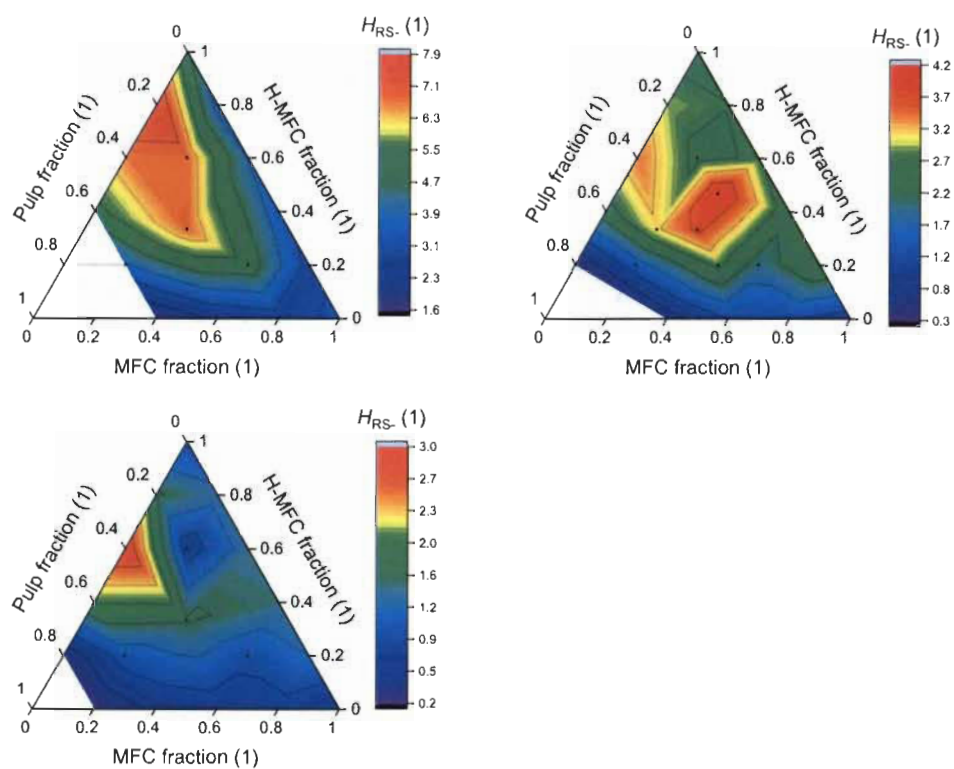


Figure 9.30: Negative hysteresis data with individual scale bars for the single dilutions, 0.5 wt% (top left), 1 wt% (top right), 1.5 wt% (bottom left) and 2 wt% (bottom right). The scales are linear.

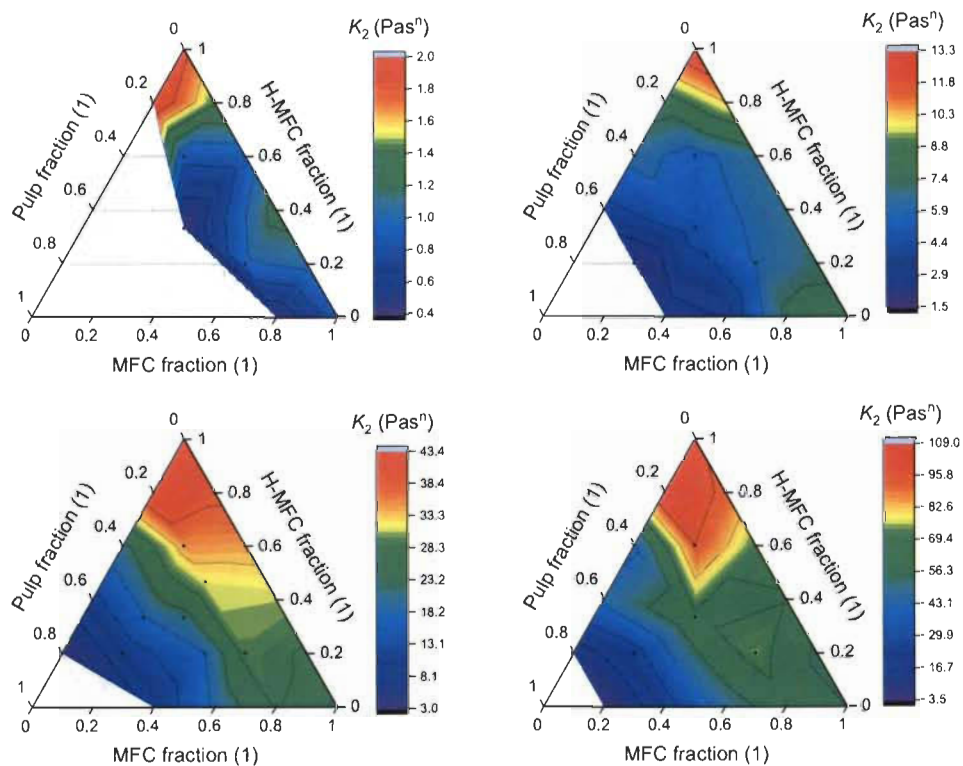


Figure 9.31: K_2 data with individual scale bars for the single dilutions, 0.5 wt% (top left), 1 wt% (top right), 1.5 wt% (bottom left) and 2 wt% (bottom right). The scales are linear.

Chapter 10 - Conclusions

The conclusions of this work can be grouped in two categories. The first category contains findings related to the selection of measurement system and protocol that are suitable for the rheological characterisation of MNFC suspensions, using a shear rheometer. It also includes the topics about the parametrisation and quantification of the so-obtained data. The second category is about the influence of the DoF and residual fibres on the rheological behaviour of MNFC suspensions. The following sections provide a discussion of both categories and go on to provide general conclusions. Detailed conclusions can be found in the respective chapters containing the publications.

10.1 Rheometer system and measurement protocol

The rheological behaviour of MNFC suspensions is very complex and obtaining reproducible, absolute results is challenging. This is manifest, for instance, when obtaining different values for a rheological property by using a different rheometer type, measurement geometry or a different measurement protocol. The general reason for such effects is that the MNFC suspension behaves differently compared to the assumptions made for interpreting the rheometer's raw data. Two prominent examples of such behaviour of MNFC suspensions are phase separation, leading for instance to the formation of a water (-rich) layer close to the measurement geometry surface and shear banding (a discontinuous shear rate profile). Such effects can lead to measurement artefacts, misinterpretation and non-reproducible data. A behaviour like this is a nuisance for experimentalists, and a significant amount of effort is put into avoiding such effects. However, it should also be borne in mind, that these effects are inherent parts of the reaction of the MNFC suspension to a deformation. So, in practice these effects may have an important influence on the overall macroscopic behaviour, and an isolated rheological treatment may not be constructive in predicting or modelling it. Then again, for understanding the suspension particulate morphology, it is necessary to at least understand these effects, or better to characterise and quantify them.

In the present work, one has not set out to characterise and quantify all the non-linear effects occurring in MNFC suspensions under flow conditions. However, instead, the phenomenological behaviour of MNFC suspensions under varying conditions has been

investigated and related to prevailing mechanistic models. Specifically, MNFC suspensions as used in this work are understood as stable, homogeneous networks of fibres and fibrils at rest, that can undergo dynamic reorganisation under flow. The reorganisation can lead to aggregation at intermediate shear rates and de-aggregation and probably orientation at increased shear rates. The macroscopic behaviour can be described as a gel at rest, having a yield stress after which it starts to flow. The flow is characterised by a generally shear thinning behaviour, following a power law. This behaviour is discontinuous, however, because of the aggregation of the fibrils at intermediate shear rates leading to a so-called transition region, typically characterised by a viscosity drop. The characteristic flow curve of MNFC suspensions (and the discussion has to be limited to MNFC to the definition used in this work) is not described consistently in the literature. Also, this work has shown that the transition region may not be very apparent for some combinations of measurement systems and suspension parameters. In the course of optimising the measurement protocol, a simple way has been found to identify the transition region more easily. For this, only the typically used fixed acquisition time setting in a flow curve measurement protocol has to be changed to allow the system to reach an equilibrium state, i.e. acquire the viscosity after it reaches a stable reading. Parallel to recording the viscosity at a given shear rate, also the acquisition time has to be recorded and evaluated. It was found that the time to reach a stable viscosity is typically low and reproducible when the shear rate is in the regular shear thinning regimes, but increases and fluctuates among repetitive measurements when being in the transition zone. The investigation of different cylinder-in-cup based measurement systems has, in principle, confirmed general findings, i.e. that smooth surfaces are prone to measurement artefacts (likely solids depletion near the measurement surfaces), roughening of the instrument geometry wall may not be an appropriate countermeasure when the roughness is not large enough, and that vane geometries are less prone to such effects. However, it has also been shown that at low deformations, below the yield point of the suspension, the characterisation is measurement system independent. Furthermore, we have shown that, generally, the trends of viscoelastic and flow curve properties as a function of the suspension solids content can also be reproduced by the different measurement systems, despite the differences in the absolute values.

In conclusion it can be stated that:

- the use of an automated acquisition time setting to get the respective times at a given shear rate for the viscosity to reach a stable reading is a valuable addition to a flow curve protocol to identify the transition region occurring within an MNFC suspension under shear;
- a vane in (serrated) cup system seems the least prone for solids depletion effects near the measurement surface;
- general trends obtained by other, different cylinder in cup systems may still be compared to each other.

10.2 Quantification of rheological data of MNFC suspensions

Despite the unusual shape of the flow curve of MNFC suspensions, its features typically are not determined quantitatively, except probably a low and high shear (rate) viscosity or sometimes the power law parameters of the shear thinning zones (yet typically without specifying the zone). As a part of this work, several additional descriptors to the ones that are generally used already have, therefore, been proposed. The intention behind these descriptors is to describe additionally the different regions of the flow curve, and so to quantify them, such that relative comparisons become possible.

When performing a shear rate loop, i.e. first increase the shear rate and then decrease it (or vice versa), hysteresis between the two flow curves can often be observed. The presence of the hysteresis is sometimes described in the literature, but to current best knowledge, no one attempted to quantify it for MNFC suspensions. It is apparent from rheo-optical investigations, that the difference in viscosity at equal shear rates following different shear rate histories is caused by different suspension particulate morphologies. So, the hysteresis clearly contains information on the ability of the system to have different structures depending on the shear situation. In a separate work we presented the evaluation of different, empirical approaches to calculate quantitative hysteresis descriptors.

To get confidence also in the data and the chosen experimental approach, selected data sets were statistically tested and evaluated. It was found that using average data of

triplicate measurements typically results in moderate standard deviations, yet apparent trends typically are significant (at a confidence level of 5 %).

Concluding, it can be said that the introduced descriptors and quantification methods have proven very useful and that they are essential to be able to investigate systematically the rheology determining factors of MNFC suspensions, as will be shown in the next section.

10.3 Influence of DoF on the rheological properties of MNFC suspensions

To investigate the influence of the DoF of an MNFC suspension on its rheological properties, not only the rheological data should be quantified, but ideally also the DoF itself. Different strategies can be found in the literature, however, only few of them are able to provide numbers of actual fibre and fibril dimensions, specifically length and width. Image analysis of micrographs was selected in this work, yet knowing the typical challenges and pitfalls, special care was taken in critically reviewing the applied method and potential results. The sample preparation step was identified to be the most challenging part of the investigation. A good dispersion of the fibrils is key for a reliable image analysis. However, it seems that unmodified MNFC tends to aggregate at high dilutions, and so typically rather inhomogeneous distributions were obtained on the sample holders. At first sight, one attempt appeared successful though. However, comparing the so obtained fibril width distributions with SEM images of freeze dried aerogels of the same materials revealed that fibrils and fibres being wider than a certain size were not found in the image analysis at all. Instead, indirect evidence of the different DoFs was obtained by visual assessment of optical and electron microscopy images and specific surface area data of the aerogels. The discrepancy may still have been a result of a non-ideal sample preparation procedure, yet it also clearly highlighted an inherent problem of this approach for characterising rather highly polydisperse materials using rather localised imaging techniques.

An extensive experimental work was carried out, investigating up to ternary mixtures of three materials having different DoFs, and at four different solids contents. The data were presented in ternary mixture diagrams, whereas the property values were visualised by coloured contour surfaces. This way of presenting data allows for an easy identification of qualitative trends with respect to the sample composition, i.e. the DoF.

Several properties and trends were in good agreement with data presented in the literature. Yet, because the present work systematically investigated the influence of the DoF, the conclusions that can be drawn from it appear to be more universal. For instance, this universality is apparent for properties where non-monotonic trends with the DoF were found. Because our mixture approach also allowed to have compositions of very broad size distributions, for example by combining a highly fibrillated MFC and unfibrillated pulp fibres, trends were obtained that were not reported so far, or have led to inconsistent conclusions within the scientific literature.

The typically reasoned mechanism behind the change of properties of particulate materials with decreasing particle size is that the number of particles per volume (or weight) increases. This, in itself, may have implications for the material's behaviour, but also the inherent change of, for example, total surface area, or surface area to volume ratio. Our data suggest, that several of the investigated properties also follow this trend, like the suspension's yield stress or high shear viscosity. However, we also have found trends, where the mechanisms may also be governed by the stiffness of the fibres and fibrils, which is directly related to the degree of fibrillation for high aspect ratio particles like fibres.

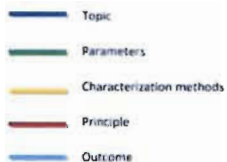
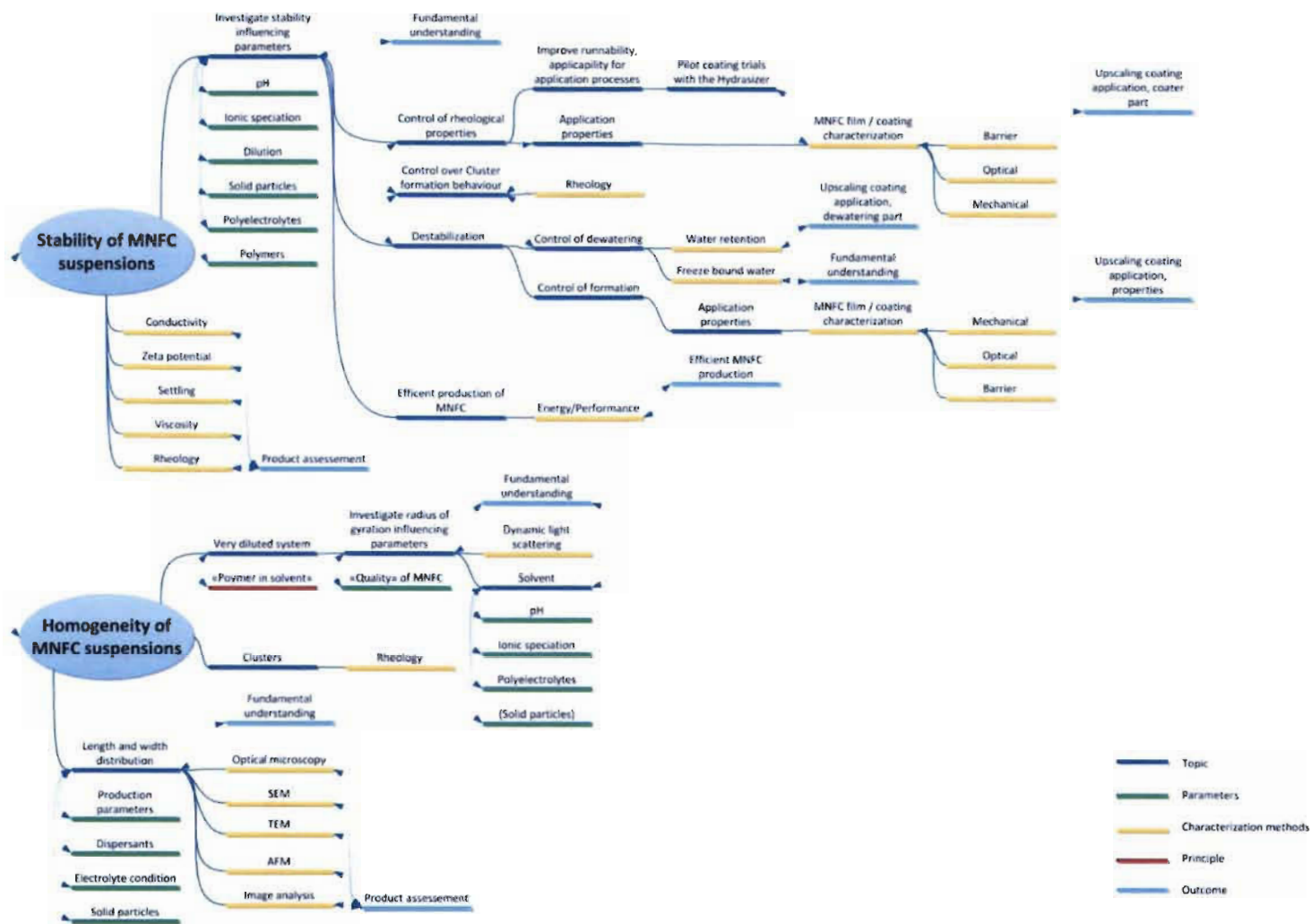
Besides the technical findings, this work has also shown that a quantification of the rheological data, in combination with adequate data presentation, can lead to very straightforward identification of qualitative trends. This, then, may serve as a starting point, for a more theoretical approach, trying to relate the observed data to physical and computational models.

10.4 Perspectives

Several general extensions of this work may be envisaged. On the one hand, optical or other structural information revealing measurement techniques could be added to the current measurement set-up and -protocols. Like this, one would be able to gain information directly on the suspension particulate morphology. This would allow to test the hypotheses that resulted from this work, and help generally to qualify the here proposed systems and protocols. On the other hand, other aspects of MNFC suspensions could be investigated, using the same approach. For instance, a systematic investigation of the influence of added charge, for example by adding cellulose derivatives or added pigment particles, could be carried out. As mentioned earlier, such investigations were planned already in the very beginning of this work, as can be seen in Figure 10.1, which is an early mind map about the potential topic of this work. Having an extensive dataset, as presented in this work, also would allow smaller trial matrices to be carried out, e.g. using DoE approaches in order to save effort and time for future studies based on the setup presented here.

Like also sketched in Figure 10.1, the findings of this work and the respective know-how is intended to serve as a basis to enable or improve (industrial) applications of MNFCs in different fields. Some of these were already applied in the meantime in some projects within my employer company, showing the actual relevance of this work for the industry.

Figure 10.1: Initial mind map on potential topics for this work.



References

- Agoda-Tandjawa G, Durand S, Berot S, Blassel C, Gaillard C, Garnier C, J.L. D (2010) Rheological characterization of microfibrillated cellulose suspensions after freezing. *Carbohydrate Polymers* 80:677-686.
- Alemдар A, Sain M (2008) Biocomposites from wheat straw nanofibers: Morphology, thermal and mechanical properties. *Composites Science and Technology* 68:557-565.
- Ankerfors M (2012) Microfibrillated cellulose: Energy-efficient preparation techniques and key properties (Licenciate thesis). KTH Royal Institute of Technology.
- Archambault D, Hamel J (2014) Cellulose Filament Demonstration, Application, Development and Commercialization, presented at Paperweek in Montreal
- Aulin C, Gällstedt M, Lindström T (2010) Oxygen and oil barrier properties of microfibrillated cellulose films and coatings. *Cellulose* 17:559-574.
- Ayse A, Sain M (2008) Isolation and characterization of nanofibers from agricultural residues - Wheat straw and soy hulls. *Bioresour.Technol.* 99:1664-1671.
- Azeredo HMC, Mattoso LHC, Avena-Bustillos RJ, Filho GC, Munford ML, Wood D, McHugh TH (2010) Nanocellulose Reinforced Chitosan Composite Films as Affected by Nanofiller Loading and Plasticizer Content. *Journal of Food Science* 75:N1-N7.
- Barnes HA (2000) Measuring the viscosity of large-particle (and flocculated) suspensions - a note on the necessary gap size of rotational viscometers. *Journal of Non-Newtonian Fluid Mechanics* 94:213-217.
- Bio-fibre (2015) Sappi to build ground-breaking nanocellulose pilot plant. <http://www.bio-fibre.eu/biofibre/Home/News/7750>. Accessed: 14.07.2015

- Chan Y, Walmsley RP (1997) Learning and Understanding the Kruskal-Wallis One-Way Analysis-of-Variance-by-Ranks Test for Differences Among Three or More Independent Groups. *Physical Therapy* 77:1755-1761.
- Charani PR, Deghani-Firouzabadi M, Afra E, Shakeri A (2013) Rheological characterization of high concentrated MFC gel from kenaf unbleached pulp. *Cellulose* 20:727-740.
- Charfeddine MA, Roussi re F, Bloch JF, Ridgway CJ, Gane PA, Mangin PJ (2014) Impact on paper properties of z-direction structuring by layered addition of Micro-Nano-Fibrillated Cellulose (MNFC), presented at Tappi International Conference on Nanotechnology for Renewable Materials in Vancouver
- Charfeddine MA, Roussi re F, Bloch JF, Ridgway CJ, Schenker M, Gane PA, Mangin PJ (2015) Effect of Carboxy-Methyl-Cellulose (CMC) as a Dispersing Agent for Micro-Nano Fibrillated Cellulose (MNFC) on z-Structured TMP Paper and MNFC Films Properties, presented at Tappi International Conference on Nanotechnology for Renewable Materials in Atlanta
- Chen WS, Yu HP, Liu YX, Chen P, Zhang MX, Hai YF (2011) Individualization of cellulose nanofibers from wood using high-intensity ultrasonication combined with chemical pretreatments. *Carbohydrate Polymers* 83:1804-1811.
- Cheng F, Li Y, Chen D (2013) Energy Consumption and Morphological Development of Eucalyptus Alkaline Peroxide Mechanical Pulp by Carboxymethyl Cellulose-assisted Refining. *BioResources* 8:2173-2185.
- Cheng Q, Wang S, Rials TG, Lee SH (2007) Physical and mechanical properties of polyvinyl alcohol and polypropylene composite materials reinforced with fibril aggregates isolated from regenerated cellulose fibers. *Cellulose* 14:593-602.

- Chinga-Carrasco G (2013) Optical methods for the quantification of the fibrillation degree of bleached MFC materials. *Micron* 48:42-48.
- Cloitre M, Bonnecaze RT (2017) A review on wall slip in high solid dispersions. *Rheologica Acta* 56:283-305.
- deMenezes AJ, Siqueira G, Curvelo AAS, Dufresne A (2009) Extrusion and characterization of functionalized cellulose whiskers reinforced polyethylene nanocomposites. *Polymer* 50:4552-4563.
- Dimic-Misic K, Gane PAC, Budtova T, Pradille C, Sixta H, Ville L, Maloney T (2015a) Influence of xylan on nanocellulose (NFC) suspension rheology and aerogel morphology, presented at 6th International Symposium on Industrial Engineering in Belgrade
- Dimic-Misic K, Gane PAC, Paltakari J (2013a) Micro- and nanofibrillated cellulose as a rheology modifier additive in CMC-containing pigment coating formulations. *Industrial and Engineering Chemistry Research* 52:16066-16083.
- Dimic-Misic K, Maloney TC, Gane PAC (2015b) Defining a strain-induced time constant for oriented low shear-induced structuring in high consistency MFC/NFC-filler composite suspensions. *Journal of Applied Polymer Science* 132:42827.
- Dimic-Misic K, Puisto A, Gane PAC, Nieminen K, Alava M, Paltakari J, Maloney T (2013b) The role of MFC/NFC swelling in the rheological behavior and dewatering of high consistency furnishes. *Cellulose* 20:2847-2861.
- Dimic-Misic K, Puisto A, Paltakari J, Alava M, Maloney T (2013c) The influence of shear on the dewatering of high consistency nanofibrillated cellulose furnishes. *Cellulose* 20:1853-1864.
- Dimic-Misic K, Salo T, Paltakari J, Gane PAC (2014) Comparing the rheological properties of novel nanofibrillar cellulose-formulated pigment coating colours with those using traditional thickener. *Nordic Pulp and Paper Research Journal* 29:253-270.

- Dukhin AS, Goetz JP (2002) *Ultrasound for Characterizing Colloids. Particle sizing, Zeta potential, Rheology*. Elsevier
- Eichhorn SJ, Dufresne A, Aranguren M, Marcovich NE, Capadona JR, Rowan SJ, Weder C, Thielmans W, Roman M, Renneckar S, Gindl W, Veigel S, Keckes H, Yano H, Abe K, Nogi M, Nakagaito AN, Mangalam A, Simonsen J, Benight AS, Bismarck A, Berglund LA, Peijs T (2010) Review: current international research into cellulose nanofibres and nanocomposites. *Journal of Material Science* 45:1-33.
- El-Gholabzouri O, Cabrerizo MA, Hidalgo-Alvarez R (1999) Comparative electrophoretic mobility and streaming current study for zeta-potential determination. *Colloids and Surfaces A: Physicochemical and Engineering Aspects* 159:449-457.
- Elazzouzi-Hafraoui S, Nishiyama Y, Putaux JL, Heux L, Dubreuil F, Rochas C (2008) The Shape and Size Distribution of Crystalline Nanoparticles Prepared by Acid Hydrolysis of Native Cellulose. *Biomacromolecules* 9:57-65.
- Eriksen O, Syverud K, Gregersen O (2008) The use of microfibrillated cellulose produced from kraft pulp as strength enhancer in TMP paper. *Nordic Pulp and Paper Research Journal* 23:299-304.
- Eronen P, Junka K, Laine J, Österberg M (2011) Interaction between water-soluble polysaccharides and native nanofibrillar cellulose thin films. *BioResources* 6:4200-4217.
- Eyholzer C (2010) *Preparation and Properties of Dried Nanofibrillated Cellulose and its Nanocomposites (Licenciate thesis)*. Luleå University of Technology.
- Fall AB, Lindström SB, Sundman O, Ödberg L, Wagberg P (2011) Colloidal stability of aqueous nanofibrillated cellulose dispersion. *Langmuir* 27:11332-11338.
- Fardim P, Holmbom B, Ivaska A, Mortha G, Laine J (2002) Critical comparison and validation of methods for determination of anionic groups in pulp fibres. *Nordic Pulp and Paper Research Journal* 17:346-351.

- Francisco M, van den Bruinhorst A, Kroona MC (2012) New natural and renewable low transition temperature mixtures (LTTMs): screening as solvents for lignocellulosic biomass processing. *Green Chemistry* 14:2153-2157.
- Gane PAC, Schoelkopf J, Gantenbein D, Schenker M (2012a) Process for the production of nano-fibrillar cellulose gels. EP2414435 A1
- Gane PAC, Schoelkopf J, Gantenbein D, Schenker M, Pohl M, Kübler B (2012b) Process for the production of nano-fibrillar cellulose suspensions. EP2414584 A1
- Gantenbein D, Schoelkopf J, Matthews GP, Gane PAC (2011) Determining the size distribution-defined aspect ratio of rod-like particles. *Applied Clay Science* 53:538-543.
- Gerrer M (2014) Commercial System to Produce Cellulose Nanofibrils, presented at Tappi International Conference on Nanotechnology for Renewable Materials in Vancouver
- Gonzalez I, Boufi S, Pelach MA, Alcala M, Vilaseca F, Mutje P (2012) Nanofibrillated cellulose as paper additive in eucalyptus pulps. *BioResources* 7:5167-5180.
- Henriksson M, Berglund LA, Isaksson P, Lindstrom T, Nishino T (2008) Cellulose nanopaper structures of high toughness. *Biomacromolecules* 9:1579-1585.
- Henriksson M, Henriksson G, Berglund LA, Lindström T (2007) An environmentally friendly method for enzyme-assisted preparation of microfibrillated cellulose (MFC) nanofibers. *European Polymer Journal* 43:3434-3441.
- Herrick FW, Casebier RL, Hamilton JK, Sandberg KR (1983) Microfibrillated cellulose: morphology and accessibility. *Journal of Applied Polymer Science* 37:797-813.
- Hii C, Gregersen OW, Chinga-Carrasco G, Eriksen O (2012) The effect of MFC on the pressability and paper properties of TMP and GCC based sheets. *Nordic Pulp and Paper Research Journal* 27:388-396.

- Ho TTT, Zimmermann T, Ohr S, Caseri WR (2012) Composites of Cationic Nanofibrillated Cellulose and Layered Silicates: Water Vapor Barrier and Mechanical Properties. *ACS Applied Materials & Interfaces* 4:4832-4840.
- Horvath AE (2003) Appropriate conditions for polyelectrolyte titration to determine the charge of cellulosic fibers (Licenciate thesis). Royal Institute of Technology Stockholm.
- Horvath AE, Lindstrom T, Laine J (2006) On the Indirect Polyelectrolyte Titration of Cellulosic Fibers. Conditions for Charge Stoichiometry and Comparison with ESCA. *Langmuir* 22:824-830.
- Hubbe MA, Moore SM, Lee SY (2005) Effects of charge ratios and cationic polymer nature on polyelectrolyte complex deposition onto cellulose. *Ind.Eng.Chem.Res.* 44:3068-3074.
- Hubbe MA, Rojas OJ, Lucia LA, Sain M (2008) Cellulosic Nanocomposites: A Review. *BioResources* 3:929-980.
- Hubbe MA, Wang F (2004) Charge-Related Measurements - A Reappraisal - Part 2: Fibre-Pad Streaming Potential. *Paper Technology* 45:27-34.
- Iotti M, Gregersen OW, Moe S, Lenes M (2011) Rheological Studies of Microfibrillar Cellulose Water Dispersions. *Journal of Polymers and the Environment* 19:137-145.
- Isogai A, Saito T, Fukuzumi H (2011) TEMPO-oxidized cellulose nanofibers. *Nanoscale* 3:71-85.
- Iwamoto S, Nakagaito AN, Yano H, Nogi M (2005) Optically transparent composites reinforced with plant fiber-based nanofibers. *Applied Physics A: Materials Science & Processing* 81:1109-1112.
- Jacobasch H-J, Bauböck G, Schurz J (1985) Problems and results of zeta-potential measurements on fibers. *Colloid and Polymer Science* 263:3-24.

- Jaycock MJ (1995) Assumptions made in the measurement of zeta-potential by streaming current/potential detectors. *Paper Technology* Jul/Aug:35-38.
- Jennings BR, Parslow K (1988) Particle size measurements: the equivalent spherical diameter. *Proceedings of the royal society of London Series, A-Mathematical physical and engineering sciences*. Vol. 419: 139-149
- Jonoobi M, Harun J, Shakeri A, Misra M, Oksman K (2009) Chemical composition, crystallinity, and thermal degradation of bleached and unbleached Kenaf Bast (*Hibiscus cannabinus*) pulp and nanofibers. *BioResources* 4:626-639.
- Josset S, Orsolini P, Siqueira G, Tejado A, Tingaut P, Zimmermann T (2014) Energy consumption of the nanofibrillation of bleached pulp, wheat straw and recycled newspaper through a grinding process. *Nordic Pulp and Paper Research Journal* 29:167-175.
- Kangas H, Lahtinen P, Sneek A, Saariaho AM, Laitinen O, Hellén E (2014) Characterization of fibrillated celluloses. A short review and evaluation of characteristics with a combination of methods. *Nordic Pulp and Paper Research Journal* 29:129-143.
- Karppinen A (2014) Rheology and flocculation of polymer-modified microfibrillated cellulose suspensions (PhD thesis). Aalto University.
- Kaukonen OV, Kunnari V, Keskinen J (2015) Energy Storage Devices Based on High Consistency Cellulose, presented at Tappi International Conference on Nanotechnology for Renewable Materials in Atlanta
- Klemm D, Heublein B, Fink HP, Bohn A (2005) Cellulose: Fascinating Biopolymer and Sustainable Raw Material. *Angewandte Chemie International Edition* 44:3358-3393.
- Kosan B, Michels C, Meister F (2008) Dissolution and forming of cellulose with ionic liquids. *Cellulose* 15:59-66.

- Kruger (2013) FPInnovations and Kruger join forces to implement a leading-edge Cellulose Filament plant. <http://www.kruger.com/en/news/a-groundbreaking-announcement-1/>. Accessed: 10.07.2015
- Laurinsilta E (2013) UPM Biofibrils - novel bio-based nanomaterial for various industrial applications, presented at EuroNanoForum2013 in Dublin
- Lavoine N, Desloges I, Dufresne A, Bras J (2012) Microfibrillated cellulose - Its barrier properties and applications in cellulosic materials: A review. *Carbohydrate Polymers* 90:735-764.
- Lavoine N, Desloges I, Khelifi B, Bras J (2014) Impact of different coating processes of microfibrillated cellulose on the mechanical and barrier properties of paper. *Journal of Material Science* 49:2879-2893.
- Lee SY (2015) Cellulose Nanofibrils: One-Dimensional Opportunity for Flexible/High-Performance Lithium-Ion Paper Batteries, presented at Tappi International Conference on Nanotechnology for Renewable Materials in Atlanta
- Leung YH, Ng AMC, Xu X, Shen Z, Gethings LA, Wong MT, Chan CMN, Guo MY, Ng YH, Djuricic AB, Lee PKH, Chan WK, Yu LH, Philipps DL, Ma APY, Leung FCC (2014) Mechanisms of antibacterial activity of MgO: Non-ROS mediated toxicity of MgO nanoparticles towards escherichia coli. *PubMed* 10:1171-83.
- Liimatainen H, Haavisto S, Haapala A, Niinimäki J (2009) Influence of adsorbed and dissolved carboxymethyl cellulose on fibre suspension dispersing, dewaterability, and fines retention. *BioResources* 4:321-340.
- Macosko CW (1994) *Rheology: Principles, Measurements and Applications*. Wiley-VCH Publishers
- Maloney T (2013) High consistency forming of microfibrillated composite webs *In* Efficient networking towards novel products and processes - Programme report 2010 - 2013. 14-29: FIBIC.

- Mezger TG (2014) *The Rheology Handbook*, 4th Edition. Vincentz Network
- Miao C, Hamad Y (2013) Cellulose reinforced polymer composites and nanocomposites: a critical review. *Cellulose* 20:2221-2262.
- Moberg T, Rigdahl M (2012) On the Viscoelastic Properties of Microfibrillated Cellulose (MFC) Suspension. *Annual Transactions of the Nordic Rheology Society* 20:123-130.
- Mohtaschemi M, Dimic-Misic K, Puisto A, Korhonen M, Maloney T, Paltakari J, Alava MJ (2014a) Rheological characterization of fibrillated cellulose suspensions via bucket vane viscosimeter. *Cellulose* 21:1305-1312.
- Mohtaschemi M, Sorvari A, Puisto A, Nuopponen M, Seppälä J, Alava MJ (2014b) The vane method and kinetic modeling: shear rheology of nanofibrillated cellulose suspensions. *Cellulose* 21:3913-3925.
- Moon RJ, Martini A, Nairn J, Simonsen J, Youngblood J (2011) Cellulose nanomaterials review: structure, properties and nanocomposites. *Chemical Society Reviews* 40:3941-3994.
- Naderi A, Lindström T (2015) Rheological Measurements on Nanofibrillated Cellulose Systems: A Science in Progress *In* *Cellulose and Cellulose Derivatives*. M.I.H. Mondal, ed 187-202: Nova Science Publishers, Inc.
- Naderi AL, T.; Sundström, J.; Pettersson, T.; Flordberg, G.; Erlandsson, J. (2014) Carboxymethylated nanofibrillated cellulose: rheological studies. *Cellulose* 21:1561-1571.
- Nakagaito AN, Yano H (2008) The effect of fiber content on the mechanical and thermal expansion properties of biocomposites based on microfibrillated cellulose. *Cellulose* 15:555-559.
- Nazari N, Kumar V, Bousfield DW, Toivakka M (2016) Rheology of cellulose nanofibers suspensions: Boundary driven flow. *Journal of Rheology* 60:1151-1159.

- Nechyporchuk O, Belgacem MN, Pignon F (2016) Current progress in Rheology of Cellulose Nanofibril Suspensions. *Biomacromolecules* 17:2311-2320.
- Nishino T, Matsuda I, Hirao K (2004) All-Cellulose Composite. *Macromolecules* 37:7683-7687.
- Nishino T, Takano K, Nakamae K (1995) Elastic-Modulus of the Crystalline Regions of Cellulose Polymorphs. *Journal of Polymer Science Part B - Polymer Physics* 33:1647-1651.
- Nogi M, Iwamoto S, Nakagaito AN, Yano H (2009) Optically Transparent Nanofiber Paper. *Advanced Materials* 20:1-4.
- Nypelö T, Pynnönen H, Österberg M, Paltakari J, Laine J (2012) Interactions between inorganic nanoparticles and cellulose nanofibrils. *Cellulose* 19:779-792.
- Österberg M, Vartiainen J, Lucenius J, Hippi U, Seppälä J, Serimaa R, Laine J (2013) A fast method to produce strong NFC films as a platform for barrier and functional materials. *ACS Appl.Mater.Interfaces* 5:4640-4647.
- Pääkkö M, Ankerfors M, Kosonen H, Nykänen A, Ahola S, Österberg M, Ruokolainen J, Laine J, Larsson PT, Ikkala O, Lindström T (2007) Enzymatic Hydrolysis Combined with Mechanical Shearing and High-Pressure Homogenization for Nanoscale Cellulose Fibrils and Strong Gels. *Biomacromolecules* 8:1934-1941.
- PaperMoney (2011) Stora Enso to Build Precommercial Microfibrillated Cellulose Plant. <http://www.globalpapermoney.org/stora-enso-to-build-precommercial-microfibrillated-cellulose-plant-cms-5599>. Accessed: 14.07.2015
- Penttillä A, Sievänen J, Torvinen K, Ojanperä K, Ketoja JA (2013) Filler-nanocellulose substrate for printed electronics: experiments and model approach to structure and conductivity. *Cellulose* 20:1413-1424.

- Peresin MS (2013) Large scale nanofibrillated cellulose films: an overview on its production, properties and potential applications, presented at CEPI and EFPRO open seminar "New ideas for the paper industry - young researchers presentation" in Helsinki
- Qvintus P (2015) Cellulose Nanofibrils (CNF) - Overcoming Challenges on the Development of Nanocellulose-Based Products, presented at Tappi International Conference on Nanotechnology for Renewable Materials in Atlanta
- Rantanen J, Dimic-Misic K, Kuusisto J, Maloney TC (2015) Optimizing the microstructure of MNFC composite paper for improved dewatering and sheet properties, presented at Tappi International Conference on Nanotechnology for Renewable Materials in Atlanta
- Rantanen J, Maloney TC (2013) Press dewatering and nip rewetting of paper containing nano- and microfibril cellulose. *Nordic Pulp and Paper Research Journal* 28:582-587.
- Ridgway CJ, Gane PAC (2011) Constructing NFC-pigment composite surface treatment for enhanced paper stiffness and surface properties. *Cellulose* 19:547-560.
- RISI (2014) Borregaard unveils Exilva microfibrillar cellulose facility plans. <http://ppimagazine.com/chemicals/west-europe/papermaking/borregaard-unveils-exilva-microfibrillar-cellulose-facility-plans#sthash.wIMnQqc4.dpuf>. Accessed: 14.07.2015
- Rodríguez-Fernández J, Pérez-Juste J, Liz-Marzán LM, Lang PR (2007) Dynamic Light Scattering of Short Au Rods with Low Aspect Ratios. *The Journal of physical chemistry* 111:5020-5025.
- Roussi re F, Charfeddine MA, Paradis J, Schenker M, Gane PAC, Mangin PJ (2015) Upgrading Thermo Mechanical Pulp with Micro-Nano Fibrillated Cellulose at pilot scale, presented at PAPTAC Paperweek in Montr al

- Roussière F, Xu X, Dubé M, Carreau P, Schoelkopf J, Gane PAC, Mangin PJ (2014) Dispersion of Micro-Nano Fibrillated Cellulose (MNFC) by Carboxy Methyl Cellulose (CMC) and its characterization, presented at Tappi International Conference on Nanotechnology for Renewable Materials in Vancouver
- Saarinen T, Lille M, Seppälä J (2009) Technical Aspects on Rheological Characterization of Microfibrillar Cellulose Water Suspensions. *Annual Transaction of the Nordic Rheology Society* 17:121-128.
- Saito T, Nishiyama Y, Putaux JL, Vignon M, Isogai A (2006) Homogeneous Suspensions of Individualized Microfibrils from TEMPO-Catalyzed Oxidation of Native Cellulose. *Biomacromolecules* 7:1687-1691.
- Schenker M, Gane PAC (2012) Toward Nano-fibrillated Pigmented Cellulose Composites, presented at Recent advances in cellulose nanotechnology research in Trondheim
- Schenker M, Gane PAC (2013) Development of pigmented composites on the basis of nano- and micro-fibrillated cellulose, presented at Tappi International Conference on Nanotechnology for Renewable Materials in Stockholm
- Schenker M, Schoelkopf J, Mangin PJ, Gane PA (2015) Pigmented Micro-Nanofibrillated Cellulose (MNFC) as packaging composite material: a first assessment, presented at PaperCon in Atlanta
- Sehaqui H, Allais M, Zhou Q, Berglund LA (2011) Wood cellulose bioscomposites with fibrous structures at micro- and nanoscale. *Composites Science and Technology* 71:382-387.
- Shimaoka T (2015) Development of Transparent Cellulose Nano Fiber Film for Flexible Displays, presented at Tappi International Conference on Nanotechnology for Renewable Materials in Atlanta

- Sim K (2014) Change in rheological properties of nanofibrillated cellulose suspension with additives, presented at Tappi International Conference on Nanotechnology for Renewable Materials in Vancouver
- Siqueira G, Bras J, Dufresne A (2009) Cellulose Whiskers versus Microfibrils: Influence of the Nature of the Nanoparticle and its Surface Functionalization on the Thermal and Mechanical Properties of Nanocomposites. *Biomacromolecules* 10:425-432.
- Siqueira G, Bras J, Dufresne A (2010) Cellulosic Bionanocomposites: A review of Preparation, Properties and Applications. *Polymers* 2:728-765.
- Sneck A, Pitkänen M, Kangas H, Tammelin T, Hellén E (2011) New approach to classification of cellulose fibrils and suitable methods for their characterization, presented at Tappi International Conference on Nanotechnology for Renewable Materials in Arlington
- Spence KL, Venditti RA, Habibi Y, Rojas OJ, Pawlak JJ (2010) The effect of chemical composition on microfibrillar cellulose films from wood pulps: Mechanical processing and physical properties. *Bioresource Technology* 101:5961-5968.
- Spence KL, Venditti RA, Rojas OJ, Habibi Y, Pawlak JJ (2011) A comparative study of energy consumption and physical properties of microfibrillated cellulose produced by different processing methods. *Cellulose* 18:1097-1111.
- Subramanian R, Kononov A, Kang T, Paltakari J, Paulapuro H (2008) Structure and properties of some natural cellulosic fibrils. *BioResources* 3:192-203.
- Suopajarvi T, Mathew A, Kekäläinen K, Grubbström G, Oksman K, Laitinen O, Niinimäki J (2010) Comparison of methods in production of microfibrillar cellulose. *IPW das Papier* 12:10-13.
- Svending P (2014) Commercial Break-Through in MFC Processing, presented at Tappi International Conference on Nanotechnology for Renewable Materials in Vancouver

- Svending P, Skuse D, Phipps J (2016) Micro Fibrillated Cellulose - A new dimension in paper making, presented at Specialty Papers EU in Manchester
- Syverud K, Stenius P (2009a) Strength and barrier properties of MFC films. *Cellulose* 16:75-85.
- Syverud K, Stenius P (2009b) Strength and barrier properties of microfibrillar cellulose (MFC) films. *Cellulose* 16:75-85.
- Syverud K, Xhanari K, Chinga-Carrasco G, Yu Y, Stenius P (2011) Films made of cellulose nanofibrils: surface modification by adsorption of a cationic surfactant and characterization by computer-assisted electron microscopy. *Journal of Nanoparticle Research* 13:773-782.
- Taheri H, Samyn P (2016) Effect of homogenization (microfluidization) process parameters in mechanical production of micro- and nanofibrillated cellulose on its rheological and morphological properties. *Cellulose* 23:1221-1238.
- Taipale T, Österberg M, Nykänen A, Ruokolainen J, Laine J (2010) Effect of microfibrillated cellulose and fines on the drainage of kraft pulp suspension and paper strength. *Cellulose* 17:1005-1020.
- Tammelin T, Hippel U, Salminen A (2013) Method for the Preparation of NFC Films on Supports. PCT/FI2012/051015
- Tscharnutter W (2000) Photon Correlation Spectroscopy in Particle Sizing *In* Encyclopedia of Analytical Chemistry. R.A. Meyers, ed: John Wiley & Sons Ltd.
- Turbak AF, Snyder FW, Sandberg KR (1983) Microfibrillated cellulose, a new cellulose product: properties, uses, and commercial potential. *Journal of Applied Polymer Science* 37:815-827.
- Veen SJ, Versluis P, Kuijk A, Velikov KP (2015) Microstructure and rheology of microfibril-polymer networks. *Soft Matter* 11:8907-8912.

- Vesterinen AH, Myllytie P, Laine J, Seppälä J (2010) The effect of water-soluble polymers on rheology of microfibrillar cellulose suspension and dynamic mechanical properties of paper sheet. *Journal of Applied Polymer Science* 116:2990-2997.
- Wagenführ A, Scholz F (2008) *Taschenbuch der Holztechnik*. Fachbuchverlag Leipzig
- Wikipedia (2015) List of food additives, Codex Alimentarius. https://en.wikipedia.org/wiki/List_of_food_additives,_Codex_Alimentarius. Accessed: 20.07.2015
- Wu CN, Saito T, Fujisawa S, Fukuzumi H, Isogai A (2012) Ultrastrong and High Gas-Barrier Nanocellulose/Clay-Layered Composites. *Biomacromolecules* 13:1927-1932.
- Xu X (2014) Study of the relationship between the dispersion of micro-nano-fibrillated-cellulose (MNFC) and their ability in curtain coating (MSc thesis). University of Quebec in Trois-Rivieres.
- Yang Q, Fujisawa S, Saito T, Isogai A (2012) Improvement of mechanical and oxygen barrier properties of cellulose films by controlling drying conditions of regenerated cellulose hydrogels. *Cellulose* 19:695-703.
- Yano H, Nakahara S (2004) Bio-composites produced from plant microfiber bundles with a nanometer unit web-like network. *Journal of Materials Science* 39:1635-1638.
- Yoshimura A, Prud'homme RK (1988) Wall slip corrections for Couette and parallel disk viscometers. *Journal of Rheology* 32:53-67.
- Zhang H, Wu J, Zhang J, He J (2005) 1-Allyl-3-methylimidazolium Chloride Room Temperature Ionic Liquid - A New and Powerful Nonderivatizing Solvent for Cellulose. *Macromolecules* 38:8272 - 8277.

Zheng H, Rantanen J, Maloney T (2014) Fibrillated Cellulose Production - Chemically Assisted Disintegration of the Fiber Cell Wall, presented at Tappi International Conference on Nanotechnology for Renewable Materials in Vancouver

Zimmermann T, Bordeanu N, Strub E (2010) Properties of nanofibrillated cellulose from different raw materials and its reinforcement potential. Carbohydrate Polymers 79:1086-1093.